

**CATIONIC SURFACTANTS INTERACTION
WITH AZO DYE IN MIXED SOLVENT MEDIA
AND ANTI-CORROSION ABILITY OF
SURFACTANTS**



A THESIS SUBMITTED TO THE
CENTRAL DEPARTMENT OF CHEMISTRY
INSTITUTE OF SCIENCE AND TECHNOLOGY
TRIBHUVAN UNIVERSITY
NEPAL

FOR THE AWARD OF
DOCTOR OF PHILOSOPHY
IN CHEMISTRY

BY

NEELAM SHAHI

FEBRUARY, 2023

**CATIONIC SURFACTANTS INTERACTION
WITH AZO DYE IN MIXED SOLVENT MEDIA
AND ANTI-CORROSION ABILITY OF
SURFACTANTS**



A THESIS SUBMITTED TO THE
CENTRAL DEPARTMENT OF CHEMISTRY
INSTITUTE OF SCIENCE AND TECHNOLOGY
TRIBHUVAN UNIVERSITY
NEPAL

FOR THE AWARD OF
DOCTOR OF PHILOSOPHY
IN CHEMISTRY

BY

NEELAM SHAHI

FEBRUARY, 2023

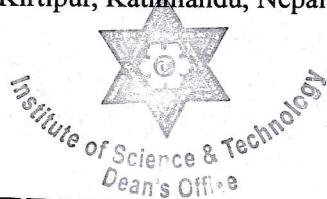


TRIBHUVAN UNIVERSITY
Institute of Science and Technology

DEAN'S OFFICE

Kirtipur, Kathmandu, Nepal

Reference No.:



EXTERNAL EXAMINERS

The Title of Ph.D. Thesis: " Cationic surfactants interaction with azo dye in mixed solvent media and anti-corrosion ability of surfactants "

Name of Candidate: Neelam Shahi

External Examiners:

- (1) Prof. Dr. Daman Raj Gautam
Amrit Science Campus
Tribhuvan University, NEPAL
- (2) Prof. Dr. Bidyut Saha
The University of Burdwan
Burdwan, INDIA
- (3) Dr. Hanna Wilczura-Wachnik
University of Warsaw
Warsaw, POLAND

August 9, 2023

(Dr. Surendra Kumar Gautam)
Asst. Dean

DECLARATION

This thesis entitled " **Cationic surfactants interaction with azo dye in mixed solvent media and anti-corrosion ability of surfactants** " which is being submitted to the Central Department of Chemistry, Institute of Science and Technology (IOST), Tribhuvan University, Nepal for the award of the degree of Doctor of Philosophy (Ph.D.), is a research work carried out by me under the supervision of Prof. Dr. Ajaya Bhattarai of Department of Chemistry, Mahendra Morang Adarsh Multiple Campus, Biratnagar, Tribhuvan University and co-supervised by Prof. Dr. Amar Prasad Yadav, of Central Department of Chemistry, Tribhuvan University.

This research is original and has not been submitted earlier in part or full in this or any other form to any university or institute, here or elsewhere, for the award of any degree.



.....
Neelam Shahi

RECOMMENDATION

This is to recommend that **Mrs Neelam Shahi** has carried out research entitled "**Cationic surfactants interaction with azo dye in mixed solvent media and anti-corrosion ability of surfactants**" for the award of Doctor of Philosophy (Ph.D.) in **Chemistry** under our supervision. To our knowledge, this work has not been submitted for any other degree.

She has fulfilled all the requirements laid down by the Institute of Science and Technology (IOST), Tribhuvan University, Kirtipur for the submission of the thesis for the award of Ph.D. degree.

Ajaya Bhattarai

.....

Prof. Dr. Ajaya Bhattarai

Supervisor

(Professor)

Department of Chemistry

Mahendra Morang Adarsh Multiple Campus

Tribhuvan University

Biratnagar, Nepal



.....

Prof. Dr. Amar Prasad Yadav

Co-Supervisor

(Professor)

Central Department of Chemistry

Tribhuvan University

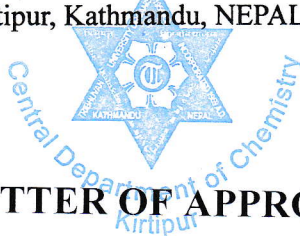
Kirtipur, Kathmandu, Nepal



त्रिभुवन विश्वविद्यालय
TRIBHUVAN UNIVERSITY
विज्ञान तथा प्रविधि अध्ययन संस्थान
Institute of Science and Technology
रसायन शास्त्र केन्द्रीय विभाग
CENTRAL DEPARTMENT OF CHEMISTRY

कीर्तिपुर, काठमाडौं, नेपाल
Kirtipur, Kathmandu, NEPAL

पत्र संख्या:
Ref. No.:



LETTER OF APPROVAL

Date: August 9, 2023

On the recommendation of Prof. Dr. Ajaya Bhattarai and Prof. Dr. Amar Prasad Yadav, this Ph.D. thesis submitted by Neelam Shahi, entitled “**Cationic surfactants interaction with azo dye in mixed solvent media and anti-corrosion ability of surfactants**” is forwarded by Central Department Research Committee (CDRC) to the Dean, IOST, T.U.

Prof. Dr. Jagadeesh Bhattarai

Professor

Head

Central Department of Chemistry

Tribhuvan University

Kirtipur, Kathmandu

Nepal

LETTER OF APPROVAL

Date:

On the recommendation of Prof. Dr. Ajaya Bhattarai and Prof. Dr. Amar Prasad Yadav, this Ph.D. thesis submitted by Neelam Shahi, entitled “ **Cationic surfactants interaction with azo dye in mixed solvent media and anti-corrosion ability of surfactants**” is forwarded by Central Department Research Committee (CDRC) to the Dean, IOST, T.U.

.....

Prof. Dr. Jagadeesh Bhattarai

Professor

Head

Central Department of Chemistry

Tribhuvan University

Kirtipur, Kathmandu

Nepal

ACKNOWLEDGEMENTS

Today, the world is in the climax of its modernization. Every people of the world are struggling to make their identity in this crew of intelligence. Without taking part in this competition, we cannot make a stable position, but we can play a trick on them. So, in my opinion, success is a word that sounds great. Here all the praises, gratitude and deepest thanks to the Almighty God, who bestowed on me his blessings and gave me full strength to finish the Ph.D. research work. During the completion of my work, I was lucky to have support from a large number of people to whom I owe sincere gratitude and thankful.

First and foremost, I would like to express my deepest gratitude to my supervisor Professor Dr. Ajaya Bhattarai, co-supervisor Prof. Dr. Amar Prasad Yadav for their valuable guidance, continuous advice, provocative discussions, constructive criticisms, encouragement, and full support from the beginning until the successful completion of the work. They are the supervisors who provide me the freedom to find out their own track and at the same time give me the instruction to recover when my steps are faltered. Hence, they were unforgettable role models to whom I hold at the highest esteem.

I would acknowledge to Prof. Dr. Jagadeesh Bhattarai, H.O.D., Central Department of Chemistry, Professor Dr. Ram Chandra Basnyat former H.O.D., Central Department of Chemistry, Kirtipur, Kathmandu, Prof. Dr. Megh Raj Pokhrel, former H.O.D., Central Department of Chemistry, Kirtipur, Professor Dr. Nirajan Parajuli, Prof. Dr. Kedar Nath Ghimire, Prof. Dr. Vinay Kumar Jha, Prof. Dr. Paras Nath Yadav of the Central Department of Chemistry for their valuable comments and evaluation of progress reports during the Ph.D. session. I would like to thank all the teaching as well as non-teaching members, staff members of the Central Department of Chemistry for their kind cooperation and assistance in various ways during the time of Ph.D work.

I acknowledge to Dr. Baburam Timilsina, Campus Chief, Prof. Dr. Mahendra Narayan Yadav (Ex-Campus Chief), Dr. Bishnu Dev Das, Assistant Campus Chief, Mr. Pramod Kherwar (Ex-Assistant Campus Chief), Mr. Sitaram Gupta (former H.O.D.), Dr. Ghanshyam Shrivastav, H.O.D., Department of Chemistry, Mahendra Morang Adarsha Multiple Campus, Biratnagar, Morang, Nepal, for granting me the various laboratory facilities and the encouragement for pursuing the Ph.D. work. Active cooperation to my research colleagues, Mr. Sanjay Singh, Mrs. Anju Kumari Das, Mr. Yuv Raj Sahu, Mr.

Janak Adhikari, Mr Rohit Kumar Dev for their well-needed guidance and helpful advice. I also acknowledge Dr. Narendra Chaudary, Dr. Deepak Kumar Gupta, Dr. Nabin Karki, Mr. Hari Bhakta Oli, Dr. Shova Neupane, Mr. Shiv Narayan Yadav, Mr. Indra Deo Gupta, Dr. RamBabu Shah, Mr. Binod Mehta for their guidance in research work. I would also acknowledge the faculty members and staff of Mahendra Morang Adarsha Multiple Campus, Biratnagar, Morang, Nepal for their assistance and kind cooperation in every step of the research work.

I am indebted from the core of heart to the University Grants Commission (UGC) Sanothimi, Bhaktapur, Nepal for providing me with the Ph.D. Fellowship.

I want to express my deepest feelings of love and compassion to my beloved Mother late. Ram Pari Devi and Father late. Assoc. Prof. Mahendra Shahi Teli for their untiring efforts so that today I can complete my Ph.D. research work. I also thank my beloved brothers Rajesh Kumar Shahi, BimLendu Shahi and sister Poonam Shahi for their continuous courage and motivation during the period of work.

Finally, I must thank very much to my husband Mr. Om Prakash Sah, for his continuous support and encouragement during the time of research work. So, I dedicate my Ph.D. work to my family.

.....

Neelam Shahi

February 2023

ABSTRACT

Due to modernization, researchers are in search of efficient compounds which must be easy to synthesis in large volume at low cost, durable, reliable, cheap for commercial applications for enhancement in dyeing and for corrosion control. In this context, surfactants are the best chemical compounds due to their aggregating nature at critical micelle concentration and such form is called micelle. The present study is dealt to its interaction with additives azo dye possessing typical dyeing features as it can be utilized for enhancing the quality of colourful substances in mixed solvent system along with its anti-corrosion ability.

The aim of the present study is to investigate the interaction between cationic surfactants dodecyl trimethyl ammonium bromide (DTAB) and cetylpyridinium chloride (CPC) with azo dye methyl red (MR) in mixed solvent media and study the anti-corrosion ability of surfactants. The interaction study is performed with the studies of UV-Vis. spectra, conductivity, surface tension, viscosity, pH, and anti-corrosion study with weight loss and potentiodynamic polarization measurements. The interactional and anticorrosion analysis has been compared at three different temperatures (298.15 K, 308.15 K and 318.15 K).

CMCs are identified at lower absorbance using UV-visible spectrophotometric techniques. From the spectral data, azo form of MR is best for interaction with cationic surfactants. The binding as well as partition parameters have been determined using Benesi-Hildebrand equation and pseudo-phase model respectively. All the spectral analysis are analysed at 0.1, 0.2, 0.3 and 0.4 volume of methanol in room temperature.

Conductometric measurements are performed to determine the CMCs both in absence and presence of MR at three different temperatures in mixed methanol media. The interaction of surfactants DTAB and CPC with MR has been identified separately through the dye-surfactant aggregation process with suppressed CMC values due to the architectural flexibility of MR in the systems. Micellization becomes more likely with MR due to the formation of a molecular complex in mixed systems. The calculated thermodynamic properties both in the absence and presence of methyl red are the standard Gibbs free energy of micellization (ΔG_m^0), the standard enthalpy of micellization (ΔH_m^0), the standard entropy of micellization (ΔS_m^0), the standard free energy of transfer (ΔG_{trans}^0) and heat capacity of micellization (ΔmC_p^0). In accordance

with ΔG_m^0 values, the mixtures show the spontaneous nature of micellization of DTAB and CPC.

CMCs are determined from the plots of surface tension and $\log[\text{surfactant}]$ in presence of MR with surface tension measurement. Surface properties are determined using CMCs to study the interaction of DTAB with MR and CPC with MR. Such surface properties are $\frac{dy}{d\log C}$, Γ_{\max} , A_{\min} , π_{CMC} , P , ΔG_{ads}^0 and pC_{20} of CPC in the presence of methyl red with respect to volume fractions of methanol at 298.15 K, 308.15 K and 318.15 K.

Viscosities in presence of MR of surfactant solution in mixed methanol system are determined at three temperatures and CMCs are obtained. Using the increased CMCs with increase in mixed volume, viscosity coefficient is determined with Jones-Dole equation. Along with this pH of surfactant solutions in presence of MR are determined at room temperature.

Anti-corrosion study of DTAB and CPC are studied to find the inhibition efficiency using weight loss method and potentiodynamic polarization method. Weight loss is obtained at three different temperatures (298.15 K, 308.15 K and 318.15 K). All the reported sample solutions were maintained at three different temperatures (298.15 K, 308.15 K and 318.15 K) of concentrations range below, above and at optimum critical micelle concentration (CMC) of the cationic surfactants. Results showed that inhibition efficiency decreases with increase in temperatures and increases with addition of concentrations of cationic surfactants. The highest inhibition efficiency of both surfactants was determined at around CMC. Both CPC and DTAB follow isotherm of Langmuir adsorption and represent as mixed type of corrosion inhibitor with predominance of cathodic reaction.

LIST OF ACRONYMS AND ABBREVIATIONS

CMC	: Critical Micelle Concentration
UV-Vis	: Ultraviolet Visible
DTAB	: Dodecyl Trimethyl Ammonium Bromide
CPC	: Cetyl Pyridinium Chloride
MR	: Methyl Red
A	: Absorbance
a.u.	: Arbitrary Unit
λ	: Wavelength
nm	: Nanometer
M or mol. L ⁻¹	: Mole Per Litre
V.F.	: Volume Fraction
T	: Absolute Temperature
VFT	: Viscous Flow Time
I.E	: Inhibition Efficiency
K	: Kelvein
CR	: Corrosion Rate
MS	: Mild Steel
kJ/mol	: Kilo Joule Per mole
NMR	: Nuclear Magnetic Resonance
pH	: Logarithmic Scale of Concentration of Hydronium ion $\log[\text{H}_3\text{O}^+]$
SEM	: Scanning Electron Microscopy
EIS	: Electrochemical Impedance Spectroscopy

TEM : Transmission Electron Microscopy

DLS : Dynamic light Scattering

LIST OF SYMBOLS

D_T	: Concentration of Dye
ΔA	: The Difference between Dye's Absorbance with and without Surfactant
ϵ_m	: Molar Absorptivity of the Dye fully Bound to Micelles
ϵ_0	: Molar Absorptivity of Dye
C_m	: Concentration of Micellized Surfactant
C_s	: Concentration of Surfactant
K_b	: Binding Constant
K_s	: Partition Constant
K_x	: Partition Coefficient
n_w	: Number of Moles of Water Per Liter
ΔG_b	: Gibb's Free Energies of Binding
ΔG_p	: Gibb's Free Energies of Partition
R	: Universal Gas Constant,
A	: Absorbance
S_1	: Premicellar Slope
S_2	: Postmicellar Slope
ΔG_m°	: Standard Gibb's Free Energy of Micelle
X_{CMC}	: Mole Fraction of CMC
ΔH_m°	: Standard Enthalpy of Micellization
ΔS_m°	: Standard Entropy of Micellization
ΔG_{trans}°	: Standard Gibb's Free Energy of Transition
$(\Delta G_m^\circ)_{methanol+water}$: Standard Gibb's Free Energy in Mixed Methanol Water

$(\Delta G_m^\circ)_{water}$: Standard Gibb's Free Energy in Water
$\Delta m C_p^0$: Heat Capacity of Micellization
V_o	: Volume of Exclusion Per Monomer in the Aggregate
$\frac{d\gamma}{d \log C}$: Slope of the γ versus $\log C$ Plot taken at CMC
Γ_{max}	: Maximum Surface Excess Concentration
A_{min}	: Area occupied Per Surfactant Molecule
π_{CMC}	: Surface Pressure
P	: Packing Parameter
ΔG_{ads}^0	: Standard Free Energy Interfacial Adsorption
pC_{20}	: Negative Logarithm of C_{20}
γ	: Surface Tension
η	: Viscosity
K	: Conductivity
W	: Weight Loss
S	: Total Area of Corrosion
T	: Time of Immersion
Θ	: Surface Coverage
K_{ads}	: The Equilibrium Constant
R^2	: Correlation Coefficient
ΔG_{ads}^0	: Standard Free of Adsorption
E_a^*	: The Apparent Activation Energy
h	: Planck's Constant
N	: Avogadro's Number
ΔH^*	: Enthalpy Change

ΔS^*	: Entropy Change
I_{corr}^0	: Corrosion Current Density in Absence of Inhibitor
I_{corr}	: Corrosion Current Density in Presence of Inhibitor
E	: Potential
I	: Current
E_{corr}	: Corrosion Potential
$\frac{n}{n_0}$: Relative viscosity of a Solution
l_c	: Maximum Chain Length
n_c	: Number of Carbon Atoms in the Alkyl Chain

LIST OF TABLES

	Page No.
Table 1: Some common methods to obtain CMC	4
Table 2: Molecular structure of DTAB, CPC, and MR	18
Table 3: CMC values of DTAB and CPC at 0.1,0.2,0.3 and 0.4 volume fractions of Methanol	30
Table 4: Values of K_b , K_s , K_x , ΔG_b and ΔG_p of DTAB and CPC at 0.1, 0.2, 0.3 and 0.4 volume fractions of methanol	30
Table 5: Values of K_b and ΔG_b of DTAB at 0.1, 0.2, 0.3 and 0.4 volume fractions of ethanol	36
Table 6: The values of CMC, α , ΔG_m^0 , ΔH_m^0 , ΔS_m^0 and ΔG_{trans}^0 of DTAB without MR and with MR at 0.1,0.2,0.3 and 0.4 methanol-water medium through three dissimilar temperatures (298.15 K, 308.15 K and 318.15K)	66
Table 7: The values of CMC, α , ΔG_m^0 , ΔH_m^0 , ΔS_m^0 and ΔG_{trans}^0 of CPC without MR and with MR at 0.1, 0.2, 0.3 and 0.4 methanol-water medium through three different temperatures (298.15 K, 308.15 K and 318.15K)	67
Table 8: Values of ΔmC_p^0 for DTAB and CPC in mixed methanol-water system	68
Table 9: The CMC values of DTAB and CPC using Surface tension method and viscosity method	78
Table 10: The values of $dy/d\log C$, T_{max} , A_{min} , Π_{cmc} , P , ΔG_{ads}^0 and pC_{20} of DTAB in the presence of MR in different volume fractions of methanol at 298.15 K, 308.15 K and 318.15 K.....	80
Table 11: The values of $dy/d\log C$, T_{max} , A_{min} , Π_{cmc} , P , ΔG_{ads}^0 and pC_{20} of CPC in the presence of MR in different volume fractions of methanol at 298.15 K, 308.15 K and 318.15 K.	81
Table 12: Essential corrosion parameters of mild steel in 0.5 M H_2SO_4 with various concentrations of DTAB and CPC obtained at 298.15 K.....	104
Table 13: Inhibition efficiency (I.E.) and surface coverage (θ) of DTAB and CPC obtained at three different temperatures.....	105
Table 14: Free energy for adsorption and equilibrium constant of DTAB and CPC as surfactant inhibitor on the mild steel surface.....	107
Table 15: Thermodynamic activation parameters for adsorption of DTAB and CPC as surfactant inhibitor on the mild steel surface.....	112
Table 16: Effect of DTAB and CPC as surfactant inhibitor on the mild steel surface studied by potentiodynamic polarization method.	114

LIST OF FIGURES

Page No.

Figure 1: Classification of Surfactant according to the composition of their head.....	1
Figure 2: Schematic representation of aggregation of surfactant depending on the concentration (Malik <i>et al.</i> , 2011).	3
Figure 3: The log of CMC varies linearly with the number of carbon atoms in the alkyl chain of a surfactant (Gohain <i>et al.</i> , 2008).....	5
Figure 4: Effect of temperature on CMC of Sodium Dodecyl Sulphate (top) and penta(ethylene glycol) nonodecyl ether (Alvares <i>et al.</i> , 2014).....	6
Figure 5: The interaction scheme between dye and surfactant for their complex formation.	8
Figure 6: Most corrosion of metals is electrochemical in nature (Malik <i>et al.</i> , 2011).....	9
Figure 7: Effect of surfactant inhibitor on change in its concentration (Elkacimi <i>et al.</i> , 2011; Malik <i>et al.</i> , 2011)	11
Figure 8: Mechanism of surfactant adsorption on metallic (Choi <i>et al.</i> , 2022; Malik <i>et al.</i> , 2011).....	12
Figure 9: Visible spectra of MR-DTAB system in 0.1 volume fraction of methanol. Here, I, II, III, IV, V, VI, VII, VIII, IX, X and MR represent the concentration of DTAB [5, 2.4, 2.2, 2, 1.8, 1.6, 1.4, 1.2, 1, 0.8 and 0] $\times 10^{-2}$ mol. L ⁻¹ respectively. Here the constant concentration of MR is 2×10^{-3} mol. L ⁻¹	24
Figure 10: Visible spectra of MR-DTAB system in 0.2 volume fraction of methanol. Here, I, II, III, IV, V, VI, VII, VIII, IX, X and MR represent the concentration of DTAB [5, 2.4, 2.2, 2, 1.8, 1.6, 1.4, 1.2, 1, 0.8 and 0] $\times 10^{-2}$ mol. L ⁻¹ respectively. Here the constant concentration of MR is 2×10^{-3} mol. L ⁻¹	24
Figure 11: Visible spectra of MR-DTAB system in 0.3 volume fraction of methanol. Here, I, II, III, IV, V, VI, VII, VIII, IX, X and MR represent the concentration of DTAB [5, 2.4, 2.2, 2, 1.8, 1.6, 1.4, 1.2, 1, 0.8 and 0] $\times 10^{-2}$ mol. L ⁻¹ respectively. Here the constant concentration of MR is 2×10^{-3} mol. L ⁻¹	25
Figure 12: Visible spectra of MR-DTAB system in 0.4 volume fraction of methanol. Here, I, II, III, IV, V, VI, VII, VIII, IX, X and MR represent the concentration of DTAB [5, 2.4, 2.2, 2, 1.8, 1.6, 1.4, 1.2, 1, 0.8 and 0] $\times 10^{-2}$ mol. L ⁻¹ respectively. Here the constant concentration of MR is 2×10^{-3} mol. L ⁻¹	25
Figure 13: Visible spectra of MR-CPC system in 0.1 volume fraction of methanol. Here, I, II, III, IV, V, VI, VII, VIII, IX, X and MR represent the concentration of CPC [1.5, 1.4, 1.3, 1.2, 1.1, 1.0, 0.9, 0.8, 0.7, 0.6 and 0] $\times 10^{-3}$ mol. L ⁻¹ respectively. Here the constant concentration of MR is 2×10^{-3} mol. L ⁻¹	26
Figure 14: Visible spectra of MR-CPC system in 0.2 volume fraction of methanol. Here, I, II, III, IV, V, VI, VII, VIII, IX, X and MR represent the concentration of CPC [1.5, 1.4, 1.3, 1.2, 1.1, 1.0, 0.9, 0.8, 0.7, 0.6 and 0] $\times 10^{-3}$ mol. L ⁻¹ respectively. Here the constant concentration of MR is 2×10^{-3} mol. L ⁻¹	27
Figure 15: Visible spectra of MR-CPC system in 0.3 volume fraction of methanol. Here, I, II, III, IV, V, VI, VII, VIII, IX, X and MR represent the concentration of CPC [1.5,	

	1.4,1.3,1.2,1.1,1,0.9,0.8,0.7,0.6 and 0] $\times 10^{-3}$ mol. L ⁻¹ respectively. Here the constant concentration of MR is 2×10^{-3} mol. L ⁻¹	27
Figure 16:	Visible spectra of MR-CPC system in 0.4 volume fraction of methanol. Here, I, II, III, IV, V, VI, VII, VIII, IX, X and MR represent the concentration of CPC [1.5, 1.4,1.3,1.2,1.1,1,0.9,0.8,0.7,0.6 and 0] $\times 10^{-3}$ mol. L ⁻¹ respectively. Here the constant concentration of MR is 2×10^{-3} mol. L ⁻¹	28
Figure 17:	Plot of absorbance against the [DTAB] profile in four different volume fractions of methanol.....	31
Figure 18:	Plot of absorbance against the [CPC] profile in four different volume fractions of methanol	31
Figure 19:	Plot of $D_T/\Delta A$ against $[C_s\text{-CMC}]^{-1}$ for MR with DTAB in four different volume fractions of methanol	32
Figure 20:	Plot of $D_T/\Delta A$ against $[C_s\text{-CMC}]^{-1}$ for MR with CPC in four different volume fractions of methanol.....	32
Figure 21:	Plot of ΔA^{-1} against $[C_{\text{dye}}+C_{\text{surfactant}}\text{-CMC}]^{-1}$ for MR with DTAB in four different volume fractions of methanol	33
Figure 22:	Plot of ΔA^{-1} against $[C_{\text{dye}}+C_{\text{surfactant}}\text{-CMC}]^{-1}$ for MR with CPC in four different volume fractions of methanol	33
Figure 23:	Visible spectra of MR-DTAB system in 0.1 volume fraction of ethanol. Here, I, II, III, IV, V and MR represent the concentration of DTAB [1, 2, 3, 4, 11 and 0] $\times 10^{-2}$ mol. L ⁻¹ respectively. Here the constant concentration of MR is 2.97×10^{-4} mol. L ⁻¹	34
Figure 24:	Visible spectra of MR-DTAB system in 0.2 volume fraction of ethanol. Here, I, II, III, IV, V and MR represent the concentration of DTAB [1, 2, 3, 4, 11 and 0] $\times 10^{-2}$ mol. L ⁻¹ respectively. Here the constant concentration of MR is 2.97×10^{-4} mol. L ⁻¹	34
Figure 25:	Visible spectra of MR-DTAB system in 0.3 volume fraction of ethanol. Here, I, II, III, IV, V and MR represent the concentration of DTAB [1, 2, 3, 4, 11 and 0] $\times 10^{-2}$ mol. L ⁻¹ respectively. Here the constant concentration of MR is 2.97×10^{-4} mol. L ⁻¹	35
Figure 26:	Visible spectra of MR-DTAB system in 0.4 volume fraction of ethanol. Here, I, II, III, IV, V and MR represent the concentration of DTAB [1, 2, 3, 4, 11 and 0] $\times 10^{-2}$ mol. L ⁻¹ respectively. Here the constant concentration of MR is 2.97×10^{-4} mol. L ⁻¹	35
Figure 27:	Plot of $D_T/\Delta A$ against $[C_s]^{-1}$ for MR with DTAB in four different volume fractions of ethanol.....	37
Figure 28:	Representative plot of conductivity against the DTAB concentration without MR (\square) and with MR (\circ) of 0.1 volume fraction of methanol in water at 298.15 K ..	39
Figure 29:	Representative plot of conductivity against the CPC concentration without MR (\circ) and with MR (∇) of 0.1 volume fraction of methanol in water at 298.15 K ..	39
Figure 30:	Plot of DTAB in absence of MR for the fitting $\ln X_{\text{CMC}}$ versus three different temperatures.....	41
Figure 31:	Plot of DTAB in presence of MR for the fitting $\ln X_{\text{CMC}}$ versus three different temperatures.....	41

Figure 32: Plot of CPC in absence of MR for the fitting $\ln X_{CMC}$ versus three different temperatures.....	42
Figure 33: Plot of CPC in presence of MR for the fitting $\ln X_{CMC}$ versus three different temperatures.....	42
Figure 34: Plot of DTAB in absence of MR of Standard enthalpy of micellization against T	43
Figure 35: Plot of DTAB in presence of MR of Standard enthalpy of micellization against T.....	44
Figure 36: Plot of CPC in absence of MR of Standard enthalpy of micellization against T.	44
Figure 37: Plot of CPC in absence of MR of Standard enthalpy of micellization against T.	45
Figure 38: Plot of conductivity against [DTAB] in absence of MR at 298.15 K	69
Figure 39: Plot of conductivity against [DTAB] in absence of MR at 308.15 K	69
Figure 40: Plot of conductivity against [DTAB] in absence of MR at 318.15 K	70
Figure 41: Plot of conductivity against [DTAB] in presence of MR at 298.15 K	70
Figure 42: Plot of conductivity against [DTAB] in presence of MR at 308.15 K.....	71
Figure 43: Plot of conductivity against [DTAB] in presence of MR at 318.15 K.....	71
Figure 44: Plot of conductivity against [CPC] in absence of MR at 298.15 K.....	72
Figure 45: Plot of conductivity against [CPC] in absence of MR at 308.15 K.....	72
Figure 46: Plot of conductivity against [CPC] in absence of MR at 318.15 K.....	73
Figure 47: Plot of conductivity against [CPC] in presence of MR at 298.15 K	73
Figure 48: Plot of conductivity against [CPC] in presence of MR at 308.15 K	74
Figure 49: Plot of conductivity against [CPC] in presence of MR at 318.15 K	74
Figure 50: Plot of surface tension versus \log [DTAB] with MR in 0.1 volume fraction of methanol at 298.15 K.....	79
Figure 51: Plot of surface tension versus \log [CPC] with MR in 0.1 volume fraction of methanol at 298.15 K.....	79
Figure 52: Plot of surface tension versus \log [DTAB] with MR in four different volume fraction of methanol at 298.15 K.....	82
Figure 53: Plot of surface tension versus \log [DTAB] with MR in four different volume fraction of methanol at 308.15 K.....	82
Figure 54: Plot of surface tension versus \log [DTAB] with MR in four different volume fraction of methanol at 318.15 K.....	83
Figure 55: Plot of surface tension versus \log [CPC] with MR in four different volume fraction of methanol at 298.15 K	83
Figure 56: Plot of surface tension versus \log [CPC] with MR in four different volume fraction of methanol at 308.15 K	84
Figure 57: Plot of surface tension versus \log [CPC] with MR in four different volume fraction of methanol at 318.15 K	84
Figure 58: Plot of viscosity against DTAB concentration with MR in 0.1 volume fraction of methanol at 298.15 K.....	87
Figure 59: Plot of viscosity against CPC concentration with MR in 0.1 volume fraction of methanol at 298.15 K.....	87

Figure 60: Plot of viscosity against DTAB concentration with MR in four different volume fractions of methanol at 298.15 K	88
Figure 61: Plot of viscosity against DTAB concentration with MR in four different volume fractions of methanol at 308.15 K	88
Figure 62: Plot of viscosity against DTAB concentration with MR in four different volume fractions of methanol at 318.15 K	89
Figure 63: Plot of viscosity against CPC concentration with MR in four different volume fractions of methanol at 298.15 K	89
Figure 64: Plot of viscosity against CPC concentration with MR in four different volume fractions of methanol at 308.15 K	90
Figure 65: Plot of viscosity against CPC concentration with MR in four different volume fractions of methanol at 318.15 K	90
Figure 66: Plot of n_r-1 against c for DTAB with MR at 298.15 K	91
Figure 67: Plot of n_r-1 against c for DTAB with MR at 308.15 K	91
Figure 68: Plot of n_r-1 against c for DTAB with MR at 318.15 K	92
Figure 69: Plot of n_r-1 against c for CPC with MR at 298.15 K.....	92
Figure 70: Plot of n_r-1 against c for CPC with MR at 308.15 K.....	93
Figure 71: Plot of n_r-1 against c for CPC with MR at 318.15 K.....	93
Figure 72: Viscosity B coefficients of DTAB with MR	94
Figure 73: Viscosity B coefficients of CPC with MR	94
Figure 74: Tautomerism of azo dye	95
Figure 75: [CPC] versus the pH profile. (A) 0.1 volume fraction of methanol	96
Figure 76: [CPC] versus the pH profile. (B) 0.2 volume fraction of methanol	96
Figure 77: [CPC] versus the pH profile. (C) 0.3 volume fraction of methanol	96
Figure 78: [CPC] versus the pH profile. (D) 0.4 volume fraction of methanol	97
Figure 79: [DTAB] versus the pH profile. (A) 0.1 volume fraction of methanol.....	97
Figure 80: [DTAB] versus the pH profile. (B) 0.2 volume fraction of methanol.....	97
Figure 81: [DTAB] versus the pH profile.(C) 0.3 volume fraction of methanol.....	98
Figure 82: [DTAB] versus the pH profile. (D) 0.4 volume fraction of methanol.....	98
Figure 83: Variation of corrosion rate of different concentrations of DTAB at 298.15 K	100
Figure 84: Variation of corrosion rate of different concentrations of CPC at 298.15 K ...	100
Figure 85: Variation of inhibition efficiency of different concentrations of DTAB at 298.15 K	101
Figure 86: Variation of inhibition efficiency of different concentrations of CPC at 298.15 K	101
Figure 87: Variation of corrosion rate of different concentrations of DTAB at three different temperatures.....	102
Figure 88: Variation of corrosion rate of different concentrations of CPC at three different temperatures.....	102
Figure 89: Variation of inhibition efficiency of different concentrations of DTAB at three different temperatures.....	103
Figure 90: Variation of inhibition efficiency of different concentrations of CPC at three different temperatures.....	103

Figure 91: Plot of C/θ against DTAB (where C is the concentration of DTAB) at three different temperatures.....	106
Figure 92: Plot of C/θ against CPC (where C is the concentration of CPC) at three different temperatures.....	107
Figure 93: Plot of $\log CR$ (DTAB) against $1/T$	109
Figure 94: Plot of $\log CR$ (CPC) against $1/T$	110
Figure 95: Plot of $\log CR/T$ (DTAB) against $1/T$	110
Figure 96: Plot of $\log CR/T$ (CPC) against $1/T$	111
Figure 97: Potentiodynamic polarization curves for MS in 0.5 M H_2SO_4 in the absence and presence of DTAB	113
Figure 98: Potentiodynamic polarization curves for MS in 0.5 M H_2SO_4 in the absence and presence of CPC	113

TABLE OF CONTENTS

	Page no.
Declaration.....	ii
Recommendation	iii
Letter of Approval.....	iv
Acknowledgements.....	v
Abstract.....	vii
List of Acronyms and Abbreviations.....	ix
List of Symbols.....	xi
List of Tables	xiv
List of Figures.....	xv
CHAPTER 1.....	1
1. INTRODUCTION.....	1
1.1 General Perspective.....	1
1.2 Surfactants.....	1
1.3 Critical Micelle Concentration (CMC)	2
1.4 Determination of Critical Micelle Concentration (CMC).....	4
1.5 Factors affecting CMC.....	5
1.5.1 Molecular structure of surfactants.....	5
1.5.2 Temperature.....	6
1.5.3. Additives.....	6
1.6 Dye and its classification	7
1.7 Influence of dye structure on aggregation.....	7
1.8 Corrosion.....	8
1.9 Surfactant inhibitor and its classification.....	9
1.10 Surfactant as corrosion inhibitor	10
1.11 CMC in corrosion inhibition	10
1.12 Rationale.....	12
1.13 Objectives.....	13
1.13.1 General objective.....	13
1.13.2 Specific objectives.....	13
CHAPTER 2.....	14

2. LITERATURE REVIEW	14
2.1 General overview	14
2.2 Surfactant Sensitized Reaction.....	14
2.3 Methods for dye-surfactant interactions.....	14
2.4 Anti-corrosion Ability of Surfactants.....	15
2.5 Applications of dye-surfactant interaction study	16
2.6 Applications of anti-corrosion study	17
CHAPTER 3	18
3. MATERIALS AND METHODS	18
3.1 Materials/ Reagents	18
3.2 Methods.....	19
3.2.1 For dye-surfactant interactions study	19
3.2.2 Anti-corrosion ability of Surfactants	21
CHAPTER 4	23
4. RESULTS AND DISCUSSION	23
4.1 Dye surfactant interaction studies	23
4.1.1 UV-Vis spectra of Cationic surfactant (DTAB)-MR interactions in methanol-water mixture.....	23
4.1.2 UV-Vis spectra of Cationic surfactant (CPC)-MR interactions in methanol- water mixture	26
4.1.3 Determination of Binding and Partition Parameters using Differential Absorption Spectra of DTAB and CPC.....	28
4.1.4 UV-Vis spectra of Cationic surfactant (DTAB)-MR interactions in ethanol- water mixture	34
4.1.5 Conductometric studies and its related thermodynamic properties of DTAB and CPC in absence and presence of MR.....	37
4.1.6. Surface tension studies and its related surface properties of DTAB and CPC in presence of MR	75
4.1.7 Viscosity studies and its related properties of DTAB and CPC in presence of MR.....	85
4.1.8 Study of pH of DTAB and CPC in presence of MR and its effects on interactions.....	95
4.2. Anti-corrosion ability of DTAB and CPC.....	98
4.2.1 Weight loss study.....	98
4.2.2 Polarization Measurements.....	112

4.2.3 Mechanism of adsorption of surfactant inhibitor on MS.....	114
CHAPTER 5	116
CONCLUSION AND RECOMMENDATIONS	116
5.1 Conclusion.....	116
5.2 Recommendations	117
CHAPTER 6	118
6. SUMMARY	118
REFERENCES	119
APPENDIX	

CHAPTER 1

1. INTRODUCTION

1.1 General Perspective

Surfactants have been a great approach to fulfil the existing need of the population. To enhance the quality of dyeing, surfactants play vital role in improving the process. The main objective of present research to diminish the environmental pollution which could be implemented using least harmful substances and must be environmentally friendly.

1.2 Surfactants

Surfactants are surface active agents which exhibit some amazing interfacial activity. All known surfactants are amphiphilic compounds possesses hydrophilic and lipophilic propensities on the same compounds (Bashir *et al.*, 2022). Polar molecules in such surfactants consisting of polar groups, non-polar groups and also ions composed of different electronegative atoms (Ma *et al.*, 2013). These molecules form a network of hydrogen bonds in water. As a result, classifying surfactants into such groups is dependent on the composition of hydrophilic groups. Surfactants are classified into groups based on the nature of their hydrophilic head groups (Sar *et al.*, 2019). Aside from that, surfactants are classified according to their use, and many surfactants have multiple uses as they are extremely useful compounds. (Isaac *et al.*, 2022). Anionic surfactants have a negative head, cationic surfactants have a positive head, nonionic surfactants have no charge in their head, and amphoteric or zwitterionic surfactants have both negative and positive heads. as shown in **Fig.** (Lavkush Bhaire *et al.*, 2015).

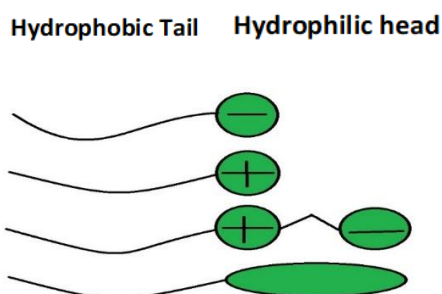


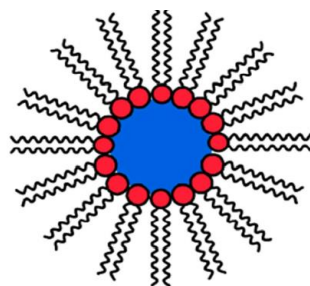
Figure 1: Classification of Surfactant according to the composition of their head.

1.3 Critical Micelle Concentration (CMC)

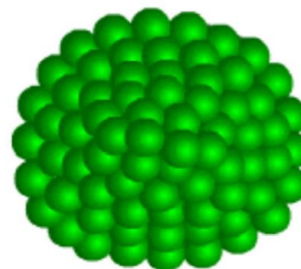
Surfactants exist as monomers in aqueous solution at low concentrations (free or unassociated surfactant molecules). These monomers form a monolayer at the interface, pack together, and lower surface and interfacial tension (Bashir *et al.*, 2022). Despite the fact that this event is highly dynamic surfactant molecules enter and exit the interface on a very quick time scale the strong interactions between molecules at the interface and their nearby neighbours allow for the determination of the monolayer's rheological properties (Ma *et al.*, 2013). With the exception of the fact that surface tension dramatically decreases with concentration, surfactant characteristics in low concentrations in water are comparable to those of simple electrolytes (Isaac *et al.*, 2022).

Surfactant monomers assemble to form a closed aggregate (micelle) at a certain concentration, with the hydrophobic tails shielded from water and the hydrophilic heads facing it. When micelles form in an aqueous medium, the critical aggregation concentration (CAC) is known as the critical micelle concentration (CMC).

The CMC is a surfactant property that indicates when monolayer adsorption is complete, and the surface-active properties are optimal. Monomer concentrations are nearly constant above the CMC. As a result, there are no significant changes in the surfactant properties of the solution because the surface activity is caused by the monomers. Micelles have no surface activity, and any increase in surfactant concentration affects the structure of micelles rather than the number of monomers in the solution.



Reverse micelle



Spherical micelle

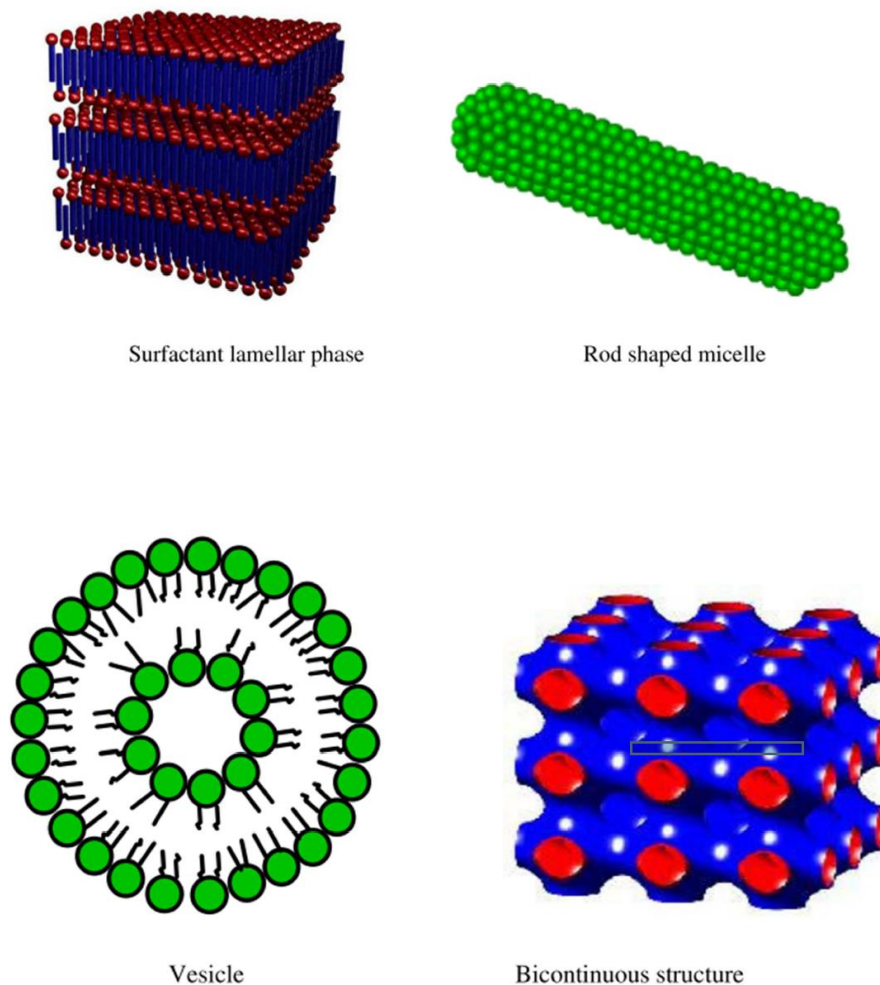


Figure 2: Schematic representation of aggregation of surfactant depending on the concentration (Malik *et al.*, 2011).

Based on the area occupied by the hydrophilic and hydrophobic groups of surfactants, a theory for aggregate structure was developed. For a surfactant aggregate structure to be stable in an aqueous system, the internal part of the aggregate must contain the hydrophobic part of the surfactant molecule, while the surface must contain the hydrophilic heads. If the polar head groups in water are ionic, they will repel each other due to the same charge repulsion. The higher the charge, the stronger the repulsion and the less likely it is to form aggregates (Malik *et al.*, 2011).

1. Spherical micelles form when the surfactant packing parameter is less than one-third (single chain surfactants with large head group areas such as anionic surfactants). The radius of the spherical aggregates is approximately equal to the maximum stretched out length of the surfactant molecule.

2. When the surfactant packing parameter is between $1/3$ and $1/2$, cylindrical micelles form (single chain surfactants with small head group areas such as non-ionic surfactants and ionic surfactants in high salt concentration). Any change in solution properties that reduces the effective size of hydrophilic head groups will cause the aggregate size and shape to change from spherical to cylindrical.
3. As the packing parameter approaches unity, the lamella flattens and becomes planar (double chain anionic surfactants in high salt concentration).

1.4 Determination of Critical Micelle Concentration (CMC)

CMC is the concentration at which micelles, or aggregates form. Beyond and after this point, several physicochemical properties (conductivity, surface tension, viscosity, density etc) of surfactant solutions are changed (Shah *et al.*, 2020; Shah & Bhattarai, 2020). A physicochemical property of interest is often plotted against the concentration of the surfactant, and the break in the plot is used to determine the CMC value of a surfactant micelle (Shah *et al.*, 2020). **Table 1** lists the techniques used to determine CMC most frequently. It should be noted that various experimental methods could result in somewhat different values for a surfactant's CMC.

Table 1: Some common methods to obtain CMC

Conductivity	(Ali <i>et al.</i> , 2014)
Ultrasonic Resonance Technology	(Horiuchi & Winter, 2015)
Surface Tension	(Menger <i>et al.</i> , 2005)
UV/Vis	(Ali <i>et al.</i> , 2014)
NMR Spectroscopy	(Alvares <i>et al.</i> , 2014)
Calorimetry	(Animesh Pan <i>et al.</i> , 2013)
Density	(Sheikh & Bhat, 2012)
Isothermal titration calorimetry	(Smith <i>et al.</i> , 2022)
Fluorescence Spectroscopy	(Lavkush Bhisare <i>et al.</i> , 2015)
Viscosity	(Sheikh & Bhat, 2012)

1.5 Factors affecting CMC

There are several factors that affect the value of CMC. It includes the molecular structure of surfactants (including hydrophobic tail, head, and counter ions), temperature and additives (such as co-solvent, azo dyes etc).

1.5.1 Molecular structure of surfactants

From the data of values of CMC of different surfactants, several general observations on the variation of the CMC with surfactant molecular structure can be made as illustrated in **Fig. 3**. The CMC decreases dramatically as the length of the alkyl chain increases seen from **Fig. 4**. It is because of increase in hydrophobicity with increase in chain length (Shah *et al.*, 2016). A fixed number of carbons in the alkyl chain is best for comparing different classes of surfactants. Non-ionic CMCs are significantly lower than ionic CMCs (Lavkush Bhaire *et al.*, 2015). The length of the alkyl chain influences the relationship. Aside from the significant difference between ionics and non-ionics, the effects of the head group are mild. Cationics usually have a higher CMC than anionics.

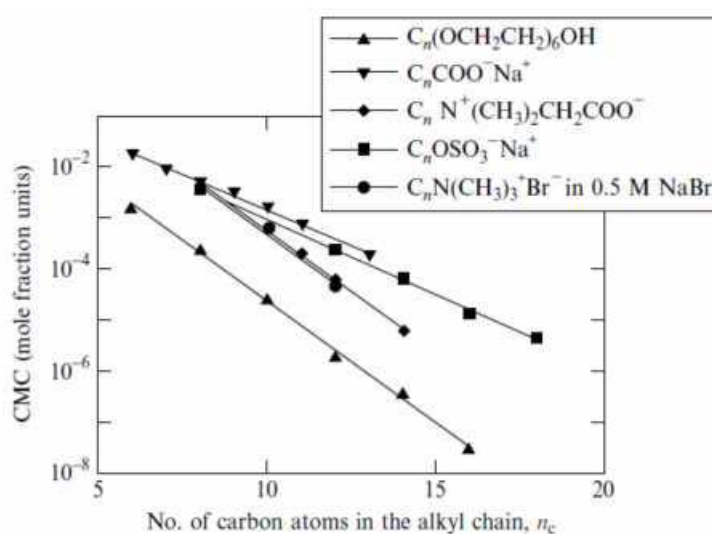


Figure 3: The log of CMC varies linearly with the number of carbon atoms in the alkyl chain of a surfactant (Gohain *et al.*, 2008).

The values of CMCs vary little depending on the nature of the charged head group. The charge of the hydrophilic head group appears to have the greatest influence. For example, the CMC of cetyltrimethylammonium chloride (CTAB) is 0.98 mM, in contrast to non-ionic surfactant, Triton X-100, the CMC is about 0.19 mM; while the CMC for SDS is 7.3 mM, for Dodecyl dimethylis(3-Sulfopropyl) ammonium hydroxide

(SB-12) is 3.5 mM (Lavkush Bhaisare *et al.*, 2015). In addition to the surfactant's relative insensitivity to the nature of the charged head group, CMCs show little dependence on the nature of the counter ion. (Singh *et al.*, 2000).

The study of physical properties of the surfactants shows that the primary factor influencing the value of the thermodynamic parameters is the length of the hydrocarbon chain. (Shehata *et al.*, 2008).

1.5.2 Temperature

The CMC fluctuates nonmonotonically over wide range (Sheikh & Bhat, 2012). The temperature dependence of CMC of Sodium Dodecyl Sulphate (SDS) is well-observed in **Fig. 4**. The CMC of non-ionic surfactant (polyoxyethylene) decreases with the rise in temperature.

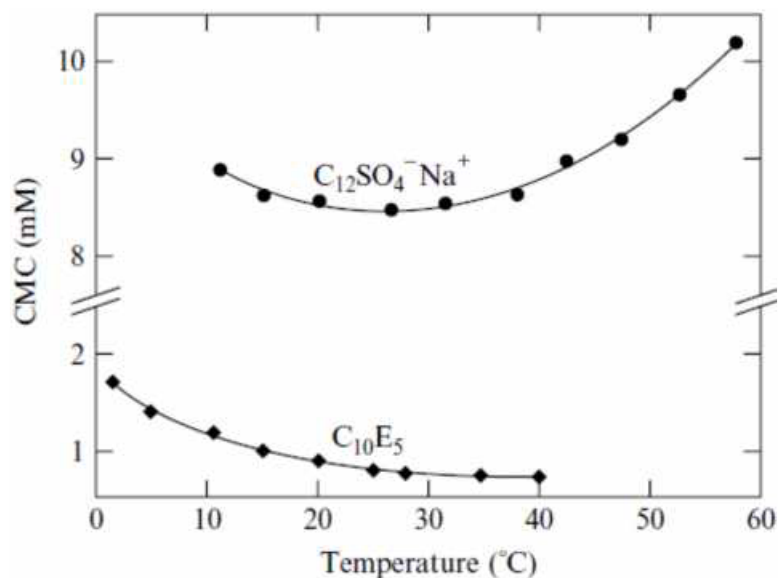


Figure 4: Effect of temperature on CMC of Sodium Dodecyl Sulphate (top) and penta(ethylene glycol) nonodecyl ether (Alvares *et al.*, 2014).

1.5.3. Additives

The external additives on the surface of surfactant molecules will vary the micellar properties of surfactants, resulting in thermodynamic changes such as Gibbs' free energy of micellization, entropy and enthalpy of micellization and many more (Bhattarai *et al.*, 2017; Shah *et al.*, 2020). Similarly, the CMC of ionic surfactant substances is altered in mixed alcohol media because the addition alcohol molecules solvate the surfactant tail portion by its hydrophobic part (Bračko & Špan, 2001). Surface properties and viscous properties of external additives such as electrolyte,

alcohol mixed in water, azo dyes, polyelectrolytes etc greatly influence on micellar activities of surfactants.

1.6 Dye and its classification

A colored substance called a dye has an affinity for the surface it is being applied on. The dye is often applied in an aqueous solution, and a mordant may be necessary to increase the dye's fastness on the fiber (M. E. Diaz Garcia & Sanz-Medel, 1986).

Dyes show significant structural variety and can be categorized according to their chemical composition or how they apply to fiber kind. Dyes need to have at least one functional group that gives the dye color, termed chromophores as well as substituents that donate or withdraw electrons to cause or amplify the chromophores' color, named as auxochrome (Muhammad & Khan, 2020). The chromophore group can serve as the foundation for categorizing dyes. Azo ($-N=N-$), nitro ($-NO_2$), methine ($-CH=$), quinoid groups and carbonyl ($-CO-$) are the most significant chromophores. The highest significant auxochromes are hydroxyl ($-OH$), carboxyl ($-COOH$), sulfonate ($-SO_3H$) and amine ($-NH_2$) groups. Furthermore, according to how soluble they are, dyes can be characterized as basic, acid, metal complex, direct, mordant, and reactive dyes or as insoluble dyes such azoic, sulfur, vat, and disperse dyes. Azo dyes, which are aromatic compounds with one or more $-N=N-$ groups, are the most common type of synthetic dyes used in industrial settings (Gokturk & Tuncay, 2003).

1.7 Influence of dye structure on aggregation

Oppositely charged dyes induced different nature of aggregation with surfactants at pre-micellar, micellar, and post micellar regions. Due to different physical and chemical properties, there is generation of hydrophilic and hydrophobic interactions. Dye molecules can be interacted with surfactant molecules due to the unique in spectra observed through spectrophotometric techniques. It has been reported in the literatures due to dye interaction with the micellar molecules there is decrease in micellar activity (Edbey *et al.*, 2018; Shah *et al.*, 2021). Many more fields are associated with the phenomenon which directly impart on solubilisation and dispersion. Such great influence brings great revolution in aggregating in nature viz-H-aggregation and J-aggregation (Dragan *et al.*, 2010, 2016). H-aggregation is related to blue shift due to solubilization of surfactant molecules with oppositely charged dye molecules and J-aggregation is related to red shift of dye molecules in absence of surface-active

molecules on dye structures. The mechanism of dye-surfactant molecules can be proposed through **Fig. 5** as shown below (M. E.Diaz Garcia & Sanz-Medel, 1986).

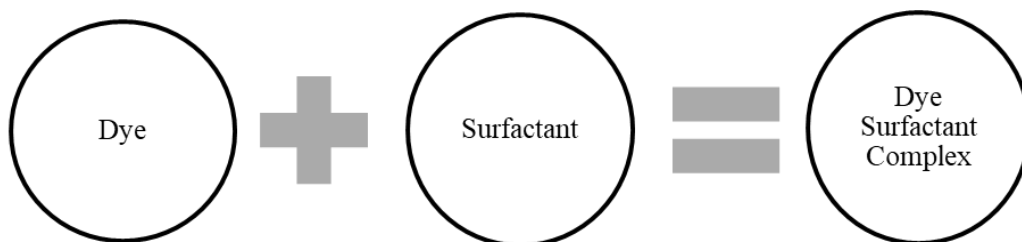


Figure 5: The interaction scheme between dye and surfactant for their complex formation

1.8 Corrosion

An electrochemical or chemical reaction that results in the irreversible destruction or damage of material or living tissue is called corrosion (Deyab, 2020). The tendency of most metals to revert to their original states causes corrosion. For instance, iron will convert into iron oxide when exposed to damp air. By directly reacting with a chemical, metals can corrode; for example, zinc can react with diluted sulfuric acid and magnesium will react with alcohols (Manonmani *et al.*, 2016). In the case of non-metallic materials, the term corrosion invariably refers to their-deterioration from chemical causes, but a similar concept is not necessarily applicable to metals. Many authorities consider that the term metallic corrosion embraces all interactions of a metal or alloy (solid or liquid) with its environment, irrespective of whether this is deliberate and beneficial or adventitious and deleterious. Thus, this definition of corrosion, which for convenience will be referred to as the transformation definition, will include, for example, the deliberate anodic dissolution of zinc in cathodic protection and electroplating as well as the spontaneous gradual wastage of zinc roofing sheet resulting from atmospheric exposure (Free *et al.*, 2004). Corrosion is the degradation of a material brought on by a reaction with its surroundings. Deterioration of the material's physical attributes is the definition of degradation. This can result in a material becoming weaker because of a reduction in cross-sectional area, a metal breaking owing to hydrogen embrittlement, or a polymer cracking from exposure to sunshine. Metals, polymers (plastics, rubbers, etc.), ceramics (concrete, brick, etc.), and composites mechanical blends of two or more materials with various properties can all be

considered materials. Due to the fact that metals are the most commonly utilized structural material (Aslam *et al.*, 2021).

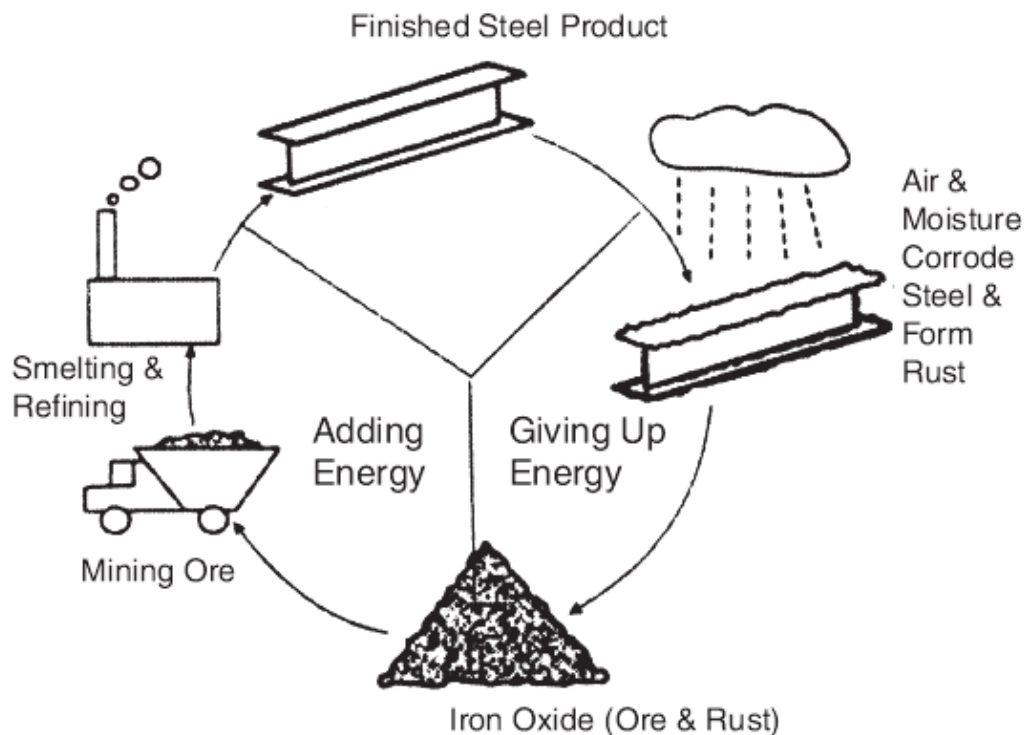


Figure 6: Most corrosion of metals is electrochemical in nature (Malik *et al.*, 2011)

Corrosion is a natural, spontaneous, and thermodynamic process. Corrosion is the metal's indication of wanting to return to its initial state as ore. **Fig. 6** correlates the corrosion life cycles of a steel product. Iron oxide (ore) is converted into finished steel product by smelting and refining. The finished steel product is converted into iron oxide because of interaction with air and moisture (Gupta, Kafle, *et al.*, 2020; Karki *et al.*, 2021).

A material will deteriorate through corrosion when it interacts with its environment. It is the process through which metallic atoms separate from the metal or combine with other elements to produce compounds. A structural element gets depleted of metal atoms until it fails, or oxides accumulate inside a conduit until it becomes clogged (Deyab, 2020).

1.9 Surfactant inhibitor and its classification

Four categories of inhibitors exist: (a) inorganic, (b) organic, (c) surfactant inhibitor, and (d) mixed substance inhibitor. A polar hydrophilic group, or "head," is joined to a

non-polar hydrophobic group, or "tail" in compounds known as surfactants, also known as surface active agents. Depending on the charge of the solid surface and the free energy change of transferring a hydrocarbon chain from water to the solid surface, the inhibitory action of surfactant molecules in aqueous solution may be caused by the physical (electrostatic) adsorption or chemisorption onto the metallic surface. A metal corrodes when there is a chemical reaction between it and its environment in which the metal is oxidized (Asefi *et al.*, 2011; Malik *et al.*, 2011).

1.10 Surfactant as corrosion inhibitor

Surfactants are the chemical substances which can be utilized for inhibiting processes to control corrosion. As corrosion is the natural phenomenon, it must be controlled. There are lots of corrosion inhibitors, among other surfactants are amphiphilic in nature which shows better inhibition efficiency. It is cheap, less toxic and easy for production (Al-Lohedan *et al.*, 1996; Aslam *et al.*, 2021; Malik *et al.*, 2011).

1.11 CMC in corrosion inhibition

The efficiency of surfactants as corrosion inhibitors can be assessed using the critical micelle concentration (CMC), a critical indicator. Interfacial aggregation lowers surface tension and is associated with corrosion inhibition because below the CMC, individual surfactant molecules or monomers tend to adsorb on exposed interfaces. Above the CMC, the surface develops several monolayers that form a protective layer on the metal surface (**Fig. 7**). As a result, any extra surfactant added to the solution above the CMC will cause the surface to adsorb in micelles or several layers. As a result, above the CMC, neither the surface tension nor the corrosion current density are considerably changed. Consequently, a surfactant inhibitor that aggregates or adsorbs at minimum concentration is excellent (Aslam *et al.*, 2021; Migahed & Al-Sabagh, 2009). Therefore, low CMC surfactants are preferred since they adsorb at low concentrations.

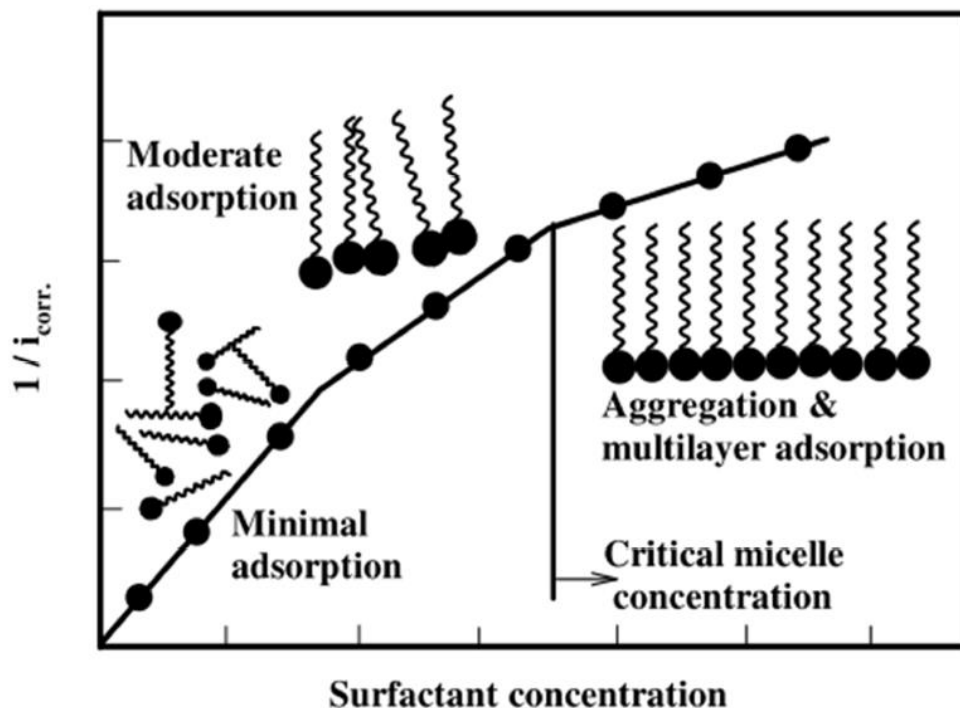


Figure 7: Effect of surfactant inhibitor on change in its concentration (Elkacimi *et al.*, 2011; Malik *et al.*, 2011)

It is well known that surfactant as corrosion inhibitor has been used effectively due to its unique properties such as aggregation and adsorption on the surface. An important prerequisite to understand corrosion inhibition by surfactant molecules is to understand the factors that affect aggregation as well as the state of aggregation of surfactant molecules on metal surfaces. Surfactant aggregation can be measured by decreasing surface tension at the air-water interface. It has been reported that, the effect of temperature on the corrosion behavior of Al in the absence and presence of different concentrations of anionic surfactants in acidic media at different temperatures has been studied (Aslam *et al.*, 2021). This means that the acceleration of the dissolution process followed by a reduction in the corrosion inhibitor's adsorption on the metal surface was caused by a rise in temperature (Al-Lohedan *et al.*, 1996).

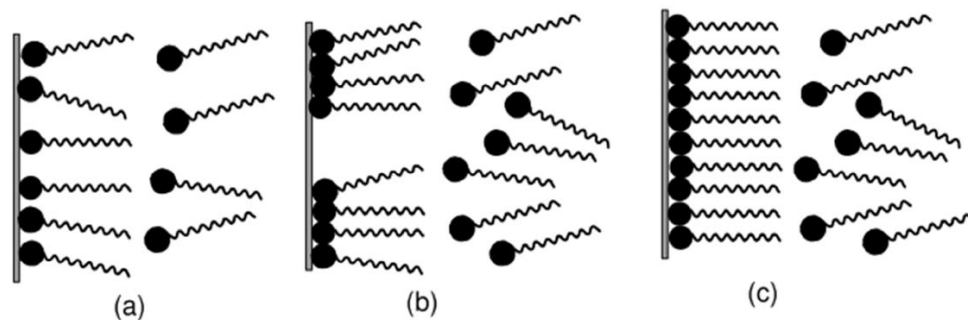


Figure 8: Mechanism of surfactant adsorption on metallic (Choi *et al.*, 2022; Malik *et al.*, 2011)

Corrosion inhibition has complex mechanism and depends on the formation of mono- or multi-dimensional protective layers on the metal surface. **Fig. 8(a)** depicts the surfactant's manner of adsorption as individual molecules at very low inhibitor concentrations. The surfactant's manner of adsorption as hemi-micelles at a moderate concentration is depicted in **Fig. 8(b)**. The beginning point to collect the surfactant in duplet, triplet, or quadruple before forming the complete micelles is known as the hemi-micelle phase in the surfactant solution (Aslam *et al.*, 2021). **Fig. 8(c)** shows the adsorption of surfactant at high concentrations.

1.12 Rationale

There are major uses of surfactants: in consumer products and in industry. A study of the interaction of surfactant with azo dye is crucial for effective and enhanced interactions with additives. By studying the interaction of mixtures with mixed solvents, we can ensure long-term use. Therefore, research into how surfactants interact with azo dye is necessary.

Metallic surfaces should be inhibited with a good inhibitor because corrosion is an electrochemical process. However, a lot of research has been done to address application-related issues. Such a study is necessary in this situation to develop concepts and pave the way for additional research projects.

As a result, there is a need for research because (i) surfactants are widely used and (ii) they have amazing micellar properties (iii) One of the main causes of economic loss is corrosion (iv) Such a study has not yet been conducted in Nepal. Therefore, this study is beneficial for both industrial and academic applications.

1.13 Objectives

1.13.1 General objective

The study was undertaken to study the interaction of cationic surfactants with Azo dyes in mixed solvent media and anticorrosion ability of the surfactants.

1.13.2 Specific objectives

Following were the specific objectives of the present research work.

- Study the interaction between DTAB and MR in mixed solvent media
- Study the interaction between CPC and MR in mixed solvent media
- Study the anti-corrosion ability of surfactants (CPC and DTAB)

CHAPTER 2

2. LITERATURE REVIEW

2.1 General overview

The chapter 2 explains the research works pertaining to surfactants interactions with azo dyes in aqueous as well as mixed solvent media and also its anticorrosion ability of surfactants. Nowadays many researchers are interested in research activities related with amphiphilic compounds due to its dual nature of interactions.

2.2 Surfactant Sensitized Reaction

Alonso *et al.*, (1984) discussed the true ternary complex of 1:3:3 through hydrophobic environment of Cetylpyridinium Bromide (CPB) twisted around chromophore. Through spectrophotometry and fluorometry analysis in this complex there is enhancement in absorptivity and bathochromic shift due to micellar media. The researchers are very much interested in such surfactant sensitive environments arising due to ion-association.

Garcia & Sanz-Medel, (1985) summarized the sensitization of the colour reaction of metal ion with dyes (chelate) and surfactants CPB of the cationic type. This brings new analytical methods which is an inexpensive in comparison to atomic spectroscopy method. Amin, (2000) used the cationic surfactant, CPB and summarized the role of micellar media in enhancing the sensitivity in the complex of the system.

Huang & Zhang, (2006) also used surfactant sensitized method of spectrophotometry to estimate orthophosphate in acidic medium. Thus, surfactant is the most significant compound for the sensitization, and it can be analysed through spectrophotometry.

2.3 Methods for dye-surfactant interactions

There are lots of techniques to study dye-surfactant interactions. Among the techniques, conductivity measurement is reported as a quick and easy method to determine the degree of interaction. Such interaction influences both the thermodynamics and kinetics of dyeing which bring quality of dyeing on fibers (Jocic, 1995).

Edbey *et al.*, (2015) also presented interactions between cationic dye (methyl violet) and anionic surfactant (Sodium Dodecyl Sulfate) by the process of solubilisation using

electrical conductivity and UV-Vis measurement. The CMC of SDS was determined and binding constant (K_b) and Gibbs Free energy parameter (ΔG_0) were evaluated. Such aggregation behaviour leads to determine the behavioral aspects of such interaction.

Wong & Park, (1986) also summarized the spectral behaviour of cationic dyes (Methylene blue and Acridine orange) individually and analysed the hydrophobic nature of the dye.

Simončič & Špan, (1998) presented that at three different temperatures, the specific conductance of dye-surfactant combinations in water-ethanol mixed solvent comprising 5, 10, 15, or 20% of ethanol was measured. Based on two theoretical models, the equilibrium constant, and other thermodynamic functions for the creation of dye-surfactant ion pairs were estimated.

Ghoreishi & Nooshabadi, (2005) concludes that the interaction study using surfactant selective electrode technique between anionic dye (azo dye) with cationic surfactant (Tetradecyl-trimethylammonium bromide-TTAB). The electromotive force data from the TTAB selective electrode was used to calculate the concentration of TTAB monomers and surfactant ions bound to dyes. This study produced the standard free energy change, ΔG_0 , and the dye-surfactant complex formation binding constant, K_b .

To enhance the interaction phenomenon between surfactant and dye, different thermodynamic parameters, surface parameters, pH values, binding and partition parameters is necessary for the establishment of better complexity and flexibility (Hosseinzadeh *et al.*, 2008; Plutino *et al.*, 2017; Prasad Tajpuriya *et al.*, 2021; Sharifi *et al.*, 2020).

2.4 Anti-corrosion Ability of Surfactants

The technological world has continued to be interested in material corrosion. Materials corrosion inhibition has been the subject of research for decades, and in many cases it has been thoroughly researched and comprehended (Shehata *et al.*, 2008).

Asefi *et al.*, (2011) studied that one of the most practical ways to prevent corrosion in acidic media is using inhibitors. Since a few years ago, there has been extensive research on the promising potential use of surfactants as corrosion inhibitors. It is generally known that surfactants frequently combine to form aggregates at surfaces and in solutions.

Malik *et al.*, (2011) reviewed the typical anticorrosion properties of various surfactant types have the potential to be employed in the industry as effective solutions to problems with corrosive on metallic surfaces to prevent material and financial loss.

Attari *et al.*, (2015) concluded that surfactants is the most significant compound which is the suitable inhibitor as explained in the literatures. The good inhibition efficiency is well observed at the CMC point of the surfactants. As reported in the papers, the mechanism of inhibition has been described through Langmuir isotherm. Langmuir isotherm is suitable to describe physisorption and chemisorption.

Arockia Selvi *et al.*, (2019) studied the compact coating of surfactant inhibitor on the metallic surface. This shows that surfactant acts as best inhibitor for the corrosion control. The use of surfactant is very easy, less toxic and environmentally friendly (Abbasov *et al.*, 2013).

Abdellaoui *et al.*, (2021) demonstrated that the cationic surfactant in presence of 1 M HCl solution acts as mixed type inhibitor with anodic type of reaction. The inhibition efficiency is obtained upto 92.98 % at 298.15 K after 6 hours immersion in the acid solution. This shows that cationic surfactant is the better inhibitor for corrosion control.

Aslam *et al.*, (2021) reviewed that use of surfactant inhibitor is very much interesting due to its capability to form film on the surface. The literature survey shows that there is few studies on cationic surfactants as corrosion inhibitor. The amazing adsorption phenomenon of cationic surfactant realizes for further study on the related field to control the corrosion.

2.5 Applications of dye-surfactant interaction study

It has been very much necessary to enhance the existing trends of dye surfactants applications. Such activities can only be improved with lots of studies. As there interactions can be utilized in chemical research, it should be implemented effectively in analytical chemistry, textile printing, photographic graphics and many others (Alehyen *et al.*, 2010; Shah *et al.*, 2021). Its applications have been reported in pharmaceutical science, production of huge personal care products, pulp, and paper printing. It has been widely utilized in analytical and photocatalyzed products (Khadka & Bhattarai, 2020; Plutino *et al.*, 2017; Sheikh & Bhat, 2012).

2.6 Applications of anti-corrosion study

As corrosion is the process of corroding the oxidized metallic bodies, it has to be controlled. The nation is losing natural beauties of natural heritage sites of metallic bodies due to corrosion, as a result, there is huge economic loss in protection which influence in tourism (Karki *et al.*, 2021). It is very much necessary to conserve the metallic surfaces. The study of anti-corrosion idealized the best inhibiting substances for corrosion control (Janati *et al.*, 2020). Also, it brings awareness to utilize the suitable inhibitor for the desired process. As it is reported that, surfactants are the good inhibitor which effectively works on the corrosion control (Abdellaoui *et al.*, 2021; Zhu *et al.*, 2021).

CHAPTER 3

3. MATERIALS AND METHODS

This chapter includes the reagents and chemicals used for the cationic surfactants interaction with azo dyes and anticorrosion ability of surfactants.

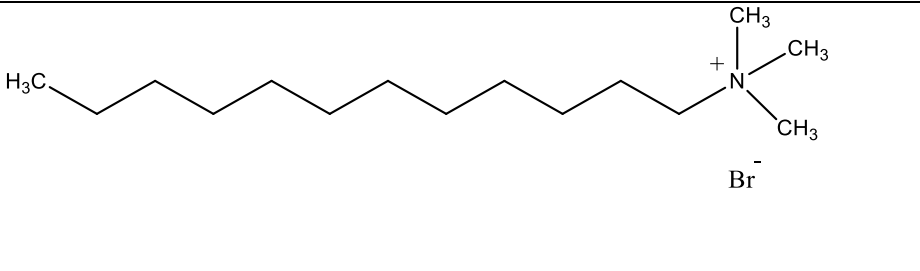
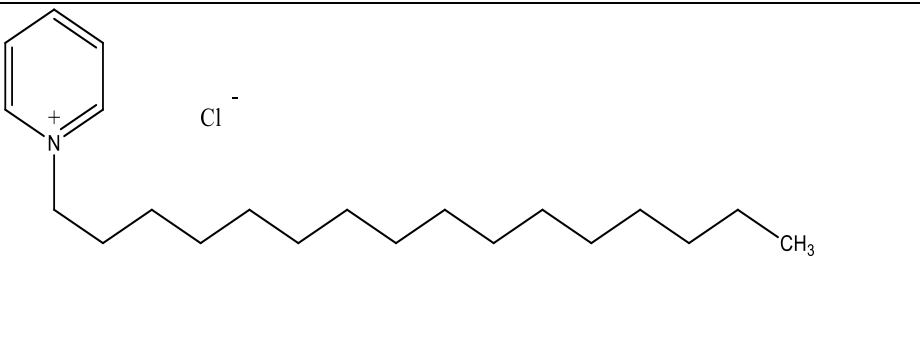
3.1 Materials/ Reagents

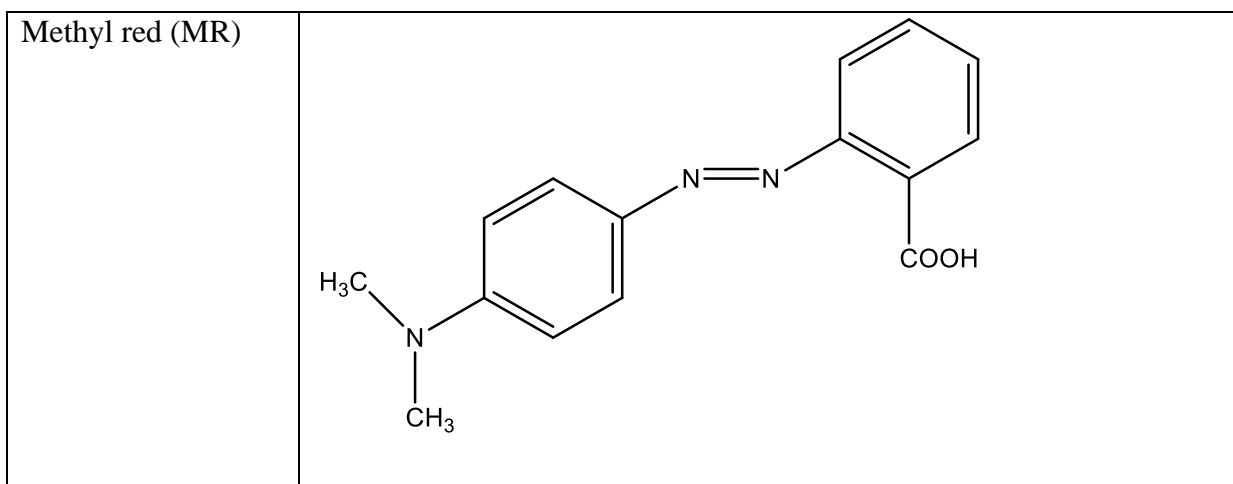
Cationic surfactants CPC and DTAB, 98% pure were purchased from Sigma Labsys in Bengaluru-03, India. It was kept in the oven for one hour before use. Azo dye MR, 98% pure was also purchased from Sigma labsys of Bengaluru-03, India. **Table 3.1** displays the molecular structure of DTAB, CPC, and MR.

Cationic surfactants have been widely used as auxiliaries in many areas due to valuable characteristics such as emulsification, spreading, water proofing and repellence (Sar *et al.*, 2019).

Methanol and Ethanol were bought from Merck, India, 99 % purity . It was purified through distillation and used as mixed solvent media (0.1, 0.2, 0.3, and 0.4 volume content of methanol). Double distilled water is used for preparing mixed media. All solvents and chemicals used during the research work were of AR (analytical reagent) grade.

Table 2: Molecular structure of DTAB, CPC, and MR

Dodecyl trimethylammonium bromide (DTAB)	
Cetyl pyridinium chloride (CPC)	



3.2 Methods

3.2.1 For dye-surfactant interactions study

For the measurement of UV-Visible spectra, conductance, surface tension, viscosity and pH, the following methodologies are adopted. Ethanol-water systems were only used for absorption spectroscopy method but not for other methods due to similar physiochemical properties between methanol and ethanol (Bhattarai *et al.*, 2017).

3.2.1.1 Preparation of mixed solvent media (0.1, 0.2, 0.3 and 0.4 volume fraction of methanol and ethanol)

First, each volume fraction of methanol and ethanol were prepared in double distilled water. Each mixed solvent was prepared at temperature 298.15 K in water bath. For 0.1, 0.2, 0.3 and 0.4 volume fraction of methanol and ethanol, the ratio of alcohol and water is 1:9, 2:8, 3:7 and 4:6 respectively. The volume of methanol above 0.4 methanol and ethanol were not used due to precipitation of surfactant molecules (Shah *et al.*, 2020). Finally, the prepared mixed media were utilized to prepare solution of CPC, DTAB and MR.

3.2.1.2 Absorption spectroscopy method

The spectrophotometric measurements were recorded by both single beam (LT-290 Model, India) and double beam (MARS ME-SP 195UV, India) UV-Visible spectrophotometer from which UV-Vis spectra were recorded at room temperature using 1 cm length quartz cuvette in the range, 300 to 700 nm.

3.2.1.3 Conductance measurement

The conductometric measurements were performed to obtain the CMC value of DTAB in the absence, as well as the presence of MR at 0.1, 0.2, 0.3 and 0.4 volume fraction of methanol at temperatures 298.15 K, 308.15 K and 318.15 K, as described in the literature (Shah *et al.*, 2020). Using a conductivity meter that was obtained from Toshniwal Instruments Mfg Pvt. Ltd., Rajasthan, India, the conductometric measurements were carried out. 0.1 M and 0.01 M KCl solutions at 298.15 K were used to calibrate the conductivity cell, which had a cell constant of 1.124. After calibration, the conductivity of double distilled water was recorded to be $1.005 \mu\text{Scm}^{-1}$.

3.2.1.4 Surface tension measurement

The surface tension was measured using easy dyne tensiometer K20S purchased from Germany was used for the density and surface tension measurement. Du Nouy ring method was adopted to measure the surface tension at three different temperatures, 298.15 K, 308.15 K and 318.15 K.

3.2.1.5 Viscosity measurement

The viscosity measurement was conducted using ManSingh Survismeter by adopting viscous flow time (VFT) method (Niraula *et al.*, 2018). In this method, time flow of solution filled in the limb are noted shown by digital stopwatch. The time flow of solution was verified in three replicated for each concentrated solution. The viscosity was determined using formula:

$$\eta_{\text{soln}} = \left(\frac{t_{\text{soln}}}{t_{\text{solv}}} \right) \left(\frac{d_{\text{soln}}}{d_{\text{solv}}} \right) \eta_{\text{solv}} \quad (3-1)$$

where,

η_{soln} = Viscosity of solution

η_{solv} = Viscosity of solvent

t_{soln} = flow time of solution

t_{solv} = flow time of solvent

d_{soln} = density of solution

d_{solv} = density of solvent

3.2.1.6 pH measurement

The pH values of solution were recorded using (a Eutech-2700, Singapore) pH meter at three different temperatures, 298.15 K, 308.15 K and 318.15 K.

3.2.2 Anti-corrosion ability of Surfactants

3.2.2.1 Weight loss method

The weight loss method is most widely used techniques for identifying the corrosion inhibition efficiency. This is most convenient for determining inhibition efficiency of the inhibitor. The data determined is not much reliable due to manual errors.

3.2.2.1.1 Preparation of solution

To prepare 0.5 M H₂SO₄, 13.76 mL of concentrated H₂SO₄ was taken in a 500 mL volumetric flask and it was diluted up to mark.

Inhibitor solution of Cationic surfactant (DTAB) of concentration 0.5 M was prepared in 0.5 M H₂SO₄ of 250 mL volumetric flask. Also, cationic surfactant (CPC) of concentration 0.5 M was prepared in 0.5 M H₂SO₄ of 250 mL volumetric flask.

3.2.2.1.2 Preparation of mild steel sample

Mild steel was cut into the piece of 2 cm × 2 cm × 0.15 cm. Sample was polished by silicon carbide paper of different grades of 100, 400, 600, 800 and 1000. Then its length, breadth and thickness were measured by Digital Vernier Caliper and washed in Hexane. Again, mild steel was polished with silicon carbide paper of grades 1200, 1500 and 2000. Then it was sonicated in ethanol for 15 minutes, dried and weighed. Mild steel sample was immersed in inhibitor solution of given concentration for 24 hours at 298.15 K, 308.15 K and 318.15 K respectively. After 24 hours samples were dried, and weight of the used samples were taken.

3.2.2.2 Potentiodynamic polarisation

Sonicated sample (used for weight loss method) was subjected for both cathodic and anodic polarization using Hokuto Denko potentiostat (HA-151B, Japan). Polarization was done using three electrode systems. Electrolytic cells were set up using mild steel samples that was used as working electrode, platinum electrode as counter electrode and saturated calomel electrode (SCE) as reference electrode. Surfactant inhibitors solution used in cell were different in different experiments. OCP (Open Circuit

Potential) was measured. Then the sample was subjected for studying cathodic and anodic polarization.

CHAPTER 4

4. RESULTS AND DISCUSSION

This chapter consists of the main findings and discusses the investigations which are UV-Vis studies, conductivity, surface tension, viscosity, and pH studies of DTAB and CPC in mixed solvent media in presence of azo dye MR. Dye-surfactant interaction is a well-known phenomenon and UV-Vis spectrophotometry, conductivity, surface tension, viscosity, and pH techniques were used to investigate this interaction between MR and DTAB, MR and CPC. Here the anticorrosion ability of surfactants using weight loss method and potentiodynamic polarization method were also studied.

4.1 Dye surfactant interaction studies

4.1.1 UV-Vis spectra of Cationic surfactant (DTAB)-MR interactions in methanol-water mixture

The simple absorption spectra of MR with and without DTAB in methanol-water mixtures are shown in **Figs. 9 to 12**. Using UV-vis spectroscopy, it can be explored the mechanism of dye-surfactant interaction. During such interaction, there is decrease in red shift due to entrapment of dye molecules in the micelle core. The micelles generate enhanced surface activity on the dye molecules throughout the interaction (Sachin *et al.*, 2019). Accordingly, the spectrum displays an abnormal hypochromic shift due to the dynamic interaction between the MR molecules containing -COOH groups and DTAB molecules containing ammonium groups (**Figs. 9 to 12**). The red shift reflects interactions between MR molecules and more methanol, which resulted in π - π stacking because azo dyes are composed of J-aggregates formed by hydrogen bonding with methanol (Dragan *et al.*, 2016).

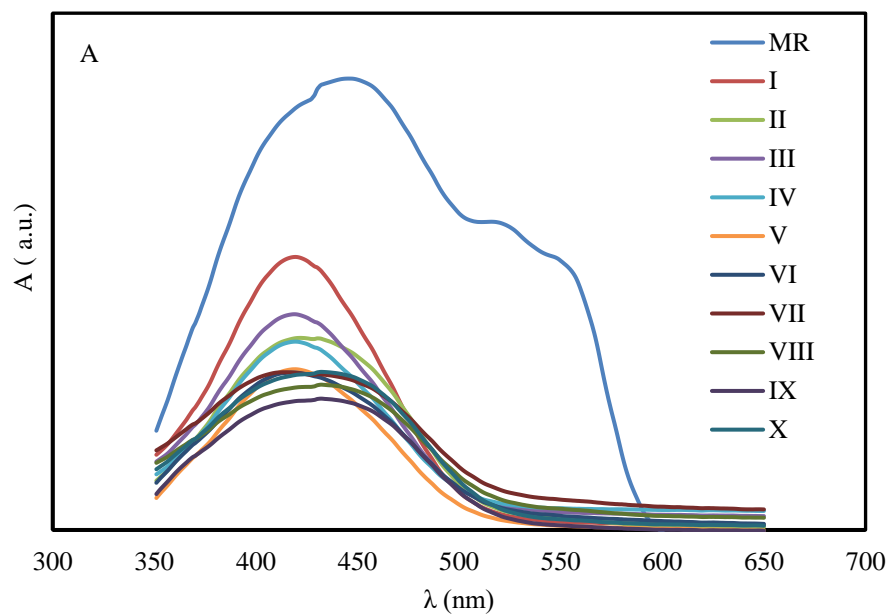


Figure 9: Visible spectra of MR-DTAB system in 0.1 volume fraction of methanol. Here, I, II, III, IV, V, VI, VII, VIII, IX, X and MR represent the concentration of DTAB [5, 2.4, 2.2, 2, 1.8, 1.6, 1.4, 1.2, 1, 0.8 and 0] $\times 10^{-2}$ mol. L⁻¹ respectively. Here the constant concentration of MR is 2×10^{-3} mol. L⁻¹

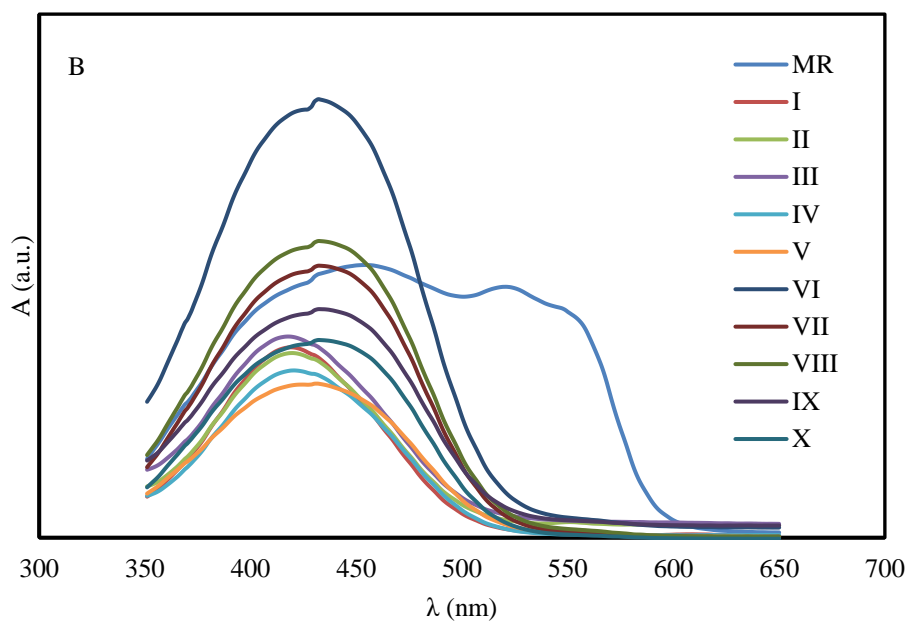


Figure 10: Visible spectra of MR-DTAB system in 0.2 volume fraction of methanol. Here, I, II, III, IV, V, VI, VII, VIII, IX, X and MR represent the concentration of DTAB [5, 2.4, 2.2, 2, 1.8, 1.6, 1.4, 1.2, 1, 0.8 and 0] $\times 10^{-2}$ mol. L⁻¹ respectively. Here the constant concentration of MR is 2×10^{-3} mol. L⁻¹

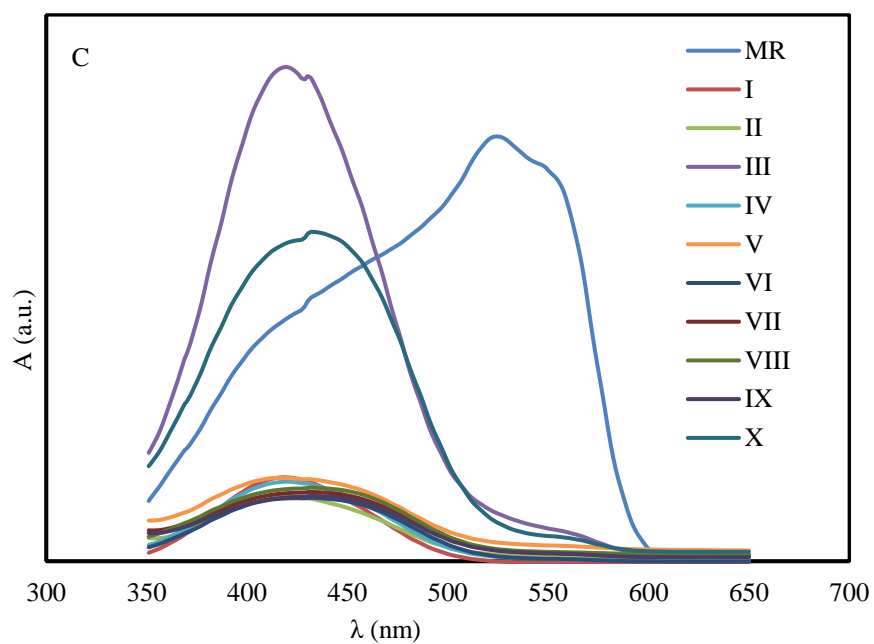


Figure 11: Visible spectra of MR-DTAB system in 0.3 volume fraction of methanol. Here, I, II, III, IV, V, VI, VII, VIII, IX, X and MR represent the concentration of DTAB [5, 2.4, 2.2, 2, 1.8, 1.6, 1.4, 1.2, 1, 0.8 and 0] $\times 10^{-2}$ mol. L $^{-1}$ respectively. Here the constant concentration of MR is 2×10^{-3} mol. L $^{-1}$

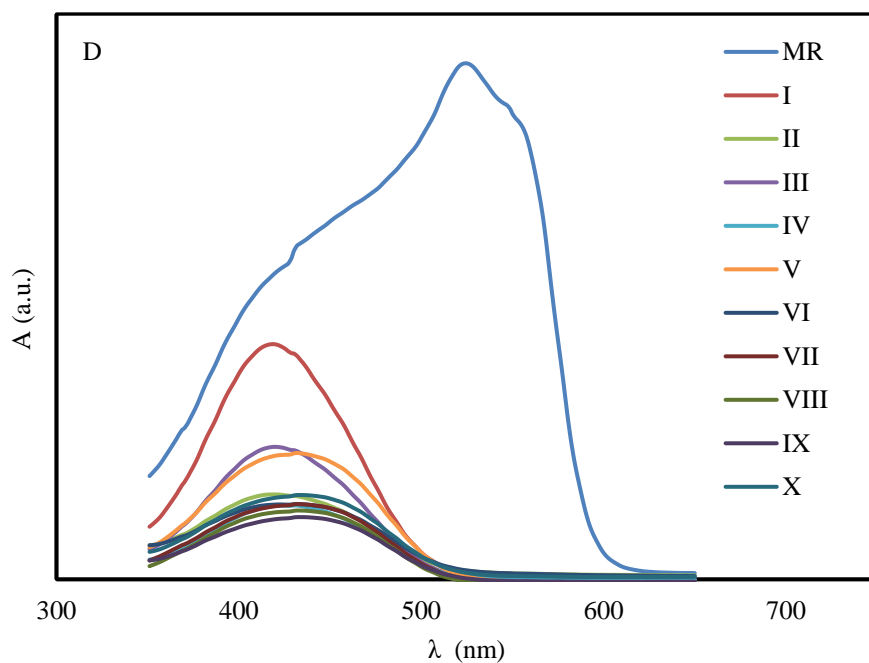


Figure 12: Visible spectra of MR-DTAB system in 0.4 volume fraction of methanol. Here, I, II, III, IV, V, VI, VII, VIII, IX, X and MR represent the concentration of DTAB [5, 2.4, 2.2, 2, 1.8, 1.6, 1.4, 1.2, 1, 0.8 and 0] $\times 10^{-2}$ mol. L $^{-1}$ respectively. Here the constant concentration of MR is 2×10^{-3} mol. L $^{-1}$

4.1.2 UV-Vis spectra of Cationic surfactant (CPC)-MR interactions in methanol-water mixture

The simple absorption spectra of MR with and without CPC in methanol-water mixtures are given in **Figs. 13 to 16**. Using UV-vis spectroscopy, the clear visible view of interaction is observed through the mechanism of dye-surfactant interaction. During such interaction, there is decrease in redshift due to dye molecules entrapment in micelles of CPC as seen in DTAB (Edbey *et al.*, 2018). Accordingly, the spectrum displays an abnormal hypochromic shift due to the dynamic interaction between the MR molecules containing -COOH groups and CPC molecules containing pyridinium groups (**Figs. 13 to 16**). The red shift declares J-aggregates which reflects interactions between MR molecules and more methanol (Plutino *et al.*, 2017).

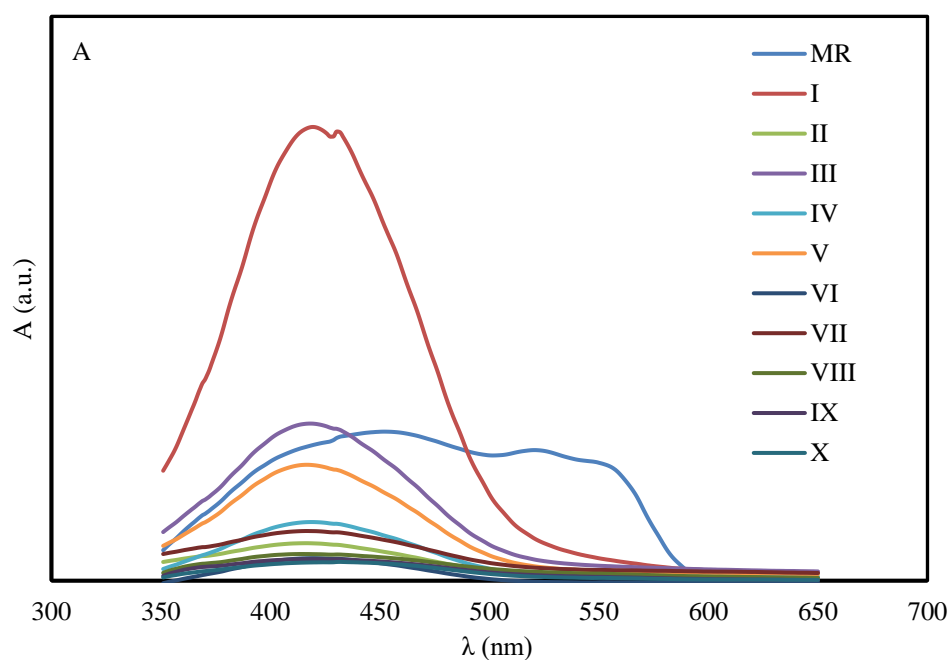


Figure 13: Visible spectra of MR-CPC system in 0.1 volume fraction of methanol. Here, I, II, III, IV, V, VI, VII, VIII, IX, X and MR represent the concentration of CPC [1.5, 1.4, 1.3, 1.2, 1.1, 1.0, 0.9, 0.8, 0.7, 0.6 and 0] $\times 10^{-3}$ mol. L $^{-1}$ respectively. Here the constant concentration of MR is 2×10^{-3} mol. L $^{-1}$

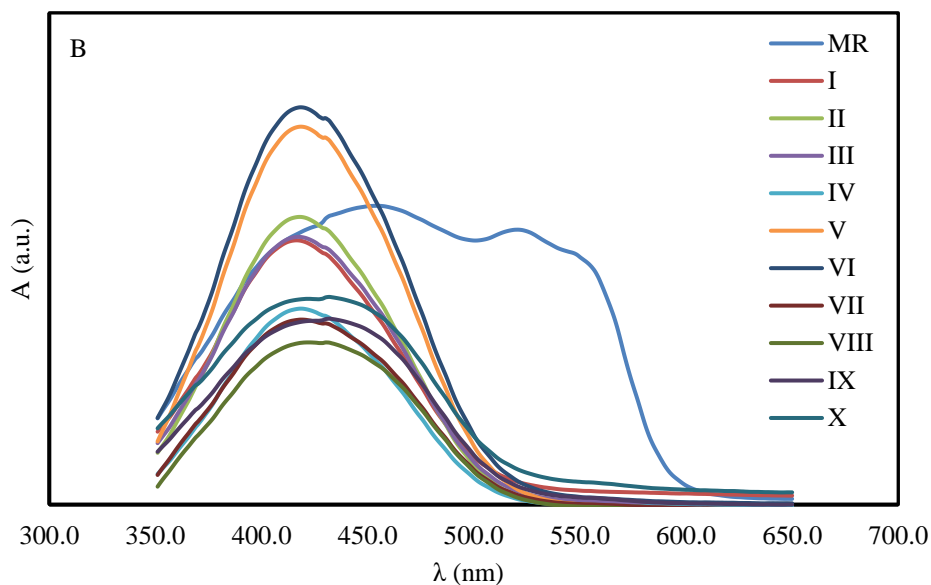


Figure 14: Visible spectra of MR-CPC system in 0.2 volume fraction of methanol. Here, I, II, III, IV, V, VI, VII, VIII, IX, X and MR represent the concentration of CPC [1.5, 1.4, 1.3, 1.2, 1.1, 1.0, 0.9, 0.8, 0.7, 0.6 and 0] $\times 10^{-3}$ mol. L $^{-1}$ respectively. Here the constant concentration of MR is 2×10^{-3} mol. L $^{-1}$

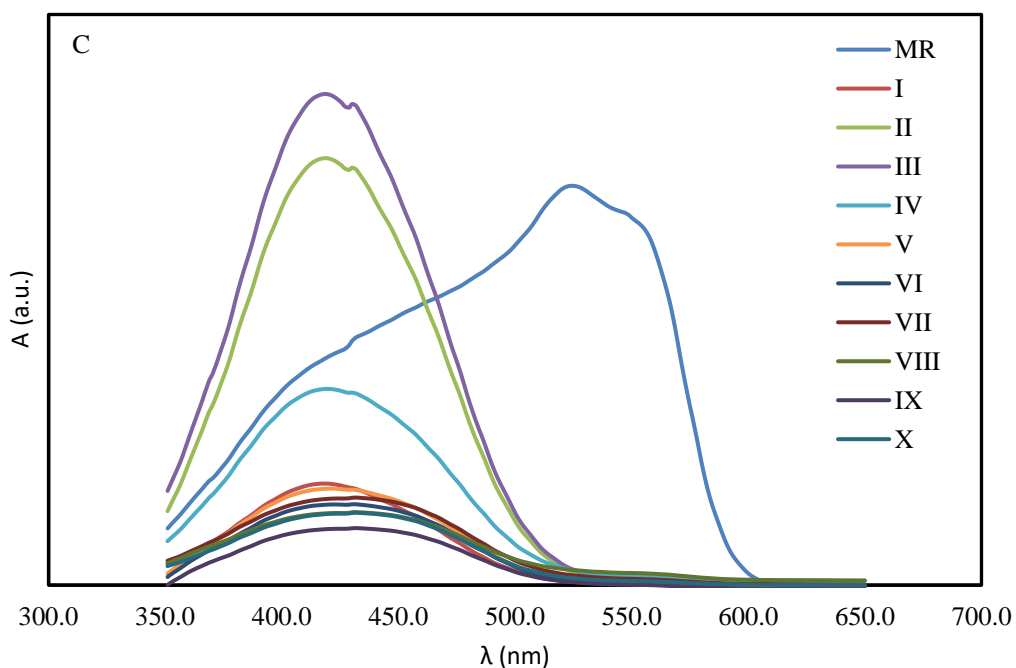


Figure 15: Visible spectra of MR-CPC system in 0.3 volume fraction of methanol. Here, I, II, III, IV, V, VI, VII, VIII, IX, X and MR represent the concentration of CPC [1.5, 1.4, 1.3, 1.2, 1.1, 1.0, 0.9, 0.8, 0.7, 0.6 and 0] $\times 10^{-3}$ mol. L $^{-1}$ respectively. Here the constant concentration of MR is 2×10^{-3} mol. L $^{-1}$

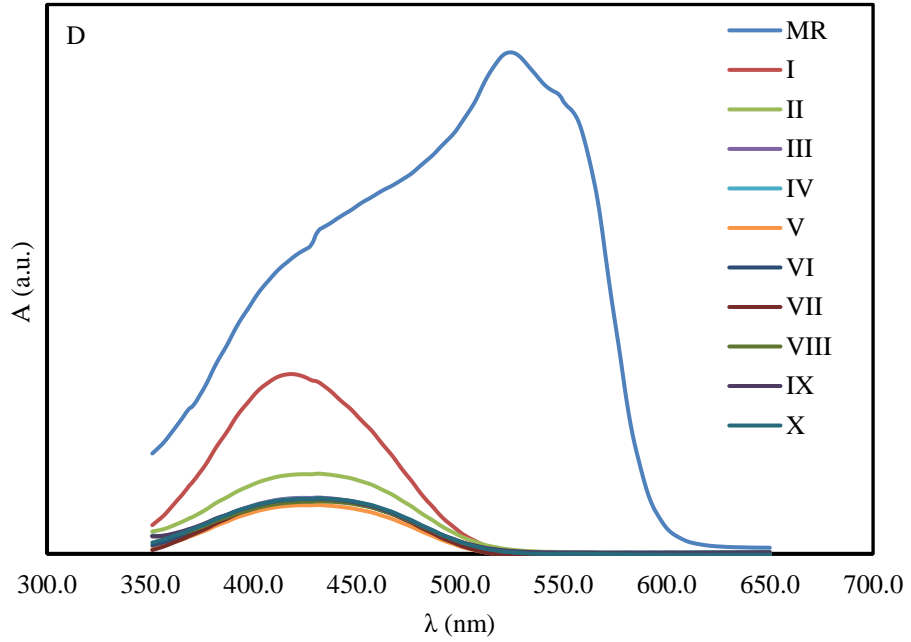


Figure 16: Visible spectra of MR-CPC system in 0.4 volume fraction of methanol. Here, I, II, III, IV, V, VI, VII, VIII, IX, X and MR represent the concentration of CPC [1.5, 1.4, 1.3, 1.2, 1.1, 1.0, 0.9, 0.8, 0.7, 0.6 and 0] $\times 10^{-3}$ mol. L⁻¹ respectively. Here the constant concentration of MR is 2×10^{-3} mol. L⁻¹

4.1.3 Determination of Binding and Partition Parameters using Differential Absorption Spectra of DTAB and CPC

At 0.1 up to 0.4 volume fraction of methanol, the CMC was determined from the plot of the absorbance – [DTAB] or [CPC] profiles. The lower absorbance value indicates the CMC value for each volume fraction of methanol as seen in **Figs. 17 and 18** and tabulated in **Table 3**.

The binding constants for molecules of dye-surfactant interactions in volume fractions of methanol were calculated with the Benesi-Hildebrand **Equation (4-1)** (Edbey *et al.*, 2018; Fazeli *et al.*, 2012).

$$\frac{D_T}{\Delta A} = \frac{1}{\epsilon_m - \epsilon_0} + \frac{1}{K_b(\epsilon_m - \epsilon_0)C_m} \quad (4-1)$$

$$\Delta A = A - A_0, \quad (4-2)$$

$$C_m = C_s - \text{CMC} \quad (4-3)$$

Dye concentration is represented by D_T in **Equation (4-1)**, while dye absorbance is represented by A in **Equation (4-2)**. The left-hand side of **Equation (4-1)** constitute of

ΔA , which shows the difference between dye's absorbance with and without surfactant expressed in **Equation (4-2)**. The right-hand side of **Equation (4-1)** consists of the terms ϵ_m , ϵ_0 , C_m and K_b represent the molar absorptivity of the dye, the absorbance molarity of the fully bound dye to micelles, the concentration of micellized CPC expressed in **Equation (4-3)** and the binding constants, respectively. Also, the term C_s represents the concentration of DTAB or CPC. The binding constants can be determined from the plots of $D_T/\Delta A$ against $1/C_m$ (**Figs. 19 and 20**) tabulated in **Table 4**.

In addition, using the partition coefficient, the concentration ratio of non-ionizing species was determined. A pseudo-phase model is used to calculate this parameter as in **Equation (4-4)** (Hosseinzadeh *et al.*, 2008; Khosa, 2010).

$$\frac{1}{\Delta A} = \frac{1}{\Delta A^\infty} + \frac{1}{K_s \Delta A^\infty (C_{Dye} + C_{surfactant} - CMC)} \quad (4-4)$$

Where, $\Delta A = A - A_0$ and $\Delta A^\infty = A^\infty - A_0$. Further, the complete absorbance of a dye attached to a surfactant is A .

$$K_s = \frac{K_x}{n_w} \quad (4-5)$$

In **Equation (4-5)**, the term K_x is the partition coefficient by following the pseudo-phase model and $n_w = 55.5 \text{ mol L}^{-1}$. Thus, K_s is the partition constant, which can be obtained from the slope of the graph plotted between ΔA^{-1} and $[C_{Dye} + C_{Surfactant} - CMC]^{-1}$ (**Figs. 21 and 22**) and K_x can also be obtained from relation **Equation (4-5)** tabulated in **Table 4** (Hosseinzadeh *et al.*, 2008).

The Gibb's free energies of binding (ΔG_b) and partition (ΔG_p) were estimated using the **Equations (4-6) and (4-7)**.

$$\Delta G_b = -RT \ln K_b \quad (4-6)$$

$$\Delta G_p = -RT \ln K_x \quad (4-7)$$

Table 3: CMC values of DTAB and CPC at 0.1,0.2,0.3 and 0.4 volume fractions of Methanol

Volume fraction of methanol	CMC of DTAB with MR (mM)	CMC of CPC with MR (mM)
0.1	10.0	0.07
0.2	18.0	0.12
0.3	16.0	1.0
0.4	12.0	1.13

Table 4: Values of K_b , K_s , K_x , ΔG_b and ΔG_p of DTAB and CPC at 0.1, 0.2, 0.3 and 0.4 volume fractions of methanol

Volume fraction of Methanol	$K_b(\text{Lmol}^{-1})$		K_s		K_x		$\Delta G_b(\text{kJmol}^{-1})$		$\Delta G_p(\text{kJmol}^{-1})$	
	DTAB	CPC	DTAB	CPC	DTAB	CPC	DTAB	CPC	DTAB	CPC
0.1	16×10^2	30.3×10^5	1.36×10^3	4.56×10^4	7.5×10^4	253.08×10^4	-18.29	-36.99	-27.83	-36.54
0.2	24×10^2	3.95×10^5	1.41×10^3	42.9×10^4	7.83×10^4	2380.9×10^4	-19.29	-31.94	-27.93	-42.10
0.3	250×10^2	14.5×10^5	13.04×10^3	192×10^4	72.36×10^4	10656×10^4	-25.10	-35.16	-33.44	-45.81
0.4	18×10^2	0.93×10^5	1.87×10^3	189×10^4	10.4×10^4	$10489. \times 10^4$	-18.58	-28.35	-28.63	-45.77

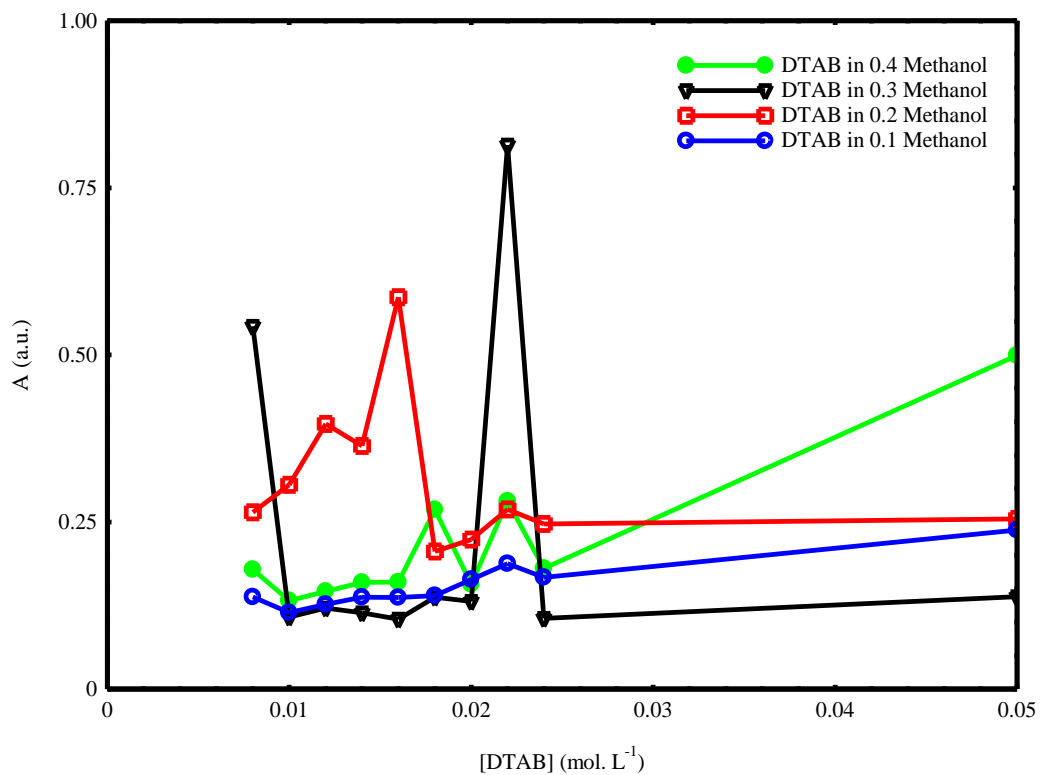


Figure 17: Plot of absorbance against the [DTAB] profile in four different volume fractions of methanol

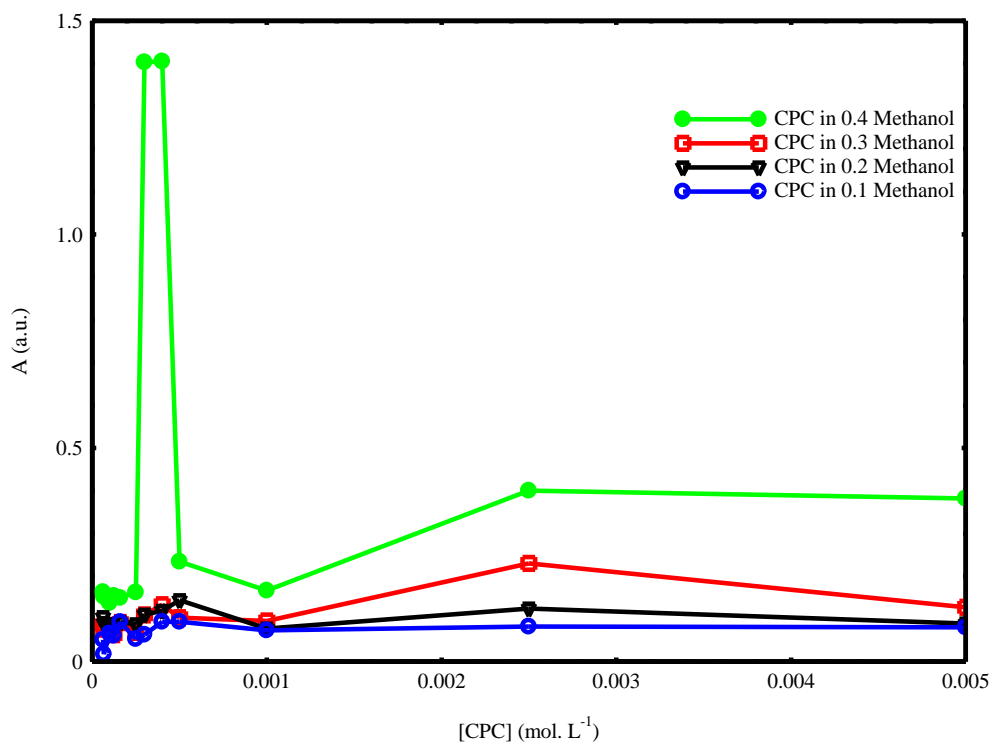


Figure 18: Plot of absorbance against the [CPC] profile in four different volume fractions of methanol

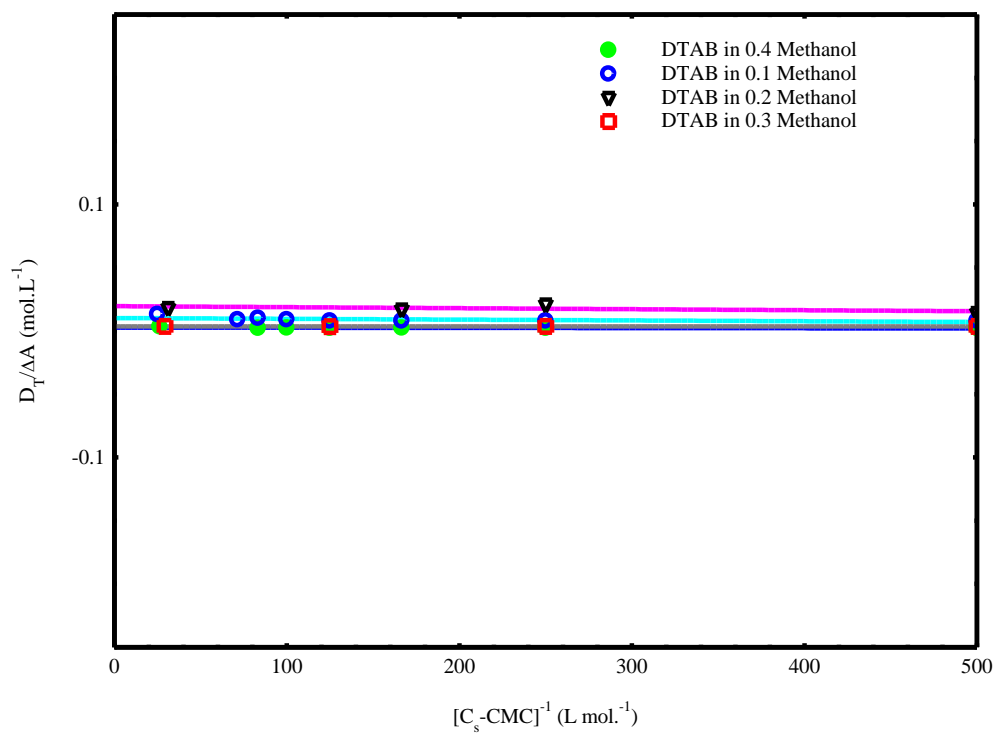


Figure 19: Plot of $D_T/\Delta A$ against $[C_s-CMC]^{-1}$ for MR with DTAB in four different volume fractions of methanol

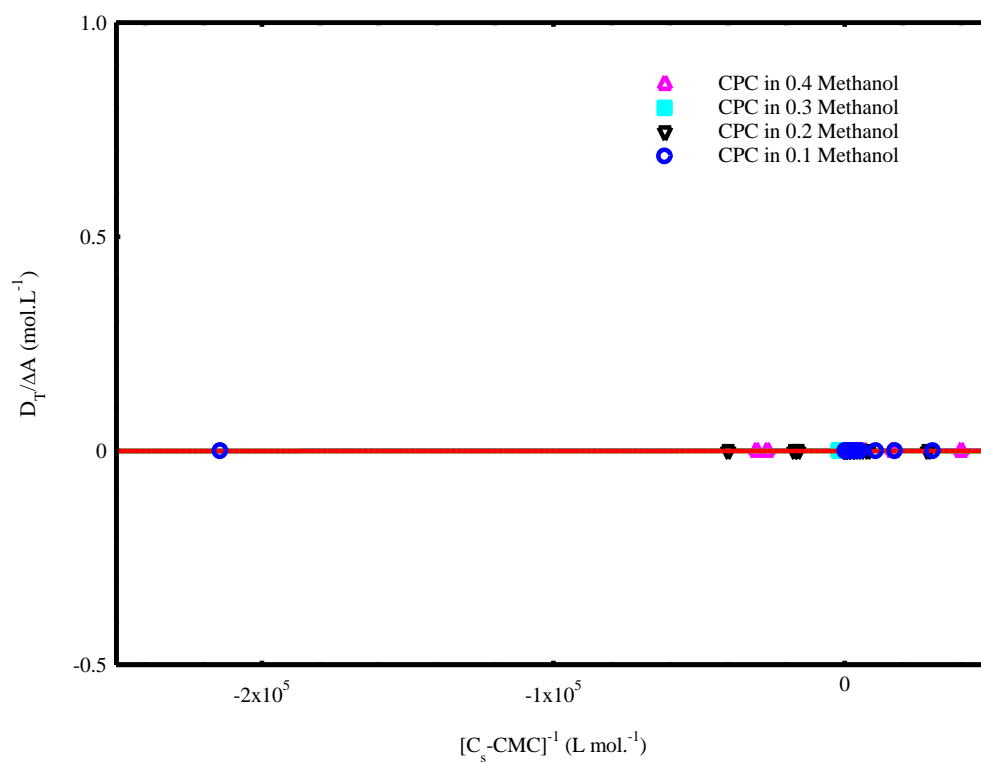


Figure 20: Plot of $D_T/\Delta A$ against $[C_s-CMC]^{-1}$ for MR with CPC in four different volume fractions of methanol

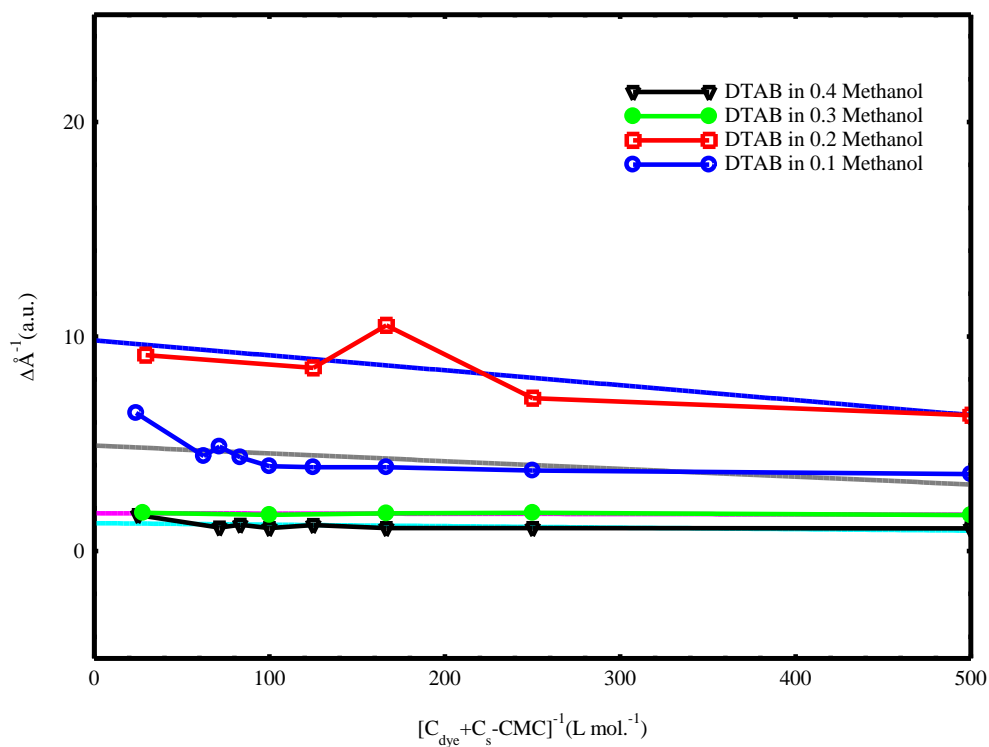


Figure 21: Plot of ΔA^{-1} against $[C_{\text{dye}} + C_{\text{surfactant}} - \text{CMC}]^{-1}$ for MR with DTAB in four different volume fractions of methanol

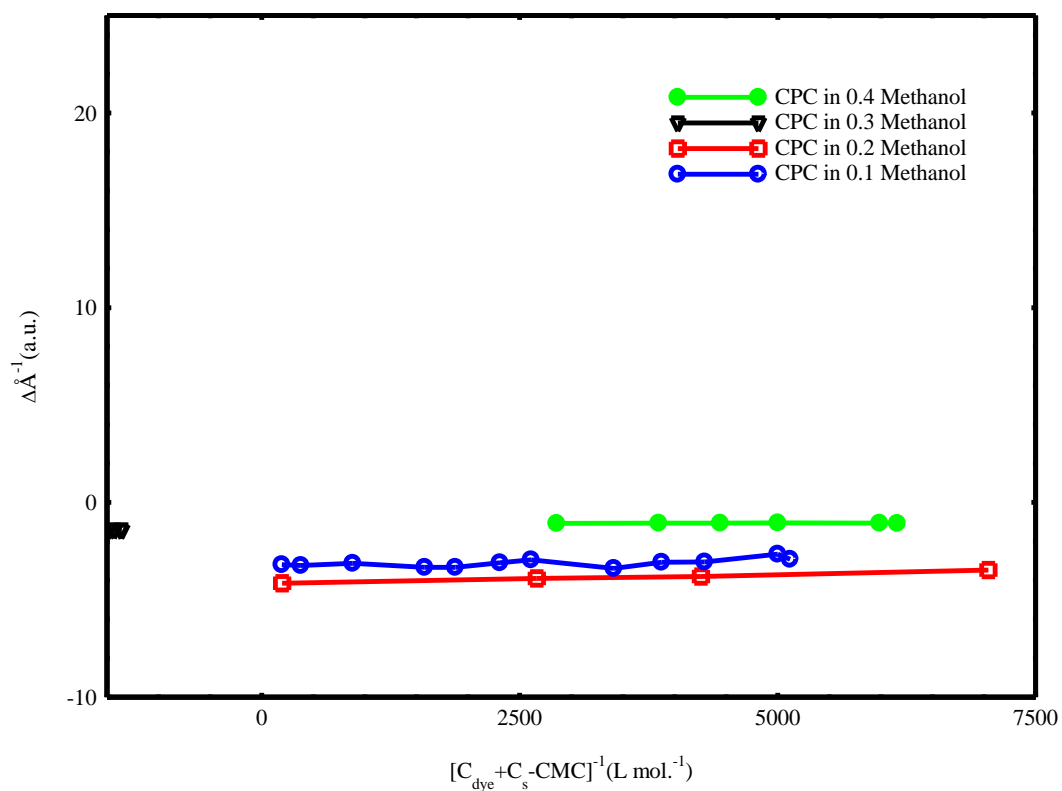


Figure 22: Plot of ΔA^{-1} against $[C_{\text{dye}} + C_{\text{surfactant}} - \text{CMC}]^{-1}$ for MR with CPC in four different volume fractions of methanol

4.1.4 UV-Vis spectra of Cationic surfactant (DTAB)-MR interactions in ethanol-water mixture

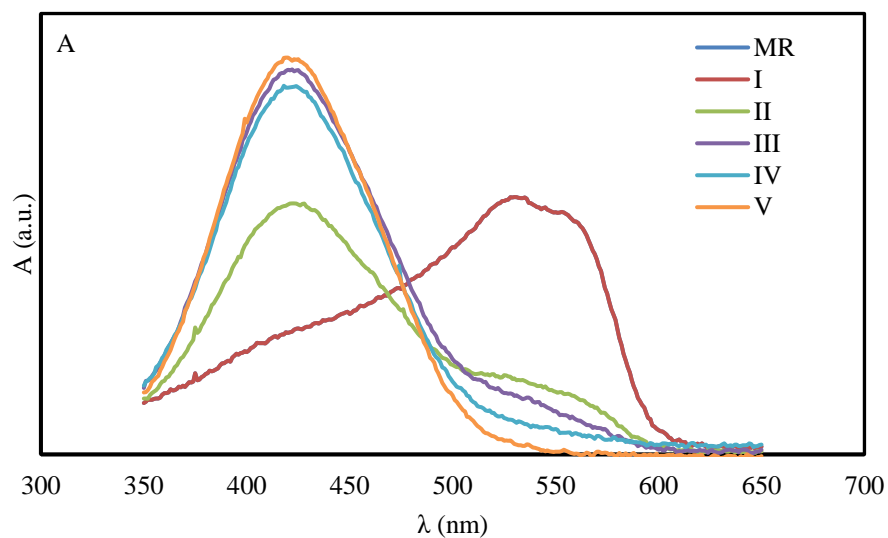


Figure 23: Visible spectra of MR-DTAB system in 0.1 volume fraction of ethanol. Here, I, II, III, IV, V and MR represent the concentration of DTAB [1, 2, 3, 4, 11 and 0] $\times 10^{-2}$ mol. L $^{-1}$ respectively. Here the constant concentration of MR is 2.97×10^{-4} mol. L $^{-1}$

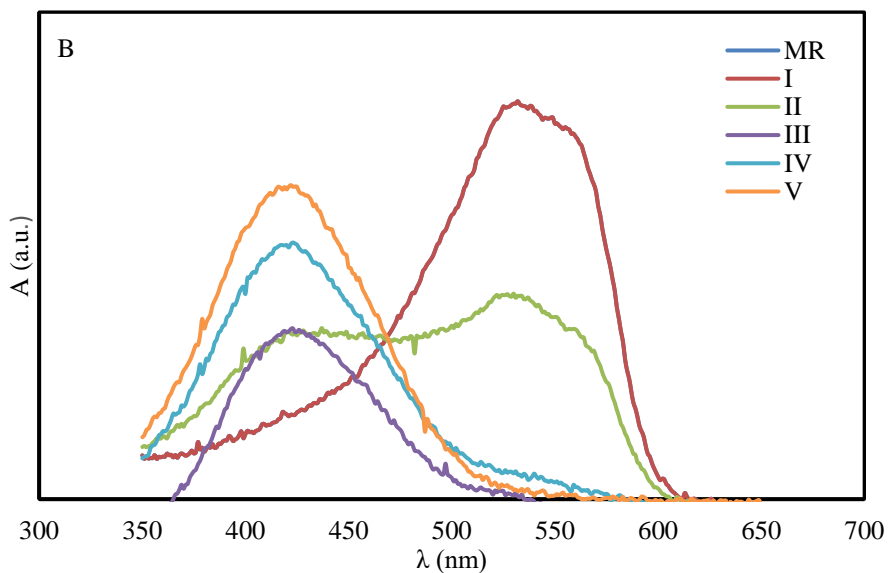


Figure 24: Visible spectra of MR-DTAB system in 0.2 volume fraction of ethanol. Here, I, II, III, IV, V and MR represent the concentration of DTAB [1, 2, 3, 4, 11 and 0] $\times 10^{-2}$ mol. L $^{-1}$ respectively. Here the constant concentration of MR is 2.97×10^{-4} mol. L $^{-1}$

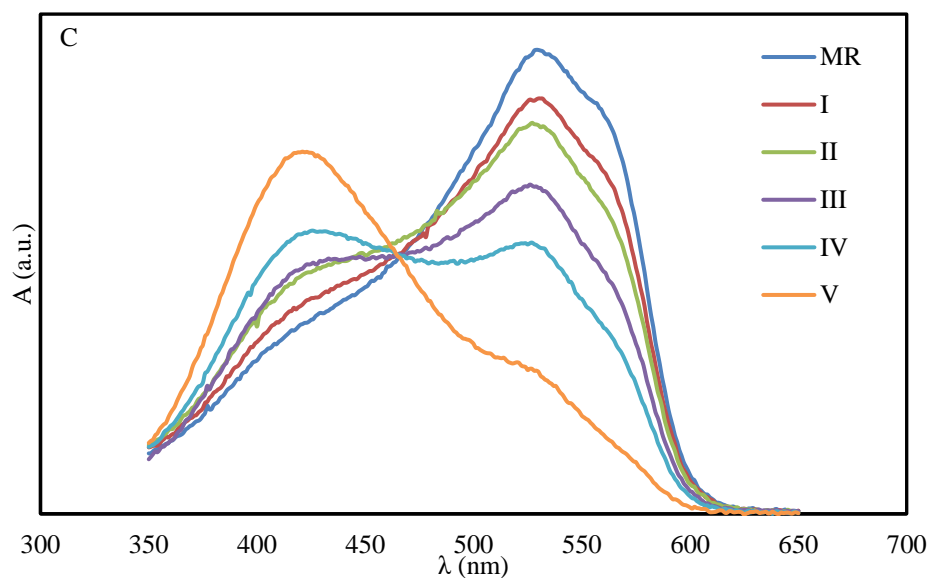


Figure 25: Visible spectra of MR-DTAB system in 0.3 volume fraction of ethanol. Here, I, II, III, IV, V and MR represent the concentration of DTAB [1, 2, 3, 4, 11 and 0] $\times 10^{-2}$ mol. L $^{-1}$ respectively. Here the constant concentration of MR is 2.97×10^{-4} mol. L $^{-1}$

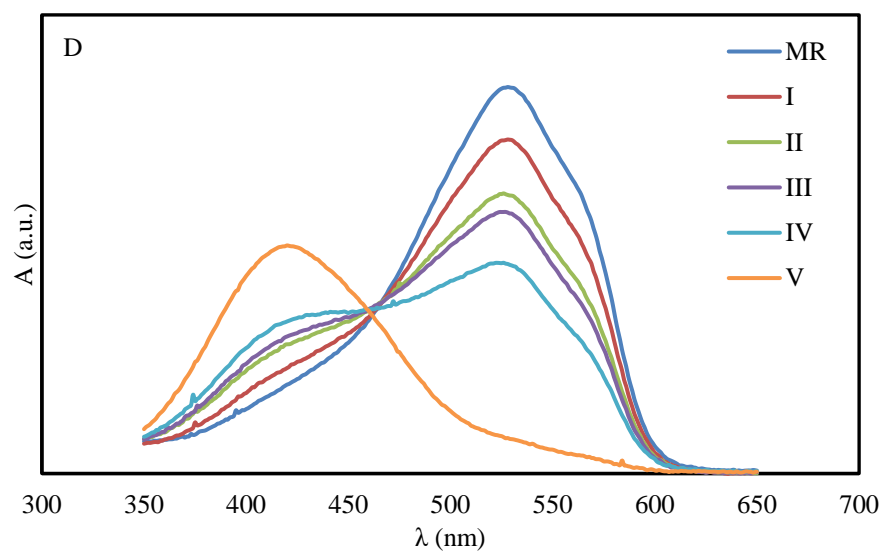


Figure 26: Visible spectra of MR-DTAB system in 0.4 volume fraction of ethanol. Here, I, II, III, IV, V and MR represent the concentration of DTAB [1, 2, 3, 4, 11 and 0] $\times 10^{-2}$ mol. L $^{-1}$ respectively. Here the constant concentration of MR is 2.97×10^{-4} mol. L $^{-1}$

The reported MR hydrazone (acidic) species peaks were discovered at ethanol volume fractions of 0.1, 0.2, 0.3, and 0.4. As a result, it was identified that the visible spectrum of methyl red is dependent on solvent, with the absorbance of methyl red in ethanol at 0.4 volume fraction being the highest among ethanol concentrations at 0.3, 0.2, and 0.1.

(Figs. 23 to 26). The addition of DTAB in the presence of varying ethanol concentrations had a significant impact on the azo dye's spectrum properties. The absorbance was increased with rised ethanol volume (Figs. 23 to 26), which contributes to the formation of molecular complex between the cationic surfactant and the azo dye as presented in Figs. 23 to 26. Due to a decrease in absorbance with a higher concentration range of ionic surfactant, the cause of electrostatic interaction on the hydrocarbon core of the surfactant was investigated at constant dye concentration (Moyá *et al.*, 2007) . Here, due to the changing status of molecular complex between MR-DTAB in Figs. 23 to 26 , there is blue shift for the higher concentration of DTAB, remaining shows red shift. Due to unusual absorption of DTAB molecules with MR, no CMC values are detected in the plots.

Analysing the visible spectra (Figs. 23-26), binding behavior is estimated using Benesi-Hildebrand Equation 4.1 without CMC values and (Edbey *et al.*, 2018; Fazeli *et al.*, 2012). K_b obtained from the Fig. 27 and using Equation 4.6, ΔG_b are tabulated in Table 5. Because MR molecules abnormally aggregate around the hydrophilic part of DTAB micelles when the volume of ethanol is 0.2, the binding value between the azo dye and the surfactant is lowest at this volume.

Table 5: Values of K_b and ΔG_b of DTAB at 0.1, 0.2, 0.3 and 0.4 volume fractions of ethanol

Volume fraction of ethanol	$K_b(\text{Lmol}^{-1})$	$\Delta G_b(\text{kJmol}^{-1})$
0.1	12.2	-6010.31
0.2	4.87	-3803.77
0.3	26.77	-7898.5
0.4	20	-7197.98

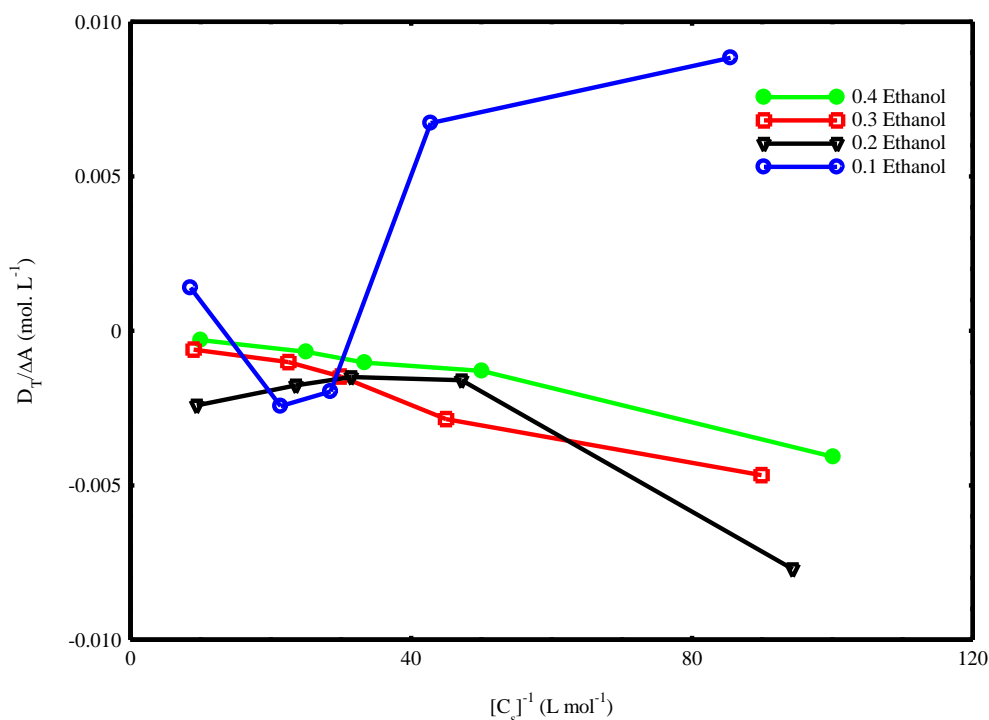


Figure 27: Plot of $D_T/\Delta A$ against $[C_s]^{-1}$ for MR with DTAB in four different volume fractions of ethanol

4.1.5 Conductometric studies and its related thermodynamic properties of DTAB and CPC in absence and presence of MR

Cationic surfactants are ionic surfactants consisting of both hydrophilic part and hydrophobic part which plays vital role in strong electrolytic solution. As a result, conductivity varies after certain concentrations, estimated as critical micelle concentration (CMC). The critical micelle concentration is that critical concentration at which micelle formation begins. It can be determined through the breakpoint between two lines. The breakpoint of the corresponding concentration is evaluated as an aggregation point called the CMC of the surfactant in the aqueous medium (Shah *et al.*, 2021). Here the system obtained both premicellar slope (S_1) and postmicellar slope (S_2) which are important slopes to determine degree of ionization (α) of surfactants in the solvent (Sachin *et al.*, 2019a). The degree of ionization is expressed as follows.

$$\alpha = \frac{S_2}{S_1} \quad (4-8)$$

In each plot of conductivity against surfactant concentrations, conductivity increases with increasing concentration of cationic surfactants (DTAB and CPC). Also, it was noticed that the upper linear part that is above the CMC values has a smaller slope than the lower linear part below the CMC values (Shah & Bhattarai, 2020; Waghmode *et*

al., 2019). It has been summarized from **Tables 6 and 7** that there is a critical change in CMC values due to different effects (**Figs. 38 to 49**). Such effects are due to additives such as azo dyes (MR), variable mixed solvent media (alcohol content in water) along with increased temperatures (Bhattarai *et al.*, 2017).

It can be seen from the representative plot (**Figs. 28 and 29**) that the CMC has been suppressed in the presence of additives (MR). The reason behind the decrease of CMC is due to the increase in the force of attraction among molecules which easily solubilizes azo dye molecules and decreases the conductivity (Moyá *et al.*, 2007). This is the outcome of higher DTAB and CPC concentrations, which lowers their ionic mobilities (Muhammad & Khan, 2020).

Tables 6 and 7 reveal the presence of a cosolvent (alcohol content in water) suppresses micellization, and it completely stops forming micelle when its mixture attains an optimum level (Niraula *et al.*, 2017). The CMC rises with rising methanol volume in water. It is due to the involvement of methanol in aggregates, where molecular species break down the aggregates (Shah *et al.*, 2016). Researchers investigated that methanol which is short-chain alcohol rises the CMC values at the concentrated bulk phase because of lower cohesive energy density in the aqueous phase which enhances the process of solubilization of the monomeric surfactant (Bhattarai *et al.*, 2017; Edbey *et al.*, 2015). In the case of ionic surfactants, the relative permittivity of the medium can be used as an alternative explanation. Alcohols with short chains lower the relative permittivity of the water, which enhances the mutual repulsion of the ionic surfactants, which would reverse micellization and rises the CMC values (Simončič & Špan, 1998).

The CMC values of DTAB and CPC are calculated from the conductivity method at three different temperatures (298.15, 308.15, and 318.15 K) but the values are very close which is matched with the literature (Bhattarai *et al.*, 2017; Shah *et al.*, 2016) of 298.15 K. The CMC is greatly influenced by the increase in temperature as investigated in relevant literature (Shah *et al.*, 2016). Thermodynamic properties are altered due to which micellization nature is varied for variable mixed solvent media at three different temperatures as shown in **Tables 6 and 7**. As a result, it is determined the increase in CMC due to increased temperatures in the same solvent system.

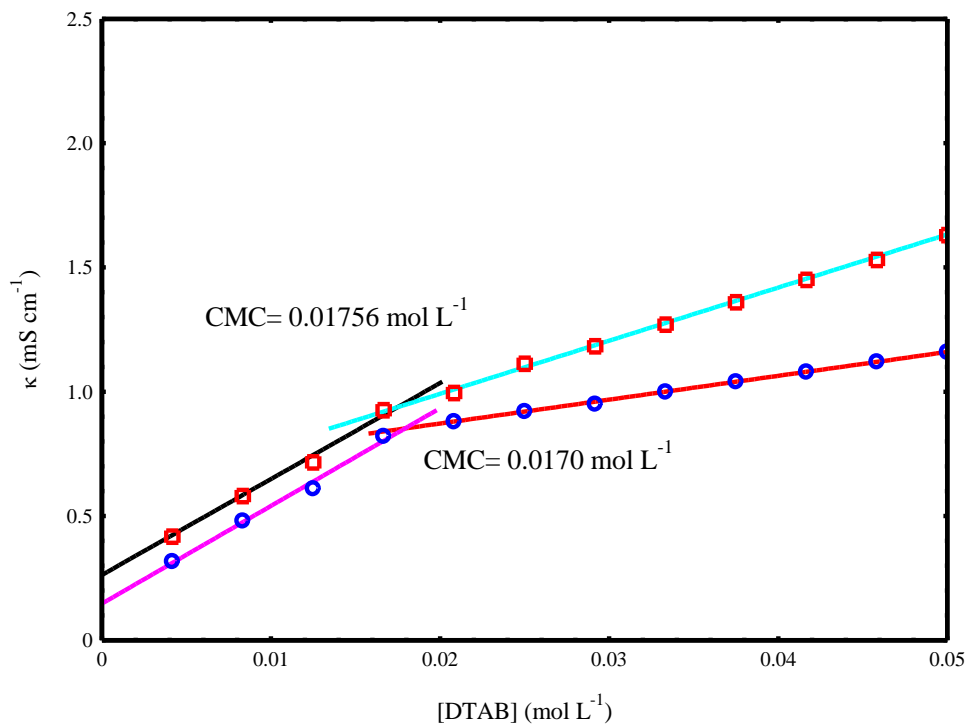


Figure 28: Representative plot of conductivity against the DTAB concentration without MR (□) and with MR (○) of 0.1 volume fraction of methanol in water at 298.15 K

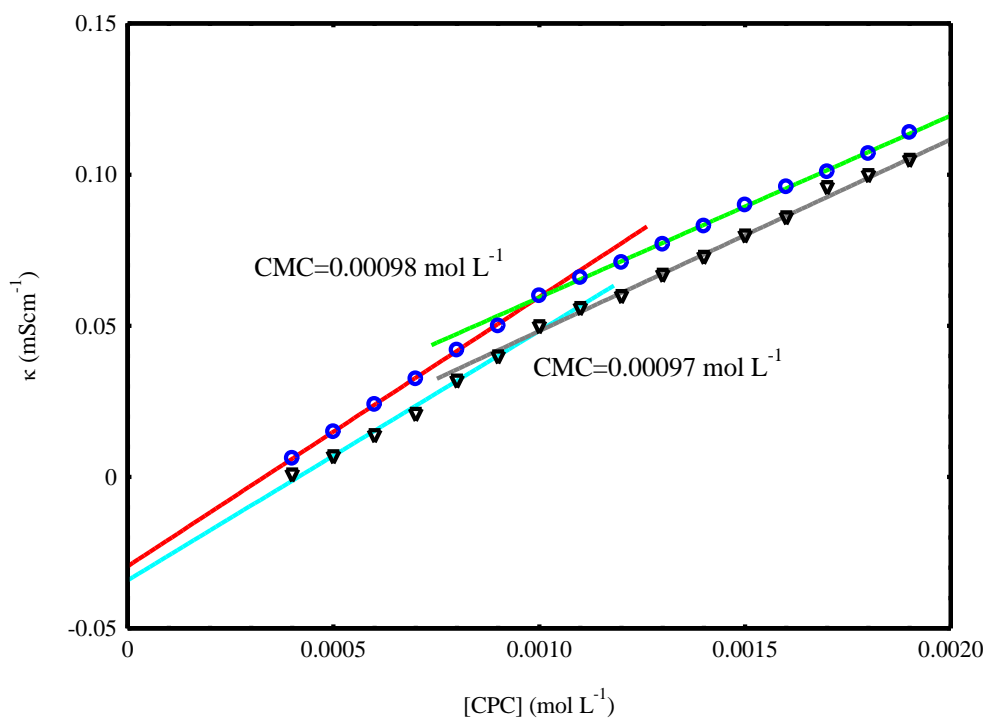


Figure 29: Representative plot of conductivity against the CPC concentration without MR (○) and with MR (▽) of 0.1 volume fraction of methanol in water at 298.15 K

Additionally, the interaction between methyl red and DTAB or CPC, interaction between mixed solvent as well as water, mixed solvent and ionic surfactant and mixed

solvent and azo dye also required to be considered. Mostly, the hydroxyl functional group of alcohol is hydrogen-bonded to the ionic head group of surfactants and thus decreases the attraction between DTAB or CPC and the azo dye. Therefore, to investigate the inhibitory impact of mixed solvents on the molecular complexes formed, assuming thermodynamic properties of mixtures, preferably solubilization of azo dyes, mixed solvent–water as well as a mixed solvent–surfactant mixture interactions. However, it is difficult to identify the reason responsible for the better inhibition effects among all. Mostly, all the determined parameters contribute more or less in variable ways (Niraula *et al.*, 2017).

Thus, the standard Gibbs free energy of micelle formation for ionic surfactant, ΔG_m° , is calculated by the relation of the pseudo-phase separation model (Ruiz, 1999).

$$\Delta G_m^{\circ} = (2 - \alpha)RT \ln X_{CMC} \quad (4-9)$$

where α denotes the degree of ionization, which was calculated with $\alpha = S_2 / S_1$ (Niraula *et al.*, 2017); S_2 is the post micellar slope and S_1 is the premicellar slope and X_{CMC} denotes the mole fraction of CMC. The CMC values along with α values were calculated by conductivity data by conventional process known as Williams' method (Ruiz, 1999).

The estimated values of ΔG_m° are negative, which denotes the spontaneous process of micellization. This spontaneity lowers with rising volume content of methanol, as a result, micellization is not more favorable. Increased negative ΔG_m° values when the azo dye content is added in mixtures, which shows that the formation of micelle becomes more beneficial with the inclusion of the azo dye.

The oppositely charged binding preferably influences ΔG_m° ; thus, ΔG_m° is one of the significant thermodynamic properties of the cationic surfactant (Shah *et al.*, 2016; Shah *et al.*, 2021).

Standard enthalpy of micellization, ΔH_m° s calculated using the relation (Bhattacharai *et al.*, 2017)

$$\Delta H_m^{\circ} = -RT^2 \left[2 - \alpha \left[\frac{\partial \ln X_{cmc}}{\partial T} \right]_P \right] \quad (4-10)$$

The term $\left(\frac{\partial \ln X_{CMC}}{\partial T}\right)$ is determined by fitting $\ln X_{CMC}$ versus temperature (Figs. 30 to 33) and taking the corresponding derivative of temperature (Bhattarai et al., 2017).

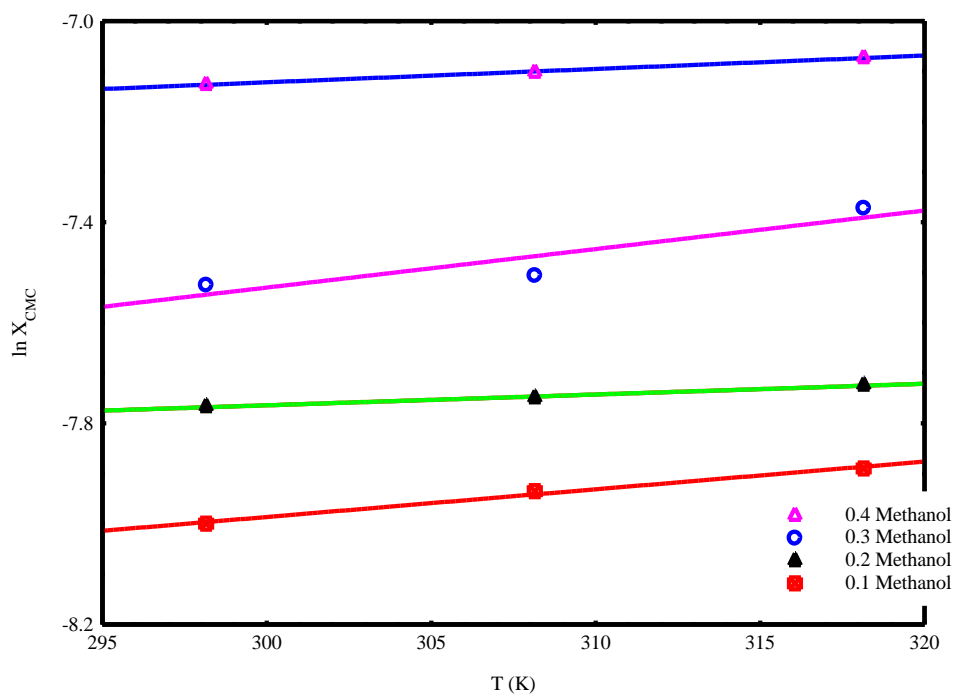


Figure 30: Plot of DTAB in absence of MR for the fitting $\ln X_{CMC}$ versus three different temperatures.

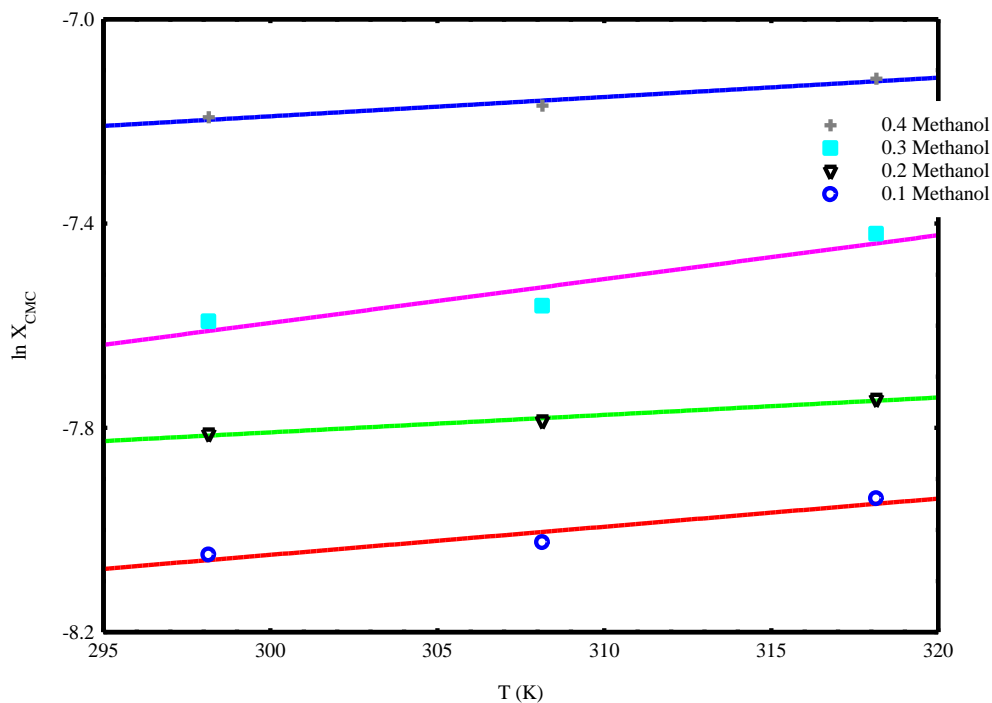


Figure 31: Plot of DTAB in presence of MR for the fitting $\ln X_{CMC}$ versus three different temperatures.

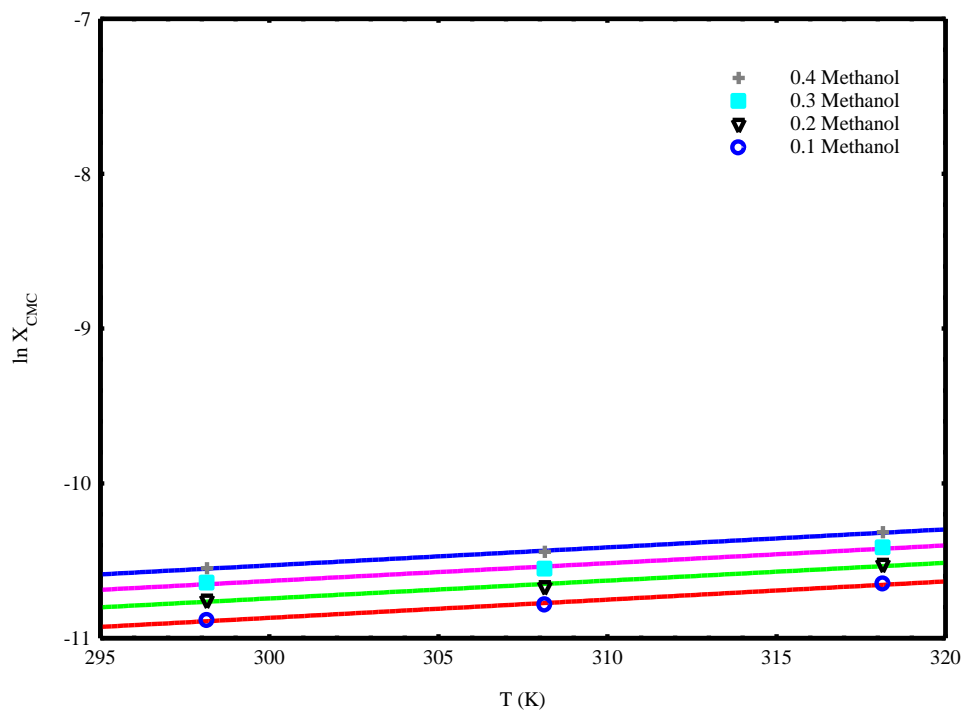


Figure 32: Plot of CPC in absence of MR for the fitting $\ln X_{CMC}$ versus three different temperatures.

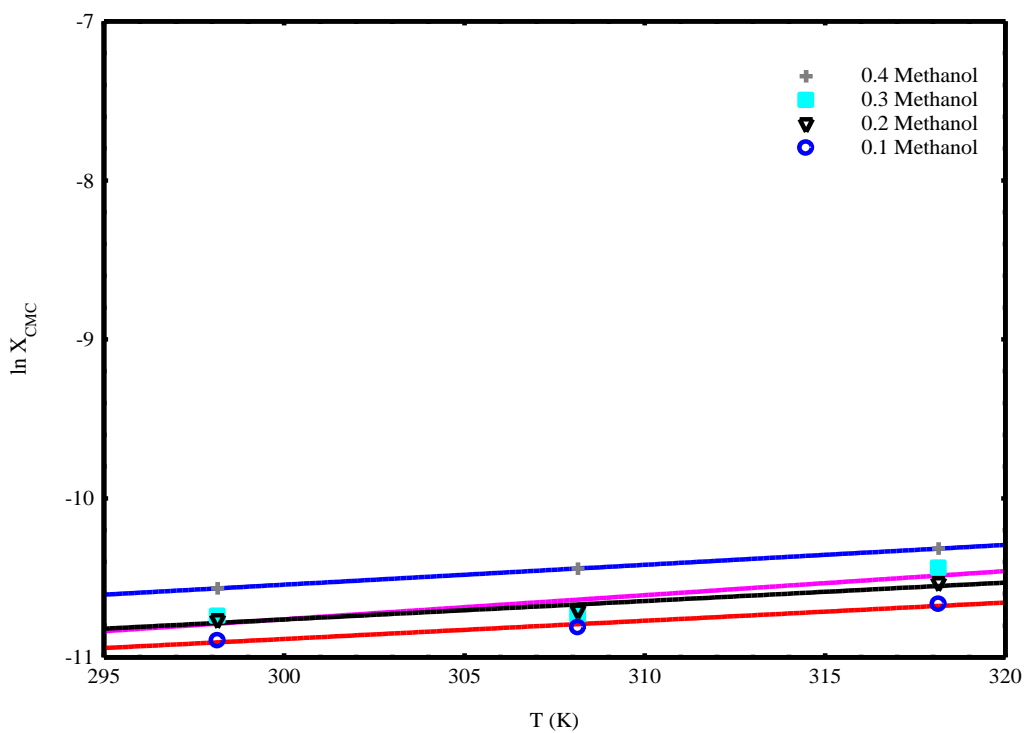


Figure 33: Plot of CPC in presence of MR for the fitting $\ln X_{CMC}$ versus three different temperatures.

Also ΔS_m° standard entropy of DTAB and CPC micellization can be obtained from the values of ΔG_m° and ΔH_m° using the relation (Bhattacharai et al., 2017a).

$$T\Delta S_m^\circ = \Delta H_m^\circ - \Delta G_m^\circ \quad (4-11)$$

The additives effect could be obtained on micellization process through the relation, (Bhattacharai et al., 2017a) denoted by $\Delta G_{\text{trans}}^\circ$.

$$\Delta G_{\text{trans}}^\circ = (\Delta G_m^\circ)_{\text{methanol+water}} - (\Delta G_m^\circ)_{\text{water}} \quad (4-12)$$

Due to presence of additives, heat capacity of micellization, $\Delta m C_p^0$ can be obtained from slope obtained in the plot of ΔH_m° against T (Figs. 34 to 37) expressed by the relation (Bhattacharai et al., 2017)

$$\Delta m C_p^0 = \frac{\partial \Delta m H^0}{\partial T} \quad (4-13)$$

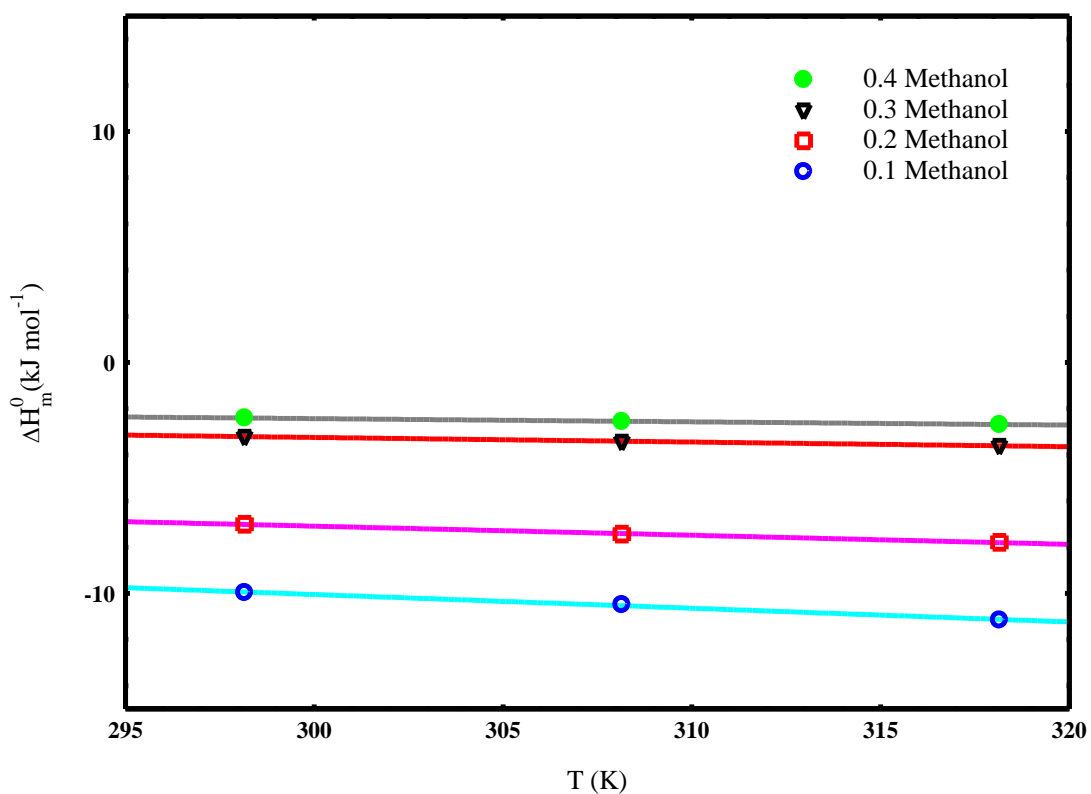


Figure 34: Plot of DTAB in absence of MR of Standard enthalpy of micellization against T

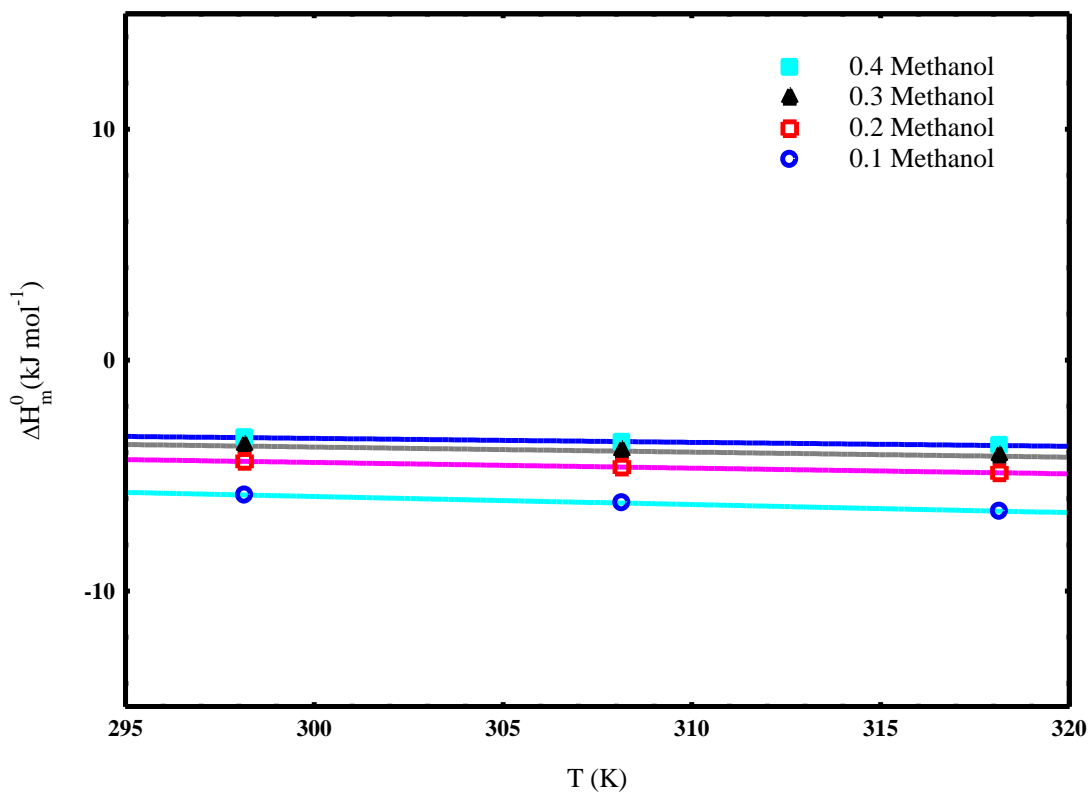


Figure 35: Plot of DTAB in presence of MR of Standard enthalpy of micellization against T.

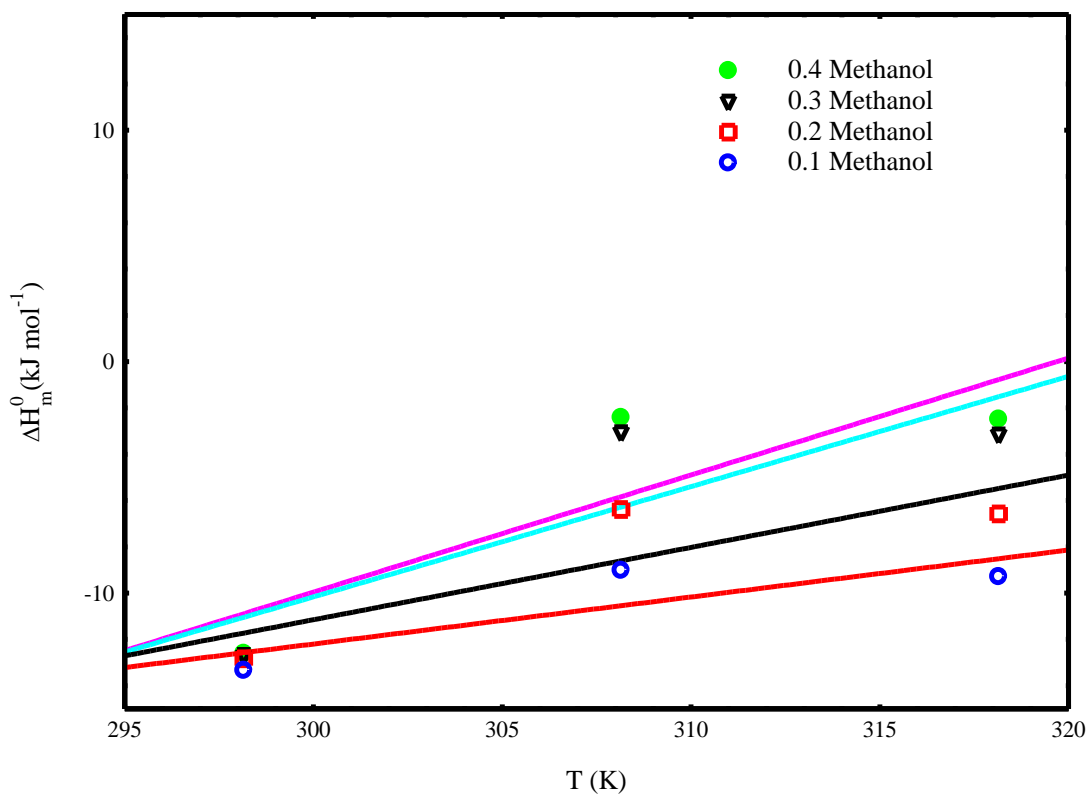


Figure 36: Plot of CPC in absence of MR of Standard enthalpy of micellization against T.

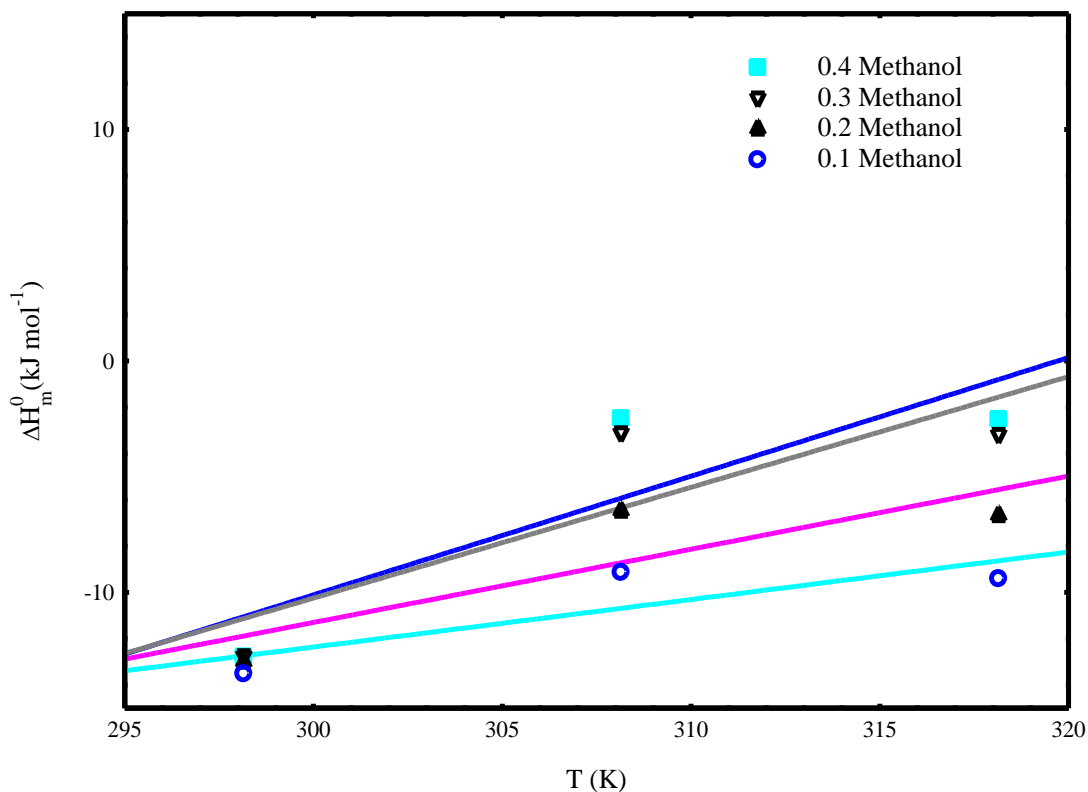


Figure 37: Plot of CPC in absence of MR of Standard enthalpy of micellization against T.

The values of α , CMC and ΔG_m^0 , ΔH_m^0 , ΔS_m^0 , ΔG_{trans}^0 , and ΔmC_p^0 of DTAB and CPC by conductivity method with or without methyl red in dissimilar volume contents of methanol-water at 298.15, 308.15, and 318.15 K are tabulated in **Tables 6, 7 and 8**. In the above section, the effect of additives such as azo dye (MR), methanol in water, etc. along with the temperature effect had been discussed from 298.15-318.15 K on CMC and ΔG_m^0 . The data show the effect of temperature and methanol solvent composition in water. The coulombic along with thermal effects are the main reason for the rise in α with the rise in methanol composition and temperature. Also, we can identify the thermodynamic effect on the parameters such as ΔH_m^0 , ΔS_m^0 , ΔG_{trans}^0 and ΔmC_p^0 . The variability in such parameters greatly influences the micellization behavior in the dyeing process. As surfactant plays a vital role in establishing an organized system for well-defined dispersing, it determined the better coloring agent (Niraula et al., 2017; Sachin et al., 2019; Shah et al., 2016).

Table 6: The values of CMC, α , ΔG_m^0 , ΔH_m^0 , ΔS_m^0 and ΔG_{trans}^0 of DTAB without MR and with MR at 0.1,0.2,0.3 and 0.4 methanol-water medium through three dissimilar temperatures (298.15 K, 308.15 K and 318.15K)

Temperature(K)	volume fraction of methanol	Degree of ionization (α)		CMC (mM) by Conductometry		ΔG_m^0 (kJ mol ⁻¹)		ΔH_m^0 (kJ mol ⁻¹)		ΔS_m^0 (J mol ⁻¹ k ⁻¹)		ΔG_{trans}^0 (kJ mol ⁻¹)	
		a	b	a	b	a	b	a	b	a	b	a	b
298.15	0.1	0.24	0.23	17.56	17.07	-41.32	-35.31	-9.96	-5.84	83.63	81.15	-4.74	1.27
	0.2	0.28	0.26	20.86	19.93	-40.29	-33.7	-7.0	-4.38	87.57	89.29	-3.71	2.88
	0.3	0.37	0.35	24.91	23.07	-39.67	-31.05	-3.2	-3.72	91.22	88.68	-3.09	5.53
	0.4	0.48	0.45	34.65	33	-38.50	-27.63	-2.4	-3.34	81.99	79.57	-1.92	8.95
308.15	0.1	0.266	0.25	18.67	17.07	-39.93	-34.81	-1.49	-6.17	76.65	74.85	-3.35	1.77
	0.2	0.29	0.28	21.15	20.37	-39.01	-33.2	-7.44	-4.63	82.45	83.49	-2.43	3.38
	0.3	0.37	0.36	25.27	23.91	-38.58	-30.74	-3.42	-3.94	87.3	83.87	-2	5.84
	0.4	0.49	0.46	35.33	33.01	-37.47	-27.37	-2.6	-3.55	77.98	75.36	-0.89	9.21
318.15	0.1	0.27	0.26	19.45	18.52	-38.07	-34.24	-11.15	-6.54	71.29	68.5	-1.49	2.34
	0.2	0.32	0.3	21.58	21.15	-37.07	-32.63	-7.79	-4.88	76.6	77.84	-0.49	3.95
	0.3	0.39	0.38	28.75	27.38	-36.22	-29.8	-3.6	-4.16	81.1	77.46	0.36	6.78
	0.4	0.51	0.5	36.14	34.6	-35.34	-26.46	-2.68	-3.69	73.68	69.64	1.24	10.12

Note: a = without MR and b = with MR

Table 7: The values of CMC, α , ΔG_m^0 , ΔH_m^0 , ΔS_m^0 and ΔG_{trans}^0 of CPC without MR and with MR at 0.1, 0.2, 0.3 and 0.4 methanol-water medium through three different temperatures (298.15 K, 308.15 K and 318.15K)

Temperature(K)	volume fraction of methanol	Degree of ionization (α)		CMC (mM) by Conductometry		ΔG_m^0 (kJ mol ⁻¹)		ΔH_m^0 (kJ mol ⁻¹)		ΔS_m^0 (J mol ⁻¹ k ⁻¹)		ΔG_{trans}^0 (kJ mol ⁻¹)	
		a	b	a	b	a	b	a	b	a	b	a	b
298.15	0.1	0.47	0.45	0.98	0.97	-41.28	-41.86	-13.34	-13.52	93.71	95.07	1.01	0.43
	0.2	0.49	0.47	1.05	1	-40.26	-40.83	-12.83	-13.00	91.98	93.32	2.03	1.46
	0.3	0.51	0.50	1.1	1.04	-39.31	-39.93	-12.66	-12.75	89.39	91.17	2.98	2.36
	0.4	0.53	0.51	1.13	1.11	-38.44	-39.02	-12.60	-12.77	86.65	88.05	3.85	3.26
308.15	0.1	0.51	0.49	1.08	1.05	-39.83	-40.47	-9.01	-9.13	100.02	101.71	2.46	1.81
	0.2	0.53	0.51	1.14	1.1	-38.88	-39.54	-6.39	-6.48	105.41	107.27	3.41	2.75
	0.3	0.55	0.52	1.2	1	-37.93	-39.38	-3.04	-3.11	113.20	117.72	4.36	2.9
	0.4	0.57	0.53	1.25	1.1	-37.01	-38.52	-2.42	-2.48	112.28	116.93	5.28	3.77
318.15	0.1	0.56	0.54	1.23	1.21	-38.02	-38.60	-9.28	-9.41	90.31	91.75	4.27	3.69
	0.2	0.58	0.56	1.31	1.3	-37.05	-37.60	-6.58	-6.68	95.75	97.19	5.24	4.69
	0.3	0.6	0.58	1.37	1.34	-36.14	-36.74	-3.13	-3.18	103.76	105.48	6.15	5.55
	0.4	0.62	0.6	1.41	1.39	-35.29	-35.85	-2.49	-2.52	103.11	104.76	7.00	6.44

Note: a = without MR and b = with MR

Table 8: Values of ΔmC_p° for DTAB and CPC in mixed methanol-water system

Cationic Surfactants	volume fraction of methanol							
	0.1		0.2		0.3		0.4	
	a	b	a	b	a	b	a	b
For DTAB	-59	-34.9	-39.3	-24.7	-20	-21.9	-14	-17
For CPC	203	513	312	479	476	316	506	205

Note: a = without MR and b = with MR

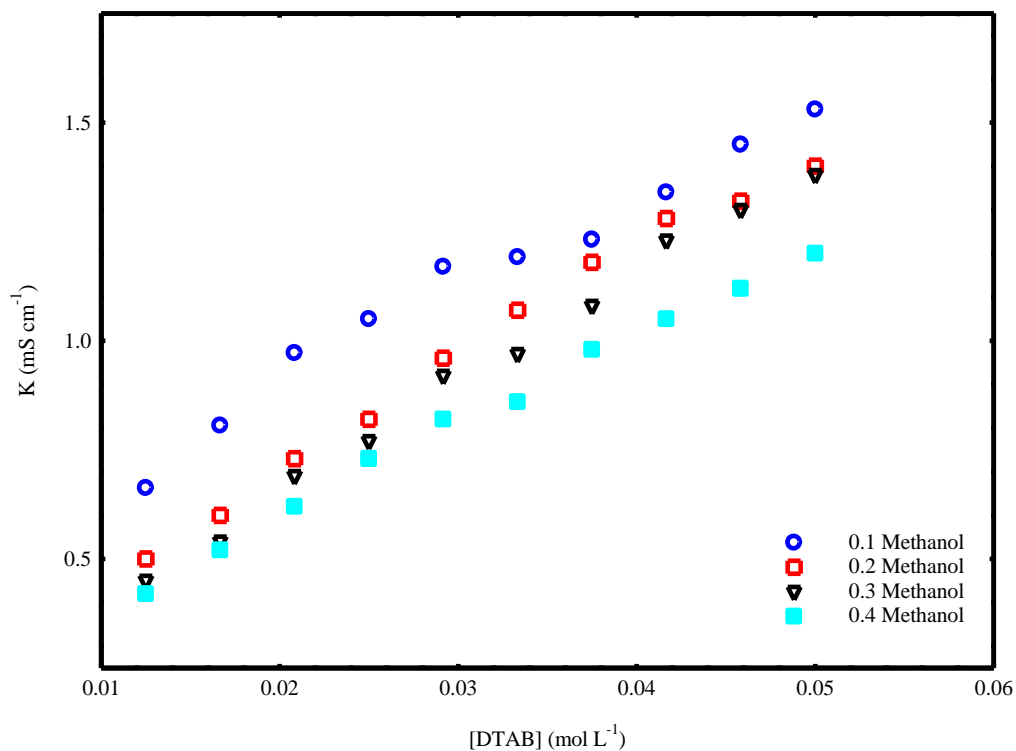


Figure 38: Plot of conductivity against [DTAB] in absence of MR at 298.15 K

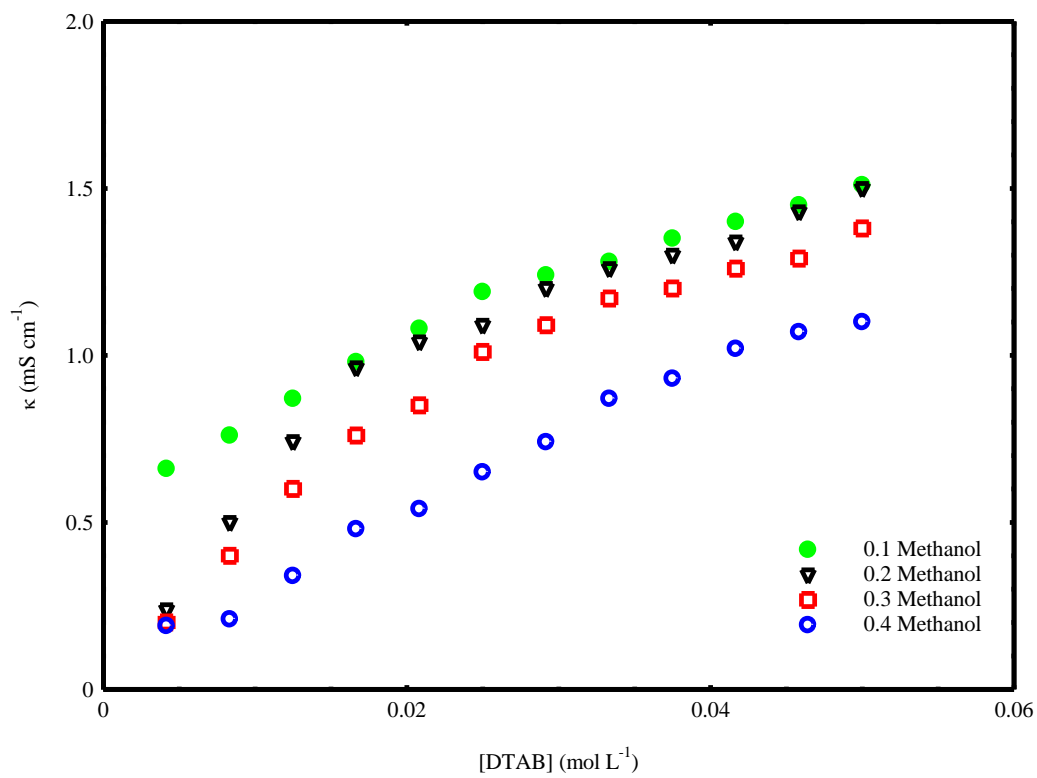


Figure 39: Plot of conductivity against [DTAB] in absence of MR at 308.15 K

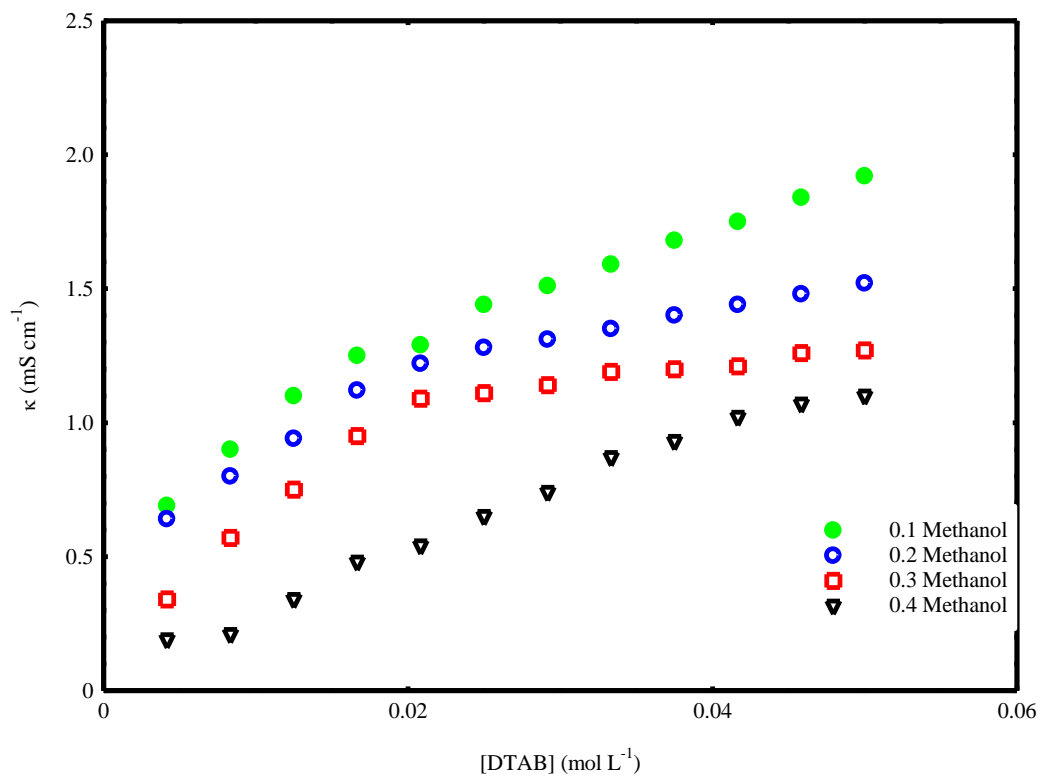


Figure 40: Plot of conductivity against [DTAB] in absence of MR at 318.15 K

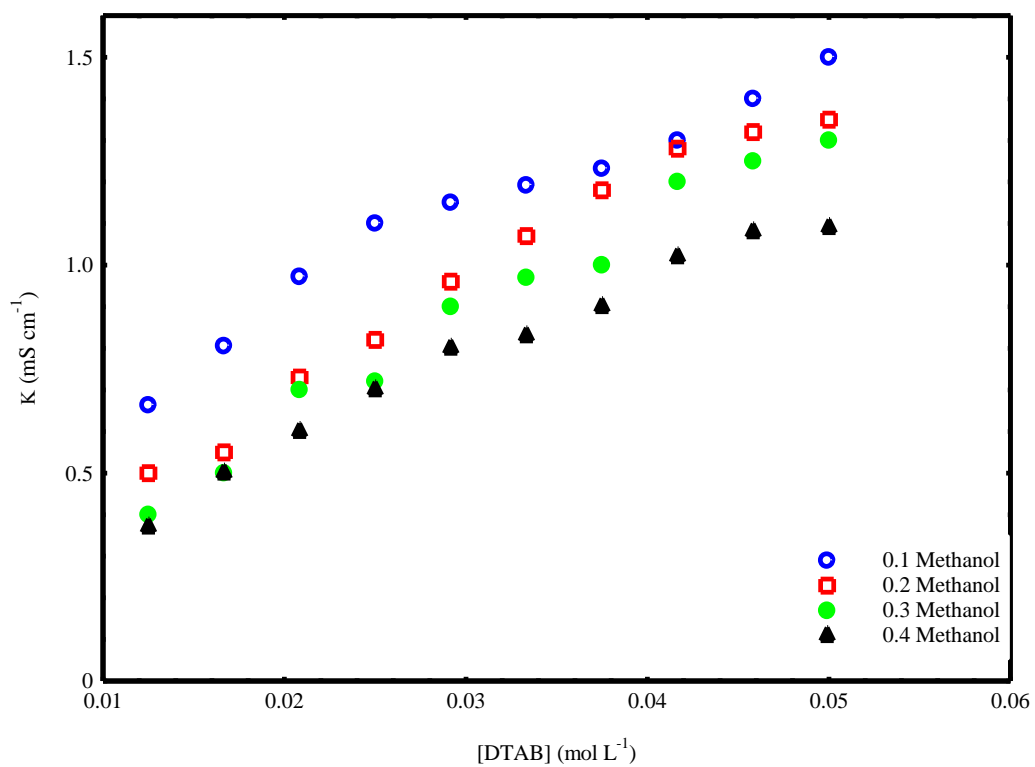


Figure 41: Plot of conductivity against [DTAB] in presence of MR at 298.15 K

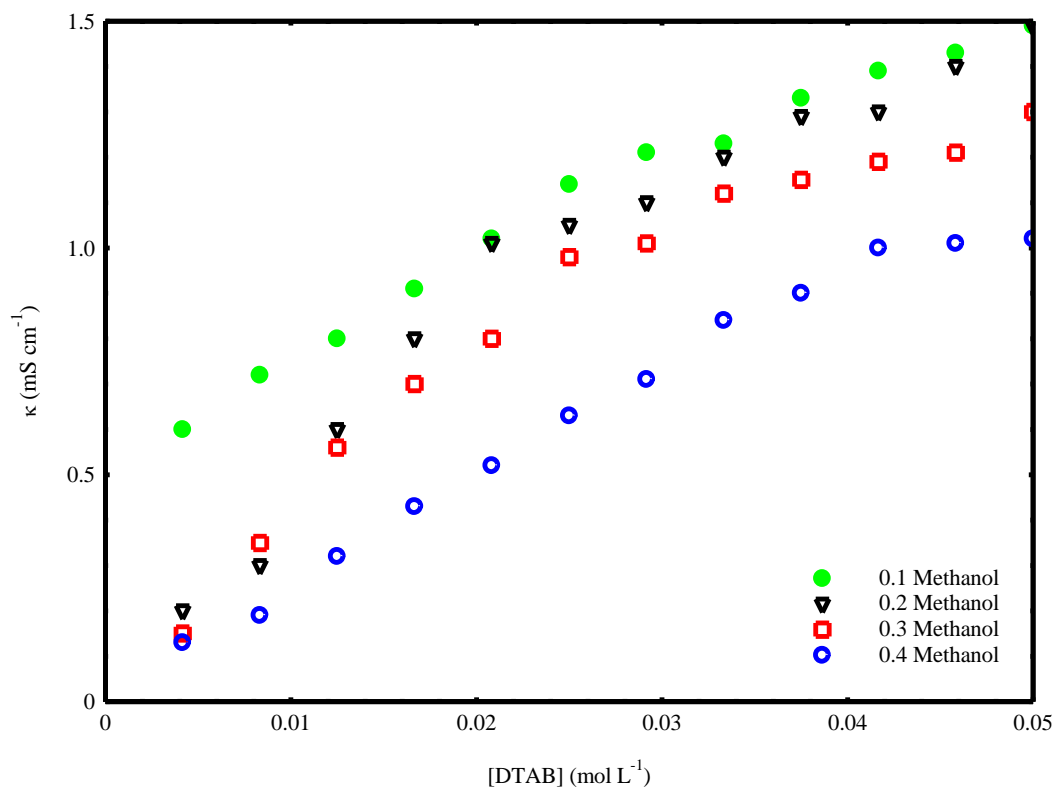


Figure 42: Plot of conductivity against [DTAB] in presence of MR at 308.15 K

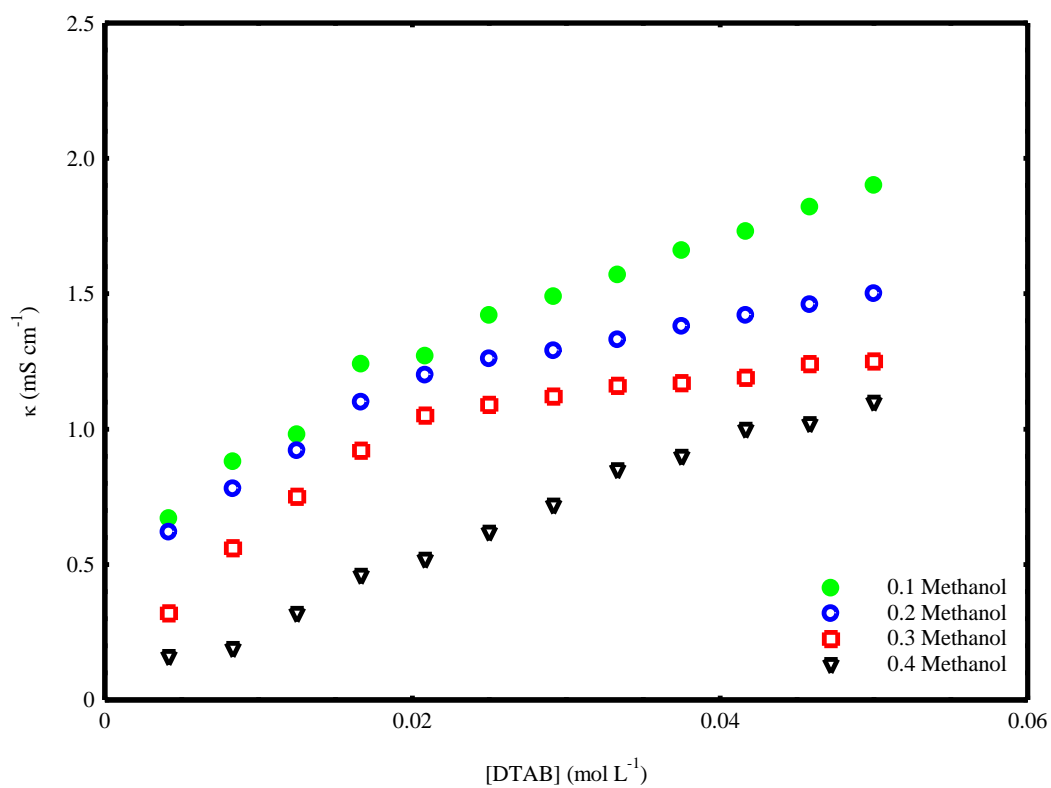


Figure 43: Plot of conductivity against [DTAB] in presence of MR at 318.15 K

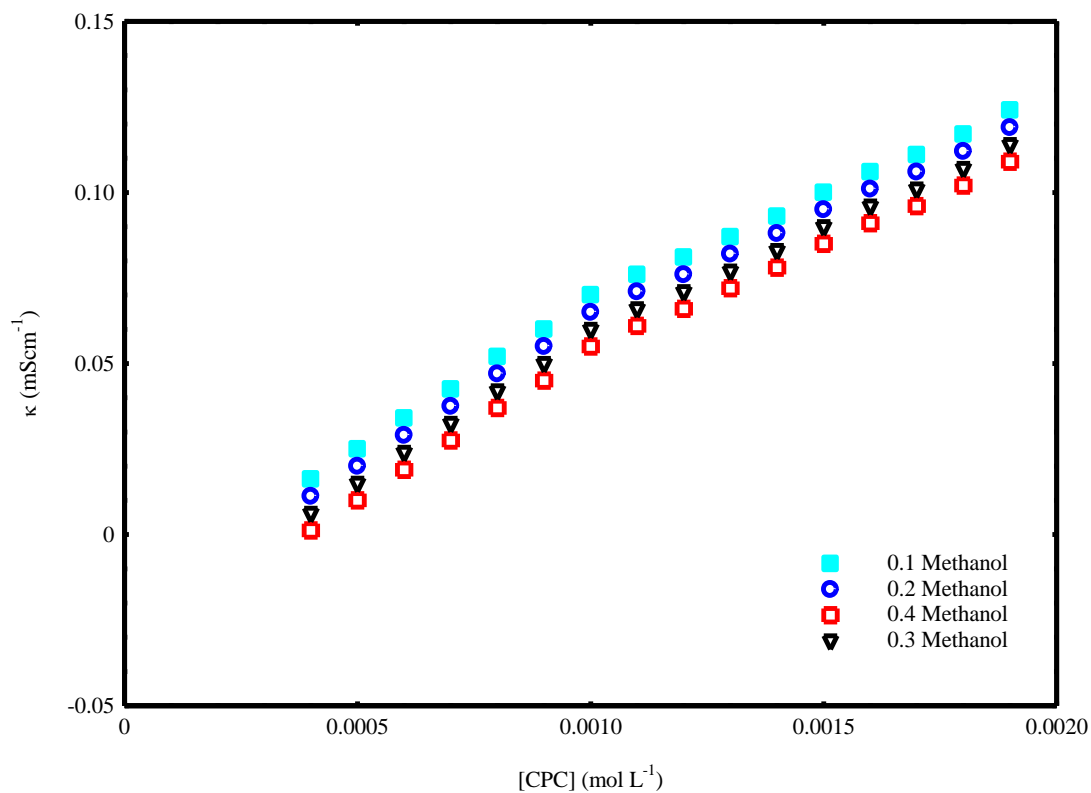


Figure 44: Plot of conductivity against [CPC] in absence of MR at 298.15 K

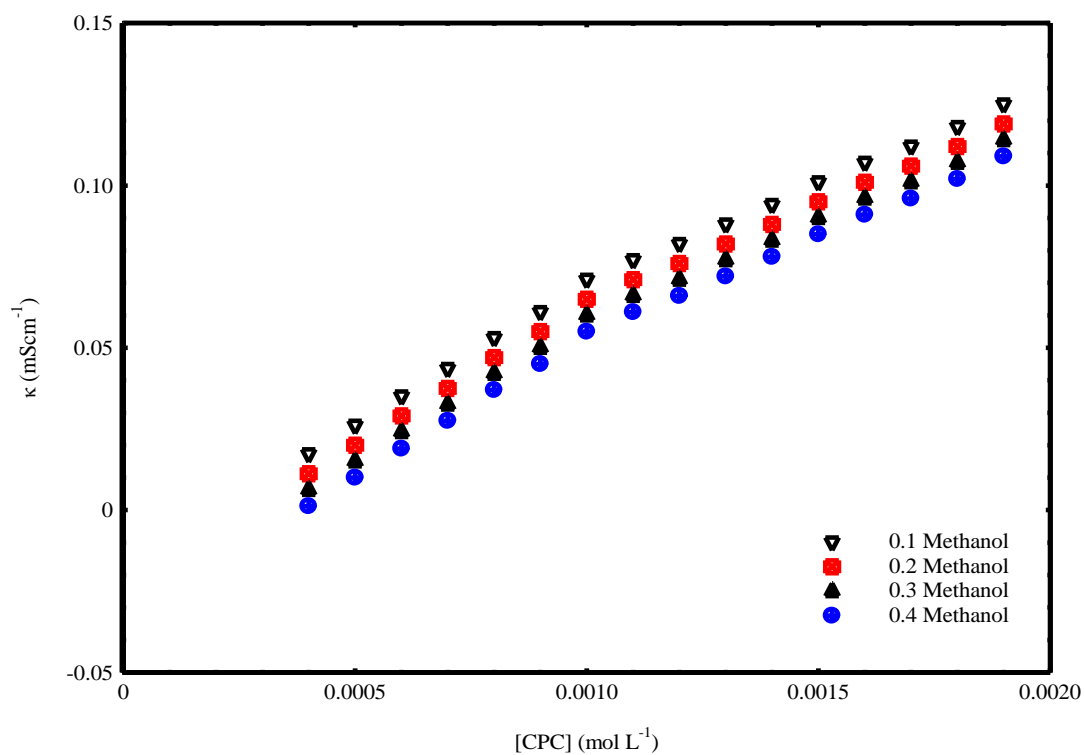


Figure 45: Plot of conductivity against [CPC] in absence of MR at 308.15 K

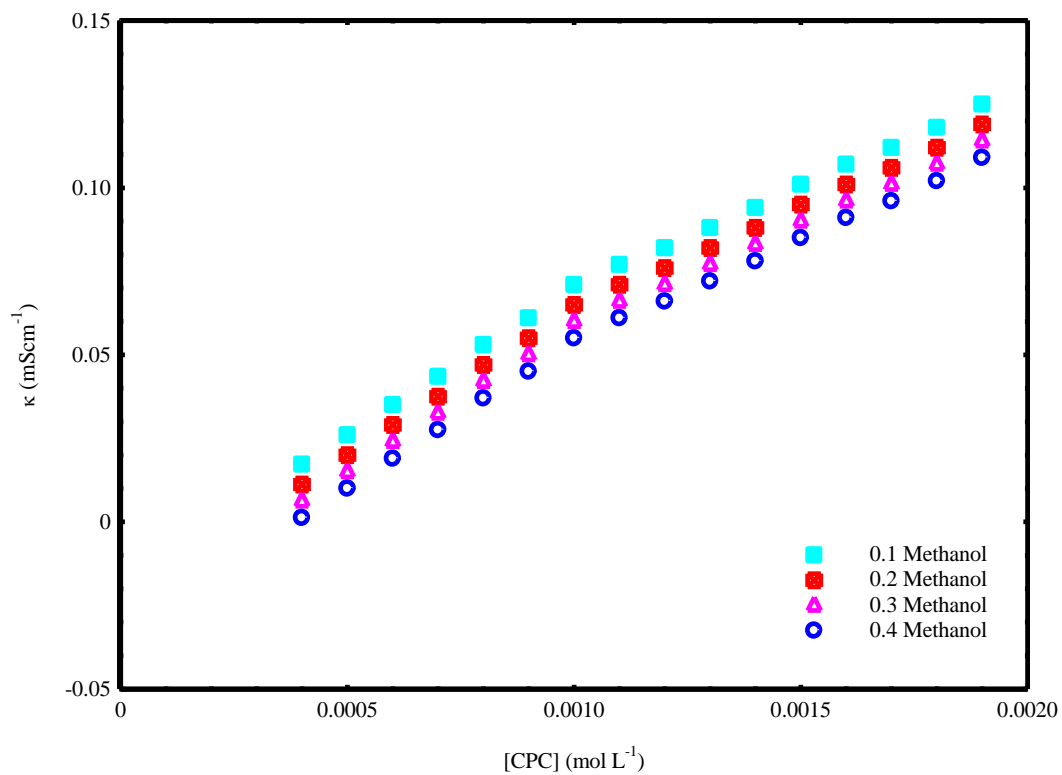


Figure 46: Plot of conductivity against [CPC] in absence of MR at 318.15 K

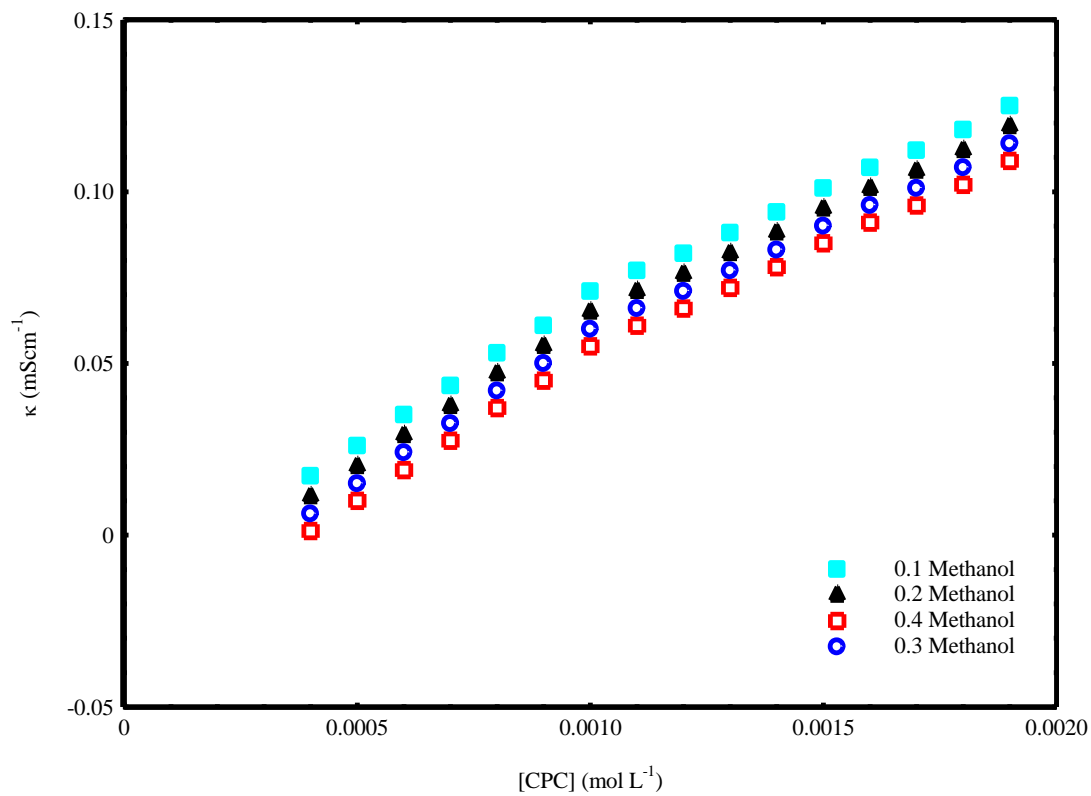


Figure 47: Plot of conductivity against [CPC] in presence of MR at 298.15 K

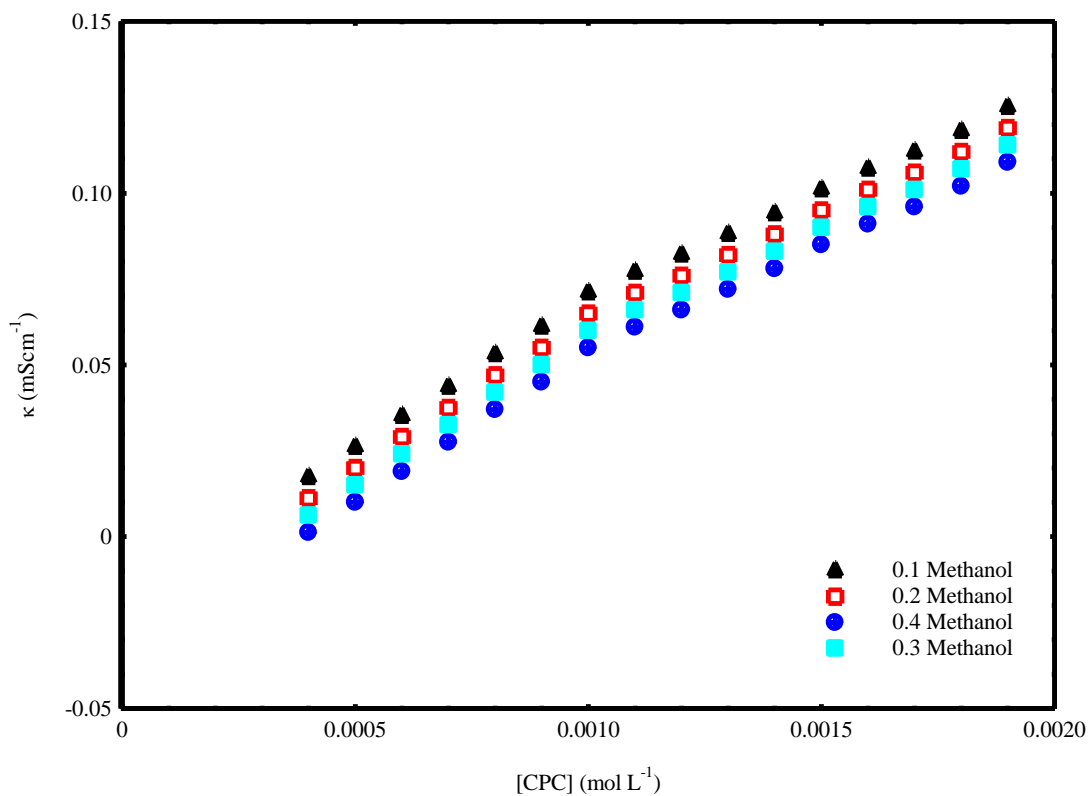


Figure 48: Plot of conductivity against [CPC] in presence of MR at 308.15 K

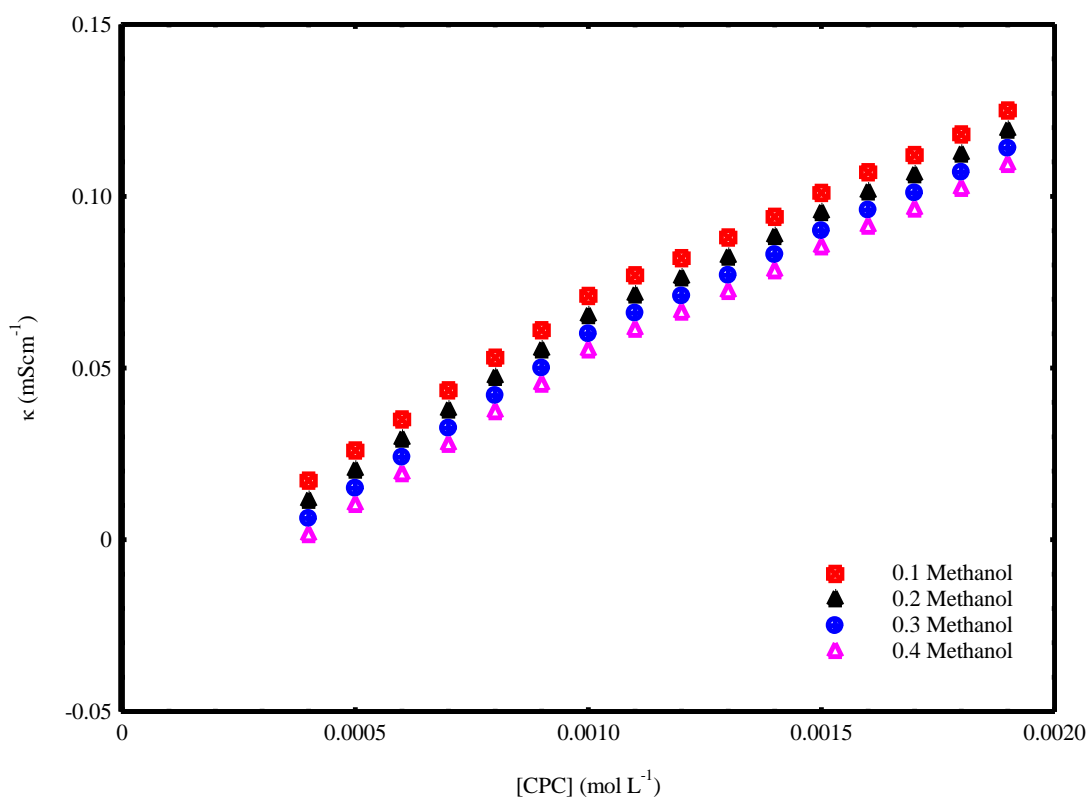


Figure 49: Plot of conductivity against [CPC] in presence of MR at 318.15 K

4.1.6. Surface tension studies and its related surface properties of DTAB and CPC in presence of MR

The surfactant has aggregation properties which reduce the surface tension on limiting values 30-40 mN m⁻¹, dependent on the chemical structure of it. The addition of external additives such as azo dye MR suppressed the micellization properties of aggregation substances. The critical concentration to form micelle is called CMC and is the most significant micellization property. The CMC value is decreased in presence of azo dye (Shah *et al.*, 2021) but increase with increase in volume of alcohol (Bhattarai *et al.*, 2017; Shah *et al.*, 2016).

Determination of CMC in presence of MR by surface tension method is presented in **Figs. 50 and 51**. CMC values of DTAB and CPC are listed in **Table 9**. Surface tension values of DTAB and CPC solutions in 0.10, 0.20, 0.30 and 0.40 volume fractions of methanol were plotted versus the surfactant's concentration to determine the CMC values at 298.15 K, 308.15 K and 318.15 K temperatures [**Figs. 52 to 57**]. It has been seen that CMC of DTAB is almost eighteen times higher than CPC. It is due to smaller size of hydrophobic tail of DTAB which shows lesser hydrophobic effect than that of CPC with larger hydrophobic tail (Sachin *et al.*, 2019). As surfactant shows both hydrophilic and hydrophobic interactions, it is highly utilized in multiple purposes. It is environmentally friendly due to significant molecular mechanisms to interact with additives (Shah *et al.*, 2020).

The variation in the pre-micellar slope $\left(\frac{d\gamma}{d \log C}\right)$ of DTAB and CPC in the presence of methyl red with volume fraction of methanol is tabulated in **Tables 10 and 11** obtained from **Figs 52 to 57**. With increasing methanol volume fraction, the slopes' negative values diminish, which shows that the surfactants' surface activity has decreased. This results is due to changes in the medium's hydrophobicity as well as dielectric constant (Mukherjee *et al.*, 2013; Niraula *et al.*, 2018). By using slope, Gibb's isotherm can be used to calculate the maximum surface excess concentration at the air/methanol-water interface, Γ_{\max} (Mukherjee *et al.*, 2013):

$$\Gamma_{\max} = -\frac{1}{2.303nRT} \left[\frac{d\gamma}{d \log C} \right]_{T,P} \quad (4-14)$$

where γ denotes the surface tension, R denotes the universal gas constant (8.314 J mol⁻¹ K⁻¹), T is the absolute temperature, C denotes the surfactant concentration and

$\left(\frac{d\gamma}{d\log C}\right)$ denotes the slope of the γ against $\log C$ plot taken at CMC. The constant n is a pre-factor that is taken as 2 for the traditional surfactant, where the surfactant ion and the center line are univalent.

The area covered for each surfactant molecule (A_{\min}) at the mixed methanol-water interface can be determined using **Equation (4-15)**,

$$A_{\min} = 1/N_A \Gamma_{\max} \quad (4-15)$$

where N_A denotes Avogadro's number.

Solubilisation of the surfactant molecules gets to the most extreme diminish in surface tension, which is shown by a parameter π_{CMC} called surface pressure. π_{CMC} is a measurement of the effectiveness of the surfactant by lowering the surface tension in the utilized solvent and is determined using **Equation (4-16)** as,

$$\pi_{\text{CMC}} = \gamma_o - \gamma_{\text{CMC}} \quad (4-16)$$

where γ_o and γ_{CMC} are the water's surface tension and surfactant solution at the CMC, respectively.

As obtained in the data, the surface excess concentration, Γ_{\max} , diminishes with increased volume fraction of methanol. This outcome is brought about by a decrease in the medium's dielectric constant and an increase in the hydrophobic effect. These elements induce the population of surfactant molecules to decline from the solvent's surface and spread throughout the bulk (Shah *et al.*, 2016). Due to the lesser concentration of DTAB and CPC molecules on the superficial or surface region, the minimum surface area, A_{\min} , increases and the surface pressure, π_{CMC} , diminishes with an increasing volume fraction of methanol (Niraula *et al.*, 2018).

This shows that the ion-pair of dye-surfactant covers more surface area at the mixed system interface than that of the surfactant alone. Additionally, the new nonionic surfactant with the bigger head group is equivalent to the dye-surfactant ion pair, which is created by electrostatic interaction, and as a result, a greater surface area per surfactant results in a lower CMC of the ion-pair surfactant (Borges *et al.*, 2017). In the presence of the dye, the values of π_{CMC} increased, indicating that dye surfactant ion pairs (DSIP) are more efficient in reducing the surface tension.

At interface, the standard free energy interfacial adsorption ($\Delta G_{\text{ads}}^{\circ}$) can be determined from the **Equation (4-17)** (Das *et al.*, 2013) as

$$\Delta G_{\text{ads}}^{\circ} = \Delta G_{\text{m}}^{\circ} - \frac{\pi_{\text{CMC}}}{\Gamma_{\text{max}}} \quad (4-17)$$

The efficiency of the surfactant to be adsorbed, or spontaneous adsorption at the surface, is indicated by a higher negative value of $\Delta G_{\text{ads}}^{\circ}$. In this experiment, it was discovered that the $\Delta G_{\text{ads}}^{\circ}$ values were less negative as the volume fraction of methanol increased, indicating poor spontaneity of surfactant molecule adsorption on the surface. However, in the presence of dye, the values of $\Delta G_{\text{ads}}^{\circ}$ turns more negative, demonstrating that the adsorption process is far more spontaneous than it is in the absence of dye.

The parameter $\text{p}C_{20}$, which is expressed in terms of the negative logarithm of C_{20} (where C_{20} is the concentration of surfactant needed to reduce the surface tension of the pure solvent by 20 mN m⁻¹), is crucial for defining how effectively a surfactant reduces surface tension. Using π_{CMC} and Γ_{max} , the value of $\text{p}C_{20}$ has been determined (Zhang *et al.*, 2017) from **Equation (4-18)** as

$$\text{p}C_{20} = \frac{\pi_{\text{CMC}} - 20}{2.303nRT\Gamma_{\text{max}}} - \log \text{CMC} \quad (4-18)$$

The $\text{p}C_{20}$ values derived from **Equation (4-18)** correlate well with $-\log C_{20}$ (result not shown), where C_{20} is the realistic concentration of surfactant solution whose corresponding surface tension value is lower than that of the methanol-water mixed solvent by 20 mN m⁻¹. The higher $\text{p}C_{20}$ value, which is determined by the medium's hydrophobicity, indicates greater adsorption effectiveness (Gompper & Schick, 2007). The $\text{p}C_{20}$ value falls as the volume fraction of methanol increases, meaning that the adsorption at the interface reduces as the population of surfactants in the bulk phase rises (Das *et al.*, 2013). With the addition of dye, surfactant effectiveness is observed to increase due to the creation of closely packed dye surfactant ion pairs (DSIP). DSIP functions as a nonionic surfactant, which is typically more effective than ionic surfactants (Shah *et al.*, 2020).

According to Israelachvili (Shah *et al.*, 2020), the packing parameter, P, is a significant parameter that predicts the shape of the micelle aggregation and may be calculated using the relation

$$P = \frac{V_o}{A_{min}l_c} \quad (4-19)$$

where V_o denotes the volume of exclusion per monomer during aggregation, as explained in Tanford's formula (Pan *et al.*, 2012; Ruiz *et al.*, 2008). $V_o = [27.4 + 26.9 n_c] \text{ \AA}^3$ and $l_c = [1.54 + 1.26 n_c] \text{ \AA}$ shows the maximum chain length and n_c denotes the total number of carbon atoms present in the alkyl chain.

From **Table 10 and 11** the P values are less than $1/3$ in presence of dye; therefore, all the aggregates shape are spherical. On increment in the volume fraction of methanol in water, the P values are diminished (Shah *et al.*, 2020). This indicates that micellar aggregates get smaller with the addition of methanol (Shah *et al.*, 2016). The P values also reduce in presence of dye due to the complex formation of a ion pair of dye-surfactant (Niraula *et al.*, 2018).

Table 9: The CMC values of DTAB and CPC using Surface tension method and viscosity method

Temperature(K)	Volume fraction of Methanol	CMC (mM)			
		DTAB		CPC	
		Surface Tension	Viscosity	Surface Tension	Viscosity
298.15	0.1	16.8	16.67	0.97	0.9
	0.2	19.8	19.94	1.04	1.0
	0.3	23.4	23.45	1	1.0
	0.4	31.9	33.33	1.11	1.1
308.15	0.1	17.1	17.17	1.16	1.14
	0.2	20.1	20.22	1.1	1.0
	0.3	24.9	23.71	1.12	1.1
	0.4	33.0	34.33	1.1	1.12
318.15	0.1	18.8	18.62	1.21	1.2
	0.2	21.2	21.0	1.3	1.3
	0.3	27.1	27.2	1.34	1.35
	0.4	34.5	34.62	1.39	1.4

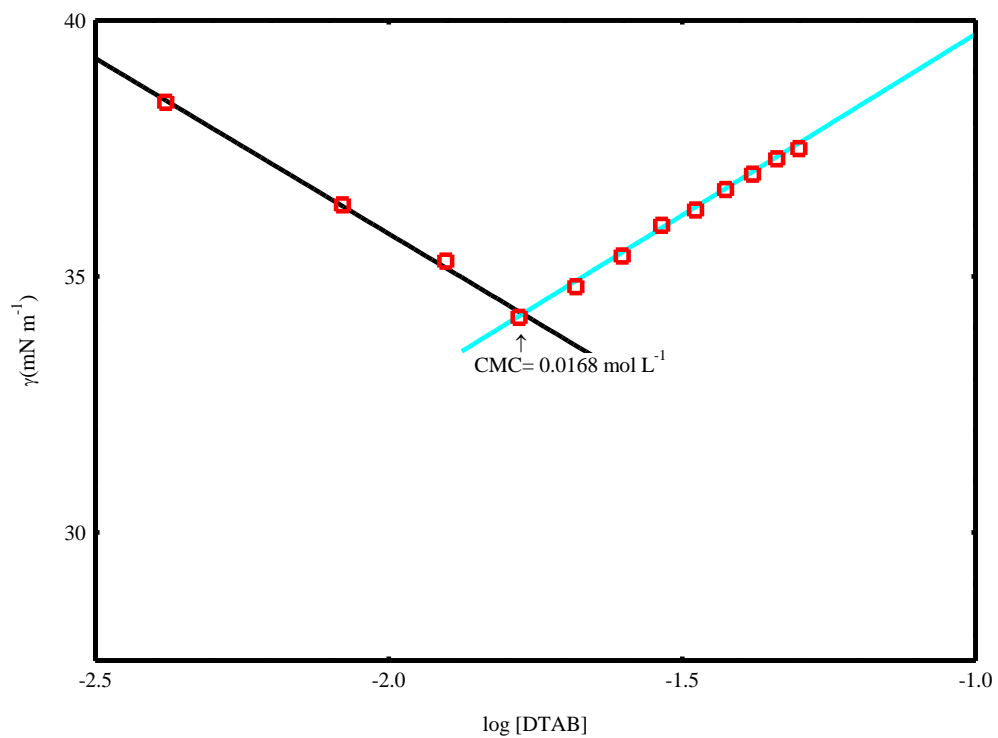


Figure 50: Plot of surface tension versus $\log[\text{DTAB}]$ with MR in 0.1 volume fraction of methanol at 298.15 K

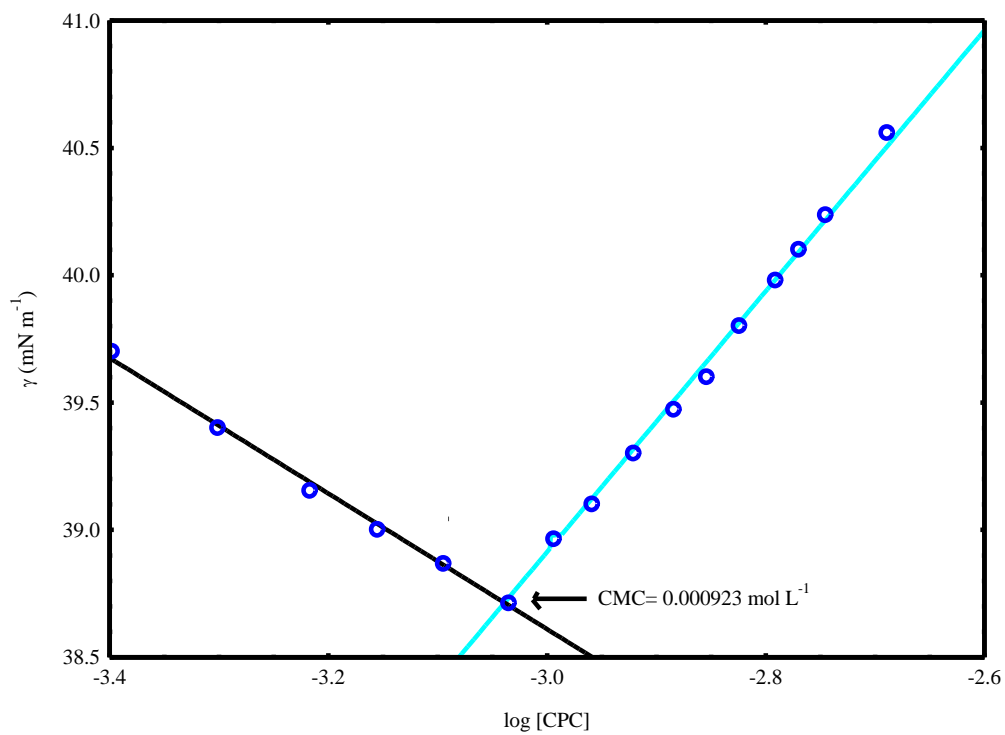


Figure 51: Plot of surface tension versus $\log[\text{CPC}]$ with MR in 0.1 volume fraction of methanol at 298.15 K

Table 10: The values of $\frac{dy}{d \log C}$, T_{\max} , A_{\min} , Π_{cmc} , P , $\Delta G_{\text{ads}}^{\circ}$ and pC_{20} of DTAB in the presence of MR in different volume fractions of methanol at 298.15 K, 308.15 K and 318.15 K.

Temperature (K)	volume fraction of Methanol	$\frac{dy}{d \log C}$	$\Gamma_{\max} 10^6$ (mol m ⁻²)	A_{\min} (Å ² molecule ⁻¹)	π_{cmc} (mN m ⁻¹)	P	$\Delta G_{\text{ads}}^{\circ}$ (kJ mol ⁻¹)	pC_{20}
298.15	0.1	-24.01	2.10	78.96	21.99	0.27	-45.76	1.77
	0.2	-15	1.31	126.39	13.53	0.17	-43.99	1.70
	0.3	-9	0.78	210.66	7.67	0.10	-40.78	1.63
	0.4	-7	0.61	270.85	3.72	0.07	-33.69	1.49
308.15	0.1	-22	1.86	89.07	20.37	0.23	-45.73	1.76
	0.2	-13	1.10	150.73	12.20	0.14	-44.27	1.69
	0.3	-6.5	0.55	301.46	6.55	0.07	-42.63	1.60
	0.4	-5.5	0.46	356.28	2.26	0.06	-32.21	1.48
318.15	0.1	-20.5	1.68	98.68	19.05	0.21	-45.56	1.72
	0.2	-11	0.90	183.92	11.08	0.11	-44.90	1.67
	0.3	-5	0.41	404.62	5.70	0.05	-34.68	1.56
	0.4	-3.7	0.30	546.79	1.52	0.04	-31.46	1.46

Table 11: The values of $d\gamma/d\log C$, T_{\max} , A_{\min} , Γ_{cmc} , P , $\Delta G_{\text{ads}}^{\circ}$ and pC_{20} of CPC in the presence of MR in different volume fractions of methanol at 298.15 K, 308.15 K and 318.15 K.

Temperature (K)	volume fraction of Methanol	$\frac{d\gamma}{d\log C}$	$\Gamma_{\max} 10^7$ (mol m ⁻²)	A_{\min} (Å ² molecule ⁻¹)	π_{cmc} (mN m ⁻¹)	P	$\Delta G_{\text{ads}}^{\circ}$ (kJ mol ⁻¹)	pC_{20}
298.15	0.1	-6.5	5.33	311.2	-41.86	0.07	-104.25	3.01
	0.2	-5.5	4.51	367.8	-40.83	0.06	-119.89	2.98
	0.3	-4.3	3.53	470.4	-39.93	0.04	-141.62	3.0
	0.4	-4.01	3.29	504.4	-39.02	0.04	-150.19	2.96
308.15	0.1	-6.2	5.09	326.2	-40.47	0.06	-103.17	2.98
	0.2	-5.2	4.27	389.0	-39.54	0.05	-122.50	2.96
	0.3	-4.01	3.29	504.4	-39.38	0.04	-150.00	3.0
	0.4	-3.8	3.12	532.3	-38.52	0.04	-158.46	2.96
318.15	0.1	-6.01	4.93	336.6	-38.6	0.06	-105.05	2.92
	0.2	-5.04	4.13	401.3	-37.6	0.05	-121.67	2.89
	0.3	-3.9	3.20	518.7	-36.74	0.04	-148.51	2.88
	0.4	-3.4	2.79	594.9	-35.85	0.03	-167.64	2.86

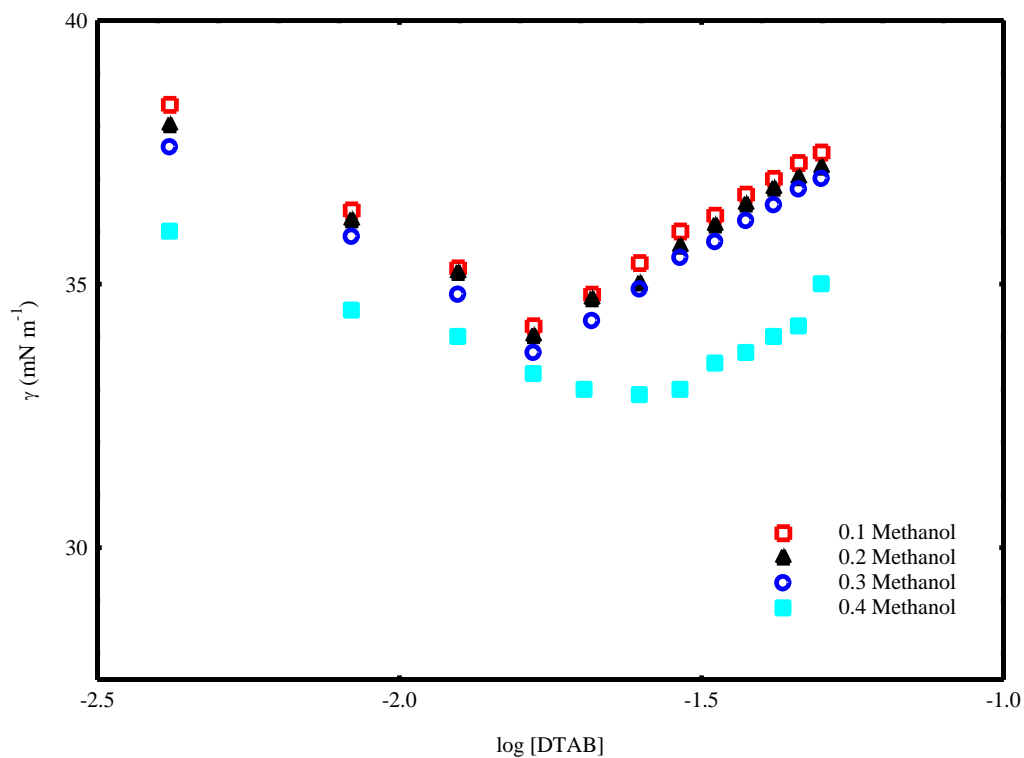


Figure 52: Plot of surface tension versus log[DTAB] with MR in four different volume fraction of methanol at 298.15 K

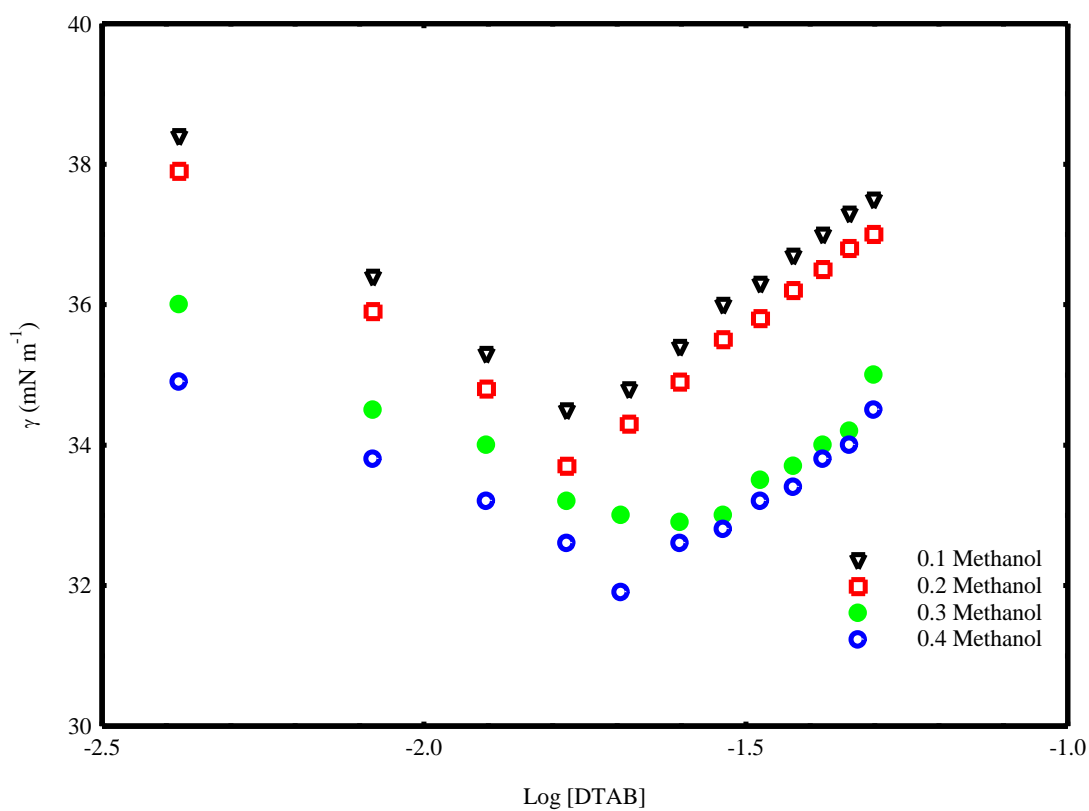


Figure 53: Plot of surface tension versus log[DTAB] with MR in four different volume fraction of methanol at 308.15 K

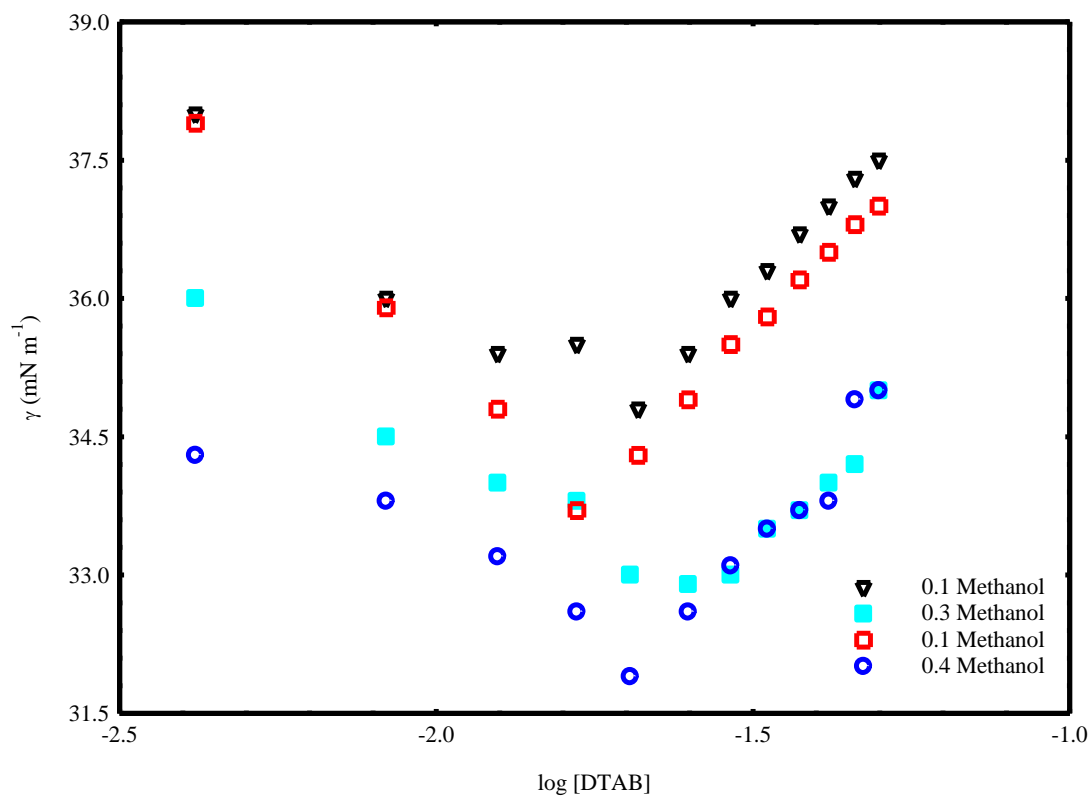


Figure 54: Plot of surface tension versus $\log[\text{DTAB}]$ with MR in four different volume fraction of methanol at 318.15 K

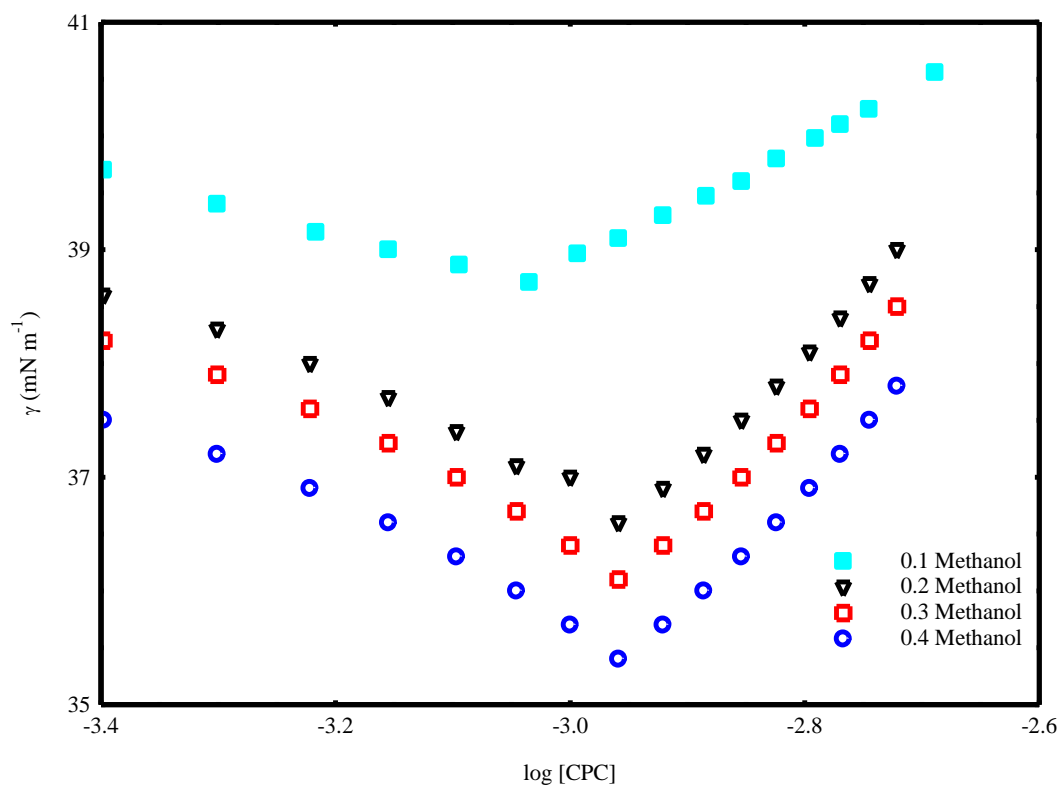


Figure 55: Plot of surface tension versus $\log[\text{CPC}]$ with MR in four different volume fraction of methanol at 298.15 K

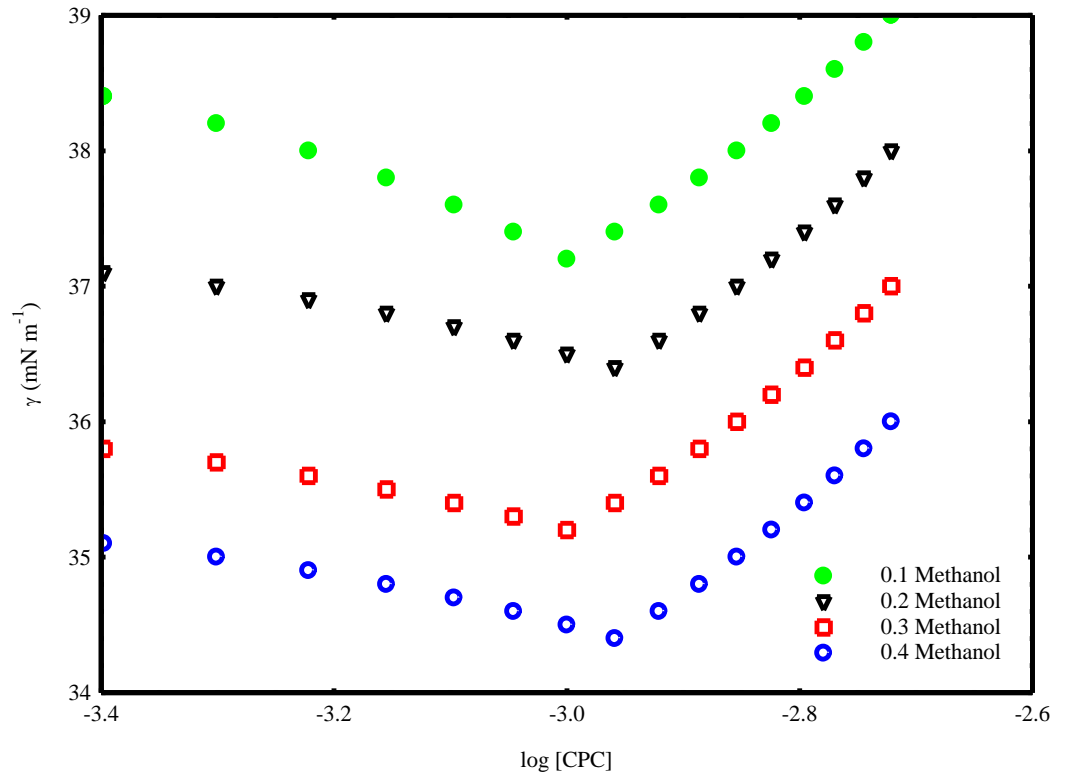


Figure 56: Plot of surface tension versus $\log[\text{CPC}]$ with MR in four different volume fraction of methanol at 308.15 K

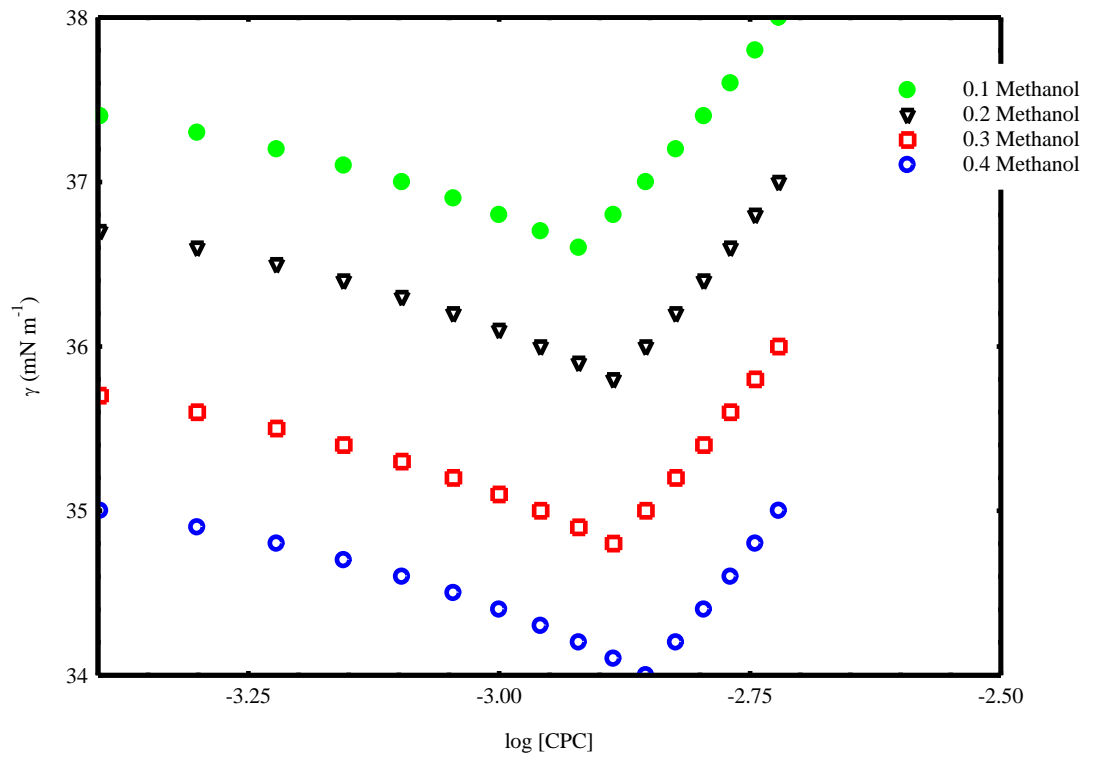


Figure 57: Plot of surface tension versus $\log[\text{CPC}]$ with MR in four different volume fraction of methanol at 318.15 K

4.1.7 Viscosity studies and its related properties of DTAB and CPC in presence of MR

Viscosity is the property of substance by virtue of which the flow of liquid molecules is resisted by the neighboring molecules. The nature of the solute and solvent interaction, is very crucial for describing the characteristics of the microemulsion as well as liquid crystal with regard to the micellar surfactant solution, is best understood through the study of viscosity (Bhattarai *et al.*, 2011; Niraula *et al.*, 2018). Due to two types of interactions solvent with solvophobic parts of surfactant molecules and solvent with solvophilic parts of surfactant molecules the interaction between the solvent and surfactants is of better interest in surfactant systems. The two interactions cause a change towards the liquid's viscous flow, which changes the liquid's numerous physiochemical properties (Shah *et al.*, 2016).

Variation of viscosity in presence of MR with concentration of DTAB and CPC solutions is depicted in **Figs. 58 and 59**, respectively. Plots of DTAB and CPC solutions at temperature, there is notable breakage known as CMC. The CMC values are presented in **Table 9** at 298.15 K, 308.15 K and 318.15 K. Viscosity fluctuation is almost constant at lower concentrations, or below CMC. However, there is a significant fluctuation in viscosity with surfactant solution concentration at higher concentrations, or above CMC. There is a linear variation. This demonstrates that the interaction between the solute and solvent is happening as the concentration rises. The increased frictional force between the solute as well as solvent is what is responsible for the viscosity increasing with concentration. The viscosity of the solution at a given temperature increases further with the addition of methanol. It can be accounted for by a reduction in the average distance between water and surfactant molecules, which results in a larger frictional force. It is also observed from **Figs. 60 to 65** that viscosity decreases with rise in temperature because as temperature rises, kinetic energy of molecules also rises which reduce the intermolecular force acting on the viscous flow with the net diminished frictional force (Maikokera & Kwaambwa, 2009; Niraula *et al.*, 2018).

The solute and solvent interaction is well studied in viscosity B coefficient by Jones-Dole equation of viscosity as shown in **Equation 4-20** (Shah *et al.*, 2016).

$$n_r = 1 + A\sqrt{c} + Bc \quad (4-20)$$

Where $n_r = n/n_0$ denotes the relative viscosity of a solution and A and B are constants. After rearranging the **Equation 4-20**

$$n_r - 1 = Bc + A\sqrt{c} \quad (4-21)$$

Here B coefficient represents interaction between solute and solvent and A coefficient denoted the electrostatic force of interions (Chandra *et al.*, 2013).

Plots of $n_r - 1$ against c for DTAB and CTAB solutions in mixed solvents in the range of post micellar region is shown in **Figs. 66 to 71** in which there are linear variations. The viscosity B coefficients are obtained from the slopes of these plots **Figs. 72 and 73**.

The differences of B values of DTAB and CPC in different volume fraction of methanol at three different temperatures are shown in **Figs. 72 and 73**, respectively.

Figs. 72 and 73 show that adding methanol and raising the temperature have a significant impact on the B values. B values rise with higher volume fractions while falling with higher temperatures. The greater contact between the solute and solvent is what causes the first effect. Methanol addition causes the solvent to become more hydrophobic, which causes the micelle to dissolve and increases the intermolecular force between the molecules of solvent and surfactant's tails. Thermal expansion that occurs as temperature rises is the cause of the effect of temperature. Lower B values show that as a result, the solute-solvent interaction weakens and the intermolecular force becomes less effective (Chandra *et al.*, 2013).

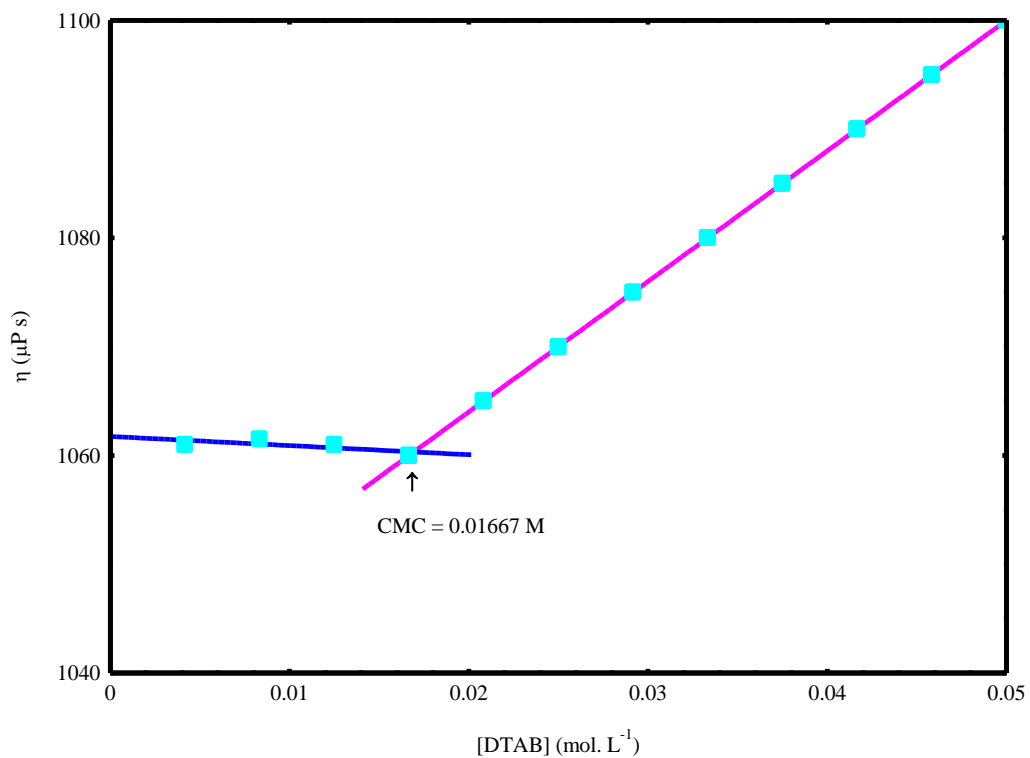


Figure 58: Plot of viscosity against DTAB concentration with MR in 0.1 volume fraction of methanol at 298.15 K

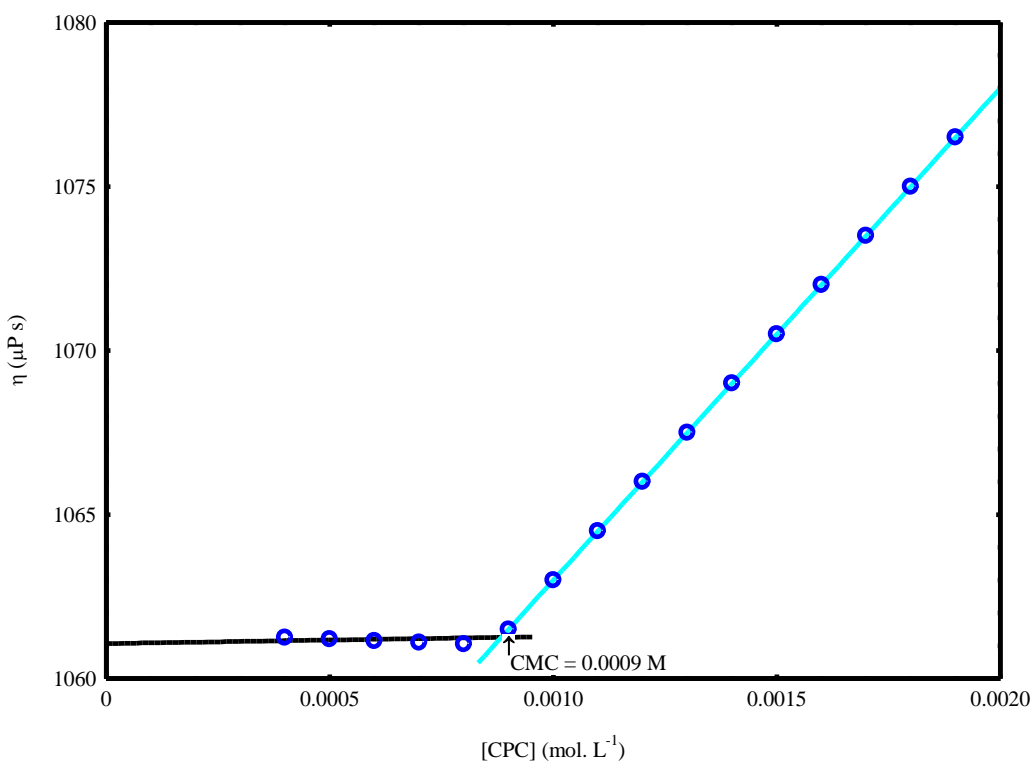


Figure 59: Plot of viscosity against CPC concentration with MR in 0.1 volume fraction of methanol at 298.15 K

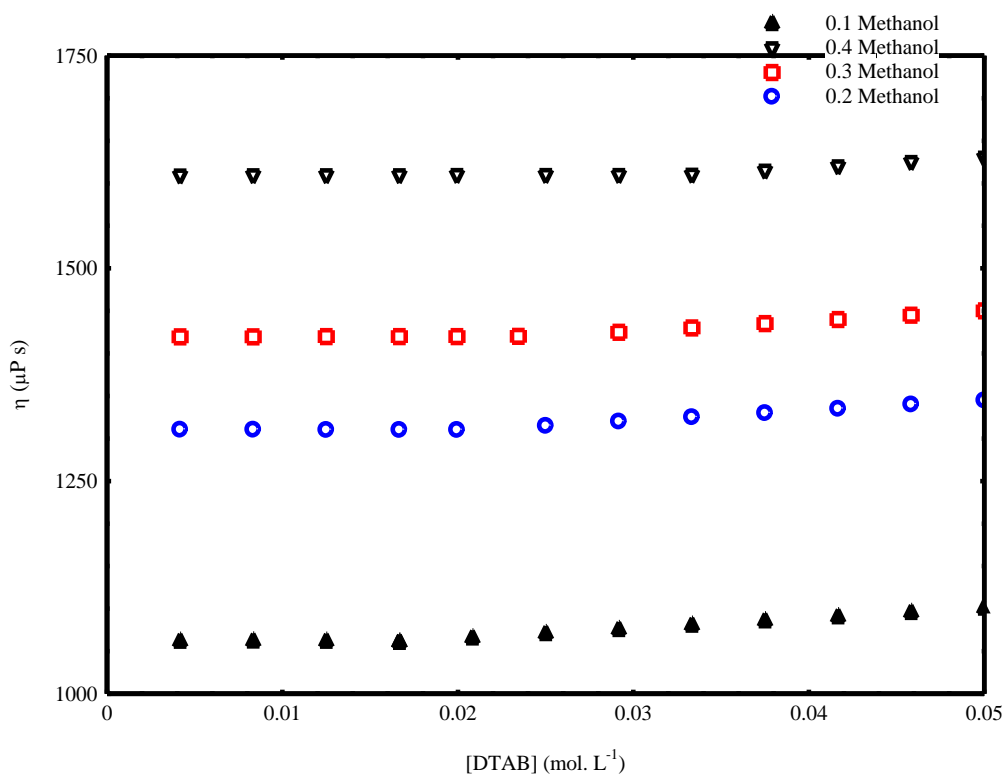


Figure 60: Plot of viscosity against DTAB concentration with MR in four different volume fractions of methanol at 298.15 K

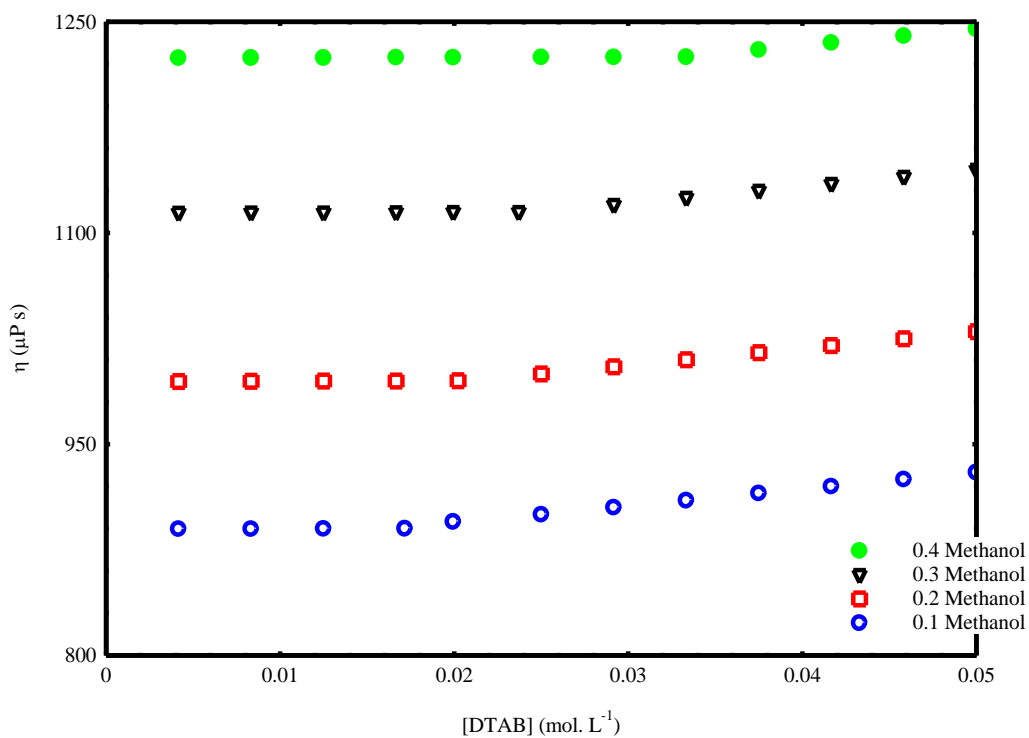


Figure 61: Plot of viscosity against DTAB concentration with MR in four different volume fractions of methanol at 308.15 K

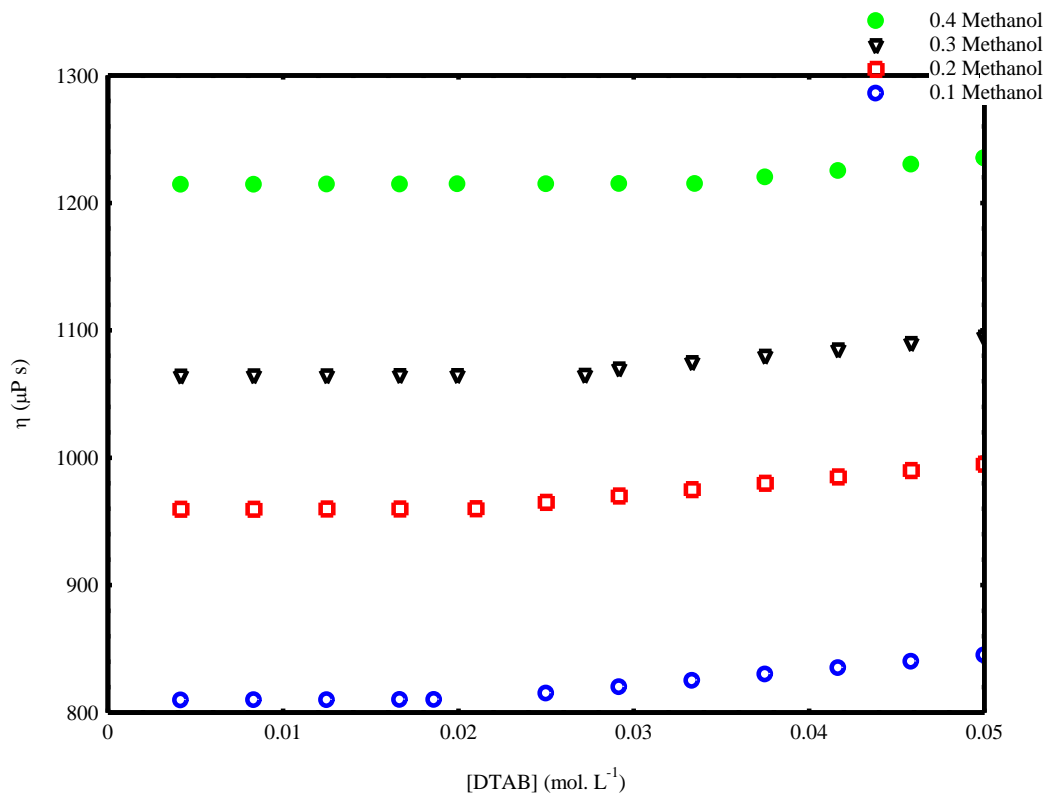


Figure 62: Plot of viscosity against DTAB concentration with MR in four different volume fractions of methanol at 318.15 K

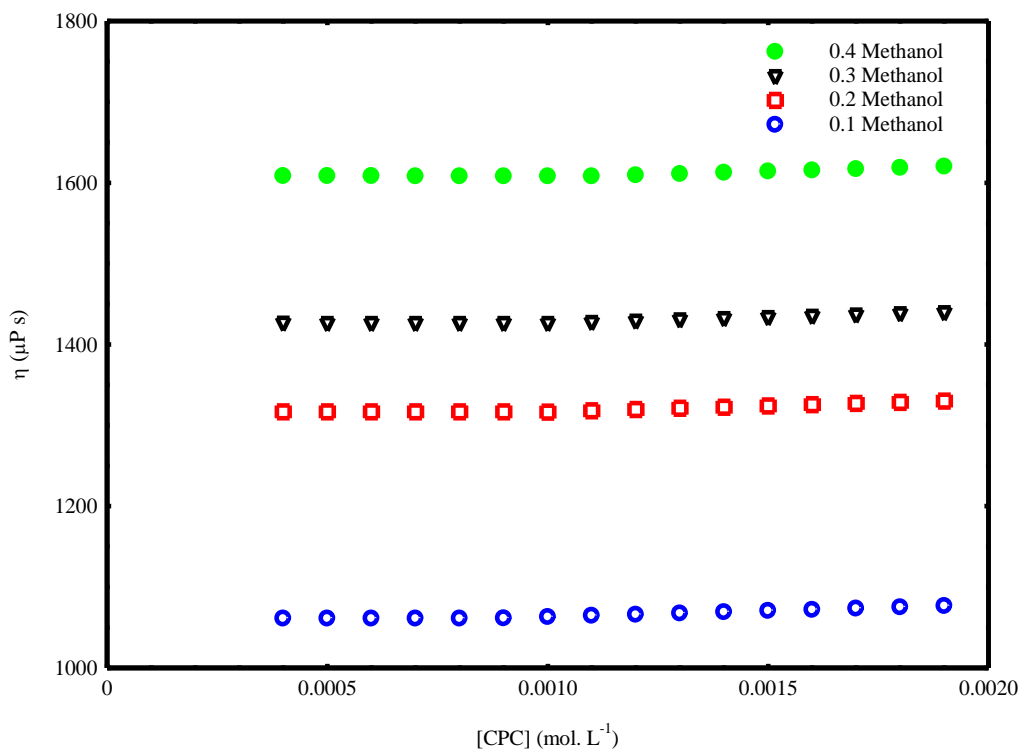


Figure 63: Plot of viscosity against CPC concentration with MR in four different volume fractions of methanol at 298.15 K

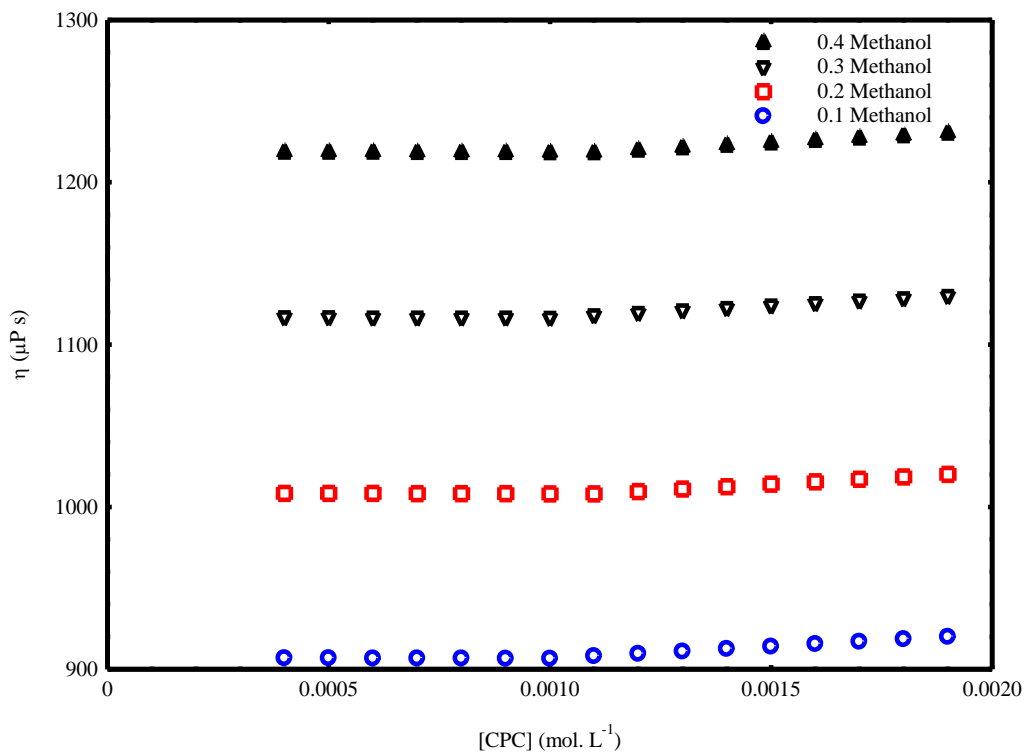


Figure 64: Plot of viscosity against CPC concentration with MR in four different volume fractions of methanol at 308.15 K

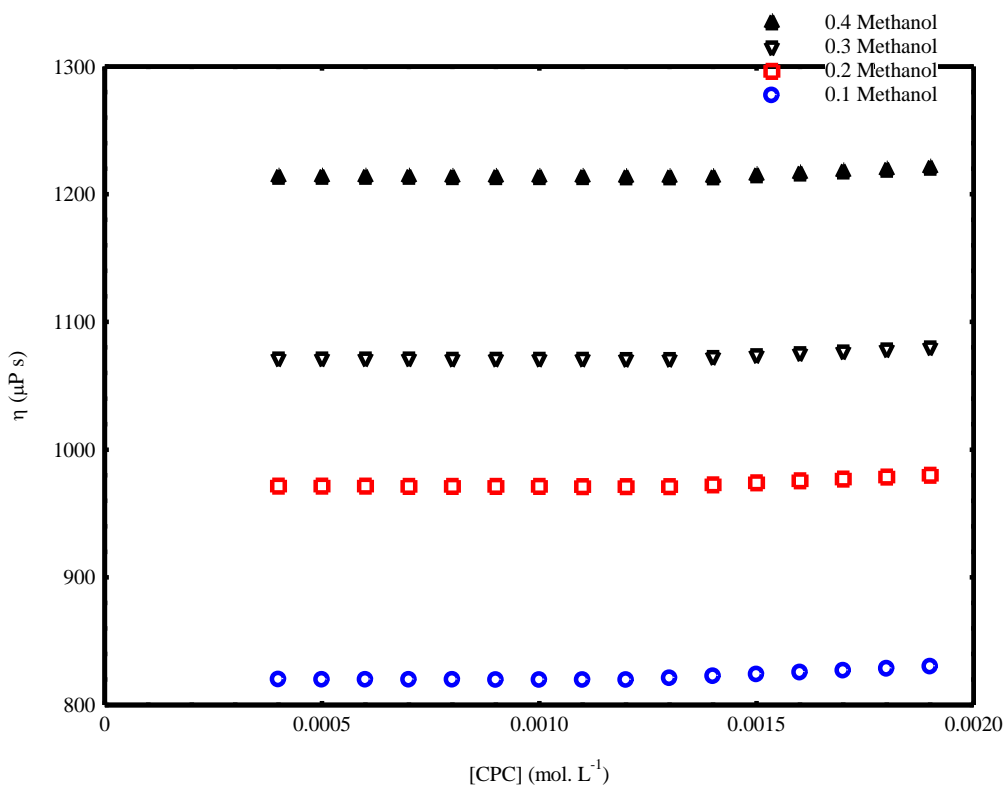


Figure 65: Plot of viscosity against CPC concentration with MR in four different volume fractions of methanol at 318.15 K

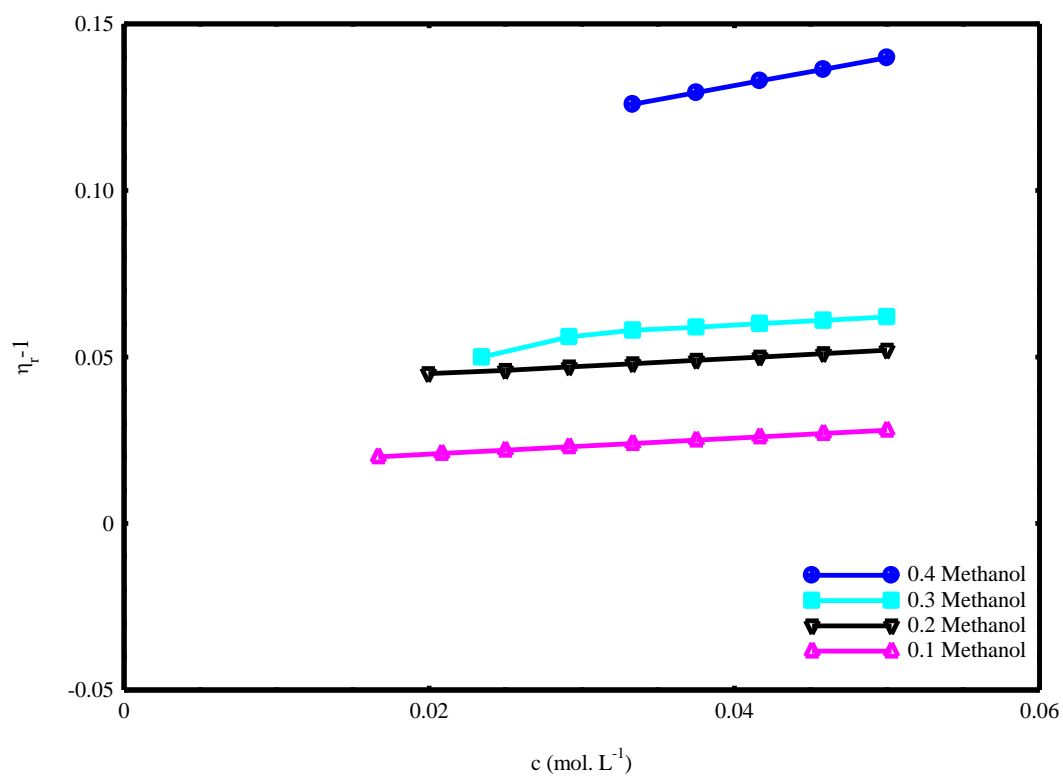


Figure 66: Plot of η_r^{-1} against c for DTAB with MR at 298.15 K

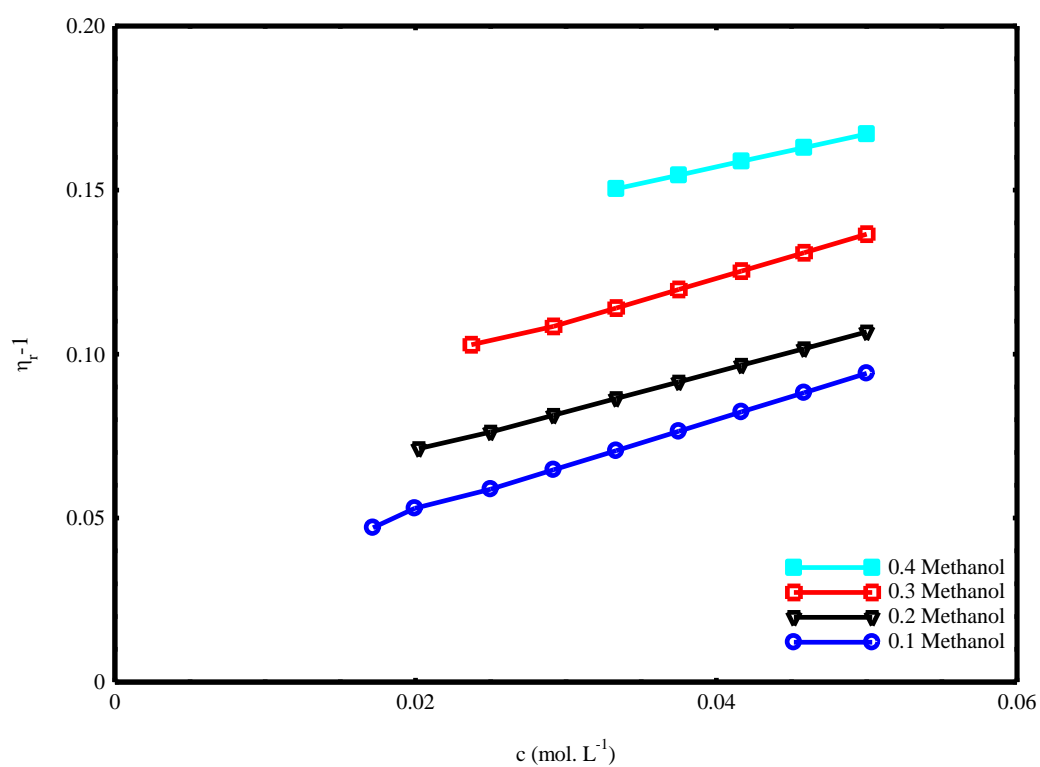


Figure 67: Plot of η_r^{-1} against c for DTAB with MR at 308.15 K

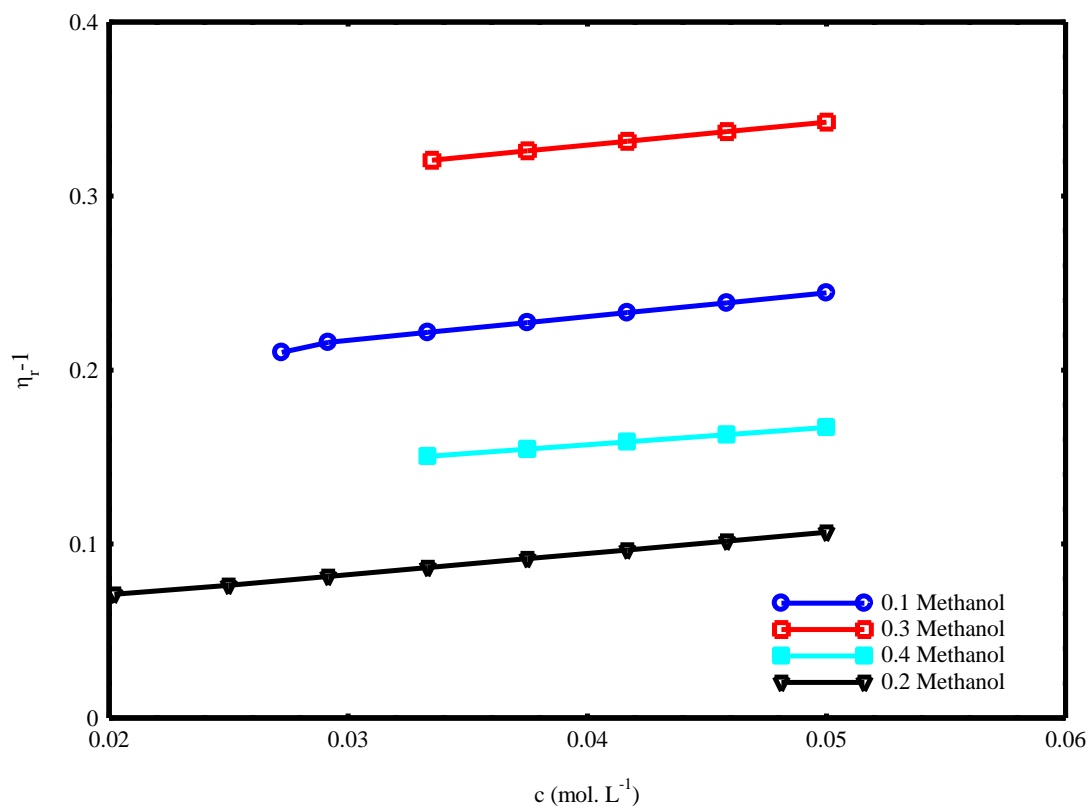


Figure 68: Plot of η_{r-1} against c for DTAB with MR at 318.15 K

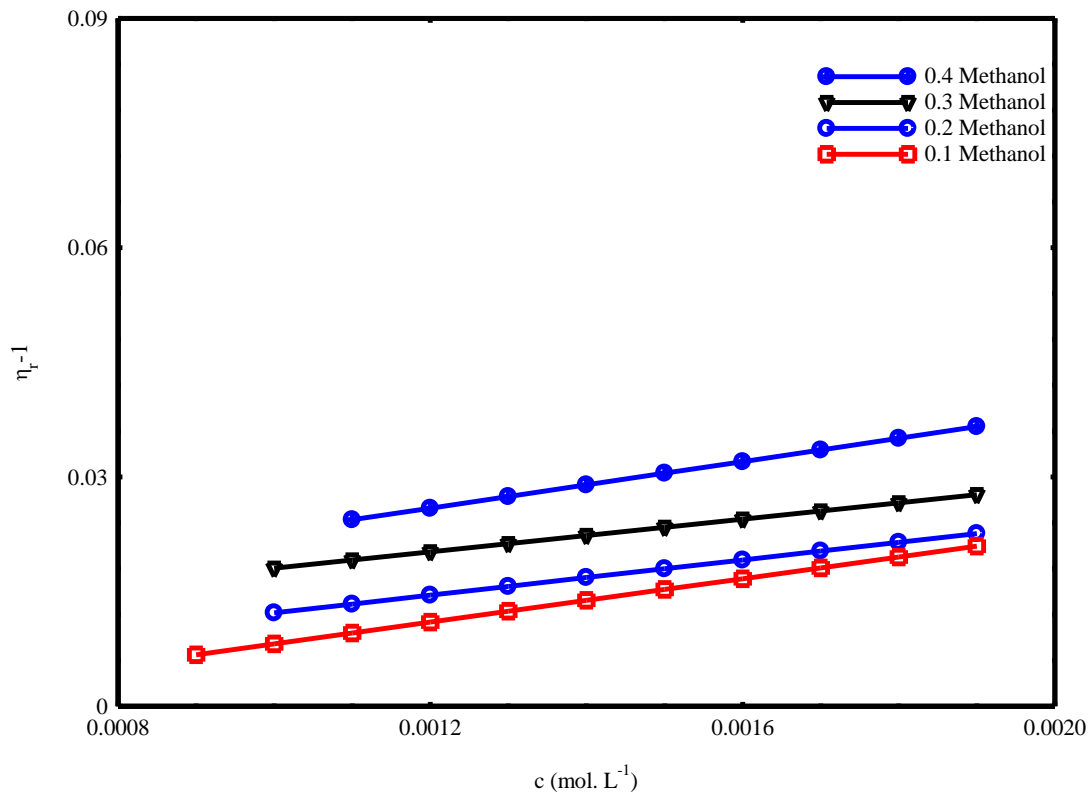


Figure 69: Plot of η_{r-1} against c for CPC with MR at 298.15 K

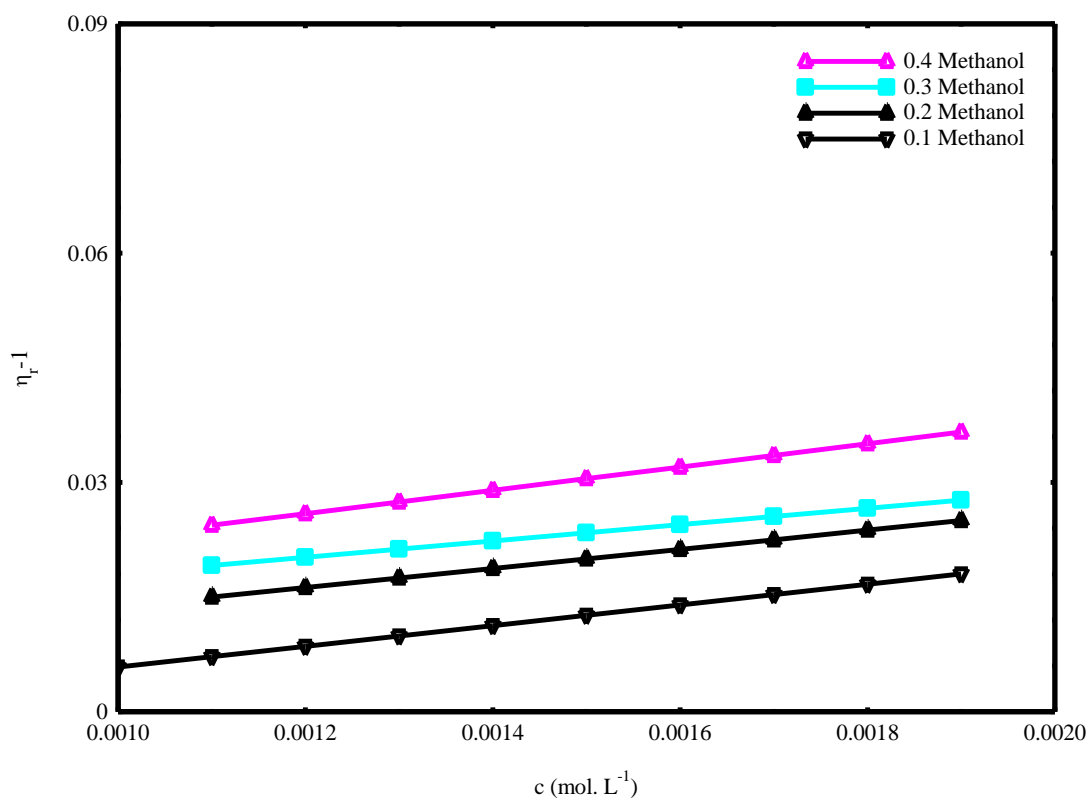


Figure 70: Plot of $n_r - 1$ against c for CPC with MR at 308.15 K

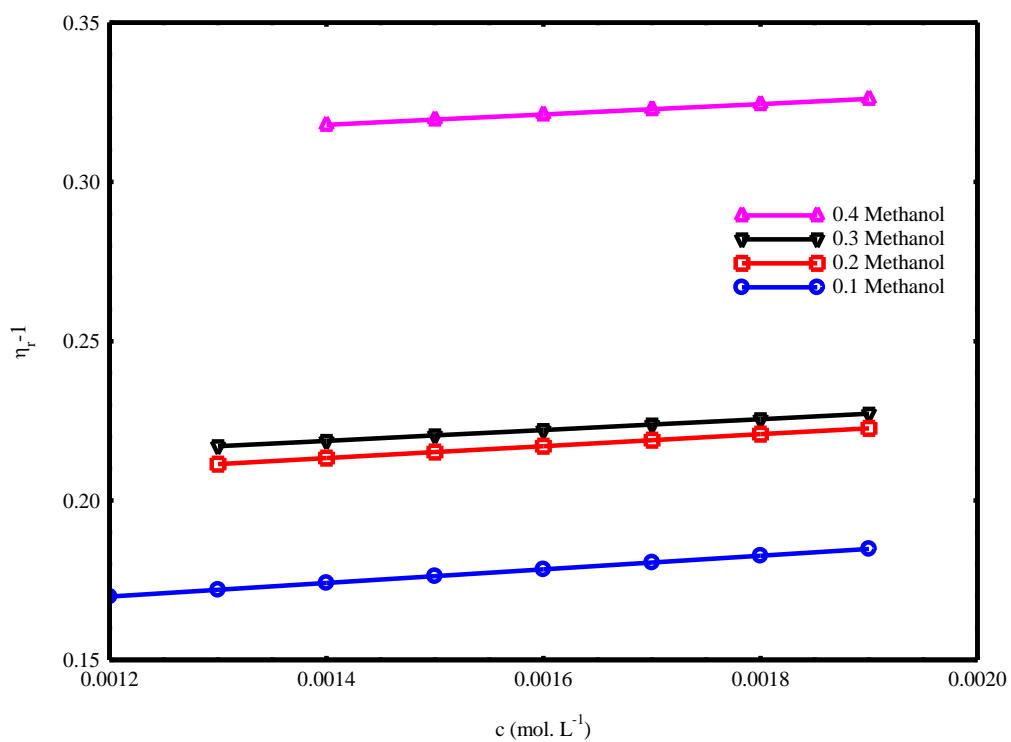


Figure 71: Plot of $n_r - 1$ against c for CPC with MR at 318.15 K

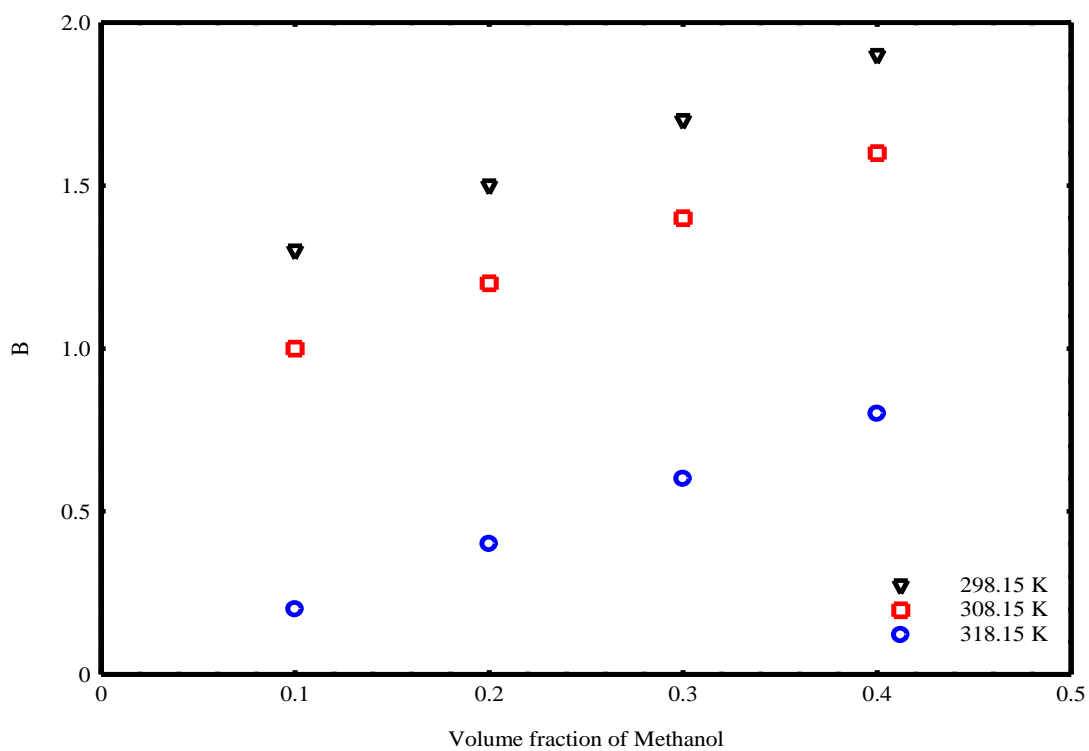


Figure 72: Viscosity B coefficients of DTAB with MR

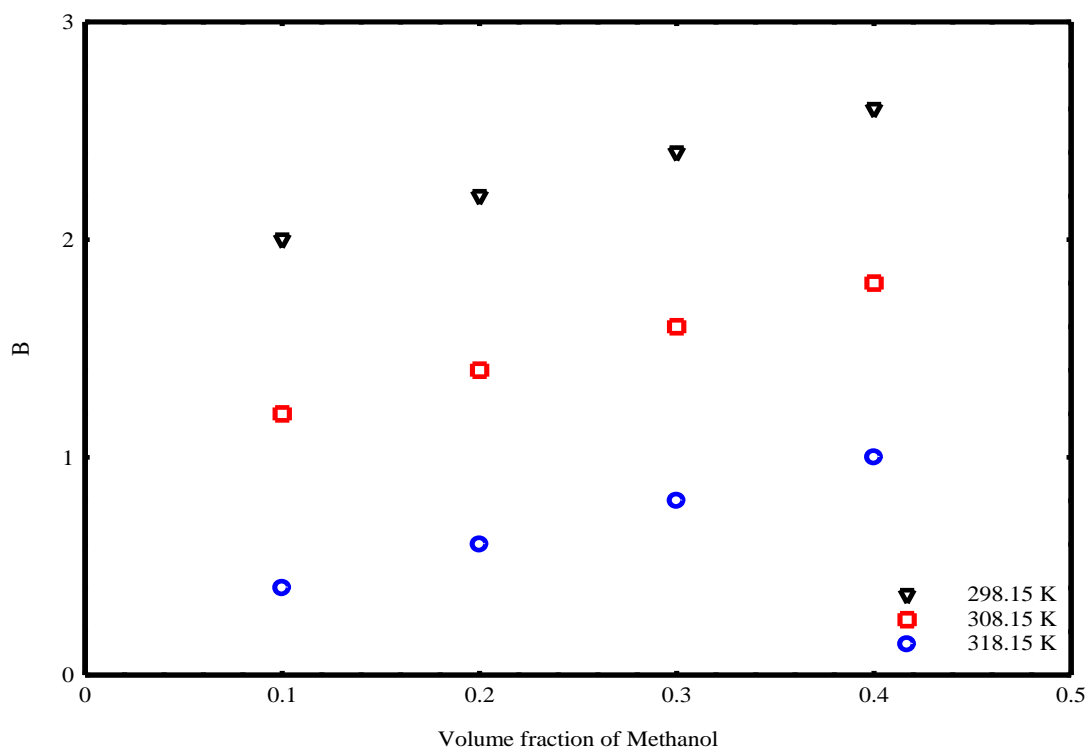


Figure 73: Viscosity B coefficients of CPC with MR

4.1.8 Study of pH of DTAB and CPC in presence of MR and its effects on interactions

The interaction between the azo dye MR and cationic surfactants DTAB and CPC is discussed in accordance with the effect of pH (Hari *et al.*, 2005). The effects are discussed in two regions i.e., below, and above CMC.

Below CMC: Protonation of azo dye occurs in an acidic region ranging pH 2-5 and due to electrostatic interactions between the charged azo dye and the surfactant monomer to form ion pairs will decrease. In accordance with this matter, the result is sorted by realizing the tautomerism of the dye as shown in **Figs. 74**.

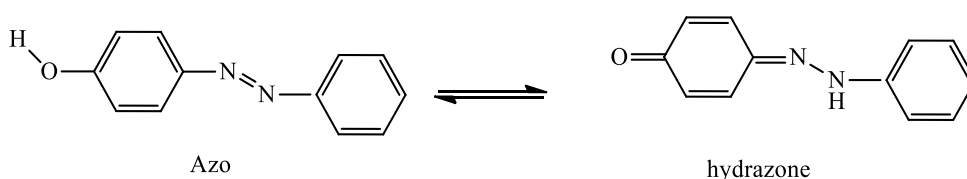


Figure 74: Tautomerism of azo dye

The azo dye consists of an azo group (-N=N-), which shifts to the hydroazo form during equilibrium in an acidic medium. However, in basic medium hydroazo form is shifted to the azo form in equilibrium (Prasad Tajpuriya *et al.*, 2021). For this methanol-water system, the value for ion pair formation was found to be at pH (5-8), as shown in **Figs. 75 and 82**.

Above CMC: The change in pH (7-8) did not affect the spectra and absorbance for the alcohol-water systems. The alteration in pH values was not affected by the solubilization of the dye into the micelle. The dye-surfactant complex is unaffected by pH variation, as discussed.

It is justified from the literature (Plutino *et al.*, 2017) that MR dye solution in aqueous solution showed red color at wavelength of maximum absorbance (λ_{\max}) 523 nm in acidic (hydrazone) form (pH = 2) and yellow color at wavelength of maximum absorbance (λ_{\max}) 431 nm in basic (azo) form (pH=8). In our case, it is obtained the pH of azo form due to unusual behavior of methyl red with CPC or DTAB and without CPC or DTAB in methanol mixed media. The only existing form did not allow us to see the isobestic points in the spectra **Figs. 9 to 16**.

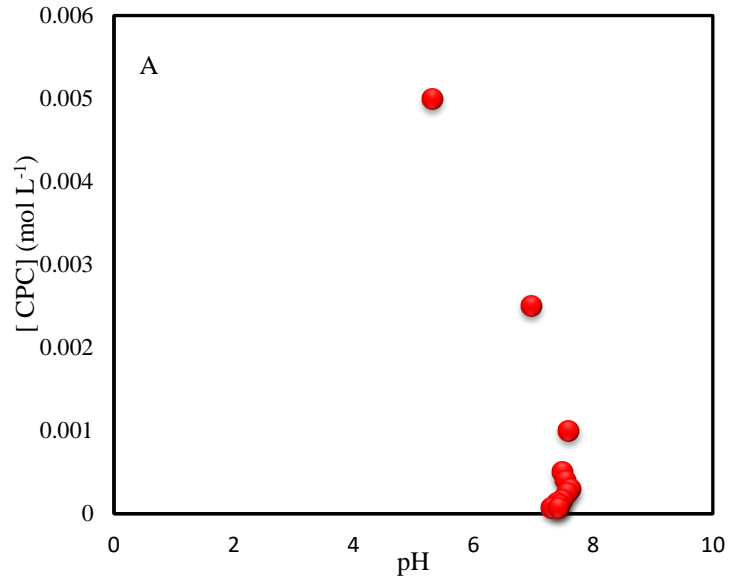


Figure 75: $[CPC]$ versus the pH profile. (A) 0.1 volume fraction of methanol

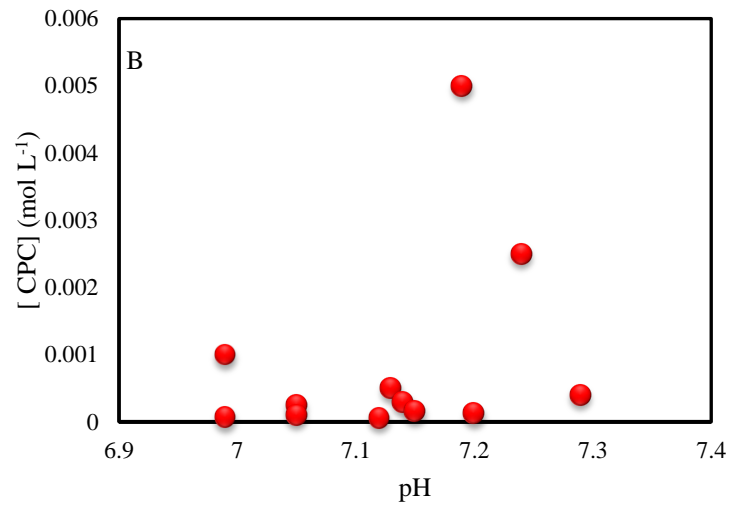


Figure 76: $[CPC]$ versus the pH profile. (B) 0.2 volume fraction of methanol

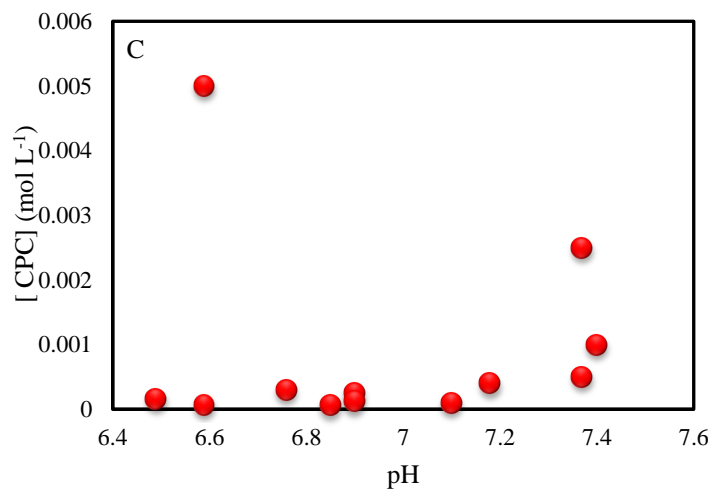


Figure 77: $[CPC]$ versus the pH profile. (C) 0.3 volume fraction of methanol

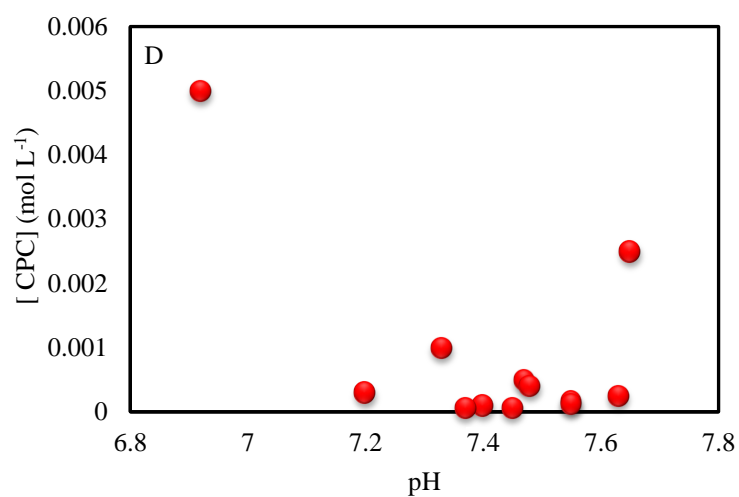


Figure 78: [CPC] versus the pH profile. (D) 0.4 volume fraction of methanol

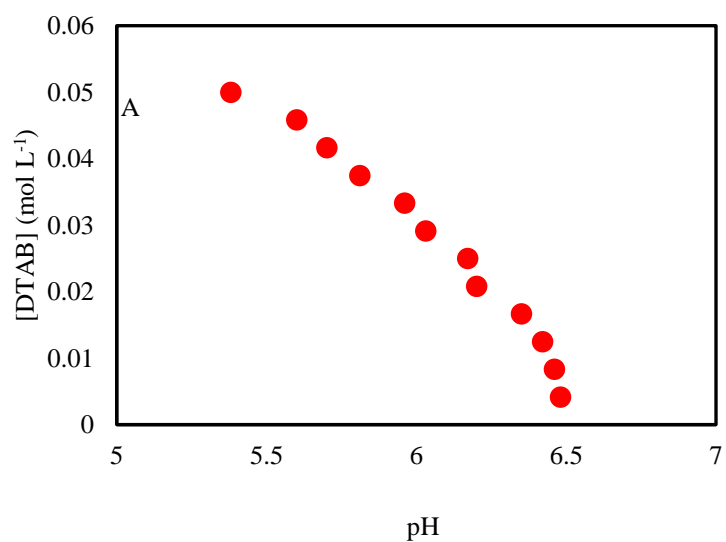


Figure 79: [DTAB] versus the pH profile. (A) 0.1 volume fraction of methanol

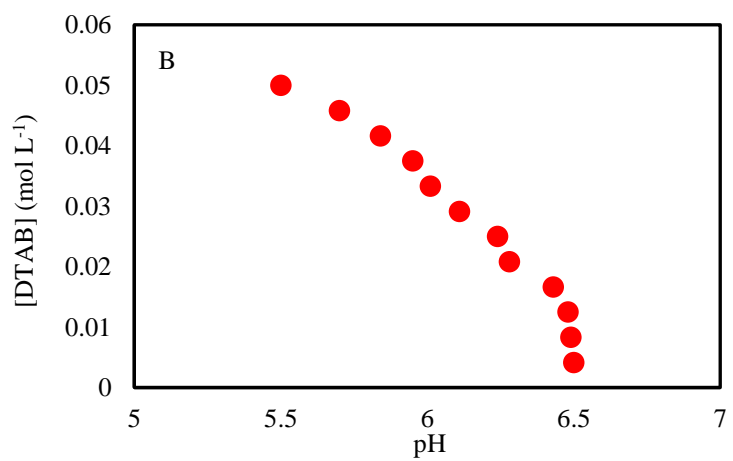


Figure 80: [DTAB] versus the pH profile. (B) 0.2 volume fraction of methanol

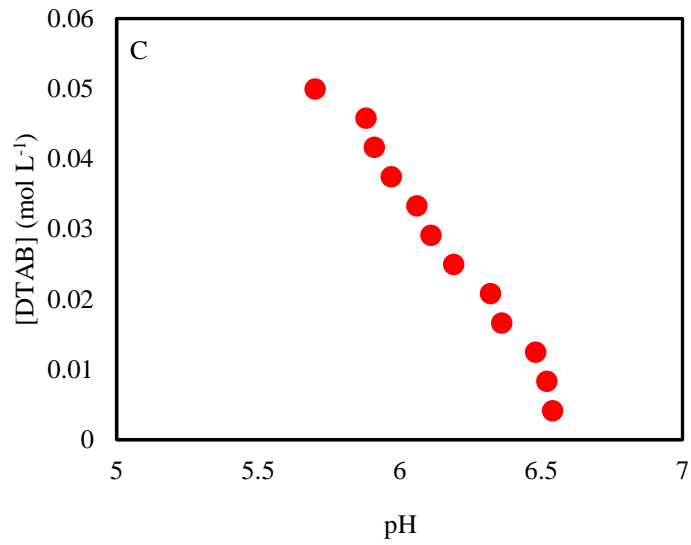


Figure 81: [DTAB] versus the pH profile.(C) 0.3 volume fraction of methanol

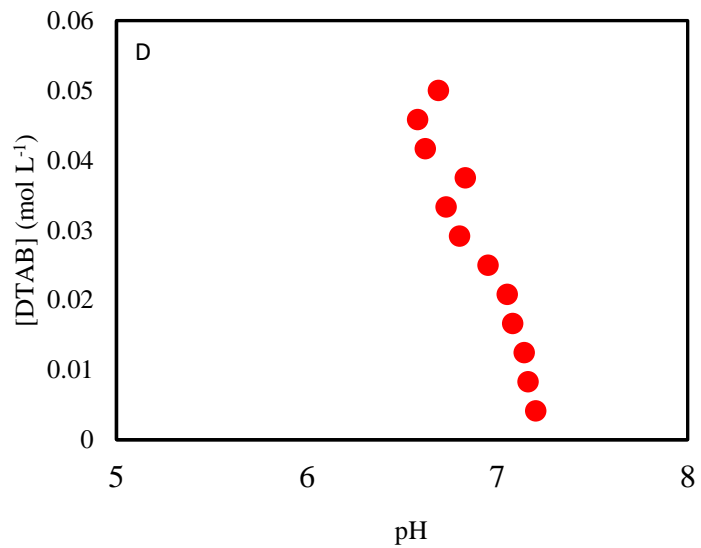


Figure 82: [DTAB] versus the pH profile. (D) 0.4 volume fraction of methanol

4.2. Anti-corrosion ability of DTAB and CPC

4.2.1 Weight loss study

The weight loss study allows the determination of several corrosion parameters (Free *et al.*, 2004; Janati *et al.*, 2020) by means of the mathematical equation given below. The corrosion rate (CR) of mild steel investigated was calculated with the following relation (Gupta, Kafle, *et al.*, 2020):

$$\text{Corrosion rate (CR)} = \frac{W}{S t} \quad (4-22)$$

where W denotes average weight loss of metal samples, S denotes the total area of corroding metal and t denotes the time of immersion. From the corrosion rate, the corrosion inhibition efficiency will be estimated. Using estimated corrosion rate, the inhibition efficiency (IE) of DTAB and CPC of the corrosion of MS has been determined as follows (Karthik *et al.*, 2014):

$$\text{IE(\%)} = (r_0 - r)/r_0 \times 100 \quad (4-23)$$

where r_0 and r denote the values of the corrosion rate in absence and presence of inhibitor, respectively.

The corroding rate and inhibition behaviour of mild steel with the addition of DTAB and CPC in 0.5 M H₂SO₄ of various concentrations at 298.15 K are shown in **Figs. 83 and 84** and **Figs. 85 and 86**, respectively. The curves in **Figs. 83 and 84** show that the corrosion rate values (g cm⁻² hr⁻¹) of MS in 0.5 M H₂SO₄ solution with DTAB and CPC decrease as the concentrations of the corrosion inhibitor (DTAB and CPC) increase. **Figs. 85 and 86** display the corrosion inhibition efficiency rises with the raised cationic surfactant concentrations (DTAB and CPC). As values included in **Table 12**, the inhibition efficiency is highest at the CMC concentrations of DTAB (0.01637 M) and CPC (0.00098 M) due to significant role of micelles on adsorption process (Bhattarai *et al.*, 2017). The CMC is the special quality of surfactant playing important role in adsorption at the interfaces. Since at the critical concentration, the surfactant molecules coagulate to form micelle of monolayer and after the CMC concentration, multi-layered molecules of micelles are generated (Malik *et al.*, 2011). Due to such phenomenon, the inhibition efficiency is highest for DTAB at 98.85% and for CPC at 98.08%. These values are the best result for confirming the suitable corrosion inhibitor for controlling corrosion.

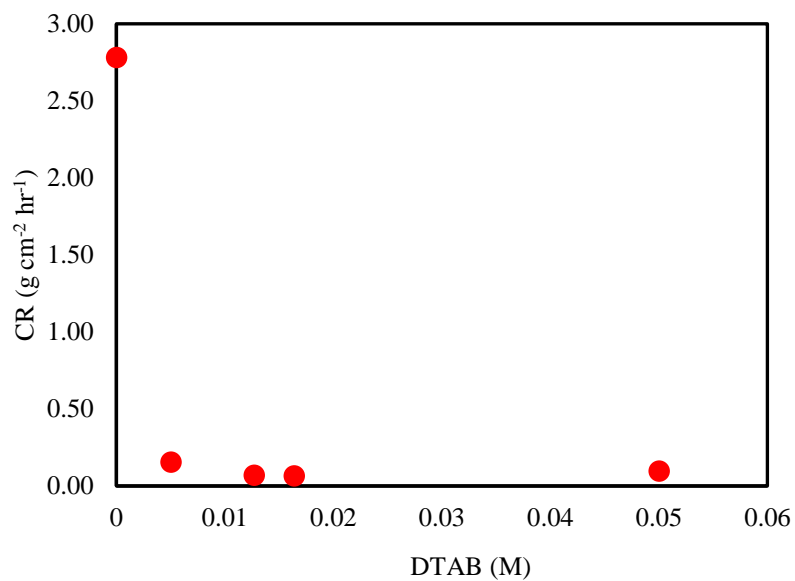


Figure 83: Variation of corrosion rate of different concentrations of DTAB at 298.15 K

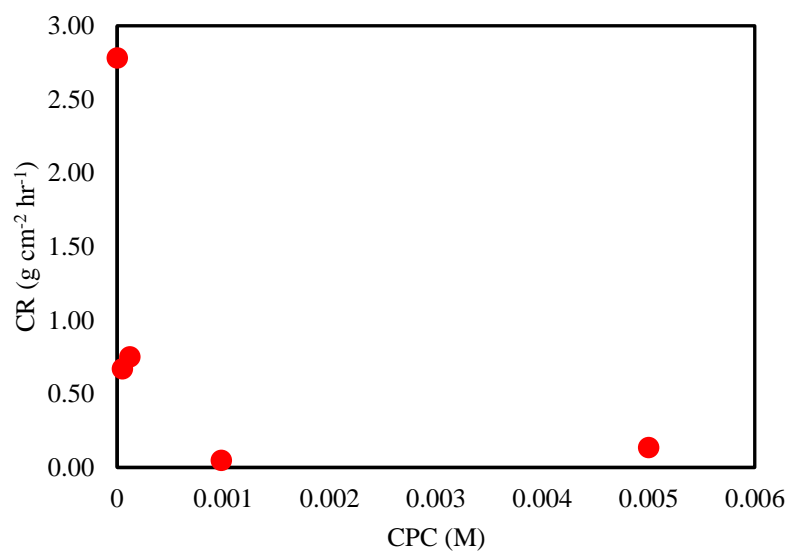


Figure 84: Variation of corrosion rate of different concentrations of CPC at 298.15 K

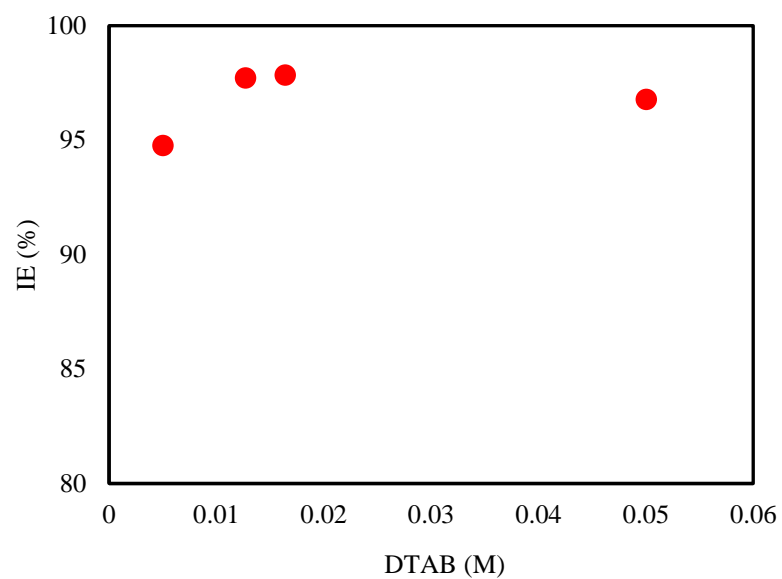


Figure 85: Variation of inhibition efficiency of different concentrations of DTAB at 298.15 K

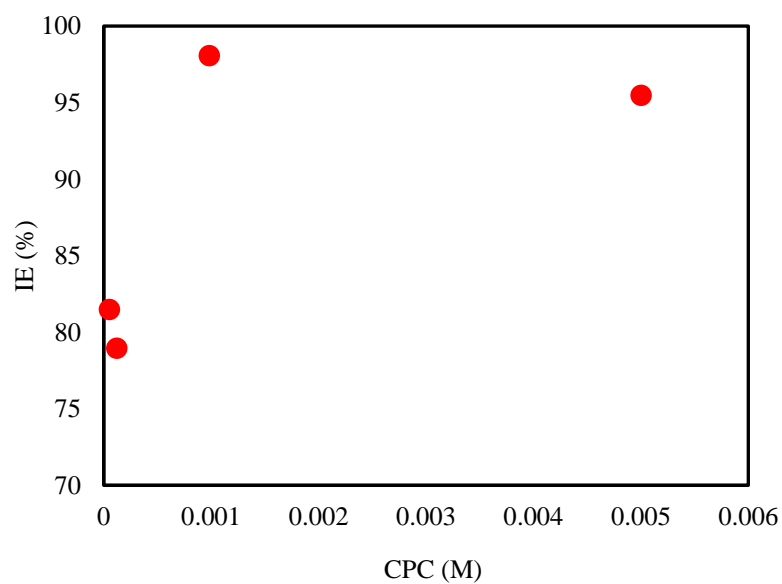


Figure 86: Variation of inhibition efficiency of different concentrations of CPC at 298.15 K

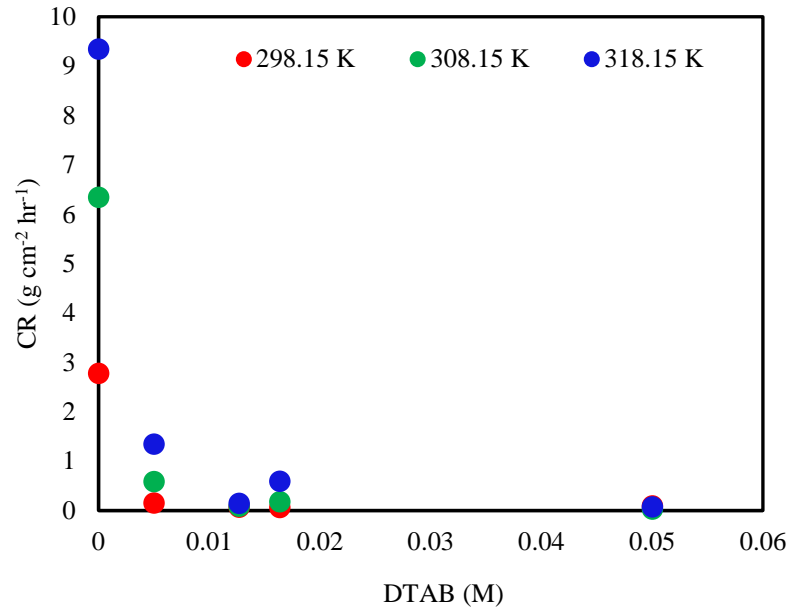


Figure 87: Variation of corrosion rate of different concentrations of DTAB at three different temperatures.

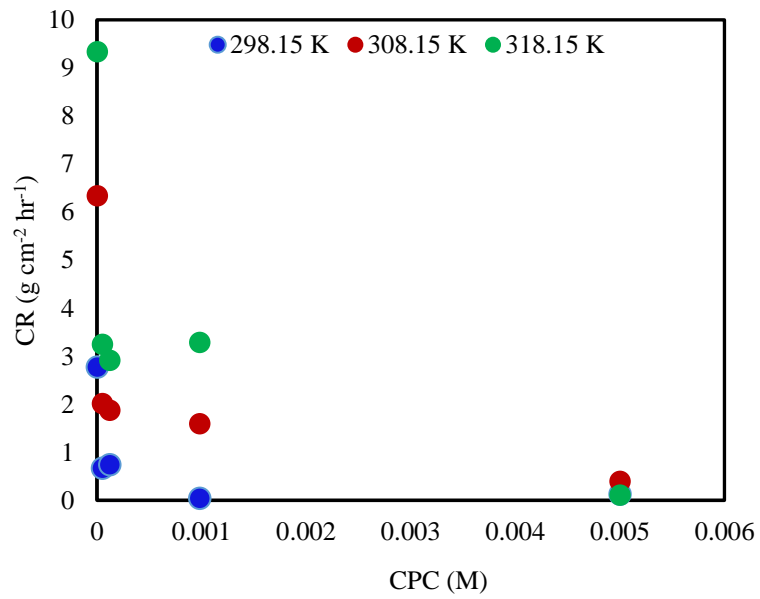


Figure 88: Variation of corrosion rate of different concentrations of CPC at three different temperatures.

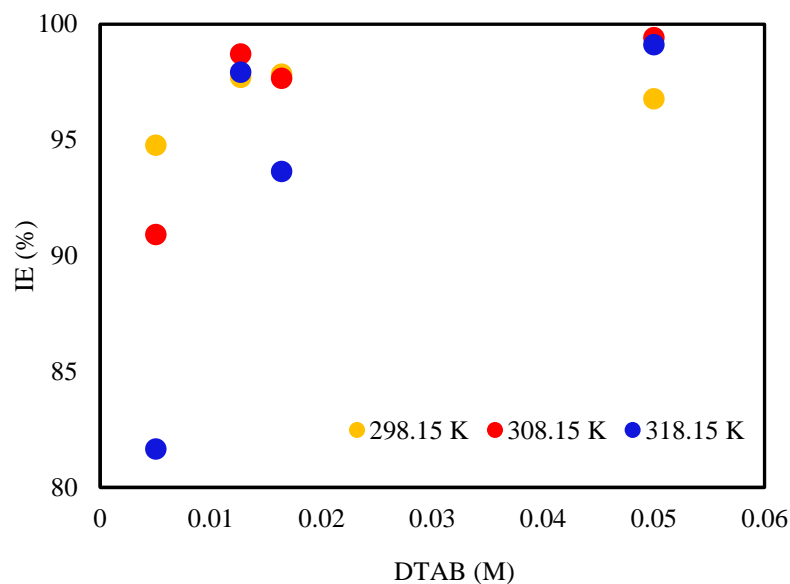


Figure 89: Variation of inhibition efficiency of different concentrations of DTAB at three different temperatures.

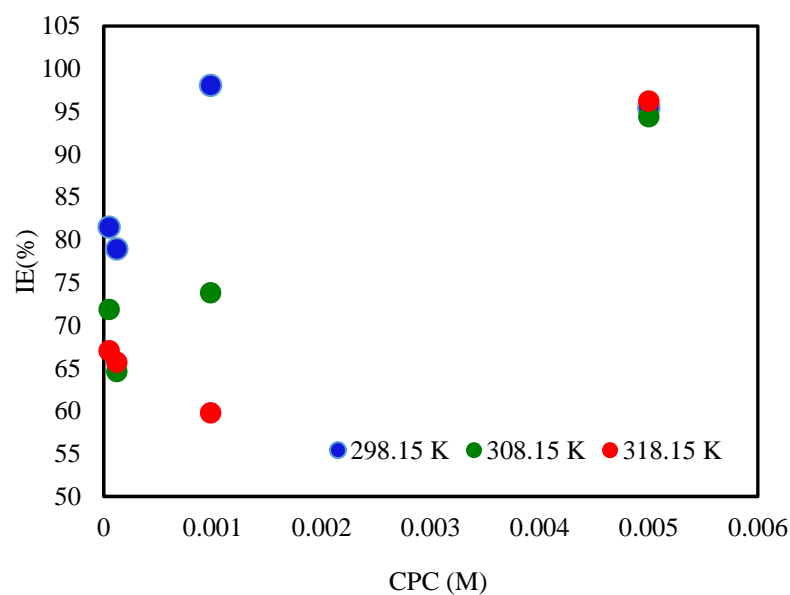


Figure 90: Variation of inhibition efficiency of different concentrations of CPC at three different temperatures.

4.2.1.1 Effect of Temperature

Generally, the corrosion rate rises with the increase in temperature (Gupta, Awasthi, *et al.*, 2020; Haldhar *et al.*, 2022). As in this thesis at low concentration of DTAB and CPC, corrosion rate is increasing at three different temperatures. However, with the increased concentration of surfactant inhibitors (DTAB and CPC), corrosion rate

decreases uniformly with the rise in temperatures at 298.15 K and 308.15 K (**Figs. 87 and 88**). As depicted in **Table 13**, and from **Figs. 89 and 90**, corrosion inhibition efficiency is well-observed up to 97.85% of 0.01637 M DTAB at 298.15 K and 98.08% of 0.00098 M of CPC at 298.15 K. From, this inhibiting efficiency of surfactants, it can be verified that there is no dissolution of metal bodies at lower temperatures (Amin *et al.*, 2011; Kumar & Karthikeyan, 2013). Kumar & Karthikeyan, (2013) stated in their work, at higher temperature, there is enhanced metal dissolution phenomenon. Due to which, there is decrease in inhibition process leading to fall in inhibition efficiency. But only at higher concentration of inhibitors (0.05 M DTAB and 0.005 M CPC)), there is increase in inhibition efficiency with rise in temperature which might be due to increase in adsorption process (Abdallah *et al.*, 2019; Kumar & Karthikeyan, 2013). Thus, there is the abnormal physical adsorption behavior of DTAB and CPC on the surface of MS. The behavior shows reverse effect of adsorption due to unfavorable micellar activity on the interface.

Table 12: Essential corrosion parameters of mild steel in 0.5 M H₂SO₄ with various concentrations of DTAB and CPC obtained at 298.15 K

[DTAB] (mM)	CR (g cm ⁻² hr ⁻¹)	IE(%)	θ	[CPC] (mM)	CR (g cm ⁻² hr ⁻¹)	IE(%)	θ
Blank	2.78	-	-	Blank	2.78	-	-
5.0	0.16	94.77	0.95	0.05	4.43	81.49	0.81
12.68	0.07	97.71	0.98	0.12	5.04	78.96	0.78
16.37	0.07	98.85	0.98	0.98	0.46	98.08	0.98
50.0	0.09	96.79	0.97	5.0	1.08	95.48	0.95

Table 13: Inhibition efficiency (I.E.) and surface coverage (θ) of DTAB and CPC obtained at three different temperatures.

[DTAB] (mM)	T (K)	IE (%)	θ	[CPC] (mM)	T (K)	IE (%)	θ
Blank	298.15	-	-	Blank	298.15	-	-
	308.15	-	-		308.15	-	-
	318.15	-	-		318.15	-	-
5.0	298.15	94.78	0.95	0.05	298.15	81.48	0.81
	308.15	90.93	0.91		308.15	71.87	0.71
	318.15	81.66	0.82		318.15	67.04	0.67
12.68	298.15	97.71	0.98	0.12	298.15	78.96	0.79
	308.15	98.7	0.99		308.15	64.61	0.65
	318.15	97.9	0.99		318.15	65.7	0.99
16.37	298.15	97.85	0.98	0.98	298.15	98.08	0.98
	308.15	97.67	0.98		308.15	73.82	0.74
	318.15	93.66	0.94		318.15	59.8	0.94
50.0	298.15	96.79	0.97	5.0	298.15	95.48	0.95
	308.15	99.42	0.99		308.15	94.4	0.94
	318.15	99.12	0.99		318.15	96.23	0.96

4.2.1.2 Adsorption Isotherm

It is generally recognized that the adsorption isotherms give valuable experiences towards mechanism of corrosion inhibition. For this purpose, surface coverage values tabulated in **Table 13** depict the basic information of interaction between the mild steel and suitable inhibitor. The surface coverage (θ) of surface-active agents was calculated using the relation (Deyab, 2020) :

$$\theta = [\text{I. E. \%}]/100 \quad (4-24)$$

After several attempts, the best fitting are obtained with Langmuir isotherm as displayed by the plots between C/θ and C with the slopes and R^2 is one (**Fig. 91**) and also very close to 1 (**Figs. 91 and 92**) indicating the adsorption of surfactant inhibitor molecules firmly follows Langmuir's adsorption isotherm relation expressed as (Aslam *et al.*, 2021; Yurt *et al.*, 2004):

$$\frac{C}{\theta} = C + \frac{1}{K_{ads}} \quad (4.25)$$

where, C = the surfactant inhibitor concentration

K_{ads} denotes the equilibrium constant for the phenomenon of adsorption/desorption of the active molecules on metallic surface.

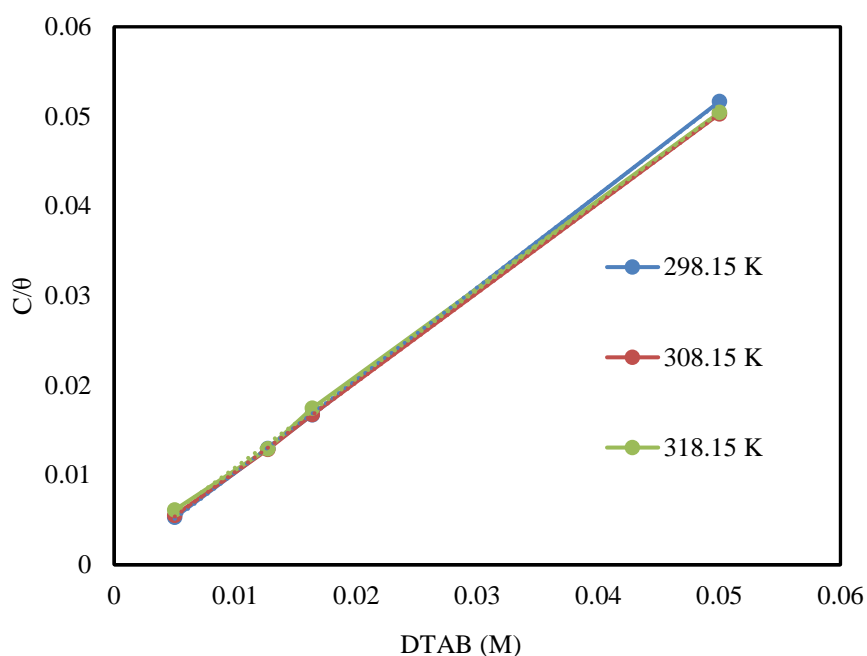


Figure 91: Plot of C/θ against DTAB (where C is the concentration of DTAB) at three different temperatures.

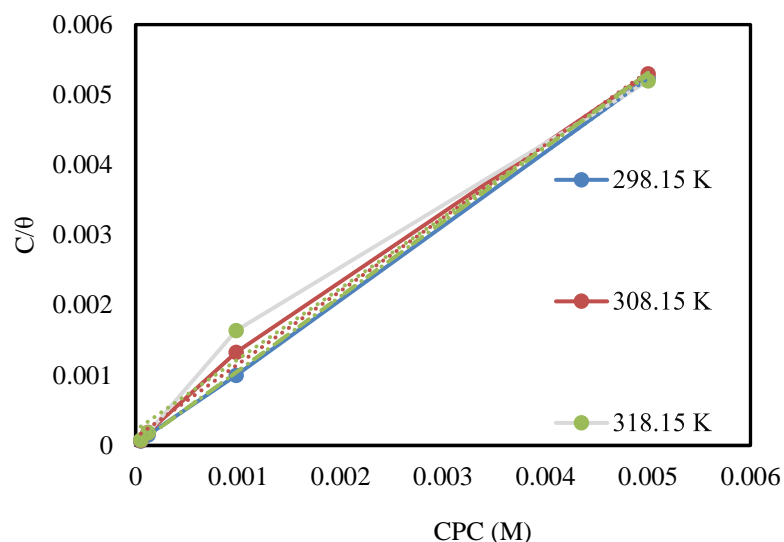


Figure 92: Plot of C/θ against CPC (where C is the concentration of CPC) at three different temperatures.

Table 14: Free energy for adsorption and equilibrium constant of DTAB and CPC as surfactant inhibitor on the mild steel surface.

For DTAB				For CPC			
T (k)	$-\Delta G_{\text{ads}}^0$ (KJmol ⁻¹)	K_{ads}	R^2	T (k)	$-\Delta G_{\text{ads}}^0$ (KJmol ⁻¹)	K_{ads}	R^2
298.15	34.5	20000	1	298.15	31.07	5000	0.985
308.15	30.33	2500	1	308.15	33.88	10000	0.997
318.15	28.89	1000	0.999	318.15	42.91	200000	0.999

K_{ads} values were obtained from the intercept of the plots for adsorption process. According to the Langmuir adsorption parameters, the equilibrium constant is related to standard free energy of adsorption through the equation (Hamid *et al.*, 1998):

$$\Delta G_{\text{ads}}^0 = -RT(55.5 K_{\text{ads}}) \quad (4-25)$$

where R indicates the Universal Gas Constant, and T is the absolute temperature.

The value of 55.5 signifies the molar concentration of water in aqueous solution expressed in per mole. The equilibrium adsorption constant as well as correlation coefficient (R^2) obtained through the linear plots between C/θ and C and the values are tabulated in **Table 14**. The negative values calculated from the above relation indicates the spontaneous process of adsorption of active agents on the MS surface. The obtained

values of free energy of adsorption, $-\Delta G_{\text{ads}}^0$ for DTAB were >28 to 34.5 kJmol^{-1} and for CPC were >31.07 to 42.91 kJmol^{-1} involves both physical adsorption and chemical adsorption of the surfactant molecules on the mild steel (Bhattarai *et al.*, 2017; Haldhar *et al.*, 2022). In this work, the chemical adsorption phenomenon is explained through free energy of adsorption of cationic surfactants on the metallic surfaces.

4.2.1.3 Thermodynamic Activation Parameters

Arrhenius put forwarded a well-known equation that determined the temperature dependence of the universal gas constant as expressed below (Attari *et al.*, 2015):

$$\log CR = \log A - \frac{E_a^*}{2.303RT} \quad (4-26)$$

where A indicates the frequency factor, E_a^* indicates the apparent activation energy, R indicates the universal gas constant and T indicates the absolute temperature.

The above Arrhenius equation predicted that plots between $\log CR$ and $1/T$ shows a linear straight line. The slope from line was generated as $(E_a^*/2.303R)$ and the intercept from the line taken as $\log A$ through the extrapolation to $(1/T=0)$. Arrhenius plots of $\log CR$ against $1/T$ at concentrations of DTAB and CPC are given in **Figs. 93 and 94**.

On the other hand, enthalpy change (ΔH^*) and entropy change (ΔS^*) of both inhibitors DTAB and CPC for activation complex formation in the transition state could be estimated from the transition state expression (Attari *et al.*, 2015):

$$\log\left(\frac{CR}{T}\right) = \left[\log\left(\frac{R}{hN}\right) + \left(\frac{\Delta S^*}{2.303 R}\right)\right] - \left(\frac{\Delta H^*}{2.303 RT}\right) \quad (4-27)$$

Where, h denotes the planck's constant and N denotes Avogadro's number.

$\log CR/T$ were plotted against $1/T$ for both DTAB and CPC in **Figs. 95 and 96**, respectively. Here, in these plots, $-\Delta H^*/2.303 R$ were used as slopes and $\log(R/hN)+(\Delta S^*/2.303 R)$ were used as intercepts from the straight lines to evaluate the ΔH^* and ΔS^* values respectively.

Table 15 shows corrosion kinetic parameters as E_a^* , ΔH^* and ΔS^* . E_a^* values are lowest for higher concentrations of DTAB and CPC for 0.05 M and 0.005 M i.e -8.18 kJmol^{-1} and 4.47 kJmol^{-1} , respectively. The concentration of cationic surfactants corresponding to its activation energy are above CMC concentrations which exhibits that micelle plays vital role in inhibition activity through adsorption on MS surfaces.

The variation in activation energy is due to difference in electrostatic characteristics of both inhibiting and uninhibiting MS surfaces and due to frequency factor (Janati *et al.*, 2020; Pakiet *et al.*, 2020). The positive signs of the enthalpies (ΔH^*) recognise the endothermic behavior of the MS dissolution process. The obtained negative values of entropies (ΔS^*) represents an association during inhibition rather than a dissociation step, meaning from reactants to generate activated complex (Karthik *et al.*, 2014).

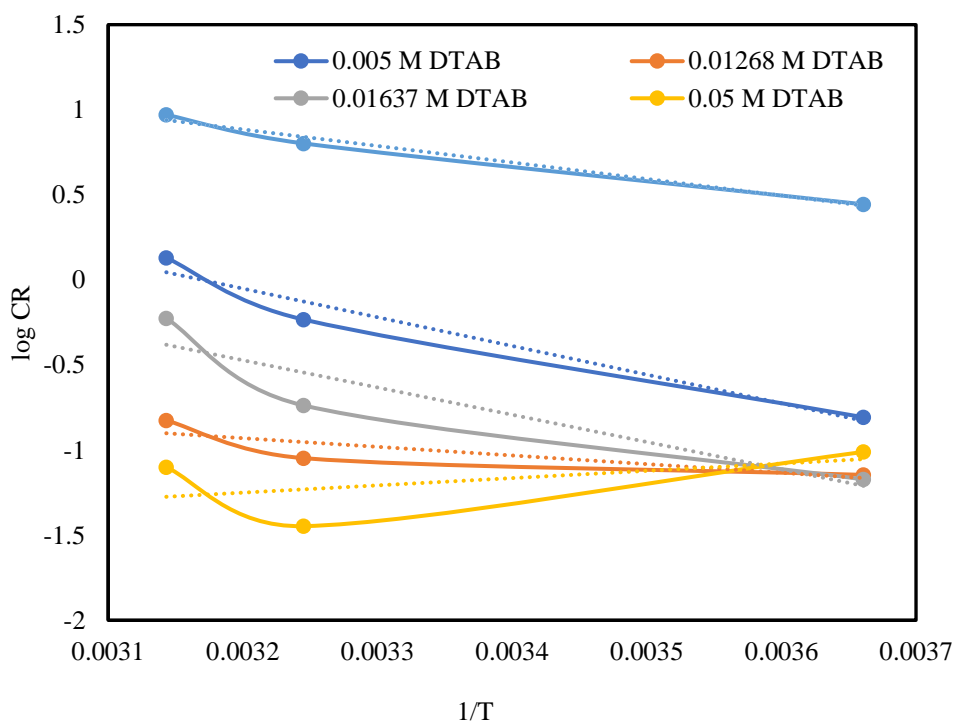


Figure 93: Plot of log CR (DTAB) against 1/T

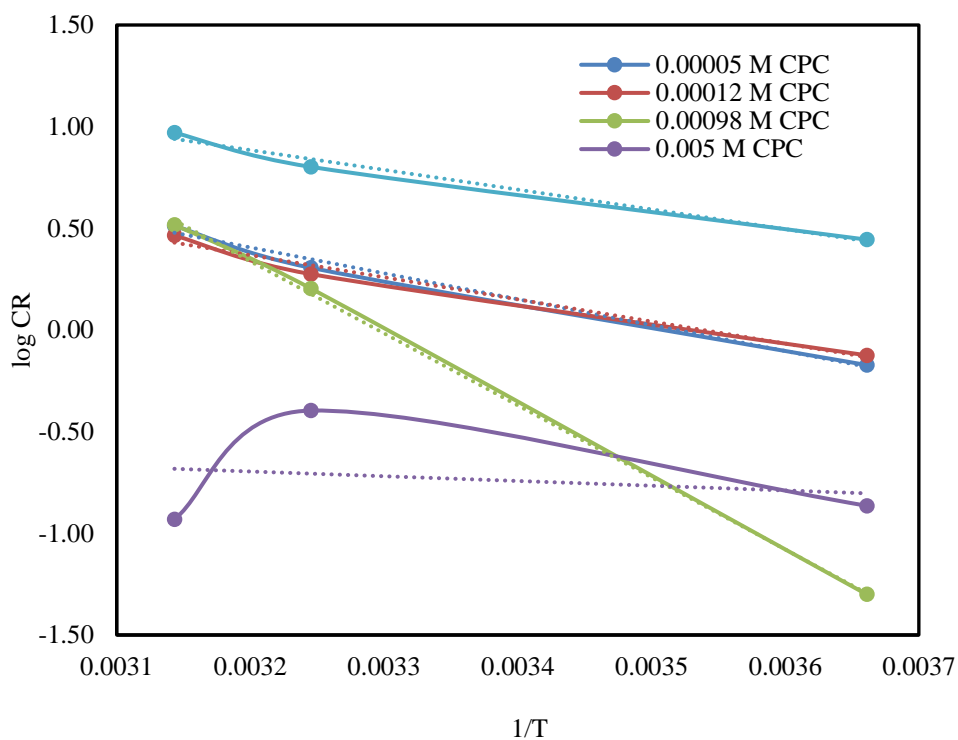


Figure 94: Plot of log CR (CPC) against $1/T$

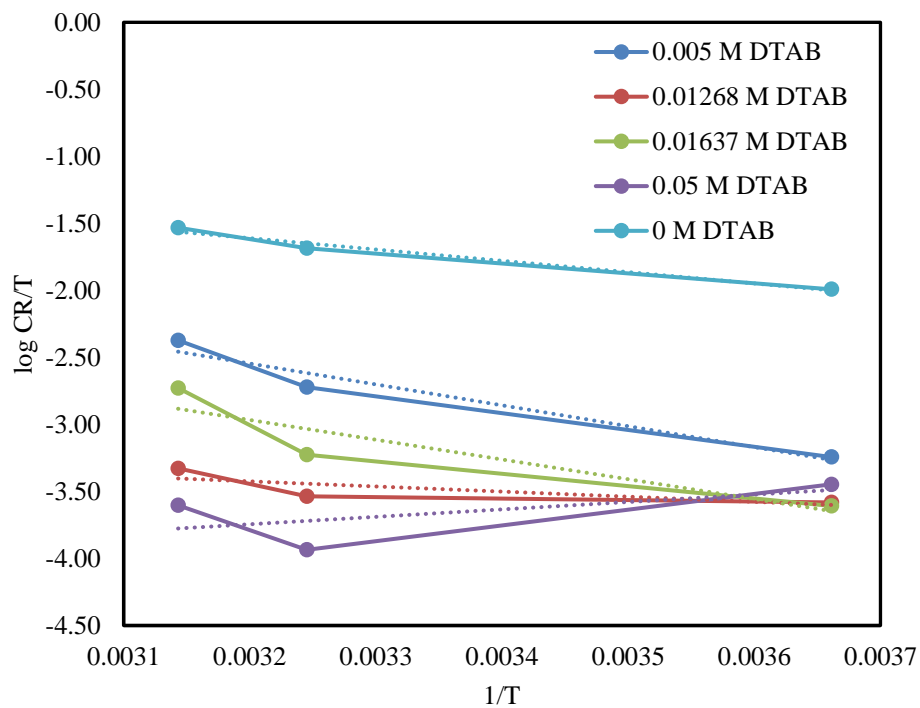


Figure 95: Plot of log CR/T (DTAB) against $1/T$

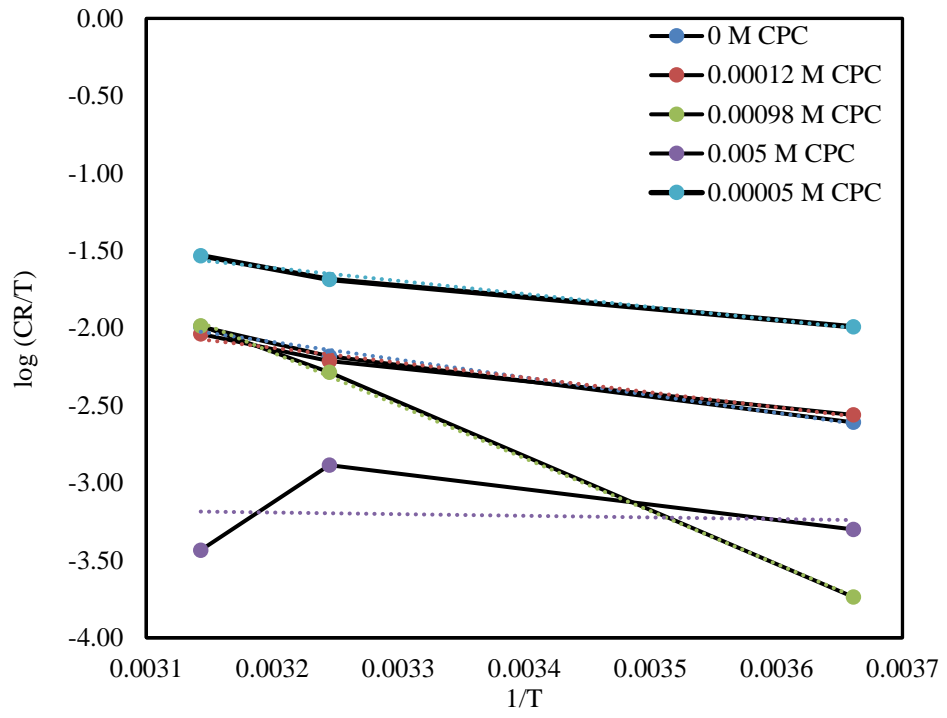


Figure 96: Plot of $\log CR/T$ (CPC) against $1/T$

Table 15: Thermodynamic activation parameters for adsorption of DTAB and CPC as surfactant inhibitor on the mild steel surface.

[DTAB] (mM)	E_a^* (KJmol ⁻¹)	ΔH^* (KJmol ⁻¹)	$-\Delta S^*$ (Jmol ⁻¹ K ⁻¹)	[CPC] (mM)	E_a^* (KJmol ⁻¹)	ΔH^* (KJmol ⁻¹)	$-\Delta S^*$ (Jmol ⁻¹ K ⁻¹)
Blank	18.6	16.16	177.30	Blank	18.6	16.16	176.73
5.0	32.28	29.84	150.84	0.05	24.37	21.93	167.42
12.68	9.73	7.29	239.83	0.12	20.82	18.39	179.51
16.37	30.65	28.22	164.10	0.98	67.81	65.37	29.71
50.0	-8.18	10.62	103.26	5.0	4.47	20.28	142.69

4.2.2 Polarization Measurements

Polarization curves for the mild steel at various concentrations of cationic surfactants (DTAB and CPC) in 0.5 M H₂SO₄ solutions are shown in **Figs. 97 and 98**. From the extrapolation of Tafel straight lines, corrosion current density (I_{corr}) and corrosion current potential (E_{corr}) were determined. The values of I_{corr} , E_{corr} and inhibition efficiency (I.E.,%) are included in **Table 16**. The I.E.% is determined using following equation (Choi *et al.*, 2022; Elkacimi *et al.*, 2011):

$$I. E. = \left(\frac{I_{corr}^0 - I_{corr}}{I_{corr}^0} \right) \times 100 \quad (4-28)$$

Where, I_{corr}^0 denotes corrosion current density in absence of inhibitor and I_{corr} denotes corrosion current density in presence of inhibitor.

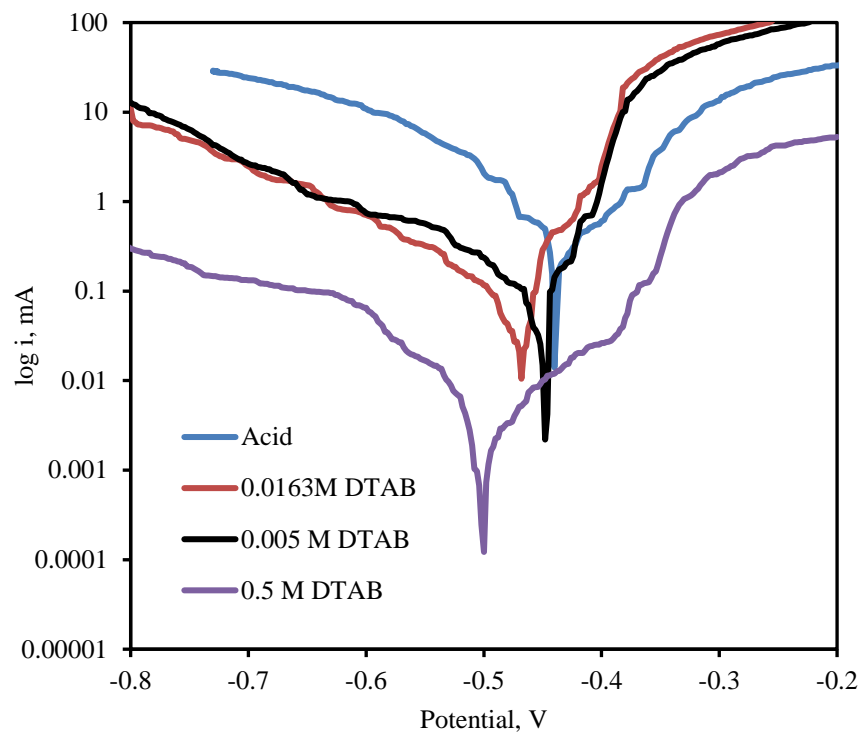


Figure 97: Potentiodynamic polarization curves for MS in 0.5 M H₂SO₄ in the absence and presence of DTAB

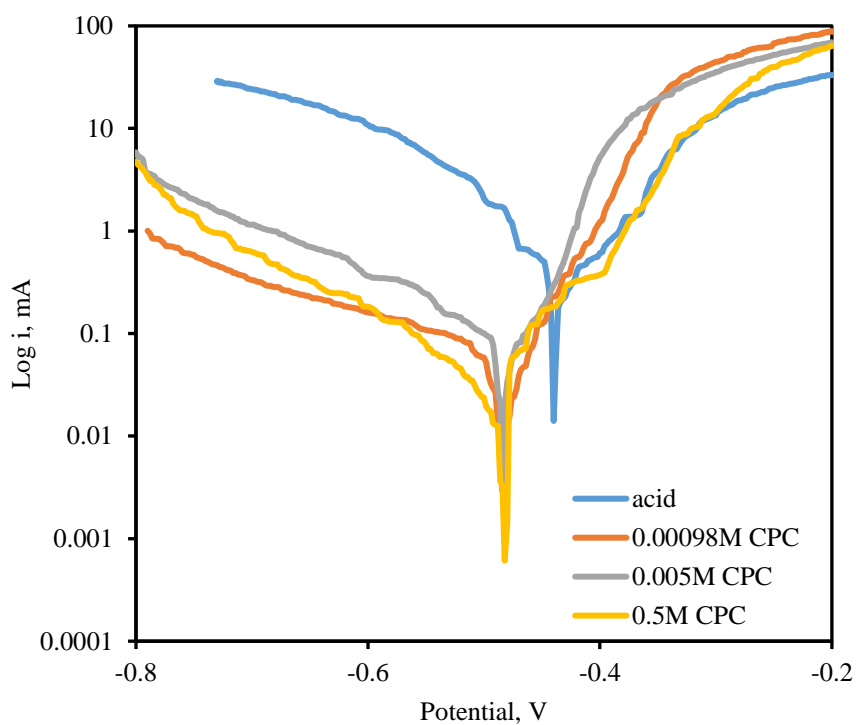


Figure 98: Potentiodynamic polarization curves for MS in 0.5 M H₂SO₄ in the absence and presence of CPC

From **Table 16** and **Figs. 97 & 98** it is clearly identified a complete effect of concentration on both lower current density and corrosion potential (E_{corr}) towards its corresponding anode and cathode branches of Tafel's plots (El Assiri *et al.*, 2020). Besides, the higher the concentration of cationic surfactants(DTAB and CPC), the more critical decrease in i_{corr} values due to DTAB and CPC adsorption molecules on the MS, allowing metallic surface to act as insulator to the amphiphilic acid solution. In addition, as cationic surfactants concentration increases, the E_{corr} values are moved to the negative value. Thus, in the presence of surfactant inhibitor, there is greater influence on the cathodic reaction than the anodic reaction at different surfactant concentrations (A. Singh *et al.*, 2020). Based on the plots of DTAB and CPC, the inhibitors show the nature of a mixed type of inhibitor indicating a predominant cathodic reaction (A. Singh *et al.*, 2010, 2020).

From the polarization plots it is evident that the selected cationic surfactants in this research work have the better adsorption capacity due to their highest inhibition efficiency (98.6% for DTAB and 89.38% for CPC) at highest concentrations of surfactant inhibitor. Thus, those surfactants could be the most essential inhibitor for corrosion control.

Table 16: Effect of DTAB and CPC as surfactant inhibitor on the mild steel surface studied by potentiodynamic polarization method.

[DTAB] (M)	E_{corr}	I_{corr}	I.E.%	[CPC] (M)	E_{corr}	I_{corr}	I.E.%
0	-0.43	0.227	-	0	-0.43	0.227	-
0.0163	-0.49	0.089	60.79	0.00098	-0.468	0.0446	80.35
0.05	-0.46	0.0494	78.23	0.005	-0.474	0.065	71.37
0.5	-0.482	0.00317	98.6	0.5	-0.502	0.0241	89.38

4.2.3 Mechanism of adsorption of surfactant inhibitor on MS

The very first step in corrosion control mechanism is the adsorption of surfactant inhibitor molecules on the MS surface. The adsorption process depends on the active species of inhibitor molecules, electrolytic solution and the nature of metallic substances. A. Singh *et al.*,(2010) reported that in the MS surface possess positive

charge in accordance with potential zero charge (PZC). The CPC & DTAB adsorb on the MS surface by

- (a) Surfactant inhibitors interact with sulphate ions (It is physical adsorption).
- (b) MS has *d*-orbitals which are vacant interact with unshared electron pairs of hetero pairs of electrons.
- (c) *d*-electron of the MS interact with *d*-orbital which are vacant.

In H₂SO₄ medium, the DTAB and CPC molecules adsorb through protonated hetero atoms (N) and SO₄⁻ ions on the MS surface.

Initially, protonated DTAB and CPC in 0.5 M H₂SO₄ solution compete with H⁺ ion for electrons on MS surface. After the evolution of H₂ gas, the cationic form of inhibitors gets to neutral form and hetero atoms with lone pair electrons brings chemical adsorption.

The higher electron density on MS surface provides more negative charge on it. To relieve the interface or surface from higher negative charge, the electron from the Fe-atom may be transferred to vacant π^* orbital (antibonding) of DTAB and CPC.

It is concluded from lots of experimental outcomes and theoretical point that I.E. of DTAB is higher than CPC due to larger effect of ammonium group in DTAB than pyridinium group in CPC (Abdallah *et al.*, 2021; Kumar & Karthikeyan, 2013; A. Singh *et al.*, 2010). Though the molecular weight of DTAB is lower than CPC along with shorter chain length of DTAB than CPC, it is experimentally verified that I.E. of DTAB is higher than CPC. It means difference in chain length greatly influence on efficiency of inhibiting activity (Arockia Selvi *et al.*, 2019; Asefi *et al.*, 2011; Karki *et al.*, 2021).

CHAPTER 5

CONCLUSION AND RECOMMENDATIONS

5.1 Conclusion

According to the the existing demand for suitable active agents for multiple purposes, surfactants have been widely used for numerous applications. In such typical conditions, cationic surfactant interactions study is very fruitful for further applications in efficient manner. To tailor their properties to a specific application, it had been studied to comprehend how dye and cationic surfactant behave in combinations of varying alcohols.

The method for analyzing the dye-surfactant interaction via a variety of spectral methods is the spectrophotometric technique. By way of adsorption events and the development of a dye surfactant complex, the changing absorbance values eventually revealed the mechanism of dye-surfactant interaction. During the interaction, the j-aggregate nature, and the pH of the azo form of MR acts an important role in the incorporation of MR by micelles of CPC and DTAB (cationic surfactant). The only basic form(azo) of MR oppose to observe the isosbestic points in the spectra of interaction. The results show that there is a decrease in CMC with MR corresponding to the series of volume fraction of methanol in comparison to the CMC values of CPC from literature without MR. The trends of change in binding and partition parameters show strong interactions between MR and CPC. Moreover, the negative values of Gibb's free energy of binding and partition illustrate the spontaneous process of the system.

Consequently, dye-surfactants interactions are well realized with conductivity, surface tension and viscosity techniques due to the reduced micelle behavior with cationic surfactants. The CMC values of DTAB and CPC rise with the rise in the volume of methanol along with the increased temperature. Due to this, the thermodynamic and surface properties are greatly influenced by the decrease in hydrophobicity in the mixed system. Micellar behavior is well inspired by the best thermodynamic parameter ΔG_m^0 as it affects the degree of ionization. Due to complex molecular flexibility, the CMC of DTAB is higher than CPC. Viscosity B coefficient determined from the viscosity

techniques allows the researchers to allocate the idea of solute-solvent interactions in presence of MR.

From this research work, experimental results visualise that DTAB and CPC are the good inhibitors for the corrosion control. Using both weight loss and potentiodynamic polarization method, it can be concluded that they are the best techniques to determine the better inhibiting compound. Therefore, cationic surfactants could act as better mixed type inhibitors with dominant cathodic reaction for corrosion control. Due to higher inhibition efficiencies of both cationic surfactants (DTAB and CPC), they can be utilized in desirable industrial fields and many more.

In short, cationic surfactants molecules are well interacted with azo dye molecules as well as cationic surfactants (DTAB and CPC) are good inhibitors for corrosion control. The studied systems are environmentally friendly and appropriate for utilisation in multiple dimensions.

5.2 Recommendations

Research is a continuous study regarding a particular concern or problem by using scientific tools and techniques. Research can predict, explain, and control theories and ideas. The study of dye-surfactant interaction can be accompanied through many other techniques such as NMR (Nuclear Magnetic Resonance), fluorometry, DLS (Dynamic light Scattering), Polarographic techniques etc. Also, anticorrosion study of surfactants can be extended using EIS (Electrochemical Impedance Spectroscopy), SEM (Scanning Electron microscopy), TEM (Transmission Electron Microscopy) etc.

CHAPTER 6

6. SUMMARY

The present research thesis is divided into six chapters. They are summarized as follows:

Chapter 1 deals with the general introduction of surfactants and its classification, dyes and its classification, role of CMC, influence of dye structure on aggregation, surfactant as corrosion inhibitor. It also highlighted the general and specific objectives of the thesis.

Chapter 2 explains the detailed literature review of the present research work, which is an important part of any research work. Here, the literature review explains the general overview of research, surfactant sensitized system, methods of dye surfactant interaction study and application of dye surfactant interaction study and anti-corrosion study.

The details of the materials or reagents used in the present research work and the methods adopted are explained in **chapter 3**.

The details of the results and discussion of the current research work are explained in **chapter 4**, which is the important backbone and skeletal part of any thesis. The explanations of various techniques are included in this Chapter. The tables and figures represent the analyzed data that are positioned at proper places in this chapter.

Chapter 5 deals with the conclusion of the present research work. The plan for the future and recommendations of the present research work are clearly explained in this chapter.

Chapter 6 explained a summary of all the various chapters of the present research thesis.

REFERENCES

- Abbasov, V. M., Abd El-Lateef, H. M., Aliyeva, L. I., Qasimov, E. E., Ismayilov, I. T., & Khalaf, M. M. (2013). A study of the corrosion inhibition of mild steel C1018 in CO₂-saturated brine using some novel surfactants based on corn oil. *Egyptian Journal of Petroleum*, **22**(4), 451–470. <https://doi.org/10.1016/j.ejpe.2013.11.002>
- Abdallah, M., Alfakeer, M., Altass, H. M., Alharbi, A. M., Althagafi, I., Hasan, N. F., & Mabrouk, E. M. (2019). The polarographic and corrosion inhibition performance of some Schiff base compounds derived from 2-amino-3-hydroxypyridine in aqueous media. *Egyptian Journal of Petroleum*, **28**(4), 393–399. <https://doi.org/10.1016/j.ejpe.2019.09.002>
- Abdallah, M., Soliman, K. A., Al-Gorair, A. S., Al Bahir, A., Al-Fahemi, J. H., Motawea, M. S., & Al-Juaid, S. S. (2021). Enhancing the inhibition and adsorption performance of SABIC iron corrosion in sulfuric acid by expired vitamins. Experimental and computational approach. *RSC Advances*, **11**(28), 17092–17107. <https://doi.org/10.1039/d1ra01010g>
- Abdellaoui, O., Skalli, M. K., Haoudi, A., Rodi, Y. K., Mazzah, A., Arrousse, N., Taleb, M., Ghibate, R., & Senhaji, O. (2021). Study of the inhibition effect of a new cationic surfactant on mild steel corrosion in a 1 M HCl solution. *Materials Today: Proceedings*, **45**, 7517–7523. <https://doi.org/10.1016/j.matpr.2021.02.316>
- Al-Lohedan, H. A., Khamis, E., & Issa, Z. A. (1996). Studies on the influence of temperature on the adsorption of some cationic surfactants on to steel. *Adsorption Science and Technology*, **13**(3), 137–152. <https://doi.org/10.1177/026361749601300301>
- Alehyen, S., Bensejjay, F., El Achouri, M., Pérez, L., & Infante, M. R. (2010). Study of the interaction between methyl orange and mono and bis-quaternary ammonium surfactants. *Journal of Surfactants and Detergents*, **13**(2), 225–231. <https://doi.org/10.1007/s11743-009-1161-3>
- Ali, A., Uzair, S., Malik, N. A., & Ali, M. (2014). Study of interaction between cationic surfactants and cresol red dye by electrical conductivity and spectroscopy methods. *Journal of Molecular Liquids*, **196**(May), 395–403. <https://doi.org/10.1016/j.molliq.2014.04.013>

- Alonso, J. I. G., Garcia, M. E. D., & Medel, A. S. (1984). *THE SURFACTANT-SENSITIZED ANALYTICAL ACID*. *31*(5), 361–366.
- Alvares, R., Gupta, S., Macdonald, P. M., & Prosser, R. S. (2014). Temperature and pressure based NMR studies of detergent micelle phase equilibria. *Journal of Physical Chemistry B*, *118*(21), 5698–5706. <https://doi.org/10.1021/jp500139p>
- Amin, A. S. (2000). The surfactant-sensitized analytical reaction of niobium with some thiazolylazo compounds. *Microchemical Journal*, *65*(3), 261–267. [https://doi.org/10.1016/S0026-265X\(00\)00119-3](https://doi.org/10.1016/S0026-265X(00)00119-3)
- Amin, M. A., Ahmed, M. A., Arida, H. A., Arslan, T., Saracoglu, M., & Kandemirli, F. (2011). Monitoring corrosion and corrosion control of iron in HCl by non-ionic surfactants of the TRITON-X series - Part II. Temperature effect, activation energies and thermodynamics of adsorption. *Corrosion Science*, *53*(2), 540–548. <https://doi.org/10.1016/j.corsci.2010.09.019>
- Arockia Selvi, J., Kamaraj, P., Arthanareeswari, M., PushpaMalini, T., Mohanapriya, S., & Subasree, N. (2019). Effect of Cetylpyridinium chloride on corrosion inhibition of mild steel in chloride environment. *Materials Today: Proceedings*, *14*, 264–270. <https://doi.org/10.1016/j.matpr.2019.04.146>
- Asefi, D., Arami, M., & Mahmoodi, N. M. (2011). Effect of Chain Length Compatibility between Surfactants and Co-Surfactants on Corrosion Inhibition of Steel. *ECS Transactions*, *35*(31), 1–10. <https://doi.org/10.1149/1.3647848>
- Aslam, R., Mobin, M., Aslam, J., Aslam, A., Zehra, S., & Masroor, S. (2021). Application of surfactants as anticorrosive materials: A comprehensive review. *Advances in Colloid and Interface Science*, *295*(July), 102481. <https://doi.org/10.1016/j.cis.2021.102481>
- Attari, H. El, Lahmadi, K., El Bribri, A., & Siniti, M. (2015). The Adsorption and Corrosion Inhibition of Non-Ionic Surfactant on Carbon Steel Surface in Hydrochloric Acid. *International Journal of Materials and Chemistry*, *5*(3), 77–83. <https://doi.org/10.5923/j.ijmc.20150503.04>
- Bashir, A., Sharifi Haddad, A., & Rafati, R. (2022). A review of fluid displacement mechanisms in surfactant-based chemical enhanced oil recovery processes:

- Analyses of key influencing factors. *Petroleum Science*, **19**(3), 1211–1235.
<https://doi.org/10.1016/j.petsci.2021.11.021>
- Bhattacharai, A., Yadav, A. K., Sah, S. K., & Deo, A. (2017). Influence of methanol and dimethyl sulfoxide and temperature on the micellization of cetylpyridinium chloride. *Journal of Molecular Liquids*, **242**, 831–837.
<https://doi.org/10.1016/j.molliq.2017.07.085>
- Borges, L. G. A., Savi, A., Teixeira, C., de Oliveira, R. P., De Camillis, M. L. F., Wickert, R., Brodt, S. F. M., Tonietto, T. F., Cremonese, R., da Silva, L. S., Gehm, F., Oliveira, E. S., Barth, J. H. D., Macari, J. G., de Barros, C. D., & Vieira, S. R. R. (2017). Mechanical ventilation weaning protocol improves medical adherence and results. *Journal of Critical Care*, **41**, 296–302.
<https://doi.org/10.1016/j.jcrc.2017.07.014>
- Bračko, S., & Špan, J. (2001). Anionic dye- Cationic surfactant interactions in water-Ethanol mixed solvent. *Dyes and Pigments*, **50**(1), 77–84.
[https://doi.org/10.1016/S0143-7208\(01\)00025-0](https://doi.org/10.1016/S0143-7208(01)00025-0)
- Chandra, A., Patidar, V., Singh, M., & Kale, R. K. (2013). Physicochemical and friccohesity study of glycine, l-alanine and l-phenylalanine with aqueous methyltrioctylammonium and cetylpyridinium chloride from T = (293.15 to 308.15) K. *Journal of Chemical Thermodynamics*, **65**, 18–28.
<https://doi.org/10.1016/j.jct.2013.05.037>
- Choi, J.-H., Dhakal, D. R., Kshetri, Y. K., Chaudhary, B., Joshi, B., Lee, S. W., & Kim, T.-H. (2022). Role of surfactants on particle deposition, wear, and corrosion behavior of TaC particle incorporated electroless nickel-phosphorus coating. *Progress in Natural Science: Materials International*, **32**(5), 655–663.
<https://doi.org/10.1016/j.pnsc.2022.10.007>
- Das, S., Mondal, S., & Ghosh, S. (2013). Physicochemical studies on the micellization of cationic, anionic, and nonionic surfactants in water-polar organic solvent mixtures. *Journal of Chemical and Engineering Data*, **58**(9), 2586–2595.
<https://doi.org/10.1021/je4004788>
- Deyab, M. A. (2020). Understanding the anti-corrosion mechanism and performance of ionic liquids in desalination, petroleum, pickling, de-scaling, and acid cleaning

- applications. *Journal of Molecular Liquids*, **309**, 113107.
<https://doi.org/10.1016/j.molliq.2020.113107>
- Dragan, E. S., Mayr, J., Häring, M., Cocarta, A. I., & Díaz, D. D. (2016). Spectroscopic Characterization of Azo Dyes Aggregation Induced by DABCO-Based Ionene Polymers and Dye Removal Efficiency as a Function of Ionene Structure. *ACS Applied Materials and Interfaces*, **8**(45), 30908–30919.
<https://doi.org/10.1021/acsami.6b09853>
- Dragan, E. S., Schwarz, S., & Eichhorn, K. J. (2010). Specific effects of the counterion type and concentration on the construction and morphology of polycation/azo dye multilayers. *Colloids and Surfaces A: Physicochemical and Engineering Aspects*, **372**(1–3), 210–216. <https://doi.org/10.1016/j.colsurfa.2010.10.023>
- Edbey, K., Bader, N., Eltaboni, F., Elabidi, A., Albaba, S., & Ahmed, M. (2015). Conductometric and Spectrophotometric Study of the Interaction of Methyl Violet with Sodium Dodecyl Sulfate. *International Research Journal of Pure and Applied Chemistry*, **9**(4), 1–7. <https://doi.org/10.9734/irjpac/2015/19603>
- Edbey, K., El-Hashani, A., Benhmid, A., Ghwel, K., & Benamer, M. (2018). Spectral Studies of Eriochrome Black T in Cationic Surfactants. *Chemical Science International Journal*, **24**(4), 1–12. <https://doi.org/10.9734/csji/2018/44312>
- El Assiri, E. H., Driouch, M., Lazrak, J., Bensouda, Z., Elhaloui, A., Sfaira, M., Saffaj, T., & Taleb, M. (2020). Development and validation of QSPR models for corrosion inhibition of carbon steel by some pyridazine derivatives in acidic medium. *Heliyon*, **6**(10). <https://doi.org/10.1016/j.heliyon.2020.e05067>
- Elkacimi, Y., Achnin, M., Aouine, Y., Touhami, M. E., Alami, A., Tourir, R., Sfaira, M., Chebabe, D., Elachqar, A., & Hammouti, B. (2011). Inhibition of mild steel corrosion by some phenyltetrazole substituted compounds in hydrochloric acid. *Portugaliae Electrochimica Acta*, **30**(1), 53–65.
<https://doi.org/10.4152/pea.201201053>
- Fazeli, S., Sohrabi, B., & Tehrani-Bagha, A. R. (2012). The study of Sunset Yellow anionic dye interaction with gemini and conventional cationic surfactants in aqueous solution. *Dyes and Pigments*, **95**(3), 768–775.
<https://doi.org/10.1016/j.dyepig.2012.03.022>

- Free, M. L., Wang, W., & Ryu, D. Y. (2004). Prediction of corrosion inhibition using surfactants. *Corrosion*, **60**(9), 837–844. <https://doi.org/10.5006/1.3287864>
- Garcia, M. E. Diaz, & Sanz-Medel, A. (1986). Dye-surfactant interactions: a review. *Talanta*, **33**(3), 255–264. [https://doi.org/10.1016/0039-9140\(86\)80060-1](https://doi.org/10.1016/0039-9140(86)80060-1)
- Garcia, M. E. Diaz, & Sanz-Medel, A. (1985). Analytical application of the complexation of Nb(V) with bromopyrogallol red in micellar media. *Talanta*, **32**(3), 189–193. [https://doi.org/10.1016/0039-9140\(85\)80058-8](https://doi.org/10.1016/0039-9140(85)80058-8)
- Ghoreishi, S. M., & Nooshabadi, M. S. (2005). Electromotive force studies about some dyes-cationic surfactants interactions in aqueous solutions. *Dyes and Pigments*, **65**(2), 117–123. <https://doi.org/10.1016/j.dyepig.2004.07.004>
- Gohain, B., Sarma, S., & Dutta, R. K. (2008). Protonated dye-surfactant ion pair formation between neutral red and anionic surfactants in aqueous submicellar solutions. *Journal of Molecular Liquids*, **142**(1–3), 130–135. <https://doi.org/10.1016/j.molliq.2008.05.015>
- Gokturk, S., & Tuncay, M. (2003). Dye-Surfactant Interaction in the Premicellar Region. *Journal of Surfactants and Detergents*, **6**(4), 325–330. <https://doi.org/10.1007/s11743-003-0277-y>
- Gompper, G., & Schick, M. (2007). Soft Matter. *Soft Matter*, **1**, 1–285. <https://doi.org/10.1002/9783527617050>
- Gupta, D. K., Awasthi, L., Das, A. K., Yadav, B., Ghimire, A., & Yadav, A. P. (2020). Corrosion Inhibition Effect of Acidic Extract of Bark of Eucalyptus Globulus on Mild Steel. *Tribhuvan University Journal*, **35**(1), 1–10. <https://doi.org/10.3126/tuj.v35i1.35828>
- Gupta, D. K., Kafle, K. A., Das, A. K., Neupane, S., Ghimire, A., Yadav, B. D., Chaudhari, Y., Karki, N., & Yadav, A. P. (2020). Study of Jatropha Curcas Extract as a Corrosion Inhibitor in Acidic Medium on Mild Steel by Weight Loss and Potentiodynamic Methods. *Journal of Nepal Chemical Society*, **41**(1), 87–93. <https://doi.org/10.3126/jncs.v41i1.30493>
- Haldhar, R., Godfrey, U. K., Chijioke, O. C., Umezurike, E. A., Ifeoma, O. P., Oke, M. O., Ichou, H., Arrousse, N., Kim, S., Dagdag, O., Ebenso, E. E., & Taleb, M.

- (2022). *Theoretical Study and Adsorption Behavior of Urea on Mild Steel in Automotive Gas Oil (AGO) Medium. Lubricants*, **10**(7), 157; <https://doi.org/10.3390/lubricants10070157>
- Hamid, Z. A., Soror, T. Y., El-Dahan, H. A., & Omar, A. M. A. (1998). New cationic surfactant as corrosion inhibitor for mild steel in hydrochloric acid solutions. *Anti-Corrosion Methods and Materials*, **45**(5), 306–311. <https://doi.org/10.1108/00035599810234605>
- Hari, A. C., Paruchuri, R. A., Sabatini, D. A., & Kibbey, T. C. G. (2005). Effects of pH and cationic and nonionic surfactants on the adsorption of pharmaceutical to a natural aquifer material. *Environmental Science and Technology*, **39**(8), 2592–2598. <https://doi.org/10.1021/es048992m>
- Horiuchi, S., & Winter, G. (2015). CMC determination of nonionic surfactants in protein formulations using ultrasonic resonance technology. *European Journal of Pharmaceutics and Biopharmaceutics*, **92**, 8–14. <https://doi.org/10.1016/j.ejpb.2015.02.005>
- Hosseinzadeh, R., Maleki, R., Matin, A. A., & Nikkhahi, Y. (2008). Spectrophotometric study of anionic azo-dye light yellow (X6G) interaction with surfactants and its micellar solubilization in cationic surfactant micelles. *Spectrochimica Acta - Part A: Molecular and Biomolecular Spectroscopy*, **69**(4), 1183–1187. <https://doi.org/10.1016/j.saa.2007.06.022>
- Huang, X. L., & Zhang, J. Z. (2006). Surfactant-sensitized malachite green method for trace determination of orthophosphate in aqueous solution. *Analytica Chimica Acta*, **580**(1), 55–67. <https://doi.org/10.1016/j.aca.2006.07.046>
- Isaac, O. T., Pu, H., Oni, B. A., & Samson, F. A. (2022). Surfactants employed in conventional and unconventional reservoirs for enhanced oil recovery—A review. *Energy Reports*, **8**, 2806–2830. <https://doi.org/10.1016/j.egyr.2022.01.187>
- Janati, A. El, Elmsellem, H., Rodi, Y. K., Ouzidan, Y., Ramdani, M., Mokhtari, M., Abdel-Rahman, I., Alaoui, I. C., Chahdi, F. O., & Kusuma, H. S. (2020). A comparative study of two corrosion inhibitors: 1,4-diallyl-6-chloroquinoxaline 2,3-(1h,4h)-dione (1a) and 1,4-diallyl-6-nitroquinoxaline-2,3-(1h,4h)-dione (1b). *International Journal of Corrosion and Scale Inhibition*, **9**(2), 644–660.

<https://doi.org/10.17675/2305-6894-2020-9-2-17>

- Jocic, D. (1995). Conductivity measurement - a simple method for determining dye/surfactant interaction. *Textile Research Journal*, **65**(7), 409–416. <https://doi.org/10.1177/004051759506500706>
- Karki, N., Neupane, S., Gupta, D. K., Das, A. K., Singh, S., Koju, G. M., Chaudhary, Y., & Yadav, A. P. (2021). Berberine isolated from Mahonia nepalensis as an eco-friendly and thermally stable corrosion inhibitor for mild steel in acid medium. *Arabian Journal of Chemistry*, **14**(12), 103423. <https://doi.org/10.1016/j.arabjc.2021.103423>
- Karthik, R., Muthukrishnan, P., Elangovan, A., Jeyaprabha, B., & Prakash, P. (2014). Extract of Cassia senna as Green Inhibitor for the Corrosion of Mild Steel in 1M Hydrochloric Acid Solution . *Advances in Civil Engineering Materials*, **3**(1), 20140010. <https://doi.org/10.1520/acem20140010>
- Khadka, B., & Bhattarai, A. (2020). Uv-vis studies on interaction between sodium dioctylsulfosuccinate (Aot) and methyl red. *Revue Roumaine de Chimie*, **65**(11), 989–996. <https://doi.org/10.33224/rrch.2020.65.11.04>
- Khosa, M. A. (2010). *Interaction of Azo Dye with Cationic Surfactant Under Different pH Conditions*. 529–537. <https://doi.org/10.1007/s11743-009-1177-8>
- Kumar, S. H., & Karthikeyan, S. (2013). *Torseamide and Furoseamide as Green Inhibitors for the Corrosion of Mild Steel in Hydrochloric Acid Medium*. *Industrial & Engineering Chemical Research* **52** (2013) 7457–7469. <https://doi.org/10.1021/ie400815w>.
- Lavkush Bhisare, M., Pandey, S., Shahnawaz Khan, M., Talib, A., & Wu, H. F. (2015). Fluorophotometric determination of critical micelle concentration (CMC) of ionic and non-ionic surfactants with carbon dots via Stokes shift. *Talanta*, **132**, 572–578. <https://doi.org/10.1016/j.talanta.2014.09.011>
- Ma, K., Cui, L., Dong, Y., Wang, T., Da, C., Hirasaki, G. J., & Biswal, S. L. (2013). Adsorption of cationic and anionic surfactants on natural and synthetic carbonate materials. *Journal of Colloid and Interface Science*, **408**(1), 164–172. <https://doi.org/10.1016/j.jcis.2013.07.006>

- Maikokera, R., & Kwaambwa, H. M. (2009). *Use of Viscosity to Probe the Interaction of Anionic Surfactants with a Coagulant Protein from Moringa oleifera Seeds*. **2009**, 1–6. <https://doi.org/10.1155/2009/927329>
- Malik, M. A., Hashim, M. A., Nabi, F., AL-Thabaiti, S. A., & Khan, Z. (2011). Anti-corrosion ability of surfactants: A review. *International Journal of Electrochemical Science*, **6**(6), 1927–1948.
- Manonmani, K. N., Manjula, P., & Vennila, T. (2016). Anti Corrosion Ability and Biocidal Efficiency of Surfactants on Mild Steel in Aqueous Environment. *IRA-International Journal of Technology & Engineering (ISSN 2455-4480)*, **3**(3), 110–126. <https://doi.org/10.21013/jte.v3.n3.p2>
- Menger, F. M., Galloway, A. L., & Chlebowski, M. E. (2005). Surface tension of aqueous amphiphiles. *Langmuir*, **21**(20), 9010–9012. <https://doi.org/10.1021/la051363l>
- Migahed, M. A., & Al-Sabagh, A. M. (2009). Beneficial role of surfactants as corrosion inhibitors in petroleum industry: A review article. *Chemical Engineering Communications*, **196**(9), 1054–1075. <https://doi.org/10.1080/00986440902897095>
- Moyá, M. L., Rodríguez, A., del Mar Graciani, M., & Fernández, G. (2007). Role of the solvophobic effect on micellization. *Journal of Colloid and Interface Science*, **316**(2), 787–795. <https://doi.org/10.1016/j.jcis.2007.07.035>
- Muhammad, M. T., & Khan, M. N. (2020). Comparative studies of natural and synthetic surfactants for dyes interactions at their second point of micellisation. *Physics and Chemistry of Liquids*, **58**(4), 473–482. <https://doi.org/10.1080/00319104.2019.1611825>
- Mukherjee, I., Moulik, S. P., & Rakshit, A. K. (2013). Tensiometric determination of Gibbs surface excess and micelle point: A critical revisit. *Journal of Colloid and Interface Science*, **394**(1), 329–336. <https://doi.org/10.1016/j.jcis.2012.12.004>
- Niraula, T. P., Chatterjee, S. K., & Bhattarai, A. (2017). Micellization of sodium dodecyl sulphate in presence and absence of alkali metal halides at different temperatures in water and methanol-water mixtures. *Journal of Molecular*

Liquids. <https://doi.org/10.1016/j.molliq.2017.12.014>

- Niraula, T. P., Shah, S. K., Chatterjee, S. K., & Bhattarai, A. (2018). Effect of methanol on the surface tension and viscosity of sodiumdodecyl sulfate (SDS) in aqueous medium at 298.15–323.15 K. *Karbala International Journal of Modern Science*, **4**(1), 26–34. <https://doi.org/10.1016/j.kijoms.2017.10.004>
- Pakiet, M., Kowalczyk, I., Leiva Garcia, R., Akid, R., & Brycki, B. (2020). Cationic clevelable surfactants as highly efficient corrosion inhibitors of stainless steel AISI 304: Electrochemical study. *Journal of Molecular Liquids*, **315**, 113675. <https://doi.org/10.1016/j.molliq.2020.113675>
- Pan, A., Naskar, B., Prameela, G. K. S., Kumar, B. V. N. P., Mandal, A. B., Bhattacharya, S. C., & Moulik, S. P. (2012). Amphiphile behavior in mixed solvent media I: Self-aggregation and ion association of sodium dodecylsulfate in 1,4-dioxane-water and methanol-water media. *Langmuir*, **28**(39), 13830–13843. <https://doi.org/10.1021/la303281d>
- Pan, Animesh, Mati, S. S., Naskar, B., Bhattacharya, S. C., & Moulik, S. P. (2013). Self-aggregation of MEGA-9 (N-Nonanoyl-N-methyl-d-glucamine) in aqueous medium: Physicochemistry of interfacial and solution behaviors with special reference to formation energetics and micelle microenvironment. *Journal of Physical Chemistry B*, **117**(25), 7578–7592. <https://doi.org/10.1021/jp400139d>
- Plutino, M. R., Guido, E., Colleoni, C., & Rosace, G. (2017). Effect of GPTMS functionalization on the improvement of the pH-sensitive methyl red photostability. *Sensors and Actuators, B: Chemical*, **238**, 281–291. <https://doi.org/10.1016/j.snb.2016.07.050>
- Prasad Tajpuriya, G., Shah, P., Shahi, N., & Bhattarai, A. (2021). UV–Vis studies of methyl red in the presence of sodium dioctylsulfosuccinate/acetone and sodium dioctylsulfosuccinate/acetone/water. *Spectrochimica Acta - Part A: Molecular and Biomolecular Spectroscopy*, **255**, 119646. <https://doi.org/10.1016/j.saa.2021.119646>
- Ruiz, C. C. (1999). Thermodynamics of micellization of tetradecyltrimethylammonium bromide in ethylene glycol-water binary mixtures. *Colloid and Polymer Science*, **277**(7), 701–707. <https://doi.org/10.1007/s003960050443>

- Ruiz, C. C., Díaz-López, L., & Aguiar, J. (2008). Micellization of sodium dodecyl sulfate in glycerol aqueous mixtures. *Journal of Dispersion Science and Technology*, **29**(2), 266–273. <https://doi.org/10.1080/01932690701707571>
- Sachin, K. M., Karpe, S. A., Singh, M., & Bhattarai, A. (2019a). Self-assembly of sodium dodecylsulfate and dodecyltrimethylammonium bromide mixed surfactants with dyes in aqueous mixtures. *Royal Society Open Science*, **6**(3). <https://doi.org/10.1098/rsos.181979>
- Sachin, K. M., Karpe, S. A., Singh, M., & Bhattarai, A. (2019b). Study on surface properties of sodiumdodecyl sulfate and dodecyltrimethylammonium bromide mixed surfactants and their interaction with dyes. *Heliyon*, **5**(4), e01510. <https://doi.org/10.1016/j.heliyon.2019.e01510>
- Sar, P., Ghosh, A., Scarso, A., & Saha, B. (2019). Surfactant for better tomorrow: applied aspect of surfactant aggregates from laboratory to industry. *Research on Chemical Intermediates*, **45**(12), 6021–6041. <https://doi.org/10.1007/s11164-019-04017-6>
- Shah, P., Jha, N., & Bhattarai, A. (2020). Physicochemical studies on the interaction between sodium dodecyl sulfate and methylene blue in methanol-water mixed solvent media. *Journal of Chemistry*, **2020**. <https://doi.org/10.1155/2020/5292385>
- Shah, P., Kumari Jha, S., & Bhattarai, A. (2021). Spectrophotometric study of the sodium dodecyl sulfate in the presence of methylene blue in the methanol–water mixed solvent system. *Journal of Molecular Liquids*, **340**, 117200. <https://doi.org/10.1016/j.molliq.2021.117200>
- Shah, S. K., & Bhattarai, A. (2020). Interfacial and Micellization Behavior of Cetyltrimethylammonium Bromide (CTAB) in Water and Methanol-Water Mixture at 298.15 to 323.15 K. *Journal of Chemistry*, **2020**. <https://doi.org/10.1155/2020/4653092>
- Shah, S. K., Chatterjee, S. K., & Bhattarai, A. (2016). Micellization of cationic surfactants in alcohol — water mixed solvent media. *Journal of Molecular Liquids*, **222**, 906–914. <https://doi.org/10.1016/j.molliq.2016.07.098>

- Shah, S. K., Chatterjee, S. K., & Bhattarai, A. (2016). The Effect of Methanol on the Micellar Properties of Dodecyltrimethylammonium Bromide (DTAB) in Aqueous Medium at Different Temperatures. *Journal of Surfactants and Detergents*, **19**(1), 201–207. <https://doi.org/10.1007/s11743-015-1755-x>
- Sharifi, S., Nazar, M. F., Rakhshanizadeh, F., Sangsefedi, S. A., & Azarpour, A. (2020). Impact of amino acids, organic solvents and surfactants on azo-hydrazone tautomerism in Methyl Red: spectral-luminescent and nonlinear optical properties. *Optical and Quantum Electronics*, **52**(2). <https://doi.org/10.1007/s11082-020-2211-3>
- Shehata, H. A., El-Wahab, A. A. A., Hafiz, A. A., Aiad, I., & Hegazy, M. A. (2008). Syntheses and characterization of some cationic surfactants. *Journal of Surfactants and Detergents*, **11**(2), 139–144. <https://doi.org/10.1007/s11743-008-1064-8>
- Sheikh, F. A., & Bhat, P. A. (2012). Effect of temperature and concentration on density, apparent molar volume, ultrasound velocity, isoentropic compressibility, viscosity, and conductivity of hexadecyldimethylethylammonium bromide. *Journal of Chemical and Engineering Data*, **57**(12), 3368–3374. <https://doi.org/10.1021/je3003404>
- Simončič, B., & Špan, J. (1998). A study of dye-surfactant interactions. Part 1. Effect of chemical structure of acid dyes and surfactants on the complex formation. *Dyes and Pigments*, **36**(1), 1–14. [https://doi.org/10.1016/S0143-7208\(97\)00001-6](https://doi.org/10.1016/S0143-7208(97)00001-6)
- Singh, A., Dayu, X., Ituen, E., Ansari, K., Quraishi, M. A., Kaya, S., & Lin, Y. (2020). Tobacco extracted from the discarded cigarettes as an inhibitor of copper and zinc corrosion in an ASTM standard D1141-98(2013) artificial seawater solution. *Journal of Materials Research and Technology*, **9**(3), 5161–5173. <https://doi.org/10.1016/j.jmrt.2020.03.033>
- Singh, A., Singh, V. K., & Quraishi, M. A. (2010). Aqueous extract of kalmegh (*andrographis paniculata*) leaves as green inhibitor for mild steel in hydrochloric acid solution. *International Journal of Corrosion*, **2010**. <https://doi.org/10.1155/2010/275983>
- Singh, R. P., Rawat, J. P., Kumar, R., & Science, S. (2000). *Effect of Cationic , Non-*

ionic and Anionic Surfactants on the Adsorption of Carbofuran on Three Different Types of Indian Soil. **2**(1), 333–346. <https://doi.org/10.1260/0263617001493477>

Smith, O. E. P., Waters, L. J., Small, W., & Mellor, S. (2022). CMC determination using isothermal titration calorimetry for five industrially significant non-ionic surfactants. *Colloids and Surfaces B: Biointerfaces*, **211**, 112320. <https://doi.org/10.1016/j.colsurfb.2022.112320>

Waghmode, T. R., Kurade, M. B., Sapkal, R. T., & Bhosale, C. H. (2019). Sequential photocatalysis and biological treatment for the enhanced degradation of the persistent azo dye methyl red. *Journal of Hazardous Materials*, **371**, 115–122. <https://doi.org/10.1016/j.jhazmat.2019.03.004>

Wong, D. H., & Park, W. (1986). **7**(2), 113–116.

Yurt, A., Balaban, A., Kandemir, S. U., Bereket, G., & Erk, B. (2004). Investigation on some Schiff bases as HCl corrosion inhibitors for carbon steel. *Materials Chemistry and Physics*, **85**(2–3), 420–426. <https://doi.org/10.1016/j.matchemphys.2004.01.033>

Zhang, C., Geng, T., Jiang, Y., Zhao, L., Ju, H., & Wang, Y. (2017). Impact of NaCl concentration on equilibrium and dynamic surface adsorption of cationic surfactants in aqueous solution. *Journal of Molecular Liquids*, **238**, 423–429. <https://doi.org/10.1016/j.molliq.2017.05.033>

Zhu, H., Li, X., Lu, X., Chen, X., Li, J., Han, X., Ma, X., & Hu, Z. (2021). Intra-/inter-molecular synergistic inhibition effect of sulfonate surfactant and 2-benzothiazolethiol on carbon steel corrosion in 3.5% NaCl solution. *Corrosion Science*, **182**, 109291. <https://doi.org/10.1016/j.corsci.2021.109291>

APPENDIX

Scientific publications

National Scientific publications

Shahi, Neelam and Bhattarai, Ajaya, (2018) A survey on applications of surfactants and their investigation for commercial utilization, Medha, Vol 5, No.1, Page-46-53, ISSN 2362-5146.

Shahi, N., & Bhattarai, A. (2017). Micellisation behavior on the dodecyltrimethylammonium bromide in the presence of Brij-35 in pure water by conductivity measurement. *Bibechana*, 15, 85–89. <https://doi.org/10.3126/bibechana.v15i0.18518>

International scientific publications

SHAHI, N., SHAH, S. K., YADAV, A. P., & BHATTARAI, A. (2021). The spectral study of azo dye and cationic surfactant interaction in ethanol-water mixture. *Journal of the Serbian Chemical Society*, 86(5), 483–494. <https://doi.org/10.2298/JSC201116020S>

SCI mago (Q3) impact factor : 1.1 SJR:0.21 H-index: 49 ISSN: 03525139, 18207421

SHAHÍ, N., SHAH, S. K., YADAV, A. P., & BHATTARAI, A. (2022). Interaction of Methyl red with Cetylpyridinium chloride in Methanol-water system. *Gazi University Journal of Science*, 2022–2024. <https://doi.org/10.35378/gujs.978088>

SCI mago (Q3) impact factor : 0.854 SJR:0.18 H-index: 20

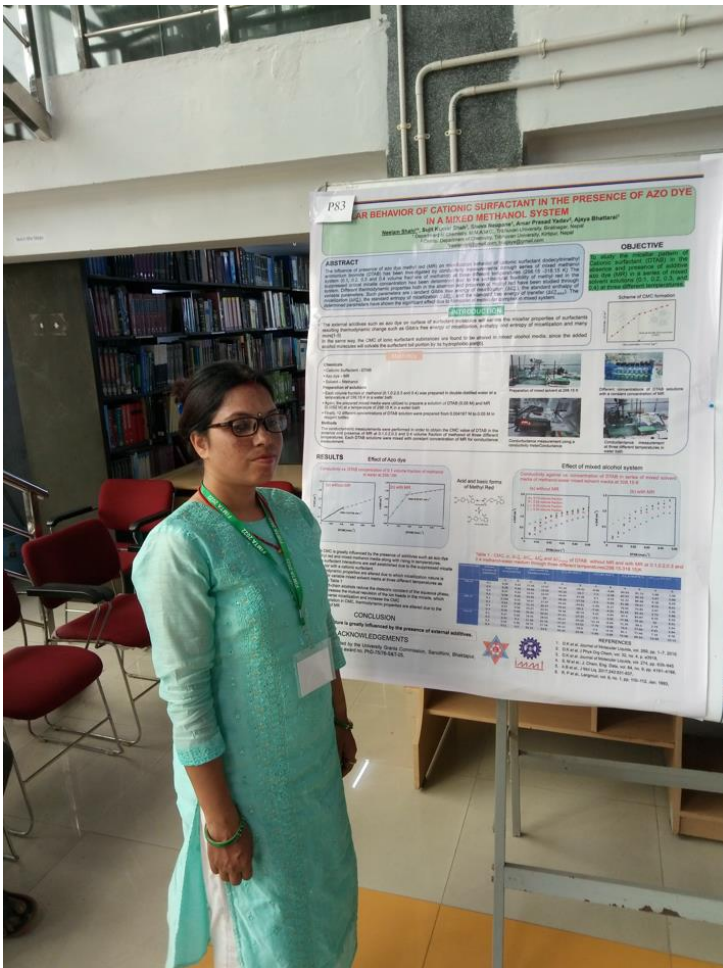
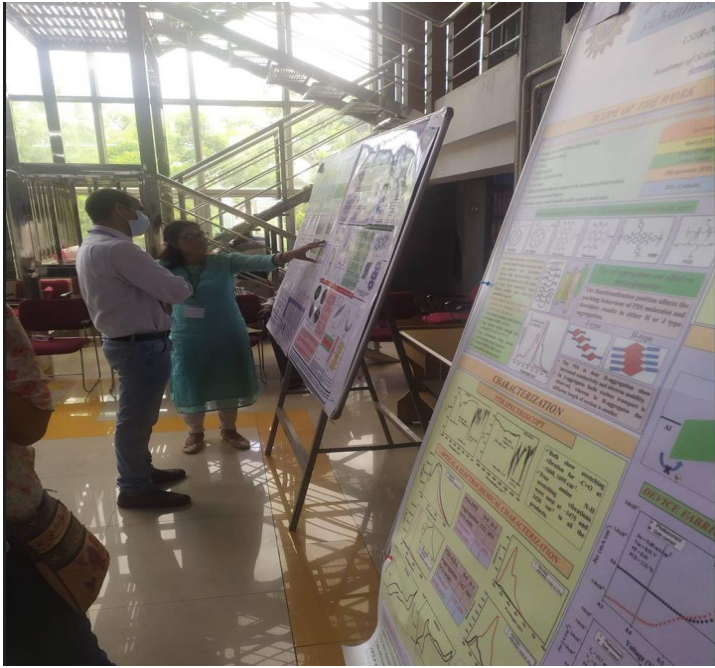
ISSN:21471762, 13039709

Participation in International conferences and workshops

- Workshop on research writing and publishing held on 8-11th May, 2019, Biratnagar, Nepal
- Consultative workshop on academic writing and publishing in Nepal Universities: Existing Practices and the gaps held on 12th September 2019, Biratnagar, Nepal
- Poster presentation in the 8th Asian conference on colloid & interface science (ACCIS 2019) held on 24-27th sept., Kathmandu, Nepal
- Poster presentation in the international conference On Frontiers in Materials for Technological Applications (FIMTA 2022) held on 03-05 Aug., 2022, Bhubaneswar, India

Poster presentations at FIMTA 2022







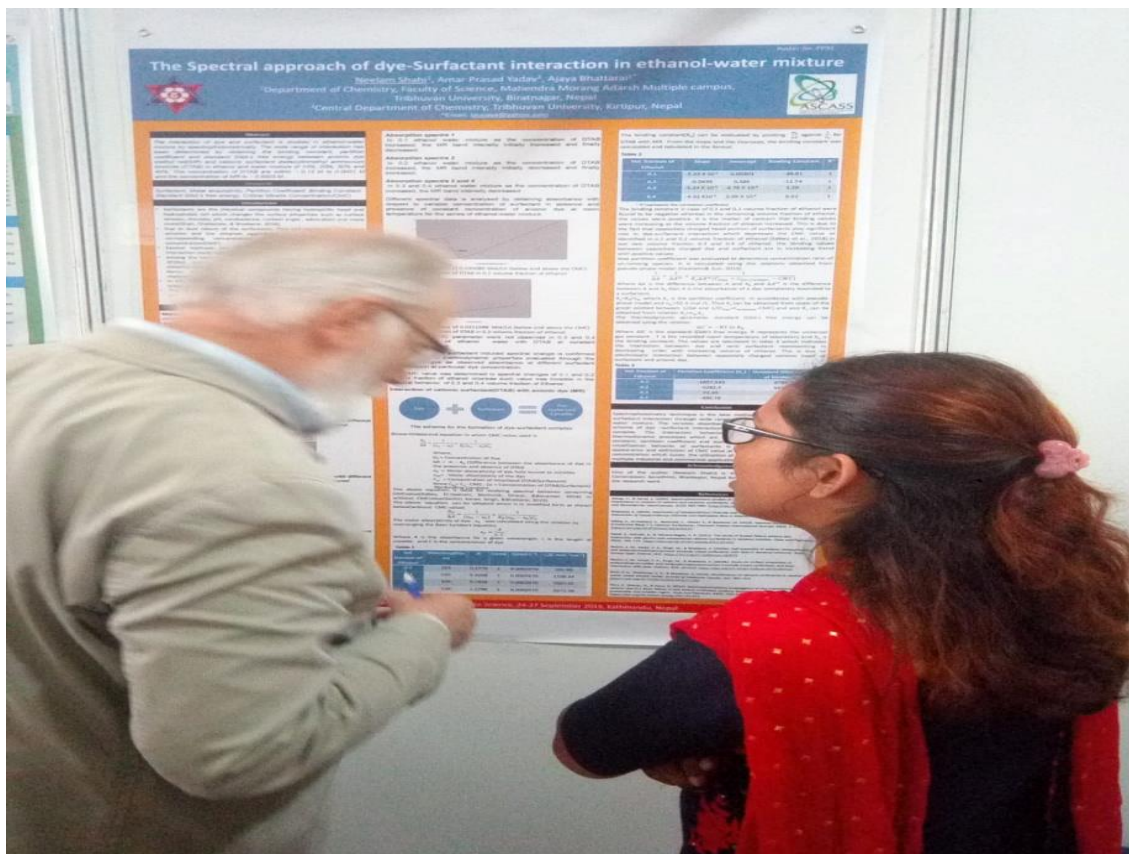
INTERNATIONAL CONFERENCE
FIMTA 2022
FRONTIERS IN MATERIALS FOR TECHNOLOGICAL APPLICATIONS
AUGUST 03-05, 2022
75
Special Anniversary
IIMT

FIMTA 2022
International Conference on
Frontiers in Materials for Technological Applications
August 03-05, 2022
PARTICIPANT
Name: NEELIMA SHRIVASTAVA
Institute: TATYASAHEB KORE UNIVERSITY
Organized by
CSIR - Institute of Materials and Materials Technology,
Bhilai, Odisha

FIMTA 2022
International Conference on
Frontiers in Materials for Technological Applications
August 03-05, 2022.

FIMTA 2022

Poster Presentation at ACCIS-2019





International Conference on
Frontiers In Materials for Technological Applications
(August 03-05, 2022)



FIMTA 2022

CERTIFICATE OF PRESENTATION

This is to certify that

NEELAM SHAHI

has made Oral/Poster presentation in the International Conference on Frontiers in
Materials for Technological Applications (FIMTA 2022) organized by CSIR-Institute of
Minerals and Materials Technology, Bhubaneswar – 751013 during **August 03-05, 2022.**




Head, HRD
CSIR-IMMT




Convener
FIMTA 2022



The 8th Asian Conference on Colloid
& Interface Science (ACCIS 2019)
Sept. 24-27, Kathmandu, Nepal



Certificate of Participation

This is to certify that
Neelam Shahi

has participated and contributed **Poster Presentation** in

The 8th Asian Conference on Colloid & Interface Science (ACCIS 2019) organized by the
Asian Society for Colloid and Surface Science (ASCASS) held in Pulchowk Campus,
Institute of Engineering, Tribhuvan University, Lalitpur, Kathmandu, Nepal.



Dr. Lok Kumar Shrestha

Dr. Lok Kumar Shrestha
Chairperson (ACCIS 2019)

September 27, 2019

Prof. Dr. Toyoko Imae

Prof. Dr. Toyoko Imae
President (ASCASS)





WORKSHOP ON RESEARCH WRITING AND PUBLISHING

8th-11th May, 2019

Certificate



This is to Certify that Mr./Mrs. Neelam Shahi
of Mahendra Morang Adarsh Multiple Campus, Biratnagar participated

in the Workshop on Research Writing & Publishing organized by Research Management cell,
Mahendra Morang Adarsh Multiple Campus, Biratnagar & supported by University Grants
Commission, Nepal held at Biratnagar from 8th-11th May, 2019.


Prof. Dr. Devendra Adhikari
(Facilitator)


Mr. Baburam Timalsena
(Campus Chief)
M.M.A.M. Campus, Biratnagar


Dr. Tilak Prasad Gautam
(Co-ordinator)
Workshop Organizing Committee,
Research Management Cell,
M.M.A.M. Campus, Biratnagar



Tribhuvan University
Mahendra Morang Adarsh Multiple Campus
www.mam.edu.np
Biratnagar, Morang, Nepal


Centre for Social Change
सामाजिक परिवर्तन केन्द्र

Academic Writing and Publishing in
Nepali Universities: Existing Practices and the Gaps
Consultative Workshop

12th September 2019
Biratnagar, Province - 1

In recognition that

Mr./Mrs./Ms. Neelam Shahi
has actively participated / facilitated / presented paper
in the workshop.


Baburam Timalsena
Campus Chief
MMAM Campus, Biratnagar


Hon. Jagan Ghimire
Chief Guest
Minister, Ministry of Social Development
Province-1


Prof. Dr. Pramod Kr. Jha
Special Guest
Member, UGC
Nepal

Grade sheet



Tribhuvan University
Institute of Science and Technology
Dean's Office

SEMESTER EXAMINATION 2075

Name of Student: Neelam Shahi

Exam Roll No.: 100021

Level: Ph.D.

Ph.D. Enrolment No.: 83/074

Department: Central Dept. of Chemistry

T.U. Regd. No.: 5-1-3-100-2005

Semester: I

Grade Sheet

Code No.	Course Title	Cr. Hrs.	Grade Point	Grade
PHS 911	Philosophy of Science	3	3.3	B+
RM 912	Research Methodology	3	3.7	A-
Sem 913	Seminar	3	3.3	B+

SGPA: 3.4

Verified By: *Sndu*

Date: *oct. 9, 2018*



K. Prasad
Asst. Dean



Tribhuvan University
Institute of Science and Technology
Dean's Office

SEMESTER EXAMINATION-2075

Name of Student: Neelam Shahi Exam Roll No.: 200020
Level: Ph.D. Ph.D. Enrolment No.: 83/074
Department: Central Dept. of Chemistry T.U. Regd. No.: 5-1-3-100-2005
Semester: 2

Grade Sheet

Code No.	Course Title	Cr. Hrs.	Grade Point	Grade
CHE 951	Advanced Research Methodology	3	3	B
CHE 955	Electrochemistry and Corrosion Science (specific)	3	3.7	A-
CHE 952	Seminar	3	3.7	A-

SGPA: 3.47

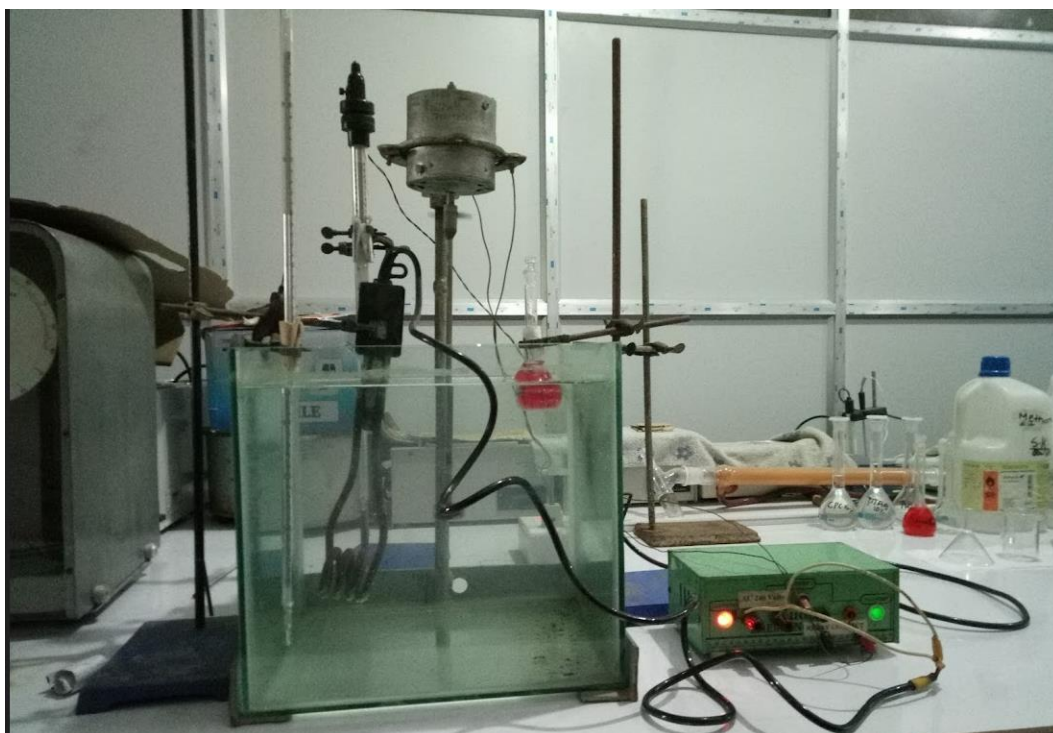
Verified By: *[Signature]*

Date: *Sept. 16, 2019*

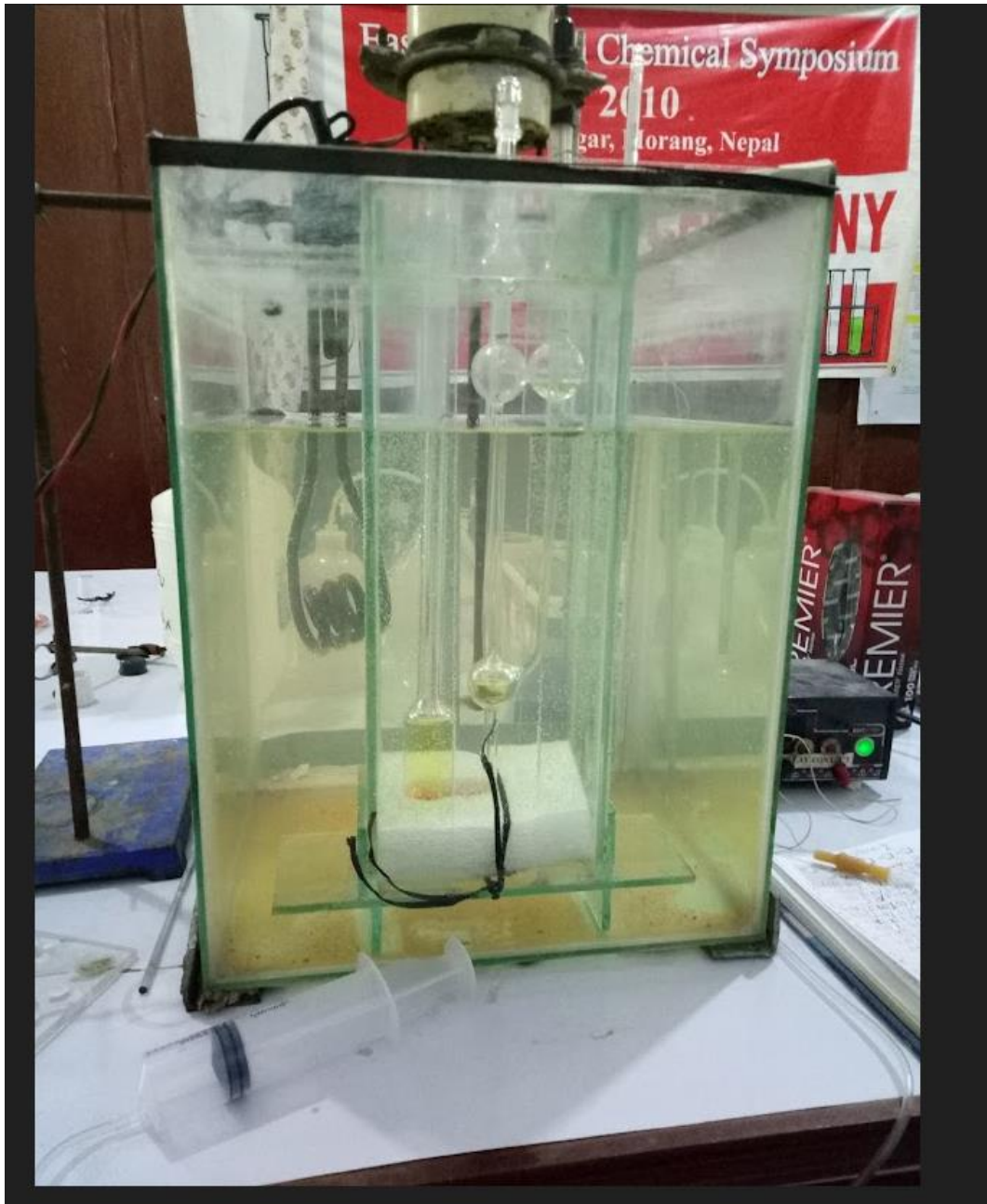
[Signature]
Asst. Dean

lab photo with equipments in Kathmandu and Biratnagar

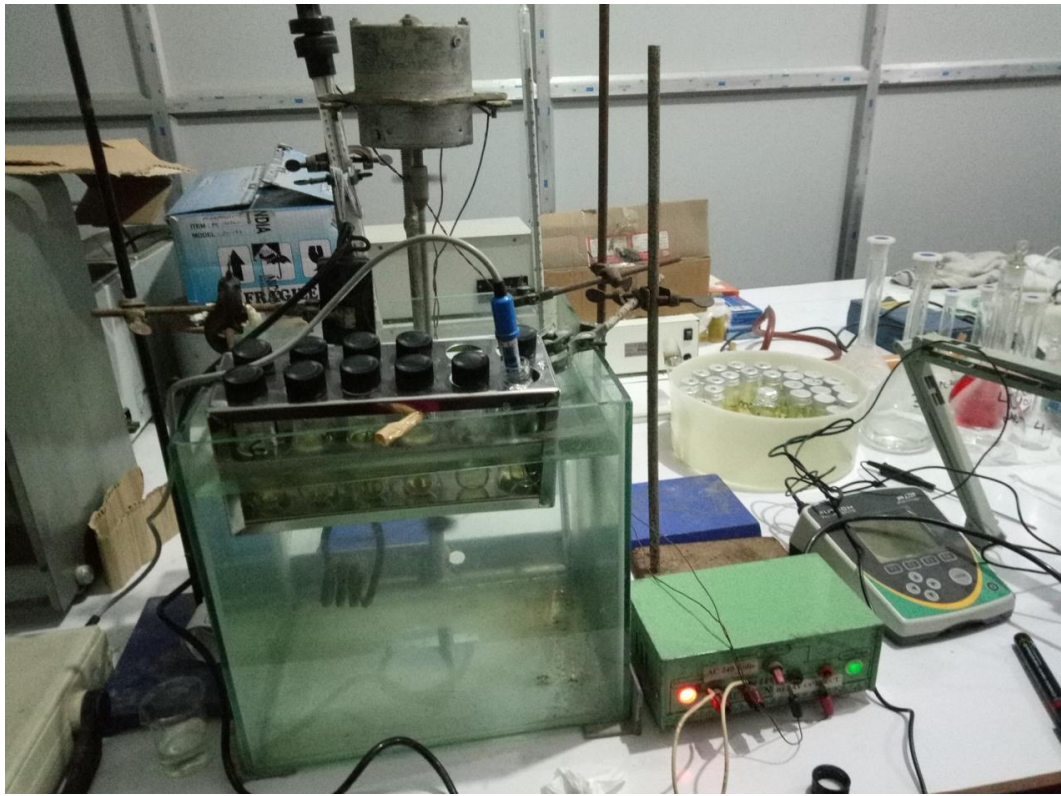




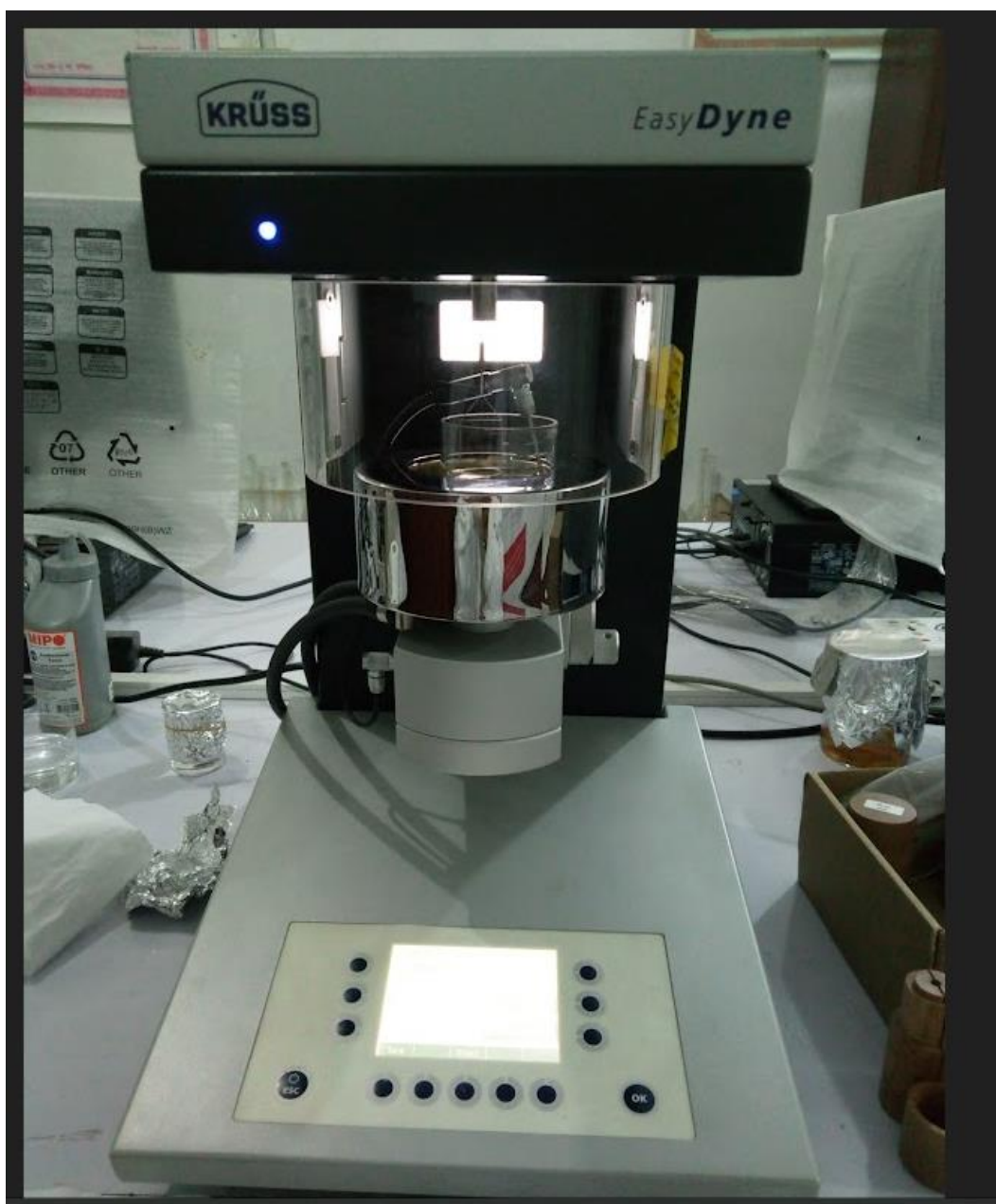
Water bath set up



ManSingh Survimeter set up in water bath



Water bath set up with solutions



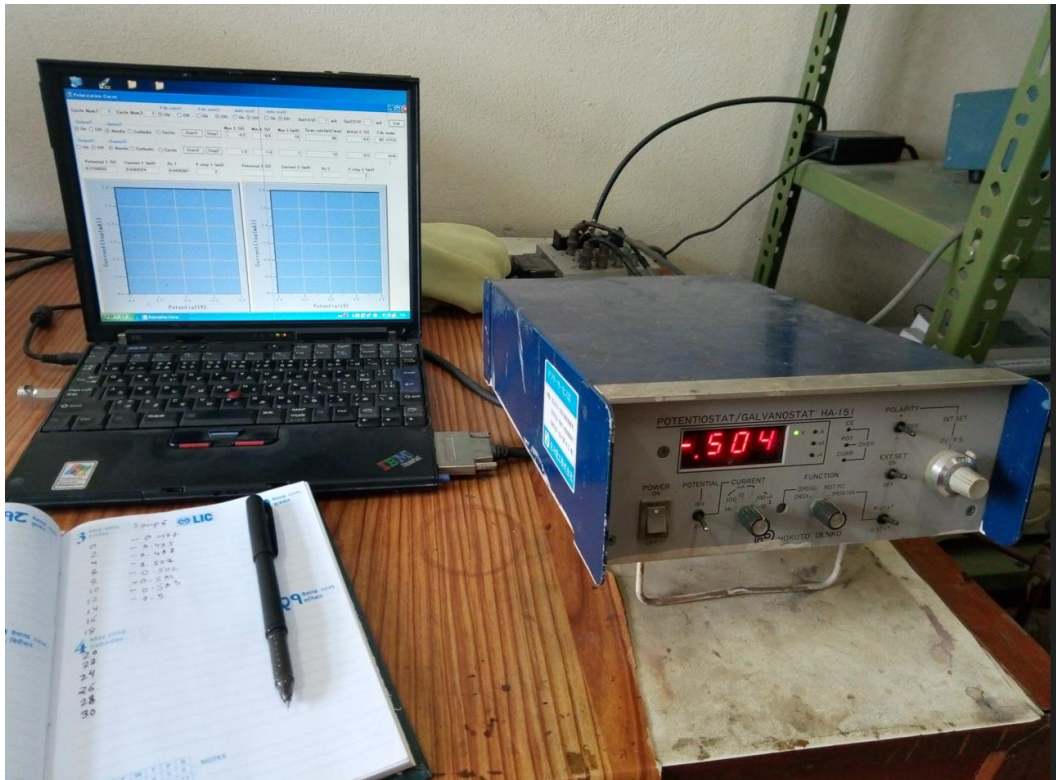
Easy dyne tensiometer K20S



Digital ultrasonic sonicator



Double beam (MARS ME-SP 195UV, India) spectrophotometer set up with desktop



Potentiodynamic polarisation using Hokuto Denko potentiostat



Solutions for weight loss study



J. Serb. Chem. Soc. 86 (5) 483–494 (2021)
JSCS–5436

The spectral study of azo dye and cationic surfactant interaction in ethanol–water mixture

NEELAM SHAHI¹, SUJIT KUMAR SHAH¹, AMAR PRASAD YADAV²
and AJAYA BHATTARAI^{1*}

¹Department of Chemistry, M.M.A.M.C., Tribhuvan University, Biratnagar, Nepal and

²Central Department of Chemistry, Tribhuvan University, Kirtipur, Nepal

(Received 16 November 2020, revised 10 March, accepted 11 March 2021)

Abstract: The interaction of the azo dye methyl red (MR) with dodecyl trimethyl ammonium bromide (DTAB) has been studied by the spectrometric methods through the azo-hydrazone tautomeric behaviour of MR for a series of the ethanol–water system (0.1, 0.2, 0.3 and 0.4 volume fractions of ethanol) at room temperature. The critical micelle concentration was determined using the conductometric technique with the increased ethanol volume, influenced by the solvent polarity and the architectural flexibility of methyl red. The azo form of methyl red brings the electrostatic interaction with the cationic surfactant through the adsorption phenomenon. The binding parameters were calculated with the aid of a modified Benesi–Hildebrand equation.

Keywords: molar absorptivity; binding constant; standard Gibbs energy.

INTRODUCTION

The performance of the interaction between dye and surfactant is one of the basic requirements for understanding the dyeing process and textile finishing.^{1–5} In order to study this process numerous researches have been performed by the selective research techniques to access the basic information of the interactions for the process of the molecular complex formation in the dye-surfactant ion pair.^{6–11}

There are no specified studies about the azo dye methyl red with cationic surfactant dodecyl trimethyl ammonium bromide, using various methods.^{12–17} The absorbance peak of methyl red was decreased, due to the photodegradation in water. It was checked after 10, 20 and 35 min (complete photodegradation) by the kinetic analysis treatment, which is based on the azo dye photosensitization.¹⁸ The anchoring position of the –COOH group at the para position of methyl red tuned the wavelength and intensity¹⁹ and showed a broad peak at 519 nm in

*Corresponding author. E-mail: bkajaya@yahoo.com
<https://doi.org/10.2298/JSC201116020S>

hydrazone form, indicating the considerable optical nonlinearities.²⁰ The visible spectrum of MR in aqueous solutions is marked by the overlap of a principal peak at 520 ± 15 nm and a shoulder peak at 435 ± 20 nm, for the hydroazo (acidic) and the azo (alkaline) species respectively.²¹

In this paper, the spectrophotometric study of the interaction between azo dye methyl red (MR) (Fig. 1) and cationic surfactant dodecyl trimethyl ammonium bromide (DTAB) (Fig. 2) is described.

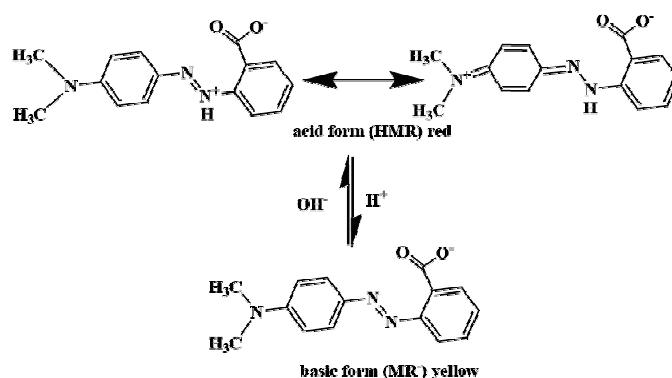


Fig. 1. Acid and basic forms of methyl red.

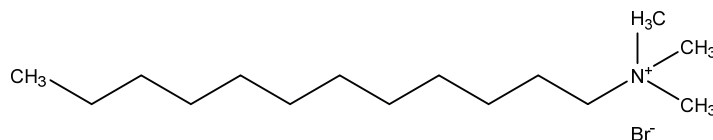


Fig. 2. Dodecyl trimethyl ammonium bromide.

The interaction between dye and surfactant plays an important role in the formation of the complex as shown in Fig. 3.

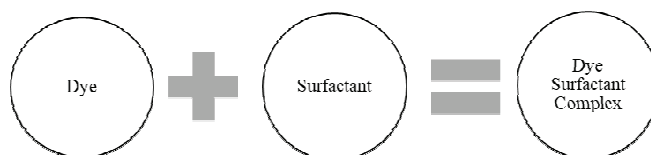


Fig. 3. The interaction between dye and surfactant for their complex formation.

To study the significance of the interaction of the molecular complex formation of the azo dye–cationic surfactant ion pair, the absorbance measurement was performed for the series of the ethanol–water systems containing the various volumes of ethanol (0.1, 0.2, 0.3 and 0.4 volume fractions of ethanol). A modified model was applied in order to determine the binding constants and the change of standard Gibbs energy of binding for the molecular complex formation

of the ion pair. The result displayed the influence of volume fraction of ethanol on the formation of dye–surfactant molecular complex and the importance of the interaction of azo dye and cationic surfactant.

Methyl red is a good example which illustrates that both the linear and non-linear optical properties can be seen through the absorbance technique. The literature shows the azo-hydrazone tautomerism of MR, with the change of surfactant charge effects and without the change in solvent polarity, generates the azo-hydrazone tautomerism as shown in Fig. 1.^{14,20,21} The optical sensitivity of azo dye makes the interaction study interesting with a cationic surfactant.¹⁴ The interaction of the azo dye and the cationic surfactant brings the flexibility in absorbance which alters the nature of spectra.^{12,13}

The present study describes the azo-hydrazone tautomerism, using the absorbance techniques along with the observation of binding constant and the change of Gibbs energy of binding of DTAB on MR, which will facilitate the advancement in the molecular design of similar derivatives, specifically a –COOH group azo dye through the photosensitized system in optical tenability. We applied a spectrophotometric technique and used the modified Benesi-Hildebrand equation in order to calculate the binding constant of methyl red, in the presence of DTAB/ethanol/water system. Such a concept was applied to calculate the binding parameters (the binding constant and the change of standard Gibbs energy of binding) for dyes (methylene blue and methyl orange) absorbance in DTAB–SDS mixed surfactant, by the absorption technique in an aqueous medium, without using critical micelle concentration (*CMC*) values.²²

EXPERIMENTAL

Chemicals

DTAB and MR were obtained from Loba Chemicals, India. Similarly, MR (95 %) was purchased from Ranbaxy, India, and used without purification and spectroscopy quality ethanol was obtained from Merck, India.

Preparation of solutions

Four types of solutions were prepared to study the interaction of MR–DTAB in the ethanol–water system.

In the first part of the study, 0.1, 0.2, 0.3 and 0.4 volume fractions of ethanol–water mixed solvent were prepared. Sequentially the surfactant (DTAB, concentration ranging from 10^{-4} to 0.12 mol L^{-1} and the azo dye MR at a constant concentration of $2.97 \times 10^{-4} \text{ mol L}^{-1}$ were prepared separately in the respective volume fraction of ethanol–water. In the second part of the study, the spectral absorbance corresponding to wavelengths ranging from 300 to 700 nm of the solution at variable concentrations of DTAB, with a constant dye concentration of MR, was obtained for the interaction study.

Methods

The spectrophotometric measurements were recorded by a single beam microprocessor UV–Vis spectrophotometer (LT-290 Model, India) from which UV–Vis spectra were registered at room temperature using 1 cm length quartz cuvette. The conductometric measure-

ments were performed in order to obtain the *CMC* value of DTAB in the absence, as well as the presence of MR at 0.1, 0.2, 0.3 and 0.4 volume fraction of ethanol, as described in the literature.

RESULTS AND DISCUSSION

UV – Vis spectra of azo dye in ethanol – water mixture

The UV–Vis spectra of MR in the ethanol-water mixture (from 0.1 to 0.4 volume fractions of ethanol) were measured at the constant dye concentration ($C_{\text{dye}} = 2.97 \times 10^{-4} \text{ mol/L}^{-1}$). When the graph displaying the relation between absorbance (A) and wavelength (λ) was plotted (Fig. 4) the redshift was observed, from 0.4 to 0.2 volume fraction of ethanol, which was due to an increase in the dielectric constant and the reduction of solubility.²³ But the redshift between 0.1 and 0.2 volume fraction of ethanol were not observed. The absorbance spectra of MR at 0.1 volume fraction of ethanol showed two broad peaks at λ_{abs} of 532 and 529 nm. However, the absorbance spectra of MR showed a slight redshift with broad peaks at λ_{abs} of 528, 529 and 532 nm for 0.4, 0.3 and 0.2 volume fraction of ethanol, respectively. The observed peaks of MR as hydrazone (acidic) species were found at 0.1, 0.2, 0.3 and 0.4 volume fraction of ethanol. Thus, the UV–Vis spectra of methyl red were found to be solvent-dependent and the absorbance of methyl red in 0.4 volume fraction of ethanol is largest among 0.3, 0.2, 0.1 volume fraction of ethanol (Table I).

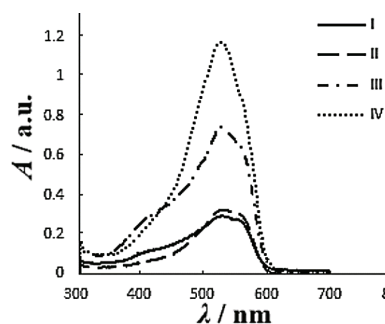


Fig. 4. Visible spectra of MR at various volume fractions of ethanol. Here, I, II, III and IV represent volume fraction of ethanol: 0.1, 0.2, 0.3 and 0.4, respectively.

TABLE I. The calculation for ϵ_0 from Eq. (4)

Volume fraction of ethanol	$\lambda_{\text{max}} / \text{nm}$	$A / \text{a. u.}$	$\epsilon_0 / \text{L mol}^{-1}\text{cm}^{-1}$
0.1	532	0.2938	989.22
0.2	532	0.3268	1100.34
0.3	529	0.7428	2501.01
0.4	528	1.1798	3972.39

UV – Vis spectra of cationic surfactant – azo dye interactions in ethanol – water mixture

The UV–Vis spectra of MR in ethanol–water–DTAB were observed at constant dye concentration. When the graph (Fig. 5) was plotted (absorbance vs. wavelength), the absorbance peak of MR in ethanol–water–DTAB showed a broad absorbance peak at λ_{abs} of 419, 424, 421 and 420 nm for 0.1, 0.2, 0.3 and 0.4 volume fraction of ethanol, respectively. The peak range is attributed to the azo form of MR within ethanol–water–DTAB. The blue shift is observed for the constant dye concentration at the variable concentration of DTAB for the spectra of 'V' of legend represented in Fig. 5 – A, B, C and D were due to the formation of H-aggregates during the electrostatic interaction in the molecular complex (Fig. 3).²⁴

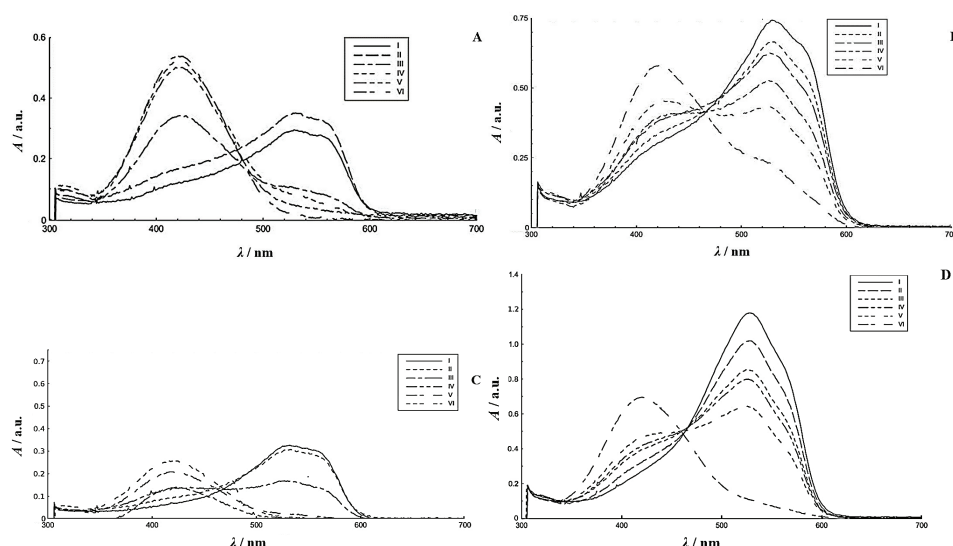


Fig. 5. Absorption spectra for methyl- red with presence and absence of DTAB; volume fraction of ethanol: 0.1 (A); 0.2 (B); 0.3 (C); 0.4 (D).

In the recent study, the interaction of CTAB (cationic surfactant) with MR is attributed to the azo form at λ_{abs} of 414 nm, whereas the interaction of AOT (anionic surfactant) with MR is subjected to the hydrazone form at $\lambda_{\text{abs}} = 519$ nm.¹⁴

In the present work, the interaction of cationic surfactant (DTAB) with the azo dye (MR) is studied through the spectrophotometric method. In the case of MR, due to its photoisomerisation, its azo(basic) form attracts the ionized surface-active agents. The ionic surfactants dissociate as electrolytes (weak or strong) which shows the adsorption phenomenon. The idealized charged spherical micelles are partially neutralized by the counterions forming the stern layer as shown in Fig. 6. The long alkyl groups of surfactants are in the interior of the micelle and the hydrophilic (polar) part of surfactants are at the surface, which exhibits the electrostatic interaction with the counterions of azo dye. Due to such

interactions, approximately 60–80 % micellized charge is neutralized by counterions and the remaining unbounded counterions are moving freely, forming the Gouy–Chapman double layer.

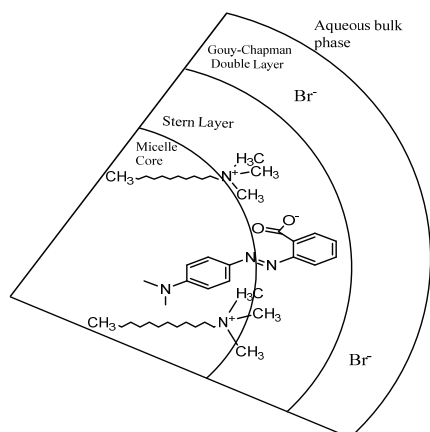


Fig. 6. A schematic structure of cationic surfactant with azo dye.²⁷

We observed the interaction through different spectral behaviour and the obtained absorbance concerning the constant concentration of azo dye in the absence and the presence of a variable concentration of DTAB, for the series of the ethanol–water mixture, at room temperature.²⁵

The spectral characteristics of azo dye were greatly influenced by the addition of cationic surfactant in the presence of various ethanol concentrations. The absorbance was increased with rised ethanol volume (Fig. 4), which contributes to the formation of molecular complex between the cationic surfactant and the azo dye as presented in Fig. 6. The origin of electrostatic interaction on the hydrocarbon core of the surfactant, at constant dye concentration, was analysed due to a decrease in absorbance with a higher concentration range of ionic surfactant.²⁶

Various natures of absorption spectra of a dye with the presence and absence of cationic surfactant had been observed for the series of the ethanol–water mixtures as shown in Fig. 5.

Absorption spectra in Fig. 5A. In 0.1 volume fraction of ethanol, as the concentration of DTAB increased the MR band intensity initially increased and finally decreased. Here, I, II, III, IV, V and VI represents the DTAB concentrations ($C/\text{mol L}^{-1}$), which were varied from as 0, 0.011695, 0.023390, 0.035085, 0.046780 and 0.116951, respectively.

The absorption spectra in Fig. 5B. In 0.2 volume fraction of ethanol, as the concentration of DTAB increased the MR band intensity initially decreased and then increased. Here, I, II, III, IV, V and VI represents the DTAB concentrations

($C/\text{mol L}^{-1}$), which were varied from as 0, 0.0105994, 0.0211988, 0.0317982, 0.0423976 and 0.1059940, respectively.

The absorption spectra in Fig. 5C and D. In 0.3 and 0.4 volume fraction of ethanol, as the concentration of DTAB increased the MR band intensity decreased. Here, in the case of Fig 5C, I, II, III, IV, V and VI represent DTAB concentrations ($C/\text{mol L}^{-1}$), which were varied as 0, 0.011122, 0.022244, 0.033366, 0.044488 and 0.111220, respectively. In the case of Fig 5D, I, II, III, IV, V and VI represent DTAB concentrations ($C/\text{mol L}^{-1}$), which were varied as 0, 0.011122, 0.022244, 0.033366, 0.044488 and 0.111220, respectively.

Analysis of cationic surfactant – azo dye interactions in ethanol – water mixture

We used the spectrophotometric technique and confirmed the surfactant induced spectral change by binding and thermodynamic properties, evaluated through the spectral changes, as the observed absorbance at different surfactant concentrations at constant dye concentration in the ethanol-water mixture, Fig. 5.

Shah *et al.*²⁸ investigated the CMC of DTAB in the ethanol–water mixture up to 0.6 volume fraction of ethanol using conductometry and tensiometry. The CMC was found to be increased up to 0.4 volume fraction of ethanol due to a decrease in hydrophobic character, with the addition of ethanol and the decrease in CMC up to 0.6 due to entrance of alcohol molecules into a micellar core. We used the conductometry technique to obtain the CMC value of DTAB in the absence, as well as in the presence of MR, at 0.1, 0.2, 0.3 and 0.4 volume fraction of ethanol. The sequential increased CMC is obtained in the adopted system, but the CMC values are suppressed with MR, in comparison to CMC values in the absence of MR.^{28,29} The decreased CMCs of DTAB, in the presence of MR is due to the change in the status of the molecular complex system.²⁹ The CMC values are listed the in Table II along with literature.²⁸

TABLE II. CMC values of DTAB in the presence and absence of MR at 298.15 K

Volume fraction of ethanol	CMC / mol L ⁻¹		
	With MR	Without MR	Without MR ²⁸
0.1	0.01497	0.01637	0.0151
0.2	0.02102	0.02178	0.0214
0.3	0.02110	0.03054	0.0325
0.4	0.02487	0.04375	0.0462

It can be seen that both the conductivity and CMC of DTAB decrease with the addition of MR, as it is presented in Fig. 7, with is in agreement with the literature.³⁰

The interaction between the dye and micellized surfactant can be described by the Eq. (1). Here, the term D, S, DS and K_b represent the dye, surfactant, dye–surfactant associate and binding constant, respectively:



Fig. 8 displays for the interaction study for the determination of the binding constant (K_b), related to the scheme on Fig. 6, which is calculated using the modified Benesi–Hildebrand Equation (2):²²

$$\frac{D_T}{\Delta A} = \frac{1}{(\epsilon_m - \epsilon_0)} + \frac{1}{K_b(\epsilon_m - \epsilon_0)C_s} \quad (2)$$

$$\Delta A = A - A_0 \quad (3)$$

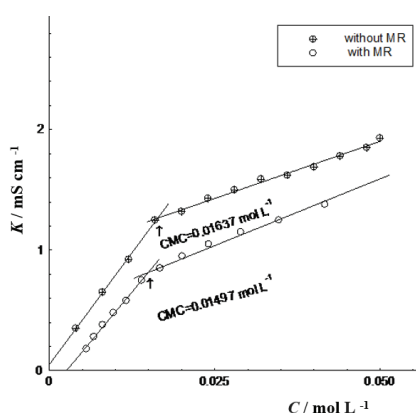


Fig. 7. Conductivity *versus* concentration of DTAB at 0.1 volume fraction of ethanol with and without MR.

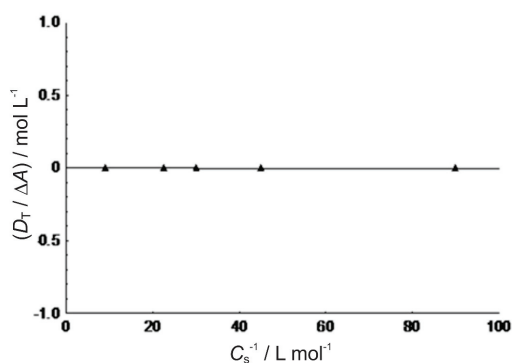


Fig. 8. The plot of $(D_T/\Delta A)$ against reciprocal of C_s for MR with DTAB at 0.3 volume fraction of ethanol. Here, $y = 3.19 \times 10^{-5}x - 8.54 \times 10^{-4}$; Max. dev. 6.05×10^{-9} , $r^2 = 1.00$.

The term D_T in Eq. (2) and A in Eq. (3) represents the concentration and the absorbance of dye. The left side of Eq. (2) consists of ΔA , which is the difference between the absorbance of dye in the presence and the absence of DTAB is expressed in Eq. (3). The right side of Eq. (2) consists of term ϵ_m , ϵ_0 , C_s and K_b which represents the molar absorptivity of the dye, the molar absorptivity of dye fully bound to micelles, the concentration of DTAB (surfactant) and the binding constant respectively. Eq. (2) can be applied for studying spectral behaviour containing *CMC* value,²⁹ or without *CMC* value.²² The molar absorptivity of dye

represented as ϵ_0 was calculated using the relation the rearranged Beer–Lambert Equation (4):

$$\epsilon_0 = \frac{A}{LC} \quad (4)$$

The Eq. (4) term consists of terms A , L and C , which represents the absorbance for a given wavelength, the length of cuvette and the concentration of dye, respectively.

The maximum wavelength corresponding to absorbance (λ_{\max} / nm), absorbance for a given wavelength (A / a.u.), length of the cuvette (L / cm), the concentration of dye (D_T / mol L⁻¹), and molar absorptivity of dye (ϵ_0 / L mol⁻¹ cm⁻¹) are the values and its interactive relationship are represented in Table I. Here, $L = 1$ cm, $C = 2.97 \times 10^{-4}$ mol L⁻¹. It can be seen that the highest molar absorptivity of azo dye at 0.4 volume fraction of ethanol is due to the influence of a higher volume of ethanol in water.²⁴

The binding constant (K_b) can be determined by plotting ($D_T/\Delta A$) against reciprocal of C_s for DTAB, with MR at 0.3 volume fraction of ethanol, as shown in Fig. 8, as a typical example. From the slope and the intercept, the binding constant was calculated at a different volume fractions of ethanol and tabulated in Table III.

TABLE III. Calculation of the slope, intercept and binding constant in the different volume fractions of ethanol

Volume fraction of ethanol	Slope $\times 10^5$	Intercept $\times 10^4$	K_b / L mol ⁻¹
0.1	6.22	7.59	12.2
0.2	1.3.3	6.48	4.87
0.3	3.19	8.54	26.77
0.4	1.48	2.96	20.00

Table III shows that the binding values, which were highest at the volume fraction of ethanol is 0.3, increased which is because the hydrophilic head portion of surfactants plays a significant role in dye-surfactant interaction.³¹ When the volume of ethanol is 0.2, the binding value between the azo dye and the surfactant is lowest, due to the abnormal aggregation around the hydrophilic portion of DTAB micelles by MR molecules.

Many researchers had reported that the addition of mixed solvent completely blocks the micellization behaviour of surfactant at a certain concentration level of mixed solvent.²⁹

The thermodynamic parameter, the change of standard Gibbs energy of binding can be obtained using Eq. (5):

$$\Delta G^\ominus = -RT \ln K_b \quad (5)$$

In Eq. (5), the left side represents the change of standard Gibbs energy of binding, ΔG^\ominus , whereas, on the right side, R represents a universal gas constant, the recorded room temperature of the laboratory is denoted by T and K_b is the binding constant. The values are presented in Table IV, which indicates the interaction between the dye and ionic surfactant, at 0.1, 0.2, 0.3 and 0.4 volume fractions. This is due to the strong electrostatic interaction between the hydrophilic cationic head of surfactant and azo dye as well as with a decrease in the dielectric constant with the addition of mixed solvent.^{30,32}

TABLE IV. Calculation of ΔG^\ominus in the different volume fractions of ethanol

Volum fraction of ethanol	$\Delta G^\ominus / \text{kJ mol}^{-1}$
0.1	-6010.31
0.2	-3803.77
0.3	-7898.50
0.4	-7197.98

CONCLUSION

Based on the spectral study of the interaction between the azo dye MR and the cationic surfactant DTAB, the following conclusions can be summarized.

The spectrophotometric technique is the best method for the study of the dye–surfactant interaction, by a wide range of spectral analysis, with typical azo-hydrazone tautomerism in the ethanol–water mixture. The variable absorbance values ultimately indicated the scheme of dye–surfactant interaction through the adsorption phenomena and the formation of a dye surfactant complex. The interaction behaviour was studied through thermodynamic processes, which were characterized by the variable binding constant and the change of standard Gibbs energy of binding. The mixed solvent media containing alcohol–water mixtures broke down the structure of water, which lowered down the dielectric constant and hence *CMC* of DTAB increases, with the addition of ethanol in water, while *CMC* values of DTAB decrease with the presence of methyl red.

Acknowledgement. This work was supported by the University Grants Commission, Sanothimi, Bhaktapur, Nepal, under the funding award no. PhD-75/76-S&T-05.

ИЗВОД

СПЕКТРОСКОПСКО ИСПИТИВАЊЕ ИНТЕРАКЦИЈЕ АЗО БОЈЕ И КАТЈОНСКОГ СУРФАКТАНТА У СМЕШИ ЕТАНОЛ–ВОДА

NEELAM SHAH¹, SUJIT KUMAR SHAH¹, AMAR PRASAD YADAV² и AJAYA BHATTARAI¹

¹Department of Chemistry, M.M.A.M.C., Tribhuvan University, Biratnagar, Nepal и ²Central Department of Chemistry, Tribhuvan University, Kirtipur, Nepal

Интеракција азо боје метил-црвена (MR) и додецилтриметиламонијум-бромида (DTAB) је спектроскопски испитивана праћењем азо-хидразон таутомерног понашања MR за серију смеша етанол–вода (запреминске фракције етанола: 0,1, 0,2, 0,3 и 0,4) на собној температури. Критична мицеларна концентрација је одређивана кондуктометријски, и

са повећањем запремине етанола на њу утиче поларност растварача и структурна флексибилност MR. Азо облик MR се адсорбује на сурфактанту електростатичким интеракцијама. Параметри везивања су израчунати применом Бенеси–Хилдебранд (Benesi–Hildebrand) једначине.

(Примљено 16. новембра 2020, ревидирано 10 марта, прихваћено 11. марта 2021)

REFERENCES

1. G. Kyzas, E. Peleka, E. Deliyanni, *Materials* **6** (2013) 184 (<https://doi.org/10.3390/ma6010184>)
2. A. Bhattarai, A. K. Yadav, S. K. Sah, A. Deo, *J. Mol. Liq.* **242** (2017) 831 (<https://doi.org/10.1016/j.molliq.2017.07.085>)
3. A. Pal, A. Garain, D. Chowdhury, M. H. Mondal, B. Saha, *Tenside Surf. Det.* **57** (2020) 401 (<https://doi.org/10.3139/113.110700>)
4. S. Tunç, O. Duman, B. Kancı, *Dyes Pigments* **94** (2012) 233 (<https://doi.org/10.1016/j.dyepig.2012.01.016>)
5. K. M. Sachin, S. A. Karpe, M. Singh, A. Bhattarai, *Roy. Soc. Open Sci.* **6** (2019) 181979 (<https://doi.org/10.1098/rsos.181979>)
6. S. Fazeli, B. Sohrabi, A. R. Tehrani-Bagha, *Dyes Pigments* **95** (2012) 768 (<https://doi.org/10.1016/j.dyepig.2012.03.022>)
7. H. Akbaş, Ç. Kartal, *Spectrochim. Acta, A* **61** (2005) 961 (<https://doi.org/10.1016/j.saa.2004.05.025>)
8. S. Malik, A. Ghosh, P. Sar, M. H. Mondal, K. Mahali, B. Saha, *J. Chem. Sci.* **129** (2017) 637 (<https://doi.org/10.1007/s12039-017-1276-4>)
9. M. F. Nazar, S. S. Shah, M. A. Khosa, *J. Surfact. Deterg.* **13** (2010) 529 (<https://doi.org/10.1007/s11743-009-1177-8>)
10. M. H. Mondal, S. Malik, B. Saha, *Tenside Surf. Det.* **54** (2017) 378 (<https://doi.org/10.3139/113.110519>)
11. M. Mondal, M. Ali, A. Pal, B. Saha, *Tenside Surf. Det.* **56** (2019) 516 (<https://doi.org/10.3139/113.110654>)
12. S. Biswas, A. Pal, *Talanta* **206** (2020) 120238 (<https://doi.org/10.1016/j.talanta.2019.120238>)
13. F. Ahmadi, M. A. Daneshmehr, M. Rahimi, *Spectrochim. Acta, A* **67** (2007) 412 (<https://doi.org/10.1016/j.saa.2006.07.033>)
14. S. Sharifi, M. F. Nazar, F. Rakhshanizadeh, S. A. Sangsefedi, A. Azarpour, *Opt. Quantum Elec.* **52** (2020) (<https://doi.org/10.1007/s11082-020-2211-3>)
15. C. Hahn, A. Wokaun, *Langmuir* **13** (1997) 391 (<https://doi.org/10.1021/la9603378>)
16. S. Chanda, K. Ismail, *IJC A* **48** (2009) 775 (<http://nopr.niscair.res.in/handle/123456789/4686>)
17. M. H. Mondal, S. Malik, A. Roy, R. Saha, B. Saha, *RSC Adv.* **5** (2015) 92707 (<https://doi.org/10.1039/c5ra18462b>)
18. R. B. Narayan, R. Goutham, B. Srikanth, K. P. Gopinath, *J. Environ. Chem. Eng.* **6** (2018) 3640 (<https://doi.org/10.1016/j.jece.2016.12.004>)
19. L. Zhang, J. M. Cole, P. G. Waddell, K. S. Low, X. Liu, *ACS Sustain. Chem. Eng.* **1** (2013) 1440 (<https://doi.org/10.1021/sc400183t>)
20. D. N. Christodoulides, I. C. Khoo, G. J. Salamo, G. I. Stegeman, E. W. Van Stryland, *Adv. Opt. Photonics* **2** (2010) 60 (<https://doi.org/10.1364/aop.2.000060>)
21. M. R. Plutino, E. Guido, C. Colleoni, G. Rosace, *Sens. Actuators, B* **238** (2017) 281 (<https://doi.org/10.1016/j.snb.2016.07.050>)

22. K. M. Sachin, S. A. Karpe, M. Singh, A. Bhattarai, *Heliyon* **5** (2019) e01510 (<https://doi.org/10.1016/j.heliyon.2019.e01510>)
23. A. A. Rafati, S. Azizian, M. Chahardoli, *J. Mol. Liq.* **137** (2008) 80 (<https://doi.org/10.1016/j.molliq.2007.03.013>)
24. M. S. Ramadan, N. M. El-mallah, G. M. Nabil, M. Sherif, *J. Dispers. Sci. Technol.* **40** (2018) 1 (<https://doi.org/10.1080/01932691.2018.1496837>)
25. K. K. Karukstis, J. P. Litz, M. B. Garber, L. M. Angell, G. K. Korir, *Spectrochim. Acta, A* **75** (2010) 1354 (<https://doi.org/10.1016/j.saa.2009.12.087>)
26. M. L. Moyá, A. Rodríguez, M. del Mar Graciani, G. Fernández, *J. Colloid Interf. Sci.* **316** (2007) 787 (<https://doi.org/10.1016/j.jcis.2007.07.035>)
27. M. E. D. Garcia, A. Sanz-Medel, *Talanta* **33** (1986) 255 ([https://doi.org/10.1016/0039-9140\(86\)80060-1](https://doi.org/10.1016/0039-9140(86)80060-1))
28. S. K. Shah, S. K. Chatterjee, A. Bhattarai, *J. Mol. Liq.* **222** (2016) 906 (<https://doi.org/10.1016/j.molliq.2016.07.098>)
29. K. Edbey, A. El-Hashani, A. Benhmid, K. Ghwel, M. Benamer, *Chem. Sci. Int. J.* **24** (2018) 1 (<https://doi.org/10.9734/csji/2018/44312>)
30. P. Shah, N. Jha, A. Bhattarai, *J. Chem-Ny.* **2020** (2020) 5292385 (<https://doi.org/10.1155/2020/5292385>)
31. A. Rodríguez, M. del M. Graciani, M. L. Moyá, *Langmuir* **24** (2008) 12785 (<https://doi.org/10.1021/la802320s>)
32. S. Bračko, J. Špan, *Dyes Pigments* **50** (2001) 77 ([https://doi.org/10.1016/S0143-7208\(01\)00025-0](https://doi.org/10.1016/S0143-7208(01)00025-0)).

See discussions, stats, and author profiles for this publication at: <https://www.researchgate.net/publication/359367127>

Interaction of Methyl red with Cetylpyridinium chloride in Methanol–water system

Article in GAZI UNIVERSITY JOURNAL OF SCIENCE · January 2022

DOI: 10.35378/guj.s.978088

CITATIONS

0

READS

39

4 authors, including:



Neelam Shahi

Mahendra Morang Adarsha Multiple Campus, Biratnagar, Nepal

5 PUBLICATIONS 5 CITATIONS

[SEE PROFILE](#)



sujit k Shah

MMAMC, Tribhuvan University, Biratnagar

29 PUBLICATIONS 246 CITATIONS

[SEE PROFILE](#)



Ajaya Bhattarai

Tribhuvan University

225 PUBLICATIONS 1,199 CITATIONS

[SEE PROFILE](#)

Some of the authors of this publication are also working on these related projects:



A Comparative Study of Conductance of Sodium Dodecyl Sulphate in Different Percentage of Ethanol Water Media at 308.15K [View project](#)



Studies on conductivity, surface tension and viscosity of alkalimetal salts in acetone-water. [View project](#)



Interaction of Methyl Red with Cetylpyridinium Chloride in Methanol-Water System

Neelam SHAHI¹ , Sujit Kumar SHAH¹ , Amar Prasad YADAV² , Ajaya BHATTARAI^{1*} 

¹ Department of Chemistry, M.M.A.M.C., Tribhuvan University, Biratnagar, Nepal

² Central Department of Chemistry, Tribhuvan University, Kirtipur, Nepal

Highlights

- This paper focuses on interaction between methyl red and cetylpyridinium chloride.
- Critical micelle concentration of cetylpyridinium chloride determined in presence of methyl red.
- 0.1 to 0.4 volume fractions of CH₃OH provided precise measure of the methyl red spectrum.

Article Info

Received: 03 Aug 2021

Accepted: 19 Jan 2022

Keywords

Azo Dye
Cationic surfactant
CMC
Absorbance
Hypochromic shift

Abstract

The interaction between methyl red (azo dye) and cetylpyridinium chloride (cationic surfactant) in the methanol-water system were studied using a spectrophotometric technique. Variable parameters like constant dye concentration and its structure, surfactant concentration, pH, absorbance, and solvent composition were studied. Using the UV-Vis technique, critical micelle concentrations (CMCs) of cetylpyridinium chloride were measured with methyl red. The spectral data were analyzed and determined the differential absorbance, binding and partition constants, partition coefficient, the Gibbs free energy of binding and partition in mixed solvent media (0.1, 0.2, 0.3, 0.4 volume fraction (v.f.)s of methanol, respectively).

1. INTRODUCTION

Organic compounds that are amphiphilic and possess hydrophilic and hydrophobic properties are surfactants that differentiate unique compounds for utilization in various activities such as washing, dispersion, antirust, anticorrosive, moistening, penetration, bubble formation, emulsifying, catalysis, solubilization, and antistat [1]. Due to such valuable activity's studies on dye-surfactant interaction are important for improving technological advancement in industrial applications [2,3]. Advanced interaction technology is significant for the further incorporation of dyes into the micellar activity of surfactants. In addition, such interaction studies assist in chemical research associated with colloidal science, biochemistry, analytical science, and photosensitization [4,5].

Based on the molecular structure of the surfactant, dyes, and solvent mixtures, we can understand the behavior of the dye and surfactant interaction. As the dielectric constant varies in mixtures of solvents, it affects dye-surfactant interactions directly, affecting cohesive energy, micellization, binding, distribution, and solubility [6].

There are some studies of methyl red (C₁₅H₁₅N₃O₂) with CPC (C₂₁H₃₈ClN) [7-12] using various methods. To conduct a detailed analysis, we reviewed the literature [8] which reported UV-Vis measurements to

*Corresponding author, e-mail: bkajaya@yahoo.com

determine how CTAB, CPC and SDS surfactants affect the dissociation constants as well as transition intervals of cresol red, methyl orange and red. There was strong interaction of dyes with cetyltrimethylammonium bromide and hexadecylpyridinium chloride. On the other hand, sodium dodecylsulphate did not affect the dissociation constants of methyl orange or cresol red, despite the relatively strong interaction between sodium dodecylsulphate and methyl red.

By kinetic analysis and complete photodegradation after 35 minutes of treatment with azo dye photosensitization, methyl red was found to have a reduced absorbance peak after 10 and 20 minutes of treatment in water [13]. The para position of the -COOH group of methyl red modulated the wavelength as well as intensity [14] and exhibited at 519 nm as the broad peak in hydrazone form, demonstrating large optical nonlinearities [15]. The remarkably visible spectrum of MR in aqueous solutions is seen as the principal peak at 520 ± 15 nm and at 435 ± 20 nm as shoulder peak, for hydroazo (acidic) as well as azo (alkaline) species respectively [16].

From the above-studied literature, we have identified that there is no specified investigation on the interaction between CPC and MR. So in this paper, we studied the interaction between methyl red (MR), a common textile dye [13] and cationic surfactant cetylpyridinium chloride (CPC) in the volume fractions of methanol 0.1, 0.2, 0.3, and 0.4 respectively at 298.15 K.

We utilize a spectrophotometric technique to assess the binding parameters of methyl red with CPC in methanol-water solutions using CMC values, by utilizing a Benesi-Hildebrand equation for the first time. Such a concept was used by our research group for the calculation of the binding parameters for dyes (methyl orange and methylene blue) using absorbance data of mixed DTAB-SDS surfactant by spectrophotometric technique in an aqueous medium without using CMC values [17]. Shahi et al. [18] also observed the strong interaction between MR and cationic surfactant dodecyltrimethyl ammonium bromide (DTAB) in the mixed solvent media. Recently Tajpuria et al. [19] investigated UV-Vis studies between MR and SDS in acetone/water systems [19]. Thus there are no investigations till now on such interaction between MR and CPC. The investigation was explored using a spectrophotometric technique to analyze the spectral behavior of interactions. An interaction capacity can be analyzed by calculating parameters such as the CMC, binding constants, partition coefficient, Gibbs free energies of binding and partition. The prescribed parameters were calculated using various equations.

However, for the first time, we used a pseudo-phase model to calculate the partition parameters of MR and CPC using CMC values in methanol-water solutions, as this concept was also previously used to study how light yellow (azo dye) (X6G) interacts with CTAB and CPC [20]. An important issue in the present study concerns the characterization of binding and partitioning parameters of CPC on MR in mixed solvent media, which will aid in the development of similar derivatives, such as a -COOH dye in optical tenability and photo-switchability. This paper would provide information about the spectral behaviour of MR in methanol-mixed media. Also due to the nontoxicity of CPC, it can be utilized for the interaction study with dyes in the medicinal, pharmaceutical, emulsion, catalytic and cosmetic industries. This study can be utilized for the improvement of optoelectronic applications [13-16]. The novelty concept of the manuscript is that in future researchers could generate ideas regarding characterising behavior on the mixture through such parameters for further studies on more co-solvent systems using different techniques.

1.1. Theory

At 0.1 up to 0.4 v.f. of methanol, the CMC was determined from the plot of the absorbance - [CPC] profiles. The lower absorbance value indicates the CMC value for each volume fraction of methanol [21].

The binding constants for dye-surfactant interactions in volume fractions of methanol were calculated with the Benesi-Hildebrand equation [17,21,22]

$$\frac{D_T}{\Delta A} = \frac{1}{\epsilon_m - \epsilon_0} + \frac{1}{K_b(\epsilon_m - \epsilon_0)C_m}, \quad (1)$$

$$\Delta A = A - A_0, \quad (2)$$

$$C_m = C_s - CMC. \quad (3)$$

Dye concentration is represented by D_T in Equation (1), while dye absorbance is represented by A in Equation (2). The left-hand side of Equation (1) consists of ΔA , which is the difference between dye's absorbance with and without CPC expressed in Equation (2). The right-hand side of Equation (1) consists of the terms ϵ_m , ϵ_0 , C_m and K_b represent the molar absorptivity of the dye, the absorbance molarity of the fully bound dye to micelles, the concentration of micellized CPC expressed in Equation (3) and the binding constants, respectively. Also, the term C_s represents the concentration of CPC.

In addition, using the partition coefficient, the concentration ratio of non-ionizing species was determined. A pseudo-phase model is used to calculate this parameter as in Equation (4) [20,23]

$$\frac{1}{\Delta A} = \frac{1}{\Delta A^\infty} + \frac{1}{K_s \Delta A^\infty (C_{Dye} + C_{surfactant} - CMC)} \quad (4)$$

where $\Delta A = A - A_0$ and $\Delta A^\infty = A^\infty - A_0$. Further, the complete absorbance of a dye attached to a surfactant is A

$$K_s = \frac{K_x}{n_w}. \quad (5)$$

In Equation (5), the term K_x is the partition coefficient by following the pseudo-phase model and $n_w = 55.5 \text{ mol L}^{-1}$. Thus, K_s is the partition constant, which can be obtained from the slope of the graph plotted between ΔA^{-1} and $[C_{Dye} + C_{surfactant} - CMC]^{-1}$ and K_x can also be obtained from relation Equation (5) [24].

The Gibbs free energies of binding (ΔG_b) and partition (ΔG_p) were calculated using the following Equations (6) and (7)

$$\Delta G_b = -RT \ln K_b, \quad (6)$$

$$\Delta G_p = -RT \ln K_x. \quad (7)$$

2. EXPERIMENTAL

2.1. Chemicals

Cationic surfactant: Cetyl pyridinium chloride (CPC) was purchased from Sigma Labs, Bengaluru-03, India, which was 98% pure. It was kept in a drying oven for one hour before use. Azo Dye: Methyl red (MR) was purchased from Sigma Labsys, Bengaluru-56003, India.

Solvent: Merck, India, provided the methanol for this experiment. It was double-distilled and used as mixed solvent media (0.1, 0.2, 0.3, and 0.4). Double-distilled water was used to prepare mixed media.

2.2. Preparation of Solutions

MR-CPC was studied in the presence of a series of volume fractions of 0.1, 0.2, 0.3, and 0.4 methanol.

- Firstly, 0.1 up to 0.4 v.f. of methanol were prepared. Sequentially surfactant (CPC) (concentration ranging from 0.0623×10^{-3} to $5 \times 10^{-3} \text{ mol. L}^{-1}$ and MR at a constant concentration of $2 \times 10^{-3} \text{ mol. L}^{-1}$ was prepared separately in the series of mixed methanol.
- Secondly, the pH values were measured at variable concentrations of CPC with constant MR concentration.

- Thirdly, spectral absorbance with corresponding wavelengths from 350 to 650 nm of the solution at different concentrations of CPC with a constant dye concentration of MR was recorded for the interacting study of the system.

2.3. Methods

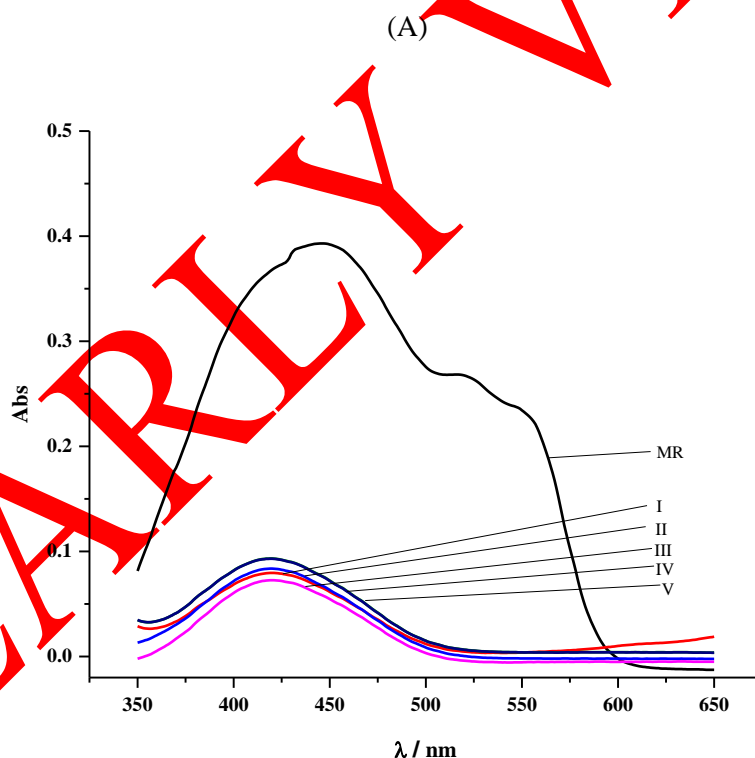
The absorbance measurements were recorded by double beam UV-Visible spectrophotometer (MARS ME-SP 195UV, India) at room temperature (298.15 K) with 1 cm length quartz cuvette. The pH values were recorded using (a Eutech-2700, Singapore) pH meter.

3. RESULTS AND DISCUSSION

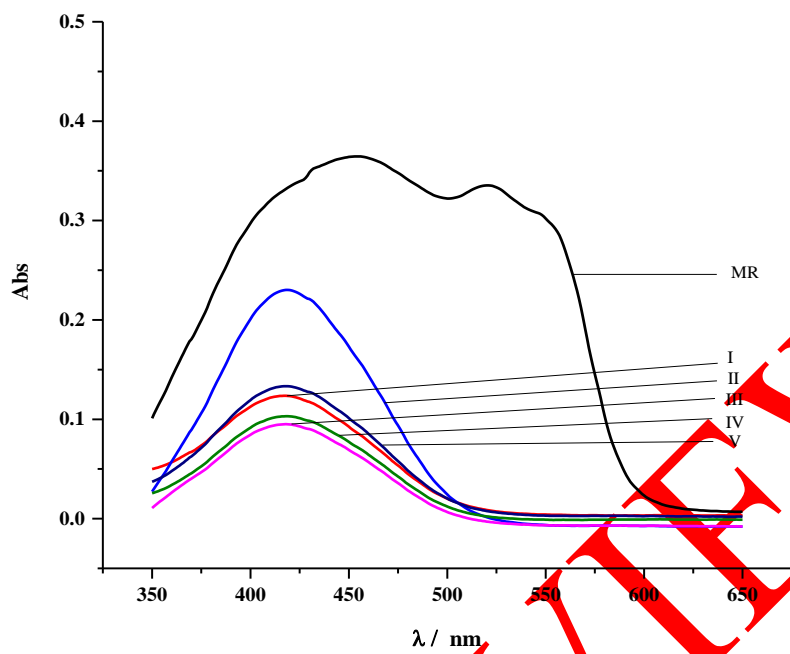
Dye-surfactant interaction is a well-determined phenomenon and we used a spectrophotometric technique to investigate this interaction between MR and CPC. The nature of the interaction is well determined and plays a significant role in the formation of dye surfactant complex which has been observed during differential absorbance with the relevant binding and partition behaviour.

The characteristic nature of the interaction is noticed through hypochromic shifts, the CMC is determined separately in different polarized methanol-water mixtures and differential absorption spectral analysis for binding and partition parameters along with the effect of pH below and above CMC.

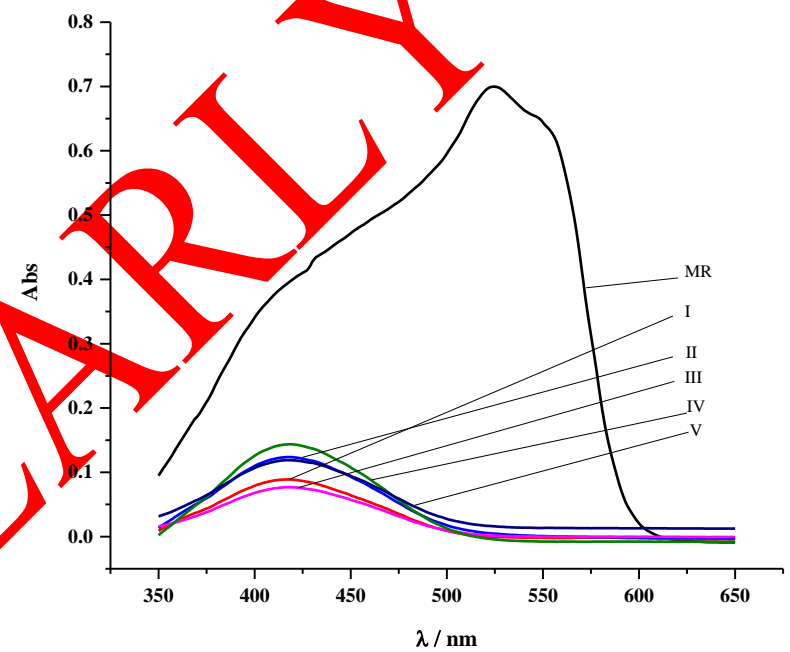
3.1. Interaction between CPC and MR



(B)



(C)



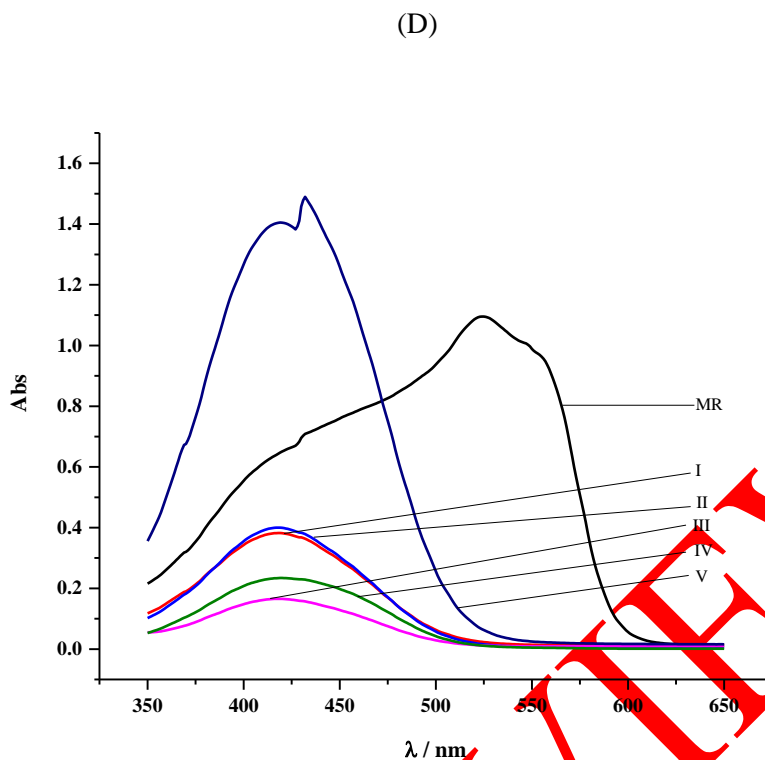


Figure 1. Visible spectra of MR-CPC system in (A) 0.1, (B) 0.2, (C) 0.3, (D) 0.4 volume fractions of methanol. Here, I, II, III, IV, V and MR represent the concentration of CPC [5, 2.5, 1, 0.5, 0.4 and 0] $\times 10^{-3}$ mol. L^{-1} respectively. Here the constant concentration of MR is 2×10^{-3} mol. L^{-1}

The simple absorption spectra of MR with and without CPC in methanol-water mixtures are given in Figure 1. The comparison revealed that the redshift of the wavelength of maximum absorbance (λ_{max}) of 30 nm, 42 nm, 112 nm, and 108 nm from 419 nm to 449 nm, 413 nm to 455 nm, 413 nm to 525 nm, and 417 nm to 525 nm for 0.1, 0.2, 0.3, and 0.4 v.f. of methanol, respectively as shown in Figure 1. The redshift increased sequentially of MR with the increase of the methanol, as described in the recent literature [9] dielectric constant decreases [25], and a reduction in solubility in the solvent.

Using UV-vis spectroscopy, we can explore the mechanism of dye-surfactant interaction. During such interaction, we observed a decrease in redshift due to the entrapment of dye molecules in the core of micelles. The micelles generate enhanced surface activity on the dye molecules throughout the interaction [18]. Accordingly, the spectrum displays an abnormal hypochromic shift due to the dynamic interaction between the MR molecules containing -COOH groups and CPC molecules containing pyridinium groups (Figure 1). The redshift reflects interactions between MR molecules and more methanol, which resulted in pi-pi stacking in Figure 2 because azo dyes are composed of J-aggregates formed by hydrogen bonding with methanol [26].

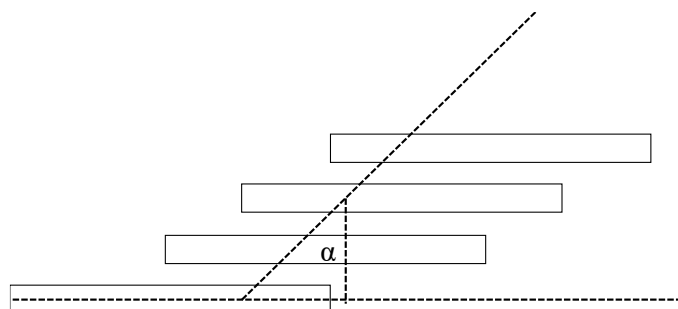


Figure 2. J- aggregate (bathochromism) [26]

Specifically, the redshift (emission) increased from 449 nm to 525 nm with increasing methanol content in water (Figure 1). This elevation is due to a revolution in the microenvironment of the solvent, leading to an increase in the absorbance value. The occupancy of a -COOH group fabricates side-by-side interaction, devise aggregation. Thus, extreme absorption materializes in solvatochromism (emission) [27].

The anionic and zwitterionic forms [14,28] of MR manifest an isosbestic point that finds the same molar extinction coefficient of the two forms of MR. However, such a point was not perceived in the spectra of the MR with CPC in the methanol-water mixtures. There is no isosbestic point in the spectra in Figure 1 due to the absence of common ions in the system [29]. In the aqueous CPC solution, methyl red may exhibit unusual behavior owing to its presence of azo and hydrazone species.

Plots of absorbance versus variable concentration of CPC with constant dye concentration in v.f. of methanol are presented in Figure 3 as the representative plot of absorbance versus [CPC] profile in 0.2 v.f. of methanol. We measured the minimum value of absorbance at a given concentration of constant dye in various surfactant concentrations, and we denoted this value as CMC. Among the absorbance concentrations of the CPC profile, the lower absorbance value signifies CMC [21]. The various absorbance-[CPC] profiles show the specified CMCs and are tabulated (Table 1).

Table 1. CMC values of CPC at 0.1, 0.2, 0.3 and 0.4 v.f.s of Methanol

Volume fraction of Methanol	0.1	0.2	0.3	0.4
CMC (mol L ⁻¹)(with MR)	0.067 x 10 ⁻³	0.125 x 10 ⁻³	1.0 x 10 ⁻³	0.1 x 10 ⁻³
Literature (mol L ⁻¹)(without MR) ^a	0.98 x 10 ⁻³	1.05 x 10 ⁻³	1.10 x 10 ⁻³	1.13 x 10 ⁻³

^aSome literature CMC values of CPC without MR obtained by conductometric measurement are given in the last row for comparison [30]

As can be seen, the CMC values increase with sequential v.f.s of methanol (0.1, 0.2, and 0.3), except for the v.f. of methanol at 0.4. In comparison to the CMC values of cationic surfactant without dye in the cosolvent, the CMC values are a decreasing trend, which explains the strong electrostatic interaction between the azo dye and surfactant. The values decrease due to the reduction of repulsive forces between the polar head of the cationic surfactant and azo dye in micelles. With the addition of dye, the absorbance, as well as CMC values, were reduced in contrast to the CMC value obtained for CPC without dye in a series of methanol-water solvent systems [30]. Abnormal behavior of reduction in the CMC value is noticed in the 0.4 v.f. of methanol because of the penetration of methanol molecules into the micelle.

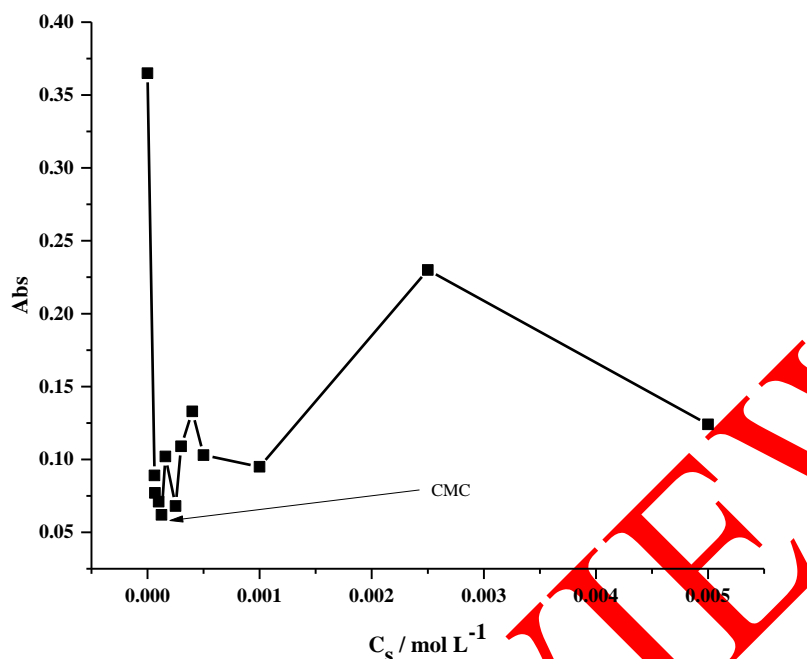


Figure 3. Representative plot of absorbance versus [CPC] profile in 0.2 volume fraction of methanol

3.2. Determination of Binding and Partition Parameters using Differential Absorption Spectra

Spectrophotometric analysis is popular for analyzing dyes that are water soluble (Direct dyes) and insoluble (lake dyes) [31]. Differential spectroscopy has proven to be the most suitable method for detecting dye-surfactant interactions [32]. Differential absorbance provides insight into the binding and partition behaviour of oppositely charged dyes and surfactants using the Benesi-Hilderbrand Equation (1) and the pseudo-phase model in Equation (4), respectively. There is an increase in differential absorbance with a greater v.f. of methanol in water as seen in Figures 4 and 5. Figures 4 and 5 show the plots to determine the binding constant and partition coefficient. Gibbs free energies of binding (ΔG_b) and partition (ΔG_p) can be determined using the binding and partition parameters with Equations (6) and (7), respectively. We evaluated the dynamic nature of interaction at the increased levels of methanol in water through differential absorbance in Table 2. The absorbance of MR from 0.1 to 0.4 shows the greater difference in nature of interaction which plays a vital role in determining the binding and partition among CPC and MR molecules. The binding constants were higher at a lower concentration of methanol and lower at 0.4 volume fraction of methanol due to its difference in polarity of the solvent. The higher partition constant and partition coefficient at 0.3 v.f. indicates the larger hydrophobic interaction than 0.2 v.f. But we also determined the interaction at 0.4 v.f. of methanol which greatly influences addressing abnormal behavior of partition. The negative values of Gibbs free energies of binding and partition represent that the system is in a stable form, which consists of spontaneous behavior of binding and partition [33].

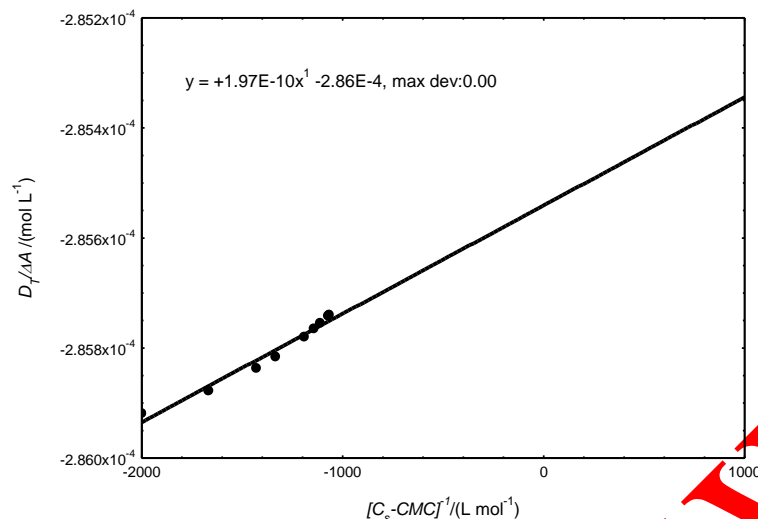


Figure 4. Plot of $\frac{D_T}{\Delta A}$ against $[C_s - CMC]^{-1}$ for MR with CPC in 0.3 volume fraction of methanol

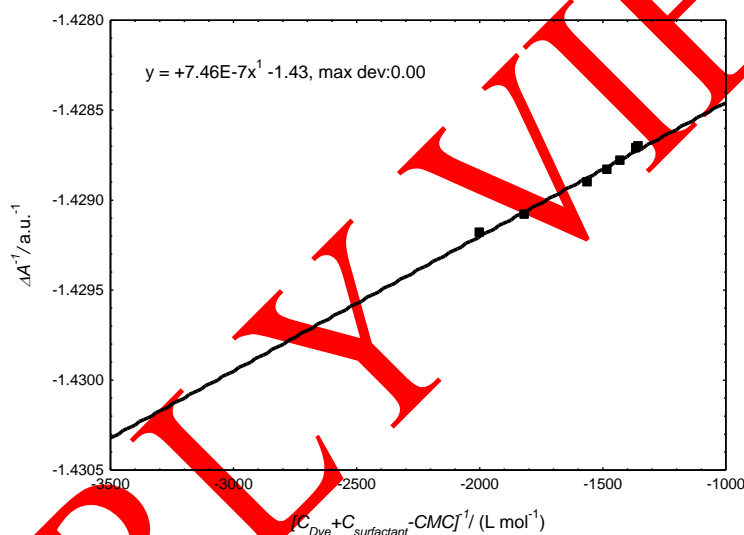


Figure 5. Plot of ΔA^{-1} against $[C_{Dye} + C_{surfactant} - CMC]^{-1}$ for MR with CPC in 0.3 volume fraction of methanol

The data are tabulated in Table 2, including, K_b , K_s , K_x , ΔG_b and ΔG_p .

Table 2. Comparison of values of K_b , K_s , K_x , ΔG_b and ΔG_p in 0.1, 0.2, 0.3 and 0.4 v.f.s of methanol

Volume fraction of Methanol	K_b (Lmol ⁻¹)	K_s	K_x	ΔG_b (kJmol ⁻¹)	ΔG_p (kJmol ⁻¹)
0.1	30.3 X 10 ⁵	4.56 X 10 ⁴	253.08 X 10 ⁴	-36.99	-36.54
0.2	3.95 X 10 ⁵	42.9 X 10 ⁴	2380.95 X 10 ⁴	-31.94	-42.10
0.3	14.5 X 10 ⁵	192 X 10 ⁴	10656 X 10 ⁴	-35.16	-45.81
0.4	0.93 X 10 ⁵	189 X 10 ⁴	10489.5 X 10 ⁴	-28.35	-45.77

3.3. Effect of pH

The pH effect is discussed when it comes to the interaction between MR and CPC [29]. The effects are discussed in two regions i.e. below and above CMC.

Below CMC: As the pH of an acidic region ranges from 2 to 5, the protonation of azo dyes will decrease because of electrostatic interactions between charged dyes and the surfactant monomer. By this matter, the result is sorted by realizing the tautomerism of the dye as shown in Figure 6.

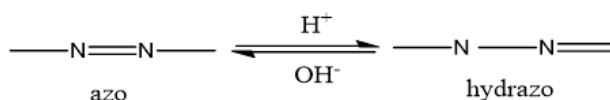
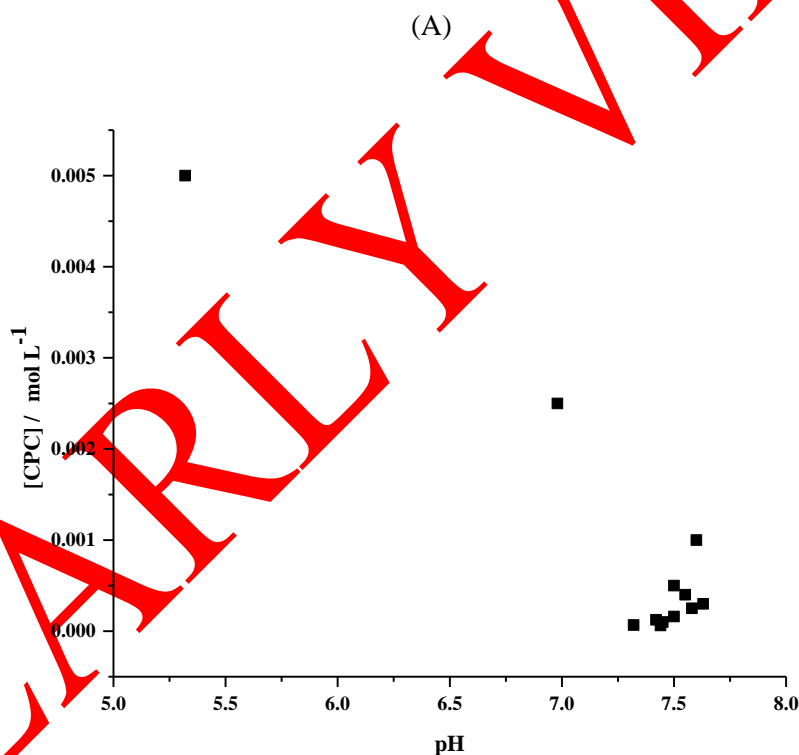


Figure 6. Tautomerism of azo dye

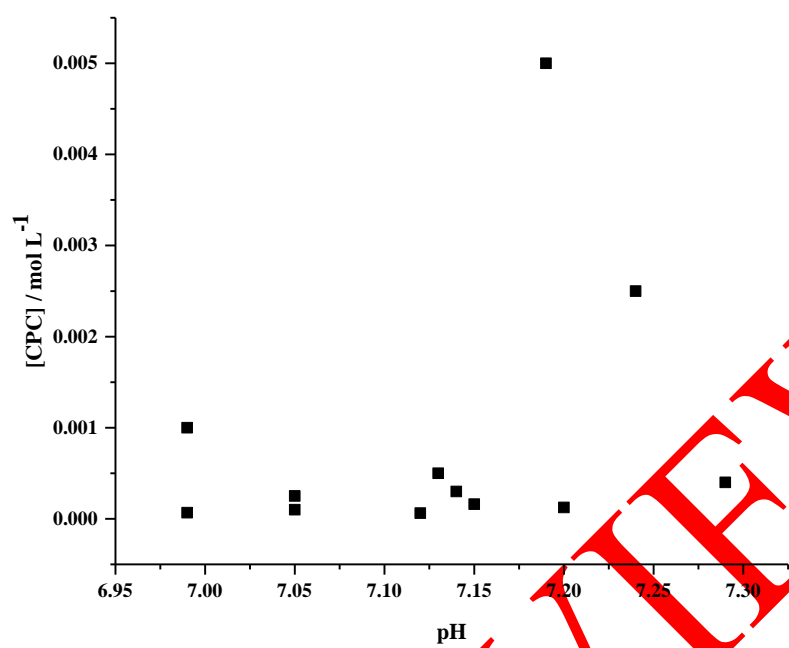
The azo dye consists of an azo group (-N=N-), which shifts to the hydroazo form during equilibrium in an acidic medium. Hydroazo ions shift to the azo form in basic media [19]; for our alcohol-water system, the appropriate pH range was found to be (5-8), as shown in Figure 7.

Above CMC: pH change (7-8) did not affect spectra and absorbance for the alcohol-water system. Diluting the dye into the micelle did not affect pH values. As discussed, pH changes do not affect the dye-surfactant complex.

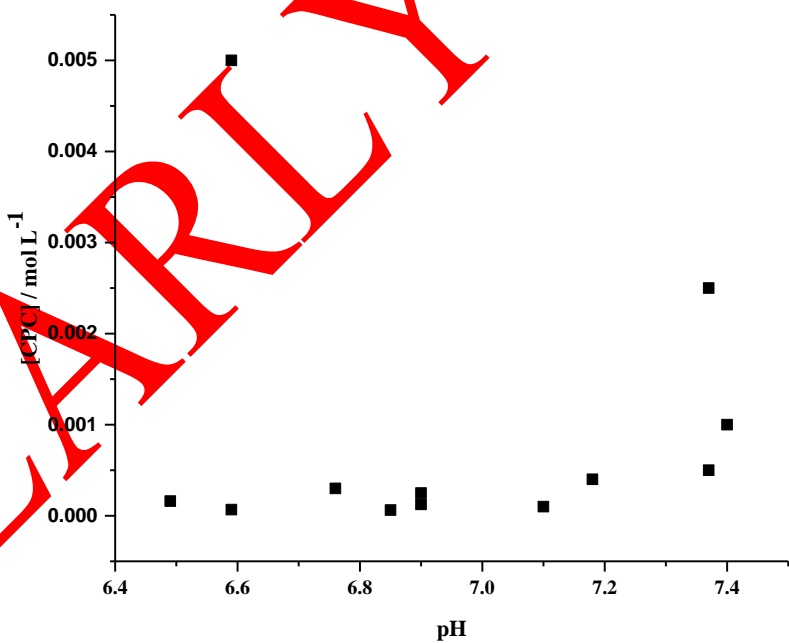
We justify from the literature [16] that MR dye solution in aqueous solution showed red color at the wavelength of maximum absorbance (λ_{max}) 523 nm in acidic (hydrazone) form (pH=2) and yellow color at the wavelength of maximum absorbance (λ_{max}) 431 nm in basic (azo) form (pH=8). In our case, we obtained the pH of azo form due to availability of basic medium of methyl red with CPC and without CPC in methanol mixed media [19]. The only existing form did not allow us to see the isosbestic points in the spectra Figure 1.



(B)



(C)



(D)

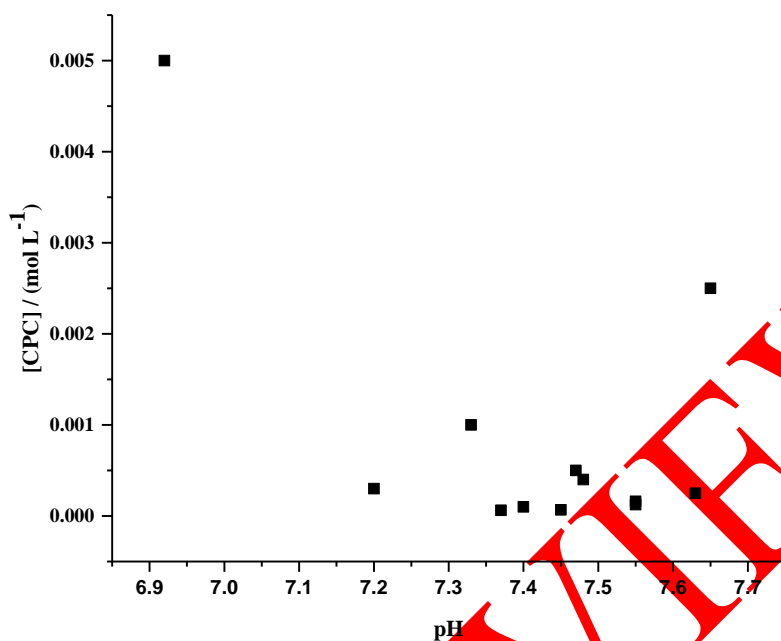


Figure 7. [CPC] versus the pH profile. (A) 0.1, (B) 0.2, (C) 0.3, and (D) 0.4 volume fractions of methanol

4. CONCLUSION

The experimental results show the interaction of MR with CPC/ CH₃OH/H₂O at room temperature. With the function of change in CPC concentration and wavelength, the abnormal hypochromic shift was seen due to the unusual behaviour of MR. During the interaction, the j-aggregate nature and the pH of the azo form of MR acts an important role in the incorporation of MR by micelles of CPC (cationic surfactant). The only basic form(azo) of MR oppose to observe the isosbestic points in the spectra of interaction. The results show that there is a decrease in CMC with MR corresponding to the series of v.f. of methanol in comparison to the CMC values of CPC from literature without MR. The trends of change in binding and partition parameters show strong interactions between MR and CPC. Moreover, the negative values of Gibb's free energy of binding and partition illustrate the spontaneous process of the system.

ACKNOWLEDGEMENTS

Under the grant award no. PhD-75/76-S&T-05, this research was funded by the Nepalese University Grants Commission, Office at Sanothimi in Bhaktapur, Nepal.

CONFLICTS OF INTEREST

No conflict of interest was declared by the authors.

REFERENCES

- [1] Ghoreishi, S.M., Behpour, M., Farsani, A.G., "Study of interaction between a cationic surfactant and two anionic azo dyes by ion-selective electrode technique and spectrophotometry", *Dyes and Pigments*, 74(3): 585–589, (2007).

- [2] Garcia, M.E.D., Sanz-Medel, A., "Dye-surfactant interactions: a review", *Talanta*, 33(3): 255–264, (1986).
- [3] Kert, M., Simoncic, B., "Importance of dye-surfactant interactions in dyeing", *Tekstilec*, 50: 187-207, (2007).
- [4] Bilksi, P., Chignell, C.F., "Properties of differently charged micelles containing rose bengal: application in photosensitization studies", *Journal of Photochemistry and Photobiology A: Chemistry*, 77: 49–58, (1994).
- [5] Bilski, P., Holt, R.N., Chignell, C.F., "Premicellar aggregates of Rose Bengal with cationic and zwitterionic surfactants", *Journal of Photochemistry and Photobiology A: Chemistry*, 110: 67–74, (1997).
- [6] Niraula, T.P., Chatterjee, S.K., Bhattarai, A., "Micellization of sodium dodecyl sulphate in presence and absence of alkali metal halides at different temperatures in water and methanol-water mixtures", *Journal of Molecular Liquids*, 250: 287-294, (2018).
- [7] Biswas, S., Pal, A., "Spectrophotometric determination of cationic surfactants in aqueous media using chrome azurol S as colour forming agent and 1-butanol as extracting solvent", *Talanta*, 206: 120-238, (2020).
- [8] Ahmadi, F., Daneshmehr, M. A., Rahimi, M., "The effect of anionic and cationic surfactants on indicators and measurement of dissociation constants with two different methods", *Spectrochimica Acta - Part A: Molecular and Biomolecular Spectroscopy*, 67(2): 412–419, (2007).
- [9] Sharifi, S., Nazar, M.F., Rakhshanizadeh, F., Sangsefedi, S.A., Azarpour, A., "Impact of amino acids, organic solvents and surfactants on azo-hydrazone tautomerism in methyl red: spectral-luminescent and nonlinear optical properties", *Optical and Quantum Electronics*, 52(2): 98, (2020).
- [10] Hahn, C., Wokaun, A., "Diffusion in surfactant systems studied by forced Rayleigh scattering", *Langmuir*, 13(3): 391–397, (1997).
- [11] Chanda, S., Ismail, K., "Surface potential and polarity at the micelle-solution interface in AOT + water system", *Indian Journal of Chemistry - Section A Inorganic, Physical, Theoretical and Analytical Chemistry*, 48(6): 775–780, (2009).
- [12] Terpko, A.T., Serafin, R.J., Bucholtz, M.L., "Conjugate acid-conjugate base equilibrium in reverse micelles", *Journal of Colloid and Interface Science*, 84(1): 202-205, (1981).
- [13] Narayan, R.B., Goutham, R., Srikanth, B., Gopinath, K.P., "A novel nano-sized calcium hydroxide catalyst prepared from clam shells for the photodegradation of methyl red dye", *Journal of Environmental Chemical Engineering*, 6(3): 3640–3647, (2018).
- [14] Zhang, L., Cole, J.M., Waddell, P.G., Low, K.S., Liu, X., "Relating electron donor and carboxylic acid anchoring substitution effects in azo dyes to dye-sensitized solar cell performance", *ACS Sustainable Chemistry and Engineering*, 1(11): 1440–1452, (2013).
- [15] Christodoulides, D.N., Khoo, I.C., Salamo, G.J., Stegeman, G.I., Van Stryland, E.W., "Nonlinear refraction and absorption: mechanisms and magnitudes", *Advances in Optics and Photonics*, 2(1): 60, (2010).
- [16] Plutino, M.R., Guido, E., Colleoni, C., Rosace, G., "Effect of GPTMS functionalization on the improvement of the pH-sensitive methyl red photostability", *Sensors and Actuators, B: Chemical*, 238: 281–291, (2017).

- [17] Sachin, K.M., Karpe, S.A., Singh, M., Bhattarai, A., "Study on surface properties of sodiumdodecyl sulfate and dodecyltrimethylammonium bromide mixed surfactants and their interaction with dyes", *Heliyon*, 5(4): e01510, (2019).
- [18] Shahi, N., Shah, S.K., Yadav, A.P., Bhattarai, A., "The spectral study of azo dye and cationic surfactant interaction in ethanol-water mixture", *Journal of the Serbian Chemical Society*, 86(5): 483-494, (2021).
- [19] Tajpuriya, G.P., Shah, P., Shahi, N., Bhattarai, A., "UV-Vis studies of methyl red in the presence of sodium dioctylsulfosuccinate/acetone and sodium dioctylsulfosuccinate/acetone/water", *Spectrochimica Acta Part A: Molecular and Biomolecular Spectroscopy*, 255: 119646, (2021).
- [20] Hosseinzadeh, R., Maleki, R., Matin, A.A., Nikkhahi, Y., "Spectrophotometric study of anionic azo-dye light yellow (X6G) interaction with surfactants and its micellar solubilization in cationic surfactant micelles", *Spectrochimica Acta - Part A: Molecular and Biomolecular Spectroscopy*, 69(4): 1183-1187, (2008).
- [21] Edbey, K., El-Hashani, A., Benhmid, A., Ghwel, K., Benamer, M., "Spectral studies of eriochrome black T in cationic surfactants", *Chemical Science International Journal*, 24(4): 1-12, (2018).
- [22] Fazeli, S., Sohrabi, B., Tehrani-Bagha, A.R., "The study of sunset yellow anionic dye interaction with gemini and conventional cationic surfactants in aqueous solution", *Dyes and Pigments*, 95(3): 768-775, (2012).
- [23] Khosa, M.A., "Interaction of azo dye with cationic surfactant under different pH conditions", *Journal of Surfactants and Detergents*, 13: 529-537, (2010).
- [24] Shah, S.S., Naeem, K., Shah, S.W.H., Laghari, G.M., "Differential absorbance measurements of amphiphilic hemicyanine dyes, solubilization study in anionic surfactant", *Colloids and Surfaces A: Physicochemical and Engineering Aspects*, 168(1): 77-85, (2000).
- [25] Bhattarai, A., Chatterjee, S.K., Deo, T.K., Niraula, T.P., "Effects of concentration, temperature, and solvent composition on the partial molar volumes of sodium lauryl sulfate in methanol (1) + water (2) mixed solvent media", *Journal of Chemical & Engineering Data*, 56(8): 3400-3405, (2011).
- [26] Karukstis, K.K., Perelman, L.A., Wong, W.K., "Spectroscopic characterization of azo dye aggregation on dendrimer surfaces", *Langmuir*, 18: 10363-10371, (2002).
- [27] Hashemi, N., Sun, G., "Intermolecular interactions between surfactants and cationic dyes and effect on antimicrobial properties", *Industrial and Engineering Chemistry Research*, 49(18): 8347-8352, (2010).
- [28] Yang, J., "Interaction of surfactants and aminoindophenol dye", *Journal of Colloid and Interface Science*, 274(1): 237-243, (2004).
- [29] Hari, A.C., Paruchuri, R.A., Sabatini, D.A., Kibbey, T.C.G., "Effects of pH and cationic and nonionic surfactants on the adsorption of pharmaceuticals to a natural aquifer material", *Environmental Science & Technology*, 39(8): 2592-2598, (2005).
- [30] Bhattarai, A., Yadav, A.K., Sah, S.K., Deo, A., "Influence of methanol and dimethyl sulfoxide and temperature on the micellization of cetylpyridinium chloride", *Journal of Molecular Liquids*, 242: 831-837, (2017).

- [31] Kaur, A., Gupta, U., "The Review on Spectrophotometric Determination of Synthetic Food Dyes and Lakes" *Gazi University Journal of Science*, 25(3): 579-588, (2012).
- [32] Shah, P., Kumari Jha, S., Bhattarai, A., "Spectrophotometric study of the Sodium dodecyl sulfate in the presence of Methylene blue in the methanol-water mixed solvent system", *Journal of Molecular Liquids*, 117200, (2021).
- [33] Buwalda, R.T., Jonker, J.M., Engberts, J.B.F.N., "Aggregation of azo dyes with cationic amphiphiles at low concentrations in aqueous solution", *Langmuir*, 15(4): 1083–1089, (1999).

EARLY VIEW